Dipartimento di / Department of

Biotecnologie e Bioscienze

Dottorato di Ricerca in / PhD program Tecnologie Convergenti per i Sistemi Biomolecolari TeCSBi Ciclo / Cycle XXXVIII

BIOACTIVE COMPOUNDS AND HEALTHY AGING:

SEARCH FOR NEW NUTRACEUTICAL COMPOUNDS THROUGH THE EXPERIMENTAL MODEL OF CHRONOLOGICAL AGING IN YEAST

Cognome / Surname Abbiati Nome / Name Francesco

Matricola / Registration number 816861

Tutore / Tutor: Prof. Ivan Orlandi

Supervisor: Prof. Marina Vai

Coordinatore / Coordinator: Prof. Andrea Galimberti

ANNO ACCADEMICO / ACADEMIC YEAR 2024/2025

“To get back one's youth, one has merely to repeat one's follies." "A delightful theory!" she exclaimed. "I must put it into practice." "A dangerous theory!" came from Sir Thomas's tight lips. Lady Agatha shook her head, but could not help being amused. Mr. Erskine listened. "Yes," he continued, "that is one of the great secrets of life. Nowadays most people die of a sort of creeping common sense, and discover when it is too late that the only things one never regrets are one's mistakes.”

The Picture of Dorian Gray by Oscar Wilde

To my 5017 Lab mates

Anna, Stefano, Luca & Davide

ABSTRACT

Over the past several decades, life expectancy in many developed countries has steadily increased, often surpassing 85 years. However, this demographic shift was not accompanied by a proportional improvement in healthspan. A significant proportion of individuals over the age of 65 suffers from chronic and debilitating conditions, including cardiovascular diseases, cancer and neurodegenerative disorders. This disparity between lifespan and healthspan has intensified scientific interest in the biological mechanisms of aging and the development of interventions aimed at mitigating age-associated decline.

Aging is governed by evolutionarily conserved pathways, allowing the use of simple model organisms to investigate its underlying biology. In this study, we employed *Saccharomyces cerevisiae*, a unicellular eukaryote which undergoes both replicative and chronological aging, two complementary models of aging, which resemble the aging process of mitotically active and post-mitotic mammalian cells, respectively. Replicative lifespan (RLS) refers to the number of daughter cells produced by a mother cell in presence of nutrients before death, while chronological lifespan (CLS) is the mean and maximum period of time of surviving cells in stationary phase. Given the strong interplay among aging, nutrient availability and metabolic regulation, we explored the effects of specific nutraceutical compounds on yeast CLS to identify potential anti-aging agents and elucidate their mechanisms of action. In particular, we decided to focus our study on three natural compounds, characterised by different, specific and unrelated chemical structures and/or composition, deriving from various natural sources.

We first investigated the impact of quercetin (QUER), a polyphenolic flavonoid with known antioxidant properties and from 2010 generally recognized as safe by the FDA. Supplementation with QUER at the onset of chronological aging (diauxic shift) significantly extended CLS. This extension correlated with reduced oxidative stress and marked alterations in carbon metabolism. Specifically, QUER enhanced gluconeogenesis *via* improved catabolism of C2 fermentation by-products and glycerol.

These effects were mediated through the Sir2-dependent activation of phosphoenolpyruvate carboxykinase and the L-glycerol 3-phosphate pathway, respectively. The resulting increase in gluconeogenic flux led to elevated trehalose accumulation, a key factor in promoting longevity. Furthermore, QUER treatment in extreme calorie restriction amplified the long-lived phenotype, reinforcing its role in modulating carbon metabolism and promoting CLS. We also examined the effects of glucosinolates (GSLs), sulfur- and nitrogen-containing glycosides present in many edible plants among which the oilseed crop Camelina (*Camelina sativa (L.)* Crantz). Its seeds contain three aliphatic GSLs: glucoarabin, glucocamelinin and homoglucocamelinin, that were purified from Camelina press cake, a by-product of oil extraction. GSL supplementation extended yeast CLS in a dose-dependent manner, primarily through enhanced mitochondrial respiration, reduced superoxide anion (ROS) levels, and increased ATP production. Additionally, GSLs preserved tricarboxylic acid cycle activity and promoted glycerol catabolism, contributing to improved phosphorylating respiration and trehalose storage, both critical for longevity. Finally, we explored the neuroprotective potential of a cocoa bean shell extract (CBSE), a by-product of cocoa processing, in models of Parkinson's disease. Using yeast and neuroblastoma cells overexpressing α-synuclein (α-syn), we demonstrated that CBSE supplementation reduced ROS level, activated autophagy and decreased protein aggregation. In neuroblastoma cells, CBSE activated AMPK and significantly reduced toxic α-syn oligomers. Surface plasmon resonance assays confirmed direct binding of CBSE to α-syn in a concentration-dependent manner, suggesting its potential to inhibit amyloid aggregation. These findings support the use of CBSE as a promising nutraceutical for the prevention of α-syn-associated neurodegenerative disorders.

In conclusion, this thesis effectively provides compelling evidence for the potential pro-longevity efficacy of molecules and compounds derived from various natural sources. Specifically, the findings lay a metabolic and molecular foundation for the development of new strategies, based on nutraceutical supplementation, aimed at narrowing the gap between lifespan extension and healthspan improvement.

TABLE OF CONTENTS

INTRODUCTION

Aging

In humans aging is inexorable [1] and globally, the world population is aging. Epidemiological data indicate that approximately 11% of the world's population is currently over the age of 60, with projections suggesting this figure will rise to 22% by 2050. However, significant country disparities exist. For instance, in Japan, 32% of the population is aged 60 or older, and the country exhibits the highest life expectancy at age 60, approximately 26 additional years. In contrast, Africa, as a continent, reports the lowest life expectancy at age 60, estimated at 17 years. In high-income countries, the proportion of individuals aged 65 and older is steadily increasing in absolute terms [2].

Aging can be conceptualized as the breakdown of self-organizing systems and a diminished capacity to adapt to environmental changes. It is characterized by a progressive and irreversible decline in physiological function across all organ systems, primarily driven by the uncontrolled-cumulative effects of cellular and molecular damage in response to various internal and external stressors [3]. The maintenance of health and survival in living organisms depends on a dynamic equilibrium between damage and repair, alteration and preservation, an overarching concept referred to as homeostasis. A

gradual decline in the intrinsic ability to regulate homeostasis effectively leads to increased susceptibility to disease and heightened physiological vulnerability [4]. Human aging is associated with a loss of complexity across a broad spectrum of physiological processes and anatomical structures, including but not limited to blood pressure regulation, gait dynamics, respiratory cycles, visual acuity and postural control. This decline ultimately results in reduced fertility and an elevated risk of morbidity and mortality [5]. Aging is marked by a set of biological features known as the hallmarks of aging (Figure 1).

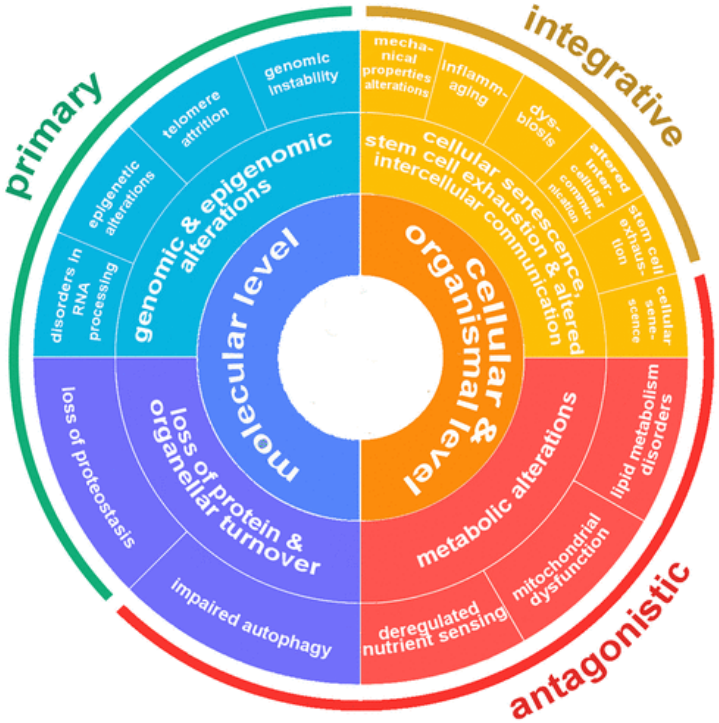

Figure 1. *Scheme of the currently identified hallmarks of aging along with their classification*. Reproduced from [4]

These are not only associated with the progressive decline in physiological function and the increased risk of age-related diseases, but they also play a direct, causative role in the aging process itself [6]. In 2013, researchers proposed a framework of nine core hallmarks which has guided much of the scientific inquiry into aging so far [7].

The first group, known as the primary hallmarks, includes genomic instability, telomere attrition, epigenetic alterations and loss of proteostasis. These mechanisms are considered the initial drivers of cellular damage. Genomic instability refers to the accumulation of DNA damage and mutations over time, which can lead to diseases such as cancer and neurodegeneration. Telomere attrition involves the gradual shortening of chromosomal ends during cell division, ultimately triggering cellular senescence. Epigenetic alterations affect gene expression without changing the DNA sequence, while the loss of proteostasis reflects the cell's declining ability to maintain proper protein folding and degradation. The second group, termed antagonistic hallmarks, includes dysregulated nutrient sensing, mitochondrial dysfunction and cellular senescence. These processes initially act as protective responses to damage but can become harmful if sustained. For instance, cellular senescence can prevent the proliferation of damaged cells, thereby reducing cancer risk, but its accumulation over time contributes to tissue dysfunction and aging. The final group, the integrative hallmarks, comprises

stem cell exhaustion and altered intercellular communication. These emerge when the damage from primary and antagonistic hallmarks surpasses the body's capacity for repair and homeostasis. As a result, the regenerative potential of tissues declines, and communication between cells becomes disrupted, further accelerating the aging process.

Over the past decade, additional features of aging have been identified. These include impaired autophagy, which hinders the clearance of damaged cellular components; disturbances in the gut microbiome or dysbiosis, which can promote systemic inflammation; and splicing dysregulation, which affects RNA processing and may drive cellular senescence. Chronic low-grade inflammation, often referred to as "inflammaging," is another widespread phenomenon, occurring even in the absence of infection and contributing significantly to age-related morbidity. Furthermore, changes in the mechanical properties of cells and tissues, such as increased stiffness, have been linked to conditions like hypertension and diabetes [4].

Recent studies have also highlighted the role of lipid metabolism in aging. For example, the accumulation of sphingolipids, particularly ceramides, in muscle tissue has been shown to impair function in older adults. Similarly, senescent cells tend to accumulate cholesterol in lysosomes, supporting the pro-inflammatory secretory phenotype associated with aging. In addition to these molecular and cellular mechanisms, several physiological changes are

commonly observed during aging. The immune system becomes less effective, increasing susceptibility to infections and certain cancers. Hormonal levels shift, with declines in growth hormone, namely testosterone and estrogen, and a rise in cortisol. Body composition also changes, with a tendency to lose muscle mass and gain fat, raising the risk of metabolic disorders. Cognitive functions such as memory and processing speed often decline, and the risk of falls and fractures increases due to weakened bones and impaired balance.

Since aging is influenced by multiple factors, including genetics, lifestyle such as diet, exercise and stress, environmental factors including pollution and climate change, and social factors such as social support and socioeconomic *status*, interventions such as lifestyle adjustments, medical treatments and social programs can help promote healthy aging and extend the lifespan. Understanding the complex interactions between these factors is essential for promoting healthy aging [4].

Nutraceutical – General introduction

Over recent decades, the Western countries have witnessed a significant rise in health awareness. Along with increasing demand for sports nutrition, an expanding geriatric population, advancements in product formulation and a

growing emphasis on preventive healthcare, have driven the growth of the nutraceuticals market [8,9].

The term "nutraceutical" was coined in 1989 by Dr. Stephen L. DeFelice, founder and chairman of the Foundation for Innovation in Medicine (FIM). He defined nutraceuticals as “a single item or combination of entities, including specific diets, that have clinical significance and may be used for disease prevention or therapy” [10,11]. This was an innovative concept and an “umbrella” term for a broad category of products derived from food sources that offer health benefits beyond basic nutritional value [11].

The global nutraceutical market was valued at USD 425.2 billion in 2023 and is projected to increase to USD 468.15 billion in 2024, reaching approximately USD 1010.83 billion by 2032. This corresponds to a compound annual growth rate (CAGR) of 10.1% during the forecast period from 2025 to 2032 [8]. Currently, Europe, the United States, and Japan collectively account for over 90% of the global nutraceutical market [9]. Despite increasing public interest, a universally accepted definition of nutraceuticals remains elusive, primarily due to country differences in regulatory frameworks governing their marketing, safety, efficacy and cultural perceptions [12].

Nutraceuticals encompass biologically active compounds found in foods that exhibit both nutritional and health advantages properties. These include natural bioactive substances such as lipids, vitamins, carbohydrates, proteins,

minerals, antioxidants, phytochemicals, fatty acids, amino acids and probiotics [13]. Depending on regional regulations, nutraceuticals may be marketed with claims related to the prevention of chronic diseases, promotion of general health, deceleration of the aging process, extension of life expectancy, or support of physiological functions.

Evidence supports the potential therapeutic applications of nutraceuticals in managing a wide range of health conditions, including respiratory infections (e.g., cough and cold), arthritis, gastrointestinal disorders, sleep disturbances, depression, cardiovascular diseases, diabetes, atherosclerosis, cancer and neurological disorders [9]. Clearly, the effective use of one of these compounds in the treatment of a pathological disease must be supported by strong scientific evidence, which nowadays remains overall poor [12].

Geroprotector - Role of nutraceuticals in anti-aging research

In the field of longevity, contemporary research is primarily directed toward the development of strategies aimed at mitigating the deleterious effects of aging [14]. In this context, the concept of “geroprotectors”, a term originally introduced by Illya Mechnikov, one of the pioneers of gerontology [15], has garnered increasing attention. This term refers to all compounds that are characterized by the ability to modulate the biological Hallmarks of Aging,

thereby delaying the onset of age-associated pathologies and enhancing physiological resilience in older individuals. Notably, several currently recognized geroprotective compounds have emerged through the repurposing of previously approved pharmaceuticals or well-characterized bioactive substances, many of which are derived from dietary natural sources [16]. The review of Rivero-Segura, N. A. *et al.* (2024) [16] provides detailed mappings of nutraceuticals to the single aging hallmarks, supported by experimental and clinical studies. An introductory summary with various examples of geroprotectors is given below:

- Genomic instability: antioxidants from grapes, coffee, turmeric and berries protect DNA from oxidative damage and improve genomic integrity
- Telomeric attrition: vitamins C, D, E, retinoic acid, curcumin, resveratrol and omega-3s (EPA/DHA) help maintain telomeric length and telomerase activity.
- Epigenetic alterations: polyphenols (curcumin, resveratrol), vitamins A, C, E modulate DNA methylation, histone modifications and miRNA expression.
- Loss of proteostasis: curcumin, cranberry proanthocyanidins, oleuropein and resveratrol enhance chaperone activity and proteasome function.

- Deregulated nutrient sensing: genistein, resveratrol, gallic acid and myoinositol modulate IIS (insulin/IGF-1 signaling), mTOR, AMPK and SIRT (sirtuin) pathways.
- Mitochondrial dysfunction: α-lipoic acid, resveratrol, apigenin and pea protein with inulin improve mitochondrial biogenesis and reduce ROS (Reactive Oxygen Species).
- Cellular senescence: fisetin, procyanidin C1, luteolin and dasatinib act as senolytics, reducing SASP (Senescence-Associated Secretory Phenotype) markers and promoting cell renewal.
- Stem cell exhaustion: resveratrol, vitamin D3 and ketogenic diets support stem cell survival and regeneration.
- Altered intercellular communication: baicalin, vitamin D, epicatechin, curcumin and ginsenosides improve neuroprotection and immune signaling.
- Disabled macroautophagy: curcumin, berberine, retinoic acid and others restore autophagic flux *via* mTOR/AMPK pathways.
- Disturbances in the gut microbiome or dysbiosis: probiotics, prebiotics, fermented foods and polyphenols modulate gut microbiota, enhancing metabolic and immune health.
- Chronic inflammation or inflammaging: resveratrol, epigallocatechin gallate, baicalin, berberine and γ-tocotrienol reduce inflammatory

cytokines and NF-κB (nuclear factor kappa-light-chain-enhancer of activated B cells) activity.

In the following paragraphs, will be discussed in detail three nutraceuticals compounds, namely quercetin, glucosinolates and cocoa bean extract, the possible pro-longevity effects of which have been evaluated in this thesis.

Quercetin

Quercetin (3,3',4',5,7-pentahydroxyflavanone) (QUER) is one of the widely occurring secondary metabolites, found abundantly in nature in plants [17] and represents a common constituent of the daily human diet.

Table 1. *Natural sources of QUER.*

Food Source	QUER content (mg/100 g)
Allium cepa Patrick (onion)	383,0
Euphorbia helioscopia	357,0
Capparis spinosa (caper bush)	180,7
Allium fistulosum (Welsh onion)	149,8
Euphorbia wallichii	146,0
Calamus scipronum (semambu)	118,8
Capsicum annuum (red chili)	80,0
Diplotaxis tenuifolia (perennial wall-rocket)	66,1
Anethum graveolens (dill)	55,1
Foeniculum vulgare (fennel)	48,8
Mangifera indica Ubá (mango)	46,9
Juniperus communis (common juniper)	46,6

Morus alba (mulberry)	35,9
Allium cepa (onion)	34,7
Prunus armeniaca (apricot)	32,2
Allium cepa red (onion)	30,7
Moringa oleifera (sohanjana)	28,1
Sambucus canadensis (american elderberry)	26,7
Eschscholzia californica (golden poppy)	26,3
Ficus religiosa (peepal)	25,6
Allium cepa (onion)	22,1
Brassica oleracea (cauliflower)	21,9
Abelmoschus esculentus (okra)	21,0
Ipomoea batatas (sweet potato)	18,9
Moringa oleifera (drumstick tree)	16,6
Sonchus oleraceus (sowthistle)	16,0
Vaccinium uliginosum (bog bilberry)	15,8
Fagopyrum esculentum (buckwheat)	15,4
Vaccinium macrocarpon (cranberry)	14,8
Asparagus officinalis (sparrow grass)	14,0
Lycium barbarum (wolfberry)	13,6
Prunus domestica (plum)	12,4
Vaccinium oxycoccos (cranberry)	12,1
Artemisia dracunculus (tarragon)	11,0
Brassica oleracea (kale)	11,0
Vitis vinifera (wine grape)	10,4
Aloe barbadensis (Aloe vera)	9,5
Rubus arcticus (Arctic bramble)	9,1
Aronia mitschurinii (Viking chokeberry)	8,9
Brassica juncea (mustard greens)	8,8
Eruca sativa (arugula)	7,9
Brassica oleracea (leaf cabbage)	7,7
Vaccinium caesariense (blueberry)	7,7
Lactuca sativa (red lettuce)	7,6
Beta vulgaris (Swiss chard)	7,5
Origanum vulgare (oregano)	7,3
Malus pumila (apple)	6,7
Cichorium intybus (green chicory)	6,5
Ficus carica (fig)	5,4
Coriandrum sativum (coriander)	5,3
Curcuma longa (turmeric)	4,9
Opuntia spp. (prickly pear)	4,9
Malpighia emarginata (acerola)	4,7

Malus domestica (apple)	4,4
Ribes nigrum Öjebyn (black currant)	4,4
Phaseolus vulgaris (French bean)	3,9
Brassica oleracea (broccoli)	3,0
Prunus avium Hartland (sweet cherry)	2,8
Prunus cerasus Schattenmorelle (sour cherry)	2,5
Helichrysum chionophyllum	1,5
Solanum lycopersicum Manisa C-33 (tomato)	0,9
Helichrysum compactum	0,6
Camellia sinensis (green tea)	ND
Ginkgo biloba (ginkgo)	ND
Hypericum perforatum (hypericum)	ND
Sophora Japonica (Japanese pagoda tree)	ND

References [17-19]. ND : not defined.

In 2010, the U.S. Food and Drug Administration (FDA) classified high-purity QUER as “Generally Recognized as Safe” (GRAS) [20], with an established safe daily intake of up to 1 g.

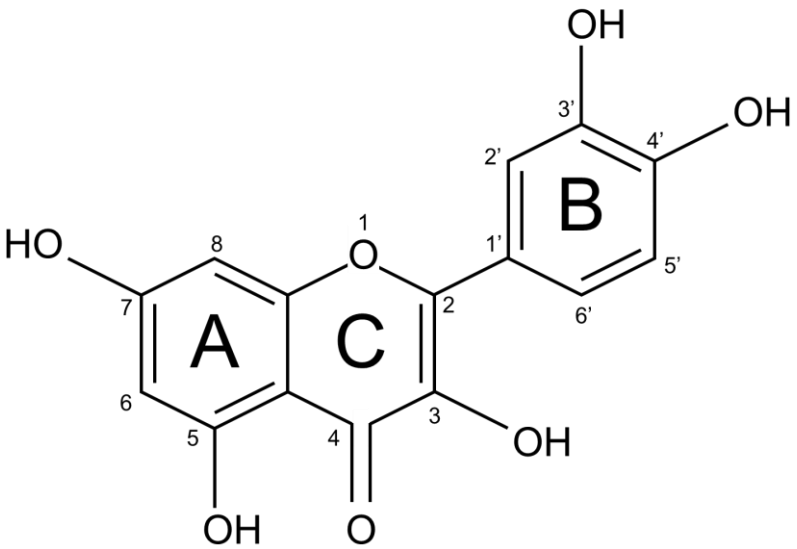

Figure 2. *Chemical structure of QUER*

QUER was first isolated and identified by Albert Szent-Györgyi in 1936. Its name is derived from the Latin word *quercetum*, meaning “forest of oaks,” reflecting its original source.

Chemically, QUER belongs to the flavonoid class of polyphenolic compounds (Figure 2). The term “flavonoid” originates from the Latin *flavus*, meaning “yellow”, which corresponds to QUER appearance as a bright lemon-yellow crystalline powder [19].

Flavonoids share a common diphenylpropane backbone (C6–C3–C6), consisting of two aromatic rings (A and B) connected by a three-carbon bridge that typically forms a heterocyclic C-ring. In QUER, this C-ring is a closed pyran structure [21]. The molecule contains five hydroxyl groups, which are critical for its biological activity [21,22]. Structurally, QUER is defined as 2-(3,4-dihydroxyphenyl)-3,5,7-trihydroxy-4H-chromen-4-one, with a molecular weight of 302.24 g/mol and a melting point of 316 °C [19]. It is practically insoluble in cold water and only sparingly soluble in hot water (0.06 mg/mL), but it dissolves readily in ethanol (2 mg/mL), lipids and organic solvents such as dimethyl sulfoxide (30 mg/mL) [23].

In plants, QUER is synthesized as part of the defense response to environmental stress [24]. It is derived from the amino acid phenylalanine *via* the phenylpropanoid pathway [25-27]. The biosynthetic route begins with the deamination of phenylalanine to cinnamic acid, followed by hydroxylation to

form p-coumaric acid, which is then activated to coumaroyl-CoA. Chalcone synthase catalyzes the condensation of three molecules of malonyl-CoA with one molecule of coumaroyl-CoA to form chalconaringenin (2′,4,4′,6′-tetrahydroxychalcone). Then chalcone isomerase facilitates the cyclization of the C-ring to yield naringenin (4′,5,7-trihydroxyflavanone). Subsequent hydroxylation by flavanone 3-hydroxylase produces dihydrokaempferol, which is further hydroxylated by flavonoid 3′-hydroxylase to form dihydroquercetin. Finally, flavonol synthase catalyzes the dehydrogenation of dihydroquercetin to yield QUER.

In nature, QUER is predominantly found in glycosylated forms, with sugar moieties such as glucose, rhamnose, or rutinose typically attached at the C-3 position *via* flavonoid glycosyltransferases. The aglycone form is relatively rare [28]. The most common glycoside is rutin, the QUER–rutinose conjugate.

QUER is among the most extensively studied flavonoids [17] both using model organisms as the nematode *Caenorhabditis elegans* and mammalian cell cultures, mice and humans [29]. Studies on mammalian cell cultures and animals indicate that QUER, as a potent free radical scavenger, neutralizes ROS, reactive nitrogen species (RNS) and carbon species (RCS). Its antioxidant capacity is primarily attributed to the catechol structure on the B-ring. Additional structural features contributing to its activity include the C-ring's

unsaturation and the presence of a 4-oxo group, which, along with the 5-hydroxyl group, enables metal ion chelation (e.g., Cu^{2+}, Fe^{2+}). The five hydroxyl groups of QUER exhibit varying reactivity in the order: 3 > 7 > 3′ > 4′ ≫ 5. These phenolic hydroxyls act as electron donors, with the catechol moiety being particularly effective in radical scavenging [20]. QUER also upregulates antioxidant enzymes such as superoxide dismutase (SOD), catalase (CAT) and glutathione (GSH) and activates the nuclear erythroid 2–related factor 2 (Nrf2), thereby promoting endogenous antioxidant defense mechanisms. It may also bind DNA, protecting it from oxidative damage [19].

Despite pharmacokinetics studies indicates that oral bioavailability of QUER is relatively low (0.17–7 μg/mL) with less than 10% of the ingested dose absorbed [29], its metabolites exhibit a slow elimination, with a half-life ranging from 11 to 48 hours, allowing for potential accumulation in plasma upon repeated intake [29].

Enzymatic activity from host and gut microbiota can also hydrolyze QUER glycosides in the aglycone form, being lipophilic, facilitating absorption across epithelial membranes *via* passive diffusion. Additionally, glycosides may be absorbed *via* active transport involving sodium-dependent glucose transporter 1 (SGLT1), and lactase-phlorizin hydrolase (LPH) can cleave sugar moieties, enhancing aglycone uptake. Once absorbed, QUER enters the hepatic portal circulation and is distributed systemically. In the intestine,

QUER undergoes extensive biotransformation into methylated, sulfated and glucuronidated metabolites, which are more bioavailable and detectable in plasma and urine. Plasma concentrations of QUER can remain elevated for up to 48 hours post-ingestion, reflecting its prolonged half-life [30].

Furthermore, various QUER delivery systems have been recently developed, including liposomes, solid lipid nanoparticles (SLNs), nanostructured lipid carriers (NLCs), polymeric and inorganic nanoparticles, extracellular vesicles, hydrogels, microgels and cyclodextrin complexes [31,32]. For instance, Qi Y. et al. [33] developed plasma exosomes loaded with QUER (Exo-QUER) and their results showed an improved brain targeting of QUER as well as significantly enhanced bioavailability of this flavonol. Furthermore, compared with free QUER, Exo-QUER better relieved the symptoms of Alzheimer Disease (AD) in mice, suggesting its therapeutic potential for better treatment of AD.

Beyond this single example, nowadays, QUER is clearly recognized for its broad therapeutic potential, including cardioprotective, neuroprotective, antimicrobial, antiviral, hepatoprotective, antidiabetic, anti-arthritic, anticancer, anti-inflammatory, anti-obesity, anti-allergic and anti-asthmatic properties. These attributes suggest a promising role in aging prevention and lifespan extension [17-19,32].

Glucosinolates

Glucosinolates (GSLs) are nitrogen- and sulfur-containing glycosides [34], synthesized as secondary metabolites by numerous plant species within the order Brassicales, which encompasses approximately thirty families [35]. Among these, members of the Brassicaceae family, such as field mustard, cauliflower, kale, garden cress, cabbage and broccoli, accumulate GSLs at high concentrations, contributing to their characteristic aroma, pungent flavor and distinctive taste [36]. Structurally, GSLs possess a conserved core comprising a β-thioglucose moiety linked *via* a sulfur atom to a (Z)-N-hydroximinosulfate ester [37], along with a variable side chain derived from amino acids (R), Methionine for aliphatic GSLs and Phenylalanine or Tryptophan for others [38] (Figure 3).

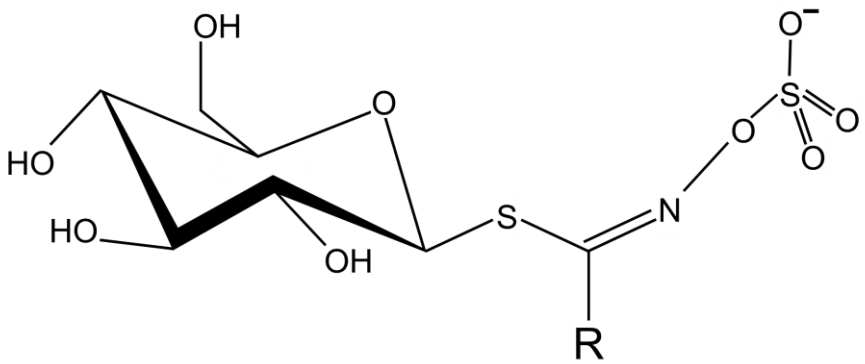

Figure 3. *Chemical structure of GSLs core*

Classification of GSLs is typically based on the nature of their amino acid precursors and the modifications of the side chain, resulting in three major

groups: aliphatic, aromatic, and indolic GSLs [37,39]. To date, over 130 distinct GSLs have been identified [39].

The composition and concentration of GSLs in plants vary significantly across species and even within cultivars, influenced by environmental conditions, agronomic practices, developmental stage, tissue type and plant health *status* [40].

GSLs play pivotal roles in plant defense, functioning both as endogenous chemical mediators against biotic and abiotic stresses [39] and as bioactive compounds with biocidal and biofumigant properties [41–44]. Upon tissue damage, GSLs are hydrolyzed by endogenous myrosinases (thioglucoside glucohydrolases, EC 3.2.1.147), which cleave the glucose moiety from the core structure. The resulting aglycone is unstable and undergoes spontaneous rearrangement to yield isothiocyanates and other degradation products, the nature of which depends on factors such as the R-group structure [39,45]. These hydrolysis products contribute to plant resistance and are also exploited in agriculture for their biofumigant activity [44].

Beyond their roles in plant physiology and agricultural applications, GSLs have garnered increasing attention for their potential health benefits in humans and animals. Numerous studies have demonstrated their anti-inflammatory, antioxidant and anticancer properties [46–50]. Moreover, GSLs have shown promising effects in the prevention and management of chronic age-

related diseases, including diabetes, neurodegenerative disorders, and cardiovascular conditions [51]. These effects have been substantiated through research in eukaryotic model organisms, as well as in animal and human studies [52].

Regarding bioavailability, intact GSLs can reach the colon, where they are metabolized by bacterial enzymes, generating a broader spectrum of metabolites [53]. Some *in vivo* studies indicate that a minor fraction of native GSLs may be absorbed in the small intestine, with up to 5% of the ingested dose detected in urine [54]. *Ex vivo* experiments using isolated rodent intestinal loops suggest this uptake may occur *via* passive or facilitated transport mechanisms [55].

Camelina (*Camelina sativa* (L.) Crantz) (Figure 4), commonly known as gold-of-pleasure, false flax, or linseed dodder, is an ancient minor oilseed crop belonging to the Brassicaceae family [56-58].

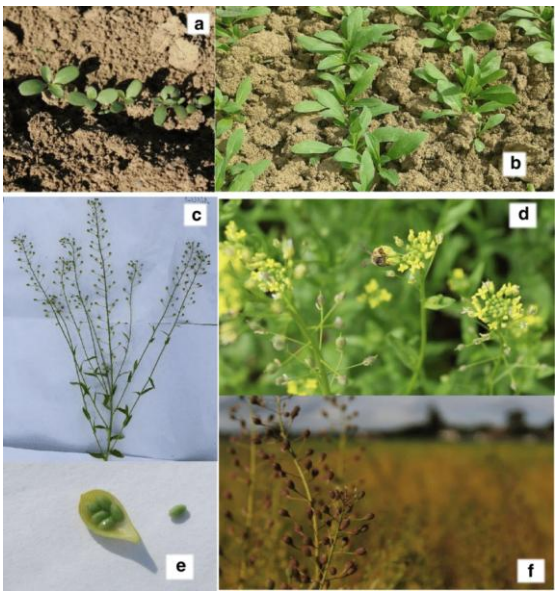

Figure 4. *Details of the Camelina plant.* (**a**) First pair of true leaves in emerged Camelina plants. (**b**) Camelina plants at the rosette stage. (**c**) Camelina branches. (**d**) Camelina inflorescences. (**e**) Pearshaped Camelina silicles. (**f**) Camelina silicles near maturity. Reproduced from [59]

Camelina seeds are notable for their accumulation of two aliphatic GSLs: glucoarabin (9-(methylsulfinyl)nonylglucosinolate; GSL9) and glucocamelinin (10-(methylsulfinyl)decylglucosinolate; GSL10), along with trace amounts of 11-(methylsulfinyl)undecylglucosinolate (GSL11) [60] (Figure 5).

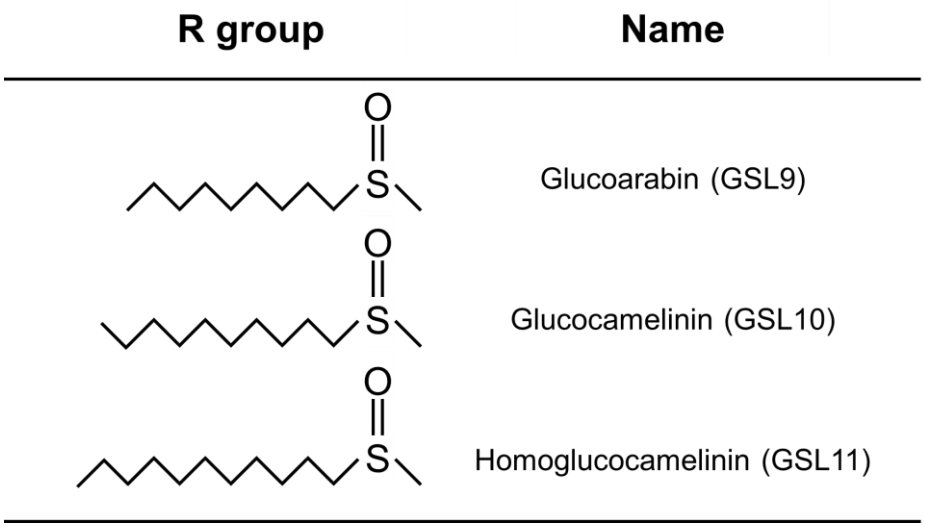

Figure 5. *Chemical structure of variable side chain (R group) of Camelina GSLs*

Native to Eastern Europe and Western Asia, Camelina is now cultivated primarily in the United States, Canada and Europe. It exhibits strong adaptability to diverse climatic and soil conditions and demonstrates high resistance to pests and diseases. Camelina is considered a low-input crop, requiring minimal water, fertilizers and pesticides [60–64]. Its favourable agronomic traits, coupled with seeds rich in oil, containing ω-3 and ω-6 fatty acids, proteins and bioactive compounds, make it a promising candidate for applications in industry, health foods and cosmetics [58].

Currently, Camelina is primarily cultivated for oil production, particularly for biolubricants [58] and biodiesel, including aviation fuels, due to its potential to reduce greenhouse gas emissions [65]. Additionally, by-products of oil extraction, such as seed press cake (meal), can be utilized as feed

supplements for livestock and poultry. These by-products also contain valuable bioactive compounds, including GSLs, which may be harnessed in pharmaceutical, cosmetic and food industries. This comprehensive utilization underscores Camelina potential as a model for environmentally and economically sustainable bio-based production systems [66,67].

Cocoa beans (Theobroma cacao L.)

Theobroma cacao L. is a small yet economically significant evergreen tree, typically reaching 4–8 meters in height. It belongs to the Sterculiaceae family and is native to the tropical regions of the Americas [68]. The species was domesticated by Mesoamerican civilizations and introduced to Europe in 1502 [69].

The fruit of *T. cacao* (Figure 6), known as a “pod,” is an elongated berry measuring 10–32 cm in length. Pod morphology, particularly color, which ranges from light green to dark green, yellow/red to deep purple—plays a crucial role in identifying varieties and populations [71]. Each pod contains 30 to 60 cocoa beans, surrounded by a sweet, mucilaginous pulp. The beans vary in shape and size, typically exhibiting a flattened form approximately 25 mm long and 8 mm thick.

Figure 6. *Theobroma cacao L. fruit.* (**a**) Diversity in fruit morphology of *Theobroma cacao L.* at CATIE, Costa Rica (some related wild types, *Herrania* spp., included), (**b**) ICGT, Trinidad. (Photo is credited to Terry Sampson) Reproduced from [70]

To be transformed into chocolate, one of the most widely consumed products globally, cocoa seeds must undergo fermentation, drying and roasting [72]. While primarily consumed for their flavor, raw cocoa and its derivatives have demonstrated beneficial effects on human health and cosmetic applications [71,73-75]. Since 1996, at least 38 human studies have investigated cocoa in various forms, revealing a multitude of biological properties. However, the high variability in cocoa processing and the composition of bioactive compounds complicates the translation of these findings into consistent clinical benefits [71].

Cocoa beans are rich in macronutrients: fiber (25–40%), lipids (10–25%), proteins (15–20%) and carbohydrates (~15%), along with micronutrients (<2%) including phosphorus, calcium, potassium, sodium, magnesium, zinc and copper [76,77]. Phenolic compounds account for approximately 12–18% of the dry weight of roasted beans. Epicatechin is the predominant polyphenol, comprising about 35% of the total polyphenol content, although its concentration decreases significantly during fermentation and drying, depending on the production location. In contrast, catechin levels tend to increase during these processes [68]. In addition to flavan-3-ols such as catechin and epicatechin, and their dimers (procyanidin B1 and B2), cocoa contains a wide variety of other polyphenols. These include procyanidins (e.g., B3: catechin-(4→8)-catechin; B4: catechin-(4→8)-epicatechin; B5: epicatechin-(4→6)-epicatechin; C1: epicatechin-(4→8)-epicatechin-(4→8)-epicatechin; D: a tetramer of epicatechin) and oligomers/polymers with 2–18 epicatechin units. Other flavonoids include flavonols (e.g., QUER and its glycosides: isoquercetin, hyperoside, quercetin-3-O-arabinoside), flavones (e.g., apigenin and its glycosides: vitexin, isovitexin, luteolin, luteolin-7-O-glucoside) and additional compounds such as dihydroquercetin, dihydrokaempferol, kaempferol-rutinoside, naringenin and its glucoside, and myricetin-glucoside [68]. Furthermore, cocoa contains methylxanthines such as caffeine and theobromine [78-82], as well as other phenolic acids including chlorogenic, coumaric,

ferulic, phenylacetic, phloretic, protocatechuic, syringic and vanillic acids, along with clovamide and dideoxyclovamide [83-86].

In the oral cavity, flavanols interact with proline-rich proteins, contributing to an astringent taste [87]. These compounds remain stable in the stomach, where acidic conditions promote hydrolysis of some oligomers into monomers and dimers, enhancing absorption in the small intestine. In the stomach, flavanols are absorbed in conjugated forms and undergo methylation and glucuronidation. Dimers and trimers are absorbed at low efficiency (<0.5%), while monomers (epicatechin and catechin) are absorbed at rates of 22–55%. In particular, epicatechin metabolites are capable of crossing the blood–brain barrier. Some glycosides are hydrolyzed by enzymes such as lactase-phlorizin hydrolase and cytosolic β-glucosidase.

In the liver, absorbed procyanidins are transported *via* the portal vein and undergo methylation, glucuronidation and sulfation, enhancing their antioxidant potential. These metabolites can circulate systemically within hours. In the colon, microbial metabolism produces additional bioactive compounds. The presence of low molecular weight metabolites in urine and feces suggests that polymeric procyanidins are degraded by gut microbiota prior to absorption. Although some studies suggest limited microbial degradation, *in vitro* experiments show that human fecal microflora can degrade these polymers within 48 hours [68].

Both *in vitro* and *in vivo* studies [68,71,88] have associated cocoa intake with a wide range of pro-healthy effects. Cocoa polyphenols neutralize free radicals and reduce oxidative stress. Cocoa flavonoids modulate inflammatory pathways and may inhibit angiogenesis and tumor growth; they also improve endothelial function and nitric oxide production, potentially reducing blood pressure, platelet aggregation and atherosclerosis risk; they enhance cerebral blood flow and neuroprotection and may improve insulin sensitivity and reduce inflammatory markers in diabetic models. Theobromine and phenylethylamine may improve mood and cognitive performance. Cocoa fibers and polyphenols act as prebiotics, promoting beneficial bacteria (e.g., *Lactobacillus*, *Bifidobacterium*), while theobromine may suppress harmful bacteria such as *E.coli* and *Clostridium* spp. Cocoa may also enhance intestinal barrier integrity and reduce inflammation. Finally, cocoa may modulate lipid metabolism, inhibit adipogenesis and influence gut microbiota, contributing to anti-obesity effects.

Global cocoa bean production during the 2015/2016 harvest season was estimated at approximately 3.97 million tons, with the shell, the by-product waste of this process, comprising up to 20% of the bean mass [78,89]. This equates to roughly 600,000 tons of biomass, most of which is discarded or used in low-value applications such as boiler fuel, animal feed, or fertilizer [78]. Recent studies suggest that cocoa shells, due to their abundance and

cost-effectiveness, hold significant potential as sustainable sources for therapeutic agents [90-92]. Additionally, new insights into the toxicological safety of two cocoa shell matrices have opened opportunities for their use in functional foods and nutraceuticals [82].

The yeast S.cerevisiae as a model system for aging research

Due to the evolutionary conservation of key cellular aging mechanisms, the budding yeast *S.cerevisiae* has become a widely utilized system for studying both cellular and organismal aging [93-95]. Commonly known as baker's or brewer's yeast, the species name *cerevisiae* derives from the traditional Gallic beer, called "cervoise" [96]. *S.cerevisiae* is a unicellular eukaryote that, under optimal growth conditions, divides approximately every 90 minutes through an asymmetric budding process, producing daughter cells that are smaller than the mother. Unbudded cells typically measure around 5 μm in diameter. *S.cerevisiae* exists in either a haploid (mating type a or α) or diploid state. Under nutrient-rich conditions, haploid cells of opposite mating types can fuse to form diploid cells. Conversely, nutrient limitation induces diploid cells to undergo meiosis and sporulation, yielding four haploid spores, two of each mating type.

Metabolically, *S.cerevisiae* is a facultative anaerobe, capable of switching between fermentative, respiratory, or mixed respiro-fermentative metabolism depending on environmental conditions, such as the type and concentration of carbon sources and the availability of oxygen.

S.cerevisiae was the first eukaryotic organism to have its genome fully sequenced, revealing a significant number of genes conserved with multicellular Eukaryotes, including mammals [97]. This milestone spurred interest in yeast as a model system, particularly given its numerous experimental advantages over mammalian cells. It has simple nutritional requirements and a rapid cell division cycle. Yeast can be genetically engineered to express human genes, and approximately 25–30% of human disease-associated genes have identifiable yeast orthologs [98]. This enables functional studies through gene deletion or overexpression. For instance, yeast models have been instrumental in elucidating the roles of *SOD1* and *YHF1*, ortholog of human genes implicated in amyotrophic lateral sclerosis and Friedreich's ataxia, respectively. Even in cases where no yeast ortholog exists, heterologous expression of human genes in yeast has enabled the modeling of diseases such as Parkinson's (PD), Huntington's (HD) and Alzheimer's (AD) [99-101].

Moreover, the metabolic flexibility of yeast allows the study of pathways relevant to metabolic disorders such as diabetes and dyslipidemia. It also serves as a platform for screening natural and synthetic compounds with

potential therapeutic benefits [102-106]. Yeast has significantly contributed to our understanding of cell growth, division, stress responses and complex disease mechanisms including cancer, mitochondrial dysfunction and apoptosis-related disorders [107].

The first study on yeast aging, published over 60 years ago, demonstrated that yeast cells possess a finite replicative capacity [108]. Remarkably, the mortality curve of yeast populations was found to resemble that of many multicellular organisms, including humans [108]. This observation led to the definition of the Replicative Life Span (RLS), which refers to the number of daughter cells a single mother cell can produce in presence of nutrients before death (Figure 7). RLS has since become a valuable model for studying aging of mitotically active cells, such as fibroblasts and leukocytes. Under optimal conditions, yeast cells grow exponentially and divide asymmetrically once they reach a critical size. Typically, mother cells undergo 25–35 divisions before entering replicative senescence. RLS is traditionally measured by manually separating daughter cells from mother cells on solid media using micromanipulation techniques [108], a labor-intensive process necessary to prevent overcrowding and maintain accurate age tracking. In recent years, microfluidic platforms have revolutionized this assay by automating the process and enhancing the precision of lifespan measurements [109]. The latter model of yeast aging, known as the Chronological Life Span (CLS), was

introduced in 1980 [110]. CLS is the mean and the maximum length of time a culture of non-dividing cells remains viable in stationary phase [111] (Figure 7). In standard CLS assays, yeast is cultured in synthetic complete medium containing 2% glucose, supplemented with excess nutrients to support auxotrophic strains. Under these conditions, yeast primarily relies on fermentative metabolism [111]. Upon glucose exhaustion, cells undergo a diauxic shift, transitioning to a strictly respiratory metabolism that utilizes ethanol and acetate produced during fermentation. This metabolic reprogramming activates stress response pathways and induces gluconeogenesis, the glyoxylate shunt and the tricarboxylic acid (TCA) cycle, all of which influence survival during the stationary phase [112-115].

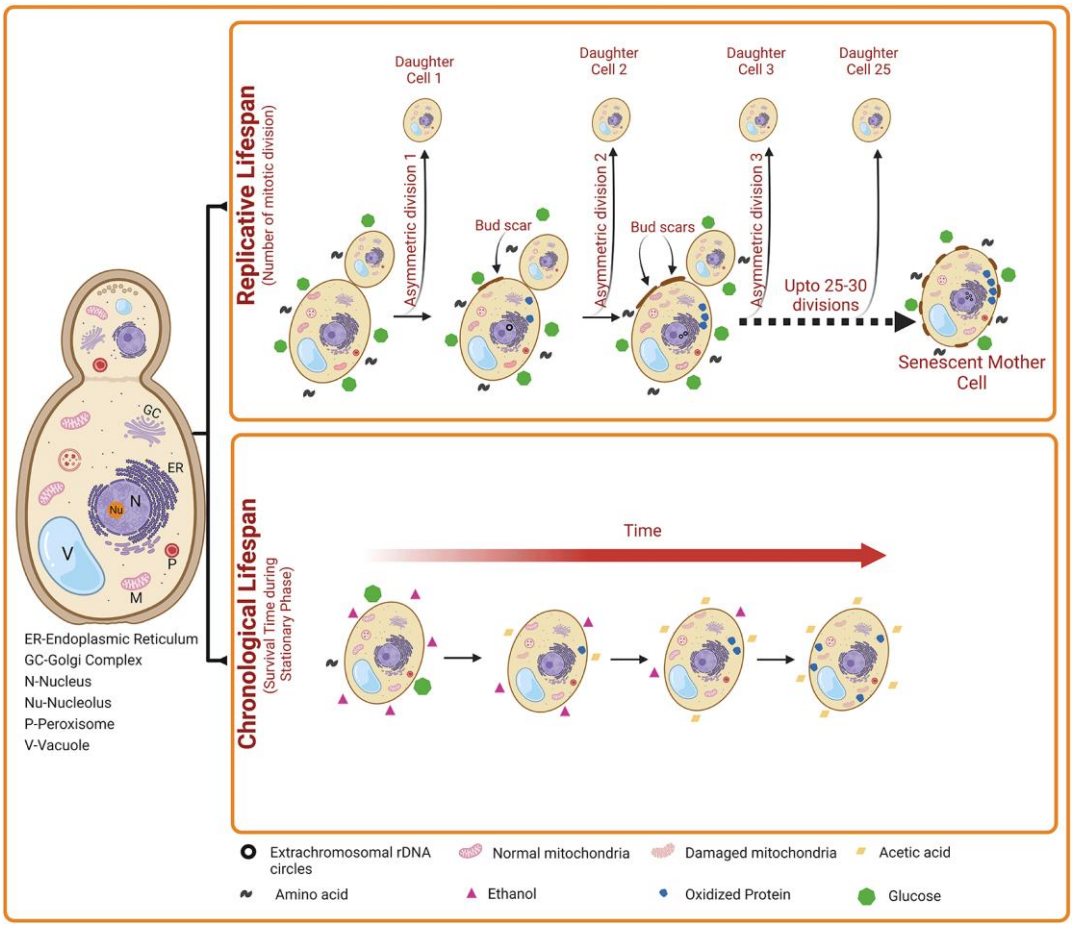

Figure 7. *The two aging patterns of S.cerevisiae*. Reproduced from [116].

CLS is typically assessed starting three days after the diauxic shift by evaluating the ability of quiescent cells to resume growth and form colonies upon plating onto fresh rich medium [111] (Figure 8). The average CLS of wild-type strains varies depending on genetic background, ranging from 6–7 days (e.g., DBY746/SP1) to 15–20 days (e.g., S288C/BY4700).

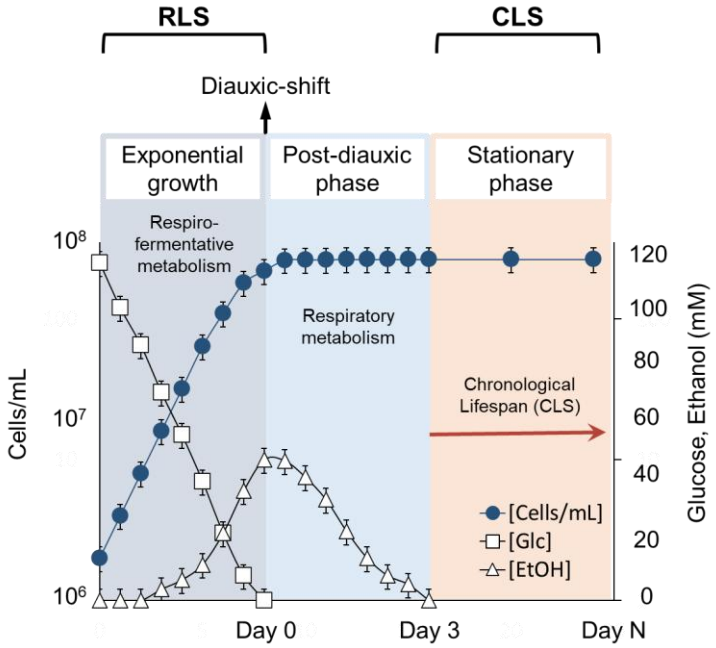

Figure 8. *Growth curve of yeast cells and metabolites production/consumption.* Yeast cells were grown in batches at 30°C in minimal medium (6.7 g/L Difco Yeast Nitrogen Base without amino acids), supplemented with 2% *w/v* glucose. Auxotrophies were compensated with four-fold excess of supplements. At designated time-points glucose and ethanol concentrations in the growth medium were determined

Carbon metabolism in S.cerevisiae

Metabolism encompasses the network of biochemical reactions required for nutrient assimilation, enabling both energy production and the generation of biosynthetic precursors. These reactions are broadly categorized into catabolic and anabolic processes. A central component of cellular metabolism is

carbon metabolism, which includes all pathways involved in the utilization of carbon sources, most notably glucose, the preferred hexose monosaccharide metabolized by yeast.

Hexose sugars, including glucose, are imported into the cell *via* a family of membrane proteins known as hexose transporters (HXT), which mediate facilitated diffusion. At least twenty such transporters are encoded by the genes *HXT1–HXT17*, *GAL2*, *SNF3* and *RGT2* [117]. Among these, *GAL2*, *SNF3* and *RGT2* exhibit distinct functional properties despite sharing high sequence similarity with other HXTs: Gal2 is specific for galactose uptake, while Snf3 and Rgt2 function as glucose sensors, responsive to high and low glucose concentrations, respectively [118]. These transporters share a conserved transmembrane helical domain architecture, whereas their N- and C-terminal cytoplasmic domains display greater variability [117]. The expression of *HXT* genes is tightly regulated by extracellular glucose levels. For instance, *HXT1* is induced under high-glucose conditions and encodes a low-affinity/high-capacity transporter, whereas *HXT2*, characterized by a low K_M, is upregulated during glucose scarcity to maximize uptake efficiency [119].

Once internalized, glucose undergoes phosphorylation and is metabolized *via* the glycolytic pathway (from the Greek “glykis,” meaning sweet), yielding pyruvate, NADH and a net gain of two ATP molecules. Glycolysis consists of a series of enzyme-catalyzed reactions, divided into two phases. The

preparatory (investment) phase involves the consumption of two ATP molecules to phosphorylate glucose intermediates. The subsequent pay-off phase generates two molecules of pyruvate, four ATP and two NADH, resulting in a net production of two ATP per glucose molecule.

Pyruvate, the end product of glycolysis, can follow three principal metabolic fates (Figure 9):

(i) In the cytosol, pyruvate can be converted to acetyl-CoA *via* the pyruvate dehydrogenase (PDH) bypass. This pathway involves three enzymatic steps: pyruvate decarboxylase converts pyruvate to acetaldehyde; acetaldehyde dehydrogenases (Ald) oxidize acetaldehyde to acetate; and acetyl-CoA synthetase (Acs) activates acetate to form cytosolic acetyl-CoA. This acetyl-CoA can then be transported into mitochondria *via* the carnitine acetyltransferase system, if carnitine is present in the medium. Or it can be used to synthesize fatty acids, since in yeast glycolytic cytosolic acetyl-CoA is the sole possible precursor for malonyl-CoA (no citrate lyase). Cytosolic acetyl-CoA is essential for biosynthetic processes, and mutants lacking this pathway are unable to grow on glucose unless acetate is supplemented in the medium [120].

(ii) Pyruvate can also undergo anaplerotic carboxylation to oxaloacetate, replenishing intermediates of the TCA cycle. This reaction is catalyzed by pyruvate carboxylase, encoded by *PYC1* and *PYC2*. Deletion of both genes impairs growth under fermentative conditions with glucose as the sole carbon

source, due to the inability to maintain TCA cycle activity and produce cytosolic oxaloacetate, a precursor for amino acid biosynthesis, particularly aspartate [121]. However, these mutants can grow on non-fermentable carbon sources such as ethanol, where the glyoxylate shunt compensates for oxaloacetate production, bypassing the need for pyruvate carboxylation. Notably, the first two fates of pyruvate, fermentation and carboxylation, are highly regulated by glucose levels and dominate under high-glucose conditions, irrespective of oxygen availability.

(iii) Pyruvate may also be transported into mitochondria for oxidative decarboxylation to acetyl-CoA by the mitochondrial PDH complex. While pyruvate can diffuse across the outer mitochondrial membrane, its passage through the inner membrane requires the mitochondrial pyruvate carrier (MPC), which links cytosolic glycolysis to mitochondrial respiration [112,122]. MPC is a heteromeric complex composed of proteins encoded by *MPC1*, *MPC2* and *MPC3* [122]. *MPC1* expression is constitutive, whereas *MPC2* and *MPC3* are differentially expressed under fermentative and respiratory conditions, respectively [123]. The PDH complex, located in the mitochondrial matrix, comprises three enzymatic components, E1, E2 and E3, each consisting of multiple subunits. This complex serves as the primary link between glycolysis and the TCA cycle and is subject to tight regulation. For example,

transcription of *LPD1*, encoding the E3 subunit, is repressed in the presence of glucose [124].

The acetyl-CoA produced by PDH enters the TCA cycle, whose primary function is to generate reducing equivalents (NADH) for the mitochondrial electron transport chain. This occurs through the oxidative decarboxylation of acetyl-CoA. In addition to its catabolic role, the TCA cycle also fulfils anabolic functions by supplying precursors for amino acid biosynthesis. The NADH generated from glycolysis, pyruvate oxidation and the TCA cycle is funnelled into the mitochondrial respiratory chain, where electrons are transferred to molecular oxygen, the terminal electron acceptor, resulting in water formation and the regeneration of NAD^+.

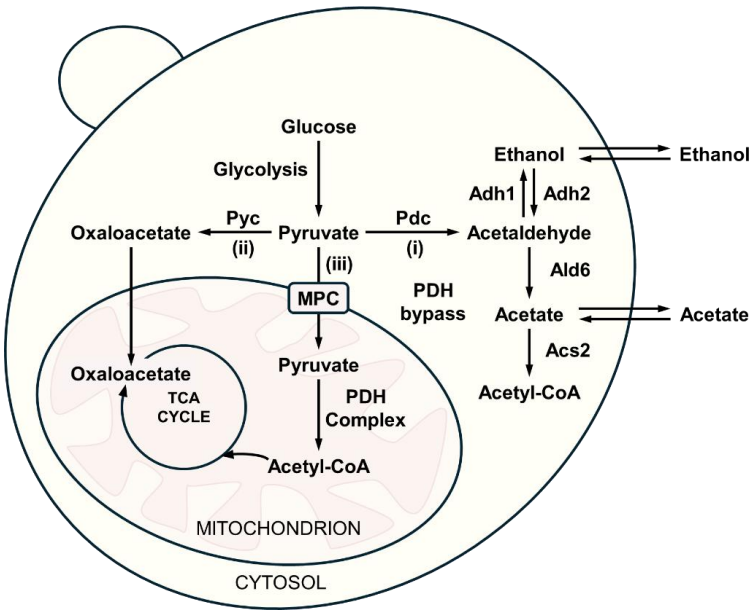

Figure 9. *Key reactions involved in pyruvate metabolism in S.cerevisiae*.

Gluconeogenesis

As previously discussed, the capacity of yeast cells to reprogram their metabolism in response to nutrient scarcity is a key determinant of the duration of the stationary phase and, consequently, CLS. Upon glucose depletion, cells undergo a highly regulated transition from a respiro-fermentative to a respiratory metabolism in which by-products of the fermentation, such us ethanol, acetate and glycerol, become substrates and are consumed [112]. Gluconeogenesis essentially reverses glycolysis in an anabolic direction, enabling the synthesis of glucose-6-phosphate. However, gluconeogenesis includes steps that are distinct from glycolysis.

The first reaction of gluconeogenesis converts oxaloacetate to phosphoenolpyruvate by phosphoenolpyruvate carboxykinase (Pck1). From this point up to the formation of fructose-1,6-bisphosphate, gluconeogenesis proceeds in the reverse direction of glycolysis. The subsequent conversion of fructose-1,6-bisphosphate to fructose-6-phosphate is catalysed by fructose-1,6-bisphosphatase (Fbp1). Both Pck1 and Fbp1 are tightly regulated by glucose availability, with their expression induced only when glucose concentrations in the medium fall below 0.005%. Notably, Pck1 catalyses the rate-limiting step of gluconeogenesis, and its activity is modulated by its acetylation state [113,125].

The acetylation and deacetylation of metabolic enzymes play a pivotal role in cellular adaptation to energy fluctuations and are regulated by acetyl-CoA, a central metabolic intermediate that links metabolism with signaling, chromatin remodeling and transcription [125]. In yeast, the NAD^+-dependent deacetylase Sir2, founding member of the Sirtuin family, is responsible for the deacetylation and subsequent inactivation of Pck1. Pck1 thus represents the first well-characterized example of a metabolic enzyme whose acetylation state directly regulates gluconeogenic flux. Furthermore, Pck1 acetylation is both necessary and sufficient to promote CLS extension under water starvation, a condition known to enhance lifespan in yeast, nematodes, fruit flies and mammals [125,126].

Gluconeogenesis is also critical during chronological aging, as it enables the synthesis of glycogen and trehalose from glucose-6-phosphate. Glycogen accumulates in both the cytoplasm and *via* macroautophagy, within the vacuole [127-129]. In batch cultures, glycogen synthesis begins before glucose is fully exhausted and peaks at the onset of the diauxic shift. During this metabolic transition, glycogen is partially degraded to support the shift to respiratory metabolism and to fuel trehalose synthesis [130]. As cells continue to grow on fermentation byproducts such as ethanol, glycogen is replenished to serve as an energy reserve during prolonged starvation.

Yeast cells also accumulate high levels of trehalose (up to 0.5 M) in response to environmental stresses such as desiccation, heat shock and nutrient starvation [127,131-134]. Trehalose enhances stress resistance through its unique biophysical properties: it preserves membrane fluidity during desiccation or freezing and stabilizes proteins, preventing their aggregation under heat and oxidative stress, functioning as a molecular chaperone [135,136]. During the post-diauxic phase, trehalose accumulates and is gradually degraded as starvation progresses, with degradation accelerating once glycogen stores are depleted [127]. This indicates that trehalose, in addition to its protective role, contributes to energy homeostasis in quiescent cells. Trehalose biosynthesis is catalyzed by Tps1, which transfers a glucosyl group from UDP-glucose to glucose-6-phosphate to form trehalose-6-phosphate (Tre-6P), and Tps2, which hydrolyzes Tre-6P into trehalose and phosphate. These enzymes form a complex with the regulatory proteins Tsl1 and Tps3 [137-141]. Although transcription of *TPS1*, *TPS2*, *TPS3* and *TSL1* is upregulated before or during the diauxic shift [142], trehalose synthesis is primarily governed by allosteric regulation of Tps1, activated by fructose-6-phosphate and inhibited by phosphate, and by substrate availability [143,144]. All four proteins are phosphorylated *in vivo*, but it remains unclear whether phosphorylation directly regulates their function [135]. As cells enter prolonged stationary phase after growth, trehalose levels tend to be maintained, whereas

glycogen stores decrease. It is clear that trehalose is preferentially maintained over glycogen as the quiescent state progresses. On exit from quiescence, when stationary-phase cells are re-exposed to glucose, trehalose plays a dominant role then glycogen [145]. This underlies the fundamental role for trehalose as a fuel reserve that enables yeast cells to survive starvation conditions and then rapidly proliferate upon return to favourable growth ones. Without sufficient trehalose stores, yeast cells would exhibit defects not only in their ability to persist in a quiescent state and to extend their CLS but also into counteract the various stresses which could affect cell longevity [146].

This process is primarily mediated by the cytoplasmic neutral trehalase Nth1, which is believed to be activated by phosphorylation following nutrient reintroduction [147]. However, the specific phosphorylation sites and the kinases involved, likely including protein kinase A (PKA) and/or Sch9 (TORC1-signalling pathway, see next paragraphs), have yet to be definitively identified [135]. Other trehalases, such as Nth2 and the vacuolar enzyme Ath1, appear to play only minor roles in trehalose mobilization during the exit from quiescence [148-150].

In the field of nutraceutical research, Orlandi *et al.* [114,115] demonstrated that supplementation with resveratrol (RSV), a naturally occurring non-flavonoid polyphenolic compound, at the diauxic shift exerts a detrimental effect

on yeast CLS. This negative impact is attributed not only to elevated levels of the superoxide anion, but also to a marked reduction in intracellular trehalose reserves. The decline in trehalose accumulation is closely linked to impaired gluconeogenesis, as evidenced by a significant decrease in the enzymatic activity of Pck1 following RSV supplementation. This reduction in activity corresponds to a decrease in the acetylated, catalytically active form of Pck1, which is subject to deacetylation by the NAD^+-dependent deacetylase Sir2, thereby downregulating gluconeogenic flux. Importantly, the adverse effects of RSV on both CLS and Pck1 activity/acetylation *status* can be reversed by the administration of nicotinamide (NAM), a non-competitive inhibitor of Sir2. NAM, the amide form of vitamin B3 and a precursor of NAD^+, is currently included in various dietary supplements (e.g., BeTotal by Haleon). Within the context of CLS, NAM supplementation at the diauxic shift inhibits Sir2-mediated deacetylation of Pck1, effectively phenocopying the metabolic profile of chronologically aging *sir2*Δ cells. These cells exhibit enhanced gluconeogenic activity and elevated trehalose levels, metabolic traits that are beneficial for long-term survival during chronological aging.

Glyoxylate shunt

In Eukaryotes, the TCA cycle occurs in the mitochondrial matrix and plays a pivotal role in utilizing non-fermentable carbon sources *via* oxidative

generation of reducing equivalents (NADH), driving aerobic respiration to yield ATP. The TCA cycle is also an important source of biosynthetic building blocks, such as α-ketoglutarate, succinyl-CoA and oxaloacetate. When yeast is grown on two-carbon compounds, such as acetate, the TCA cycle by itself cannot supply adequate amounts of biosynthetic precursors unless alternative reactions are available [151]. *S.cerevisiae*, thus, employs a modification of the TCA cycle called the glyoxylate shunt, which converts two-carbon acetate units into four-carbon dicarboxylic acids by bypassing oxidative decarboxylation. The glyoxylate shunt consists of five reactions catalysed by isocitrate lyase (Icl1), malate synthase (Mls1), citrate synthase (Cit2), aconitase (Aco1/2) and malate dehydrogenases (Mdh2/3). The first two enzymes, Icl1 and Mls1, are unique to the glyoxylate shunt and are encoded by *ICL1* and *MLS1*, respectively. Icl1 is localized solely in the cytosol and Mls1 is targeted primarily into the cytosol in cells grown on carbon sources other than fatty acids, such as ethanol, whereas it is mainly peroxisomal in oleic acid-grown cells. Deletion of the *ICL1* gene in standard CLS assays results in a short-lived phenotype and impaired acetate metabolism, underscoring the essential role of this pathway in chronological survival [113].

The glyoxylate shunt shares three of the five reactions with the TCA cycle that are catalysed by Mdh2/3, Aco1/2 and Cit2. Three Mdh genes, *MDH1*, *MDH2* and *MDH3*, encoding mitochondrial, cytosolic and peroxisomal

variants, have been identified in *S.cerevisiae*. The cytosolic isozyme Mdh2, but not the peroxisomal enzyme Mdh3, functions in the glyoxylate shunt, whereas the mitochondrial isoform Mdh1 participates in the TCA cycle. Two isoenzymes Aco1/2 encoded by a single gene, *ACO1*, are distributed between two distinct subcellular compartments, the mitochondria and the cytosol, and participate in the TCA cycle and the glyoxylate shunt, respectively. Three distinct *S.cerevisiae* genes encoding citrate synthases have been identified: *CIT1* and *CIT3* code for the mitochondrial isoforms and *CIT2* for the peroxisomal isoform. While the mitochondrial Cit1 is involved in the TCA cycle, its peroxisomal isoform Cit2 functions in the glyoxylate shunt. Cit3 has been identified as a mitochondrial dual-specific citrate and methylcitrate synthase functional for propionate metabolism, a process by which the propionate is converted to methylmalonyl-CoA and then to succinyl-CoA, which enters the TCA cycle [151].

In the context of chronological aging, the glyoxylate shunt is indispensable, as it enables the anabolic conversion of cytosolic acetyl-CoA into glucose-6-phosphate. Through the condensation of two acetyl-CoA molecules, succinate is produced. This succinate is transported into mitochondria *via* the succinate–fumarate antiporter Sfc1. Within the mitochondria, fumarate is converted to malate by fumarase (Fum1), which is present in both the cytosol

and mitochondria. Malate is subsequently converted to oxaloacetate, which serves as a key substrate for gluconeogenesis [152].

Glycerol metabolism

Glycerol is a naturally occurring organic compound whose structure contains three carbon atoms bonded to three hydroxyl (-OH) groups. It is a ubiquitous molecule in biological systems, forming the structural backbone of phospholipids and triacylglycerols, key components of cellular membranes and major forms of lipid storage, respectively [153]. In *S.cerevisiae*, glycerol plays multiple roles in carbon metabolism. It is produced as a by-product during the fermentation of glucose and its formation, which consumes NADH, is essential for maintaining cytosolic redox balance [154]. The necessity of glycerol production for redox homeostasis is underscored by the observation that mutants deficient in glycerol biosynthesis are unable to grow under anaerobic conditions [155]. Beyond its role in NADH reoxidation, glycerol biosynthesis has also been implicated in providing protection against environmental stresses, particularly hyperosmotic and thermal stress [153]. Under aerobic conditions, it can serve as the sole carbon and energy source [153].

In the context of CLS, Wei M. *et al*. [156] demonstrated that the gene expression profiles of long-lived *tor1*Δ, *sch9*Δ and *ras2*Δ mutants are marked by the upregulation of key genes involved in glycerol biosynthesis. This metabolic

reprogramming toward glycerol production represents a crucial shift in the physiology of these longevity-associated mutants. In these strains, the depletion of pro-aging carbon sources such as glucose and ethanol is increased, favoring glycerol accumulation. This metabolic state closely resembles the effects of calorie restriction (CR), a condition in yeast achieved by reducing the amount of glucose in growth medium, typically from 2% to 0.5% or lower. This nutritional restriction extends both RLS and CLS. Notably, glycerol functions as a "phantom carbon source": it does not suppress the activation of stress-responsive transcription factors Msn2/4 and Gis1. These factors are critical for enhancing stress resistance and modulating longevity, both in long-lived mutants and in cells subjected to CR. Furthermore, since glycerol is actively taken up by cells and contributes modestly to survival under starvation conditions, it likely serves as a nutritional substrate that supports long-term viability [156].

The primary and best-characterized pathway for glycerol biosynthesis in *S.cerevisiae* involves the NADH-dependent reduction of dihydroxyacetone phosphate (DHAP) to glycerol 3-phosphate (G3P) by cytosolic glycerol 3-phosphate dehydrogenase (cG3Pdh activity), followed by dephosphorylation of G3P to glycerol *via* glycerol 3-phosphatase (Gpp activity). This anabolic G3P pathway constitutes the major, if not exclusive, route for glycerol production during osmoregulation and anaerobic redox balancing [157].

In yeast, cG3Pdh activity is encoded by two isogenes, *GPD1* and *GPD2*, while Gpp activity is encoded by *GPP1* and *GPP2*. Under non-stress conditions, *GPP1* is the predominant isoform. Mutants lacking cG3Pdh activity fail to produce glycerol [155], and among the two isoforms, Gpd1 is considered the most physiologically relevant [158-160]. The precursor DHAP can be derived either from glycolysis or from gluconeogenesis when non-fermentable carbon sources are utilized.

In yeast, the catabolic or, so called, dissimilatory pathway for glycerol involves its phosphorylation by glycerol kinase, encoded by *GUT1*, followed by oxidation *via* a FAD-dependent mitochondrial glycerol 3-phosphate dehydrogenase (Gut2), which is localized on the outer surface of the inner mitochondrial membrane [153,157]. This enzyme transfers electrons from $FADH_2$ directly to the mitochondrial respiratory chain, and the resulting DHAP enters the glycolytic/gluconeogenesis pathway.

Glycerol uptake in *S.cerevisiae* is primarily mediated by the membrane protein Stl1, which functions as a glycerol/proton symporter. This transporter facilitates active import of glycerol by coupling its translocation to the inward movement of protons, thereby exploiting the proton gradient across the plasma membrane. The critical role of Stl1 in glycerol assimilation is demonstrated by the complete loss of glycerol uptake and growth in synthetic glycerol media upon deletion of the *STL1* gene. *STL1* expression is transiently

induced under osmotic stress, but its activity declines as the cell shifts to endogenous glycerol production, indicating a tightly regulated adaptation to environmental conditions. Fps1, another protein associated with glycerol transport, belongs to the major intrinsic protein (MIP) family. Although initially proposed to facilitate glycerol uptake, subsequent studies have shown that Fps1 primarily mediates glycerol efflux, particularly under hyperosmotic conditions. The non-essential role of Fps1 in glycerol import is supported by the observation that *FPS1* deletion mutants retain the ability to grow on glycerol. Thus, Fps1 appears to function mainly in the regulation of intracellular glycerol concentrations, especially in response to osmotic stress.

Although glucose depletion is known to trigger regulatory cascades that enable the utilization of alternative respiratory carbon sources [153], specific regulatory mechanisms governing glycerol utilization remain poorly understood. For instance, the transcriptional activator Cat8 has been shown to influence *STL1* derepression during the diauxic shift [161]. Cat8 is essential for growth on non-fermentable carbon sources [162] and activates gene expression by binding to carbon source-responsive elements (CSREs) in target promoters [163,164]. Another key transcription factor is Adr1, which, in cooperation with Ino2 and Ino4, is required for the derepression of *GUT1* [165]. The expression of *GUT2* is regulated by the protein kinase Snf1 and the Hap2-Hap5 complex, which activates transcription of numerous nuclear genes

encoding mitochondrial proteins [166]. Both *GUT1* and *GUT2* are repressed by the negative regulator Opi1 in the presence of glucose [164,165]. Additional regulatory factors such as Rsf1 [167,168] and Rsf2 (also known as Zms1) [169] have been implicated in glycerol metabolism. Deletion of *RSF1* results in dysregulated expression of genes involved in both glycerol biosynthesis and catabolism, reduced transcription of *HAP4* (a component of the Hap2-Hap5 complex), and increased expression of stress response genes [170].

Pathways linking metabolism, nutrient availability and longevity in yeast

The metabolic state and longevity of *S.cerevisiae* are strongly influenced by the availability and type of nutrients. In response to nutritional stimuli, several key metabolic regulators are activated. Among these, the PKA-, TORC1- and SNF1-signaling pathway play a central role.

The PKA-signaling network

The PKA (Protein Kinase A) pathway is recognized as the principal glucose-sensing signaling cascade in yeast, regulating approximately 90% of the

genes involved in the diauxic shift [171]. PKA is a heterotetrameric holoenzyme composed of two catalytic (C) subunits and a regulatory (R) subunit dimer, forming a R_2C_2 complex [172]. The catalytic subunits are encoded by *TPK1*, *TPK2* and *TPK3*, each producing distinct isoforms, while the regulatory subunit is encoded by *BCY1*. The Bcy1 dimer inhibits the catalytic subunits by acting as a pseudosubstrate. Binding of adenosine cyclic monophosphate (cAMP) to Bcy1 subunits alleviates their inhibitory activity and releases the catalytic subunits, each of which phosphorylates distinct, but partially overlapping sets of target proteins [173,174].

Intracellular cAMP levels are tightly regulated by its synthesis *via* adenylate cyclase (Cyr1) and degradation by phosphodiesterases Pde1 and Pde2. Two parallel pathways converge on Cyr1 to integrate nutrient signals. The former involves the GTP-bound forms of Ras1 and Ras2, which directly activate adenylate cyclase. Their GTP-loading *status* is modulated by GTPase-activating proteins Ira1 and Ira2, and guanine nucleotide exchange factors Cdc25 and Sdc25 [175,176]. PKA itself participates in a feedback loop by inhibiting cAMP synthesis and promoting its degradation [135]. The latter pathway involves extracellular nutrient sensing *via* a G-protein-coupled receptor (GPCR) system, comprising the receptor Gpr1, the Gα protein Gpa2, its GAP Rgs2, and the Gβ subunit Asc1 [177,178]. This GPCR module plays a relatively minor role in regulating quiescence [135].

Beyond cAMP regulation, PKA activity is modulated by additional mechanisms. For example, PKA phosphorylates Bcy1 at Ser145, destabilizing it through an unknown process [135]. Bcy1 also undergoes dynamic relocalization from the nucleus to the cytoplasm as cells approach stationary phase, indicating spatial and temporal regulation of PKA activity [179]. PKA promotes cellular growth by stimulating ribosome biogenesis through the regulation of Ribosomal Protein (RP) genes, rDNA genes and Ribosome biogenesis (Ribi) genes, which encode components involved in rRNA processing, ribosome assembly and translation [135]. Among its roles in protein synthesis, PKA favors nuclear localization of the transcription factor Sfp1, which positively influences RP and Ribi gene expression [135]. Also, PKA phosphorylates and inhibits Maf1, a repressor of RNA Polymerase III, thereby enhancing transcription of 5S rDNA and tRNA [180,181].

In addition to promoting growth, PKA suppresses stress responses. One of its key targets is Yak1, a dual-specificity kinase. During the diauxic shift, when PKA activity declines, Yak1 translocates to the nucleus and phosphorylates several stress-related targets, including Bcy1 [182,183], the heat shock transcription factor Hsf1 [183] and the zinc-finger transcription factor Msn2 [184]. Msn2, together with its paralog Msn4, regulates the expression of approximately 200 genes containing stress response elements under various environmental stress conditions, such as glucose limitation [135].

PKA also directly phosphorylates Msn2 at critical residues within its nuclear localization signal (NLS) and possibly within its nuclear export signal (NES), thereby inhibiting nuclear import and potentially promoting export [185-187].

Another key regulator of stress response is Rim15, a member of the PAS kinase family (containing a N-terminal Per-Arnt-Sim domain) that promotes entry into quiescence and is directly inhibited by PKA phosphorylation [188]. Rim15 regulates the expression of nutrient-responsive and oxidative stress genes, trehalose and glycogen accumulation, cell cycle arrest, survival in stationary phase and autophagy. These processes involve Msn2/4 and the transcription factor Gis1, which controls PDS element-regulated genes [135]. Rim15 may also coordinate transcriptional activation with post-transcriptional mRNA protection by phosphorylating Igo1 and Igo2 [189]. These proteins interact with the decapping activator Dhh1 to protect newly transcribed mRNAs from degradation during the transition to quiescence [190].

Finally, PKA inhibits autophagy by phosphorylating the kinase Atg1 and its regulator Atg13, preventing the formation of the Atg1-Atg13 complex at the preautophagosomal structure, which is essential for autophagy initiation [191-193].

Lastly, PKA orchestrates key metabolic transitions as yeast cells approach or enter the diauxic shift phase [135]. It antagonizes the switch from glycolysis to gluconeogenesis and suppresses trehalose and glycogen synthesis

through multiple mechanisms, including activation of glycolytic enzymes 6-phosphofructo-2-kinase Pfk2 and pyruvate kinases Pyk1/2, inhibition of the gluconeogenic fructose 1,6-bisphosphatase Fbp1, as well as, activation of the neutral trehalase Nth1 and glycogen phosphorylase Gph1.

The TORC1-signaling network

Nutrients serve as essential sources of energy and molecular building blocks required for organismal growth. The ability to effectively respond to fluctuations in nutrient availability is critical for maintaining cellular viability. The highly conserved Target of Rapamycin (TOR) proteins are central components of a key signaling pathway that regulates the growth of proliferating yeast in response to nutrient cues [135,194].

TOR was initially identified in *S.cerevisiae* through mutations that conferred resistance to the growth-inhibitory effects of rapamycin, a clinically significant immunosuppressive macrolide produced by *Streptomyces hygroscopicus* and first isolated in 1972 on Easter Island (Rapa Nui) [195]. Shortly thereafter, homologs of TOR were discovered in mammalian cells [194].

TOR assembles into two structurally and functionally distinct complexes: TOR complex 1 (TORC1) and TOR complex 2 (TORC2). Of these, only TORC1 is sensitive to rapamycin when this compound is bound to the peptidyl-prolyl isomerase Fpr1 [also known as FK506-binding protein 12

(FKBP12) in mammals] [196]. The architecture of TORC1 is highly conserved across Eukaryotes [197]. In yeast, TORC1 comprises the catalytic subunit Tor1 or Tor2, the conserved subunits Kog1 and Lst8, and the fungal-exclusive subunit Tco89 [197-199].

TORC1 activity is modulated by the availability and quality of carbon and nitrogen sources, as well as by various stress conditions. Consistent with this, TORC1 is inhibited under carbon or nitrogen starvation, oxidative or osmotic stress, and upon caffeine treatment [200,201].

Two primary upstream regulatory branches of TORC1 involve the highly conserved Rag GTPases and the Pib2-mediated pathway [202]. Specifically, TORC1 is regulated by the Rag GTPases Gtr1 and Gtr2, which form a heterodimer capable of binding and hydrolyzing GTP [203,204]. In the presence of amino acids, Gtr1 is GTP-bound and Gtr2 is GDP-bound, a configuration that promotes TORC1 activation. This conformation facilitates interaction with TORC1 subunits Kog1 and Tco89. Under nitrogen-limiting conditions, Gtr1 hydrolyzes GTP to GDP while Gtr2 becomes GTP-bound, resulting in a conformational shift that diminishes TORC1 interaction and inhibits its activation. Recruitment of the Gtr1-Gtr2 heterodimer and TORC1 to the vacuolar membrane is mediated by the EGO ternary complex (EGO-TC), composed of Ego1/Meh1, Ego2 and Ego3/Slm4. EGO-TC acts as a scaffold to form the

EGO complex (EGOC) in association with the Gtr1-Gtr2 heterodimer [204-208].

The nucleotide-binding states of the Rag GTPases are regulated by Guanine nucleotide Exchange Factors (GEFs) and GTPase-Activating Proteins (GAPs), which respectively promote the active (Gtr1-GTP) and inactive (Gtr1-GDP) states [194]. In yeast, the GAP activity of the SEACIT (SEAC Inhibiting TORC1) subcomplex promotes the inactive Gtr1-GDP state. SEACIT includes Npr2, Npr3 and Iml1/Sea1. Its activity is antagonized by the SEACAT (SEAC Activating TORC1) subcomplex, which comprises Seh1, Sec13, Rtc1/Sea2, Mtc5/Sea3 and Sea4. Together, SEACIT and SEACAT constitute the SEAC complex [204,207,210]. The active Gtr2-GDP state is promoted by the Lst4-Lst7 heterodimer, which also exhibits GAP activity [204,211].

In *S.cerevisiae*, an additional TORC1-activating pathway is mediated by the protein Pib2, which functions independently of the Rag GTPases and does not associate with the EGO-TC [212].

Active TORC1 promotes anabolic processes essential for cell growth while repressing catabolic processes under nutrient-rich conditions. The primary anabolic pathway regulated by TORC1 is protein biosynthesis, which is modulated at multiple levels, including ribosome biogenesis, mRNA stability,

translation initiation and the expression of high-affinity amino acid permeases [213].

The principal downstream effector of TORC1 in yeast is the AGC-family protein kinase Sch9. TORC1-mediated phosphorylation of Sch9 regulates diverse processes such as ribosome biogenesis, translation initiation, protein synthesis, sphingolipid metabolism, cell cycle progression, cell size, stress responses and autophagy [214]. Sch9 localizes to both the cytosol and vacuolar membranes and redistributes to the cytosol under carbon starvation. Full activation of Sch9 requires phosphorylation at multiple residues by various kinases, including TORC1, which targets several sites in its C-terminal region. Conversely, Sch9 is inhibited by Snf1-mediated phosphorylation at Ser^{288} during carbon starvation [215].

As a central signaling hub, Sch9 regulates numerous downstream effectors, including the PKA pathway, with which it shares overlapping targets. Additionally, Sch9 modulates stress responses by influencing the activity of various kinases and transcription factors and plays a role in proteasomal and autophagic degradation. Notably, deletion of Sch9 extends CLS and RLS in yeast cells [214].

Additional downstream targets of TORC1 include the protein phosphatases PP2A and PP2A-like enzymes, whose activity is modulated *via* the regulatory

protein Tap42. This regulation influences amino acid metabolism, stress responses and autophagy [216].

Active TORC1 also phosphorylates the transcription factor Gln3, thereby repressing the transcription of genes required for growth on non-preferred nitrogen sources [214,216,217]. Furthermore, TORC1 negatively regulates macroautophagy by phosphorylating and inhibiting Atg13, a component of the Atg1 kinase complex [216-218]. At signaling endosomes, TORC1 phosphorylates Vps27, a protein involved in multivesicular body sorting, to suppress microautophagy [218,221-223]. Additionally, TORC1 directly inhibits autophagy through phosphorylation of Ypt1 [224].

To promote ribosomal protein synthesis, TORC1 indirectly regulates the phosphorylation of the ribosomal protein Rps6. More recently, TORC1 has been shown to directly phosphorylate and activate another AGC-family protein kinase, Ypk3. Activated Ypk3 phosphorylates Rps6 at Ser^{232} and Ser^{233} both *in vivo* and *in vitro*, in a manner analogous to S6K in mammalian cells [225-227]. In parallel, TORC1 promotes ribosome biogenesis by directly phosphorylating the transcription factor Sfp1, enhancing its nuclear localization and/or its binding to ribosomal protein RP and possibly Ribi gene promoters, thereby stimulating their expression [228-230].

Recently, two novel TORC1 substrates have been identified: Ser3 and its paralog Ser33. These 3-phosphoglycerate dehydrogenases and alpha-

ketoglutarate reductases are directly phosphorylated by TORC1 in a Pib2-dependent manner, providing new evidence for TORC1 direct involvement in the regulation of amino acid biosynthesis [231,232].

The SNF1-signaling network

In *S.cerevisiae*, the SNF1 (Sucrose Non-Fermenting 1) protein kinase complex, a yeast ortholog of the mammalian AMP-activated protein kinase (AMPK), plays a pivotal role in coordinating nutrient availability and environmental stress with cellular processes such as growth, cell cycle progression and stress responses [233]. Upon nutrient depletion or exposure to environmental stressors, SNF1 is rapidly activated [234,235], inducing metabolic and transcriptional [236] reprogramming to facilitate adaptation to restrictive growth conditions [233,237].

SNF1 is essential for growth on alternative carbon sources such as sucrose, maltose or galactose, and non-fermentable substrates like ethanol and glycerol. It is also a key regulator of the metabolic shift from fermentation to oxidative phosphorylation under glucose-limiting conditions.

The SNF1 complex is a heterotrimer composed of an α-catalytic subunit (Snf1), one of three β-subunits (Gal83, Sip1, or Sip2) and a γ-regulatory subunit (Snf4) [237]. Structurally, Snf1 contains an N-terminal kinase domain (KD) and a C-terminal regulatory domain (RD), which includes an

autoinhibitory domain (AID) [238,239]. Interaction between the RD and AID maintains the SNF1 complex in an inactive conformation [240]. Activation requires phosphorylation of threonine 210 (Thr^{210}) within the activation loop (T-loop) of Snf1 [238]. Under high glucose conditions, Snf1 is cytosolic, but upon glucose depletion and activation, it translocates to the nucleus [241].

The β-subunits (Gal83, Sip1, Sip2) serve as scaffolds facilitating the interaction between Snf1 and Snf4 and modulate complex localization and substrate specificity [239]. Snf4 regulates the conformational state of SNF1 and binds adenine nucleotides (AMP, ADP, ATP), contributing to SNF1 activation [237,239,242,243]. Full activation of Snf1 requires phosphorylation at Thr^{210} by one of three upstream kinases, Sak1, Tos3, or Elm1, collectively referred to as SNF1 Activating Kinases (SAKs) [237]. Inactivation is mediated by Protein Phosphatase 1, PP1 (Glc7-Reg1), which dephosphorylates Snf1 at Thr^{210} in glucose-rich conditions [237]. Notably, Glc7-Reg1 activity appears to be glucose-independent [244]. The Glc7-Reg2 complex also contributes to Snf1 dephosphorylation following glucose readdition, particularly after prolonged carbon starvation [235,245]. Additionally, the PP2A-like phosphatase Sit4 exhibits partially overlapping activity with PP1 in regulating SNF1 signaling [246].

During energy stress, Snf1 is phosphorylated at Thr^{210} by SAKs, adopting an open, active conformation. This is further stabilized by ADP binding to Snf4

and its interaction with the AID domain of Snf1. In contrast, under glucose-rich conditions, PP1 (Glc7-Reg1) dephosphorylates Snf1, reverting it to an inactive state, a process enhanced by ATP binding to Snf4 [239,247].

SNF1 regulates the transcription of over 400 genes [233]. One of its primary targets is Mig1, a transcriptional repressor that is phosphorylated by SNF1 under low glucose conditions, leading to its nuclear export [248,249]. Mig1 represses approximately 90 genes activated by SNF1, including *SUC2*, *HXT2/4* and genes encoding TCA cycle enzymes [233].

In response to alkaline stress, SNF1 phosphorylates and inhibits Mig2, a Mig1 homolog [250,251]. Under endoplasmic reticulum (ER) stress, SNF1 activation promotes expression of *ATG39*, facilitating ER-phagy [252]. SNF1 also induces transcription of gluconeogenic genes *via* activation of transcription factors Cat8, Sip4, and Rds2 [164,165,239,253].

Furthermore, SNF1 enhances the expression of genes involved in ethanol and fatty acid metabolism through activation of Adr1 [163,239,254]. It also directly phosphorylates Acc1, an enzyme catalyzing the conversion of acetyl-CoA to malonyl-CoA, bypassing transcriptional regulation [255].

Under low glucose conditions, SNF1 phosphorylates and activates Gln3, which regulates genes required for growth on non-preferred nitrogen sources. SNF1 indirectly modulates PKA activity by phosphorylating Cyr1,

leading to reduced cAMP levels and decreased PKA signaling [234]. To fine-tune the stress response, SNF1 phosphorylates transcriptional activators Msn2 and Msn4 [256]. Additionally, SNF1 positively regulates autophagy by directly phosphorylating and activating Atg1 [128,257].

Scope of the thesis and synopsis

The average age of the population in industrialized countries is steadily rising. However, this demographic shift is not accompanied by a corresponding improvement in quality of life. Age-related diseases, such as diabetes, metabolic disorders, neurodegenerative conditions and cardiovascular illnesses, are becoming increasingly prevalent, with significant social and economic consequences. Currently, considerable efforts are being directed toward identifying and developing dietary supplement-based interventions that could serve as safe and effective strategies to promote healthy aging. In this context, the yeast *S.cerevisiae* is widely recognized as a valuable experimental model for studying aging and age-associated diseases.

The *corpus* (Chapter 1-3) of the thesis illustrates three studies conducted during my doctorate in the context of nutraceutical research, developed on the unifying model of yeast chronological aging, each concerned a different and unrelated potential dietary supplement-based intervention. In particular, on the one hand we considered a molecule that is extremely well known for

its beneficial effects (QUER), while on the other hand we included two extracts that are almost unknown from a nutraceutical perspective. Moreover, we intentionally selected nutraceutical interventions with different levels of formulation complexity, ranging from a pure compound (QUER), to an extract mainly composed of three closely related chemical species (GSL extract), and finally to a highly complex mixture (cocoa extract). It should be emphasized once again that, unlike QUER—which can be extracted from multiple sources—both the GSL and cocoa extracts align with the principles of a circular economy, as they are obtained from specific waste products of other industrial processes.

The selection of these three interventions was also guided by their expected differences in reactivity. As discussed in the previous sections, QUER and GSLs are anticipated to exhibit distinct reactivities due to their different molecular structures. These structural differences imply divergent physicochemical properties and, consequently, different bioavailability and delivery profiles. Furthermore, they are likely to differ substantially in their molecular-level reactivity and in their modulation of cellular pathways. The situation is even more complex in the case of the cocoa extract, where the coexistence of numerous compounds with diverse reactivities must be considered, along with the potential for synergistic enhancement or attenuation of their respective beneficial effects.

Synopsis of the *corpus*:

Chapter 1 is focused on the effects of QUER on yeast CLS. The study demonstrates that QUER supplementation at the diauxic shift significantly extends CLS. This extension is accompanied by reduced oxidative stress and a metabolic shift favoring gluconeogenesis and trehalose accumulation, both of which are associated with enhanced cellular longevity. Mechanistically, the study identifies the sirtuin Sir2 and glycerol metabolism as key mediators of QUER's beneficial effects on yeast aging, highlighting its potential as a dietary supplement for promoting healthy aging.

Chapter 2 describes our study about the anti-aging potential of GSLs extracted from the seed-press cake of *Camelina sativa*. We demonstrate that GSL extract supplementation significantly extends yeast CLS in a dose-dependent manner. The pro-longevity effect of GSLs is attributed to their ability to preserve mitochondrial functionality, promote a more efficient phosphorylating respiration and remodulate carbon metabolism. These effects consist of the maintenance of TCA cycle activity, particularly succinate dehydrogenase (SDH) function, and elevated levels of TCA intermediates such as citrate, succinate, malate and fumarate. GSLs also stimulate the glyoxylate shunt and gluconeogenesis, leading to increased trehalose accumulation. Combined supplementation of GSLs with nicotinamide (the water-soluble active form of Vitamin B3), a known Sir2 inhibitor, results in additive effects on CLS.

Overall, the findings highlight the potential of Camelina-derived GSLs as natural compounds capable of promoting healthy aging through metabolic reprogramming and mitochondrial preservation.

Chapter 3 includes a study which explores the neuroprotective potential of a cocoa bean shell extract (CBSE), a food industry by-product, in mitigating α-synuclein (α-syn) toxicity, a hallmark of Parkinson's disease (PD). Using both yeast and human neuroblastoma cell models overexpressing α-syn, we demonstrate that CBSE significantly reduces protein aggregation and oxidative stress, while enhancing cellular longevity. Overall, the findings support the use of CBSE as a promising nutraceutical candidate with anti-aggregant and antioxidant properties. Its ability to directly interact with α-syn and modulate cellular stress responses highlights its potential for preventing or mitigating neurodegenerative processes associated with protein misfolding.

CHAPTER 1

Sir2 and Glycerol Underlie the Pro-Longevity Effect of Quercetin during Yeast Chronological Aging

by Francesco Abbiati, Stefano Angelo Garagnani, Ivan Orlandi and Marina Vai

https://doi.org/10.3390/ijms241512223

1.1 Introduction

Quercetin (3,3',4',5,7-pentahydroxyflavone) (QUER) is a natural polyphenolic compound belonging to flavonols, a sub-class of flavonoids. Its name comes from the Latin word "quercetum", meaning forest of oaks. However, QUER occurrence, as a secondary metabolite, is widely distributed among plants where it is involved in different physiological processes from seed germination to pollen growth and in providing plant tolerance against some biotic and abiotic stresses [258]. QUER is among the abundant major naturally occurring flavonoids in the human diet via vegetables and fruits. It is found in fruits such as apples, cherries, and berries (blueberries and cranberries) and vegetables such as asparagus, broccoli, peas, green peppers, and onions [259–261]. In particular, onions (red varieties) have a high content of QUER (about 1.31 mg/100 g of fresh weight) [263]. In 2010, the American Food and Drug Administration notified high-purity QUER as "Generally Recognized as Safe" (GRAS) [20]. Currently, QUER is marketed as a dietary supplement with various claims and statements concerning its health benefits [20]. Indeed, the biological beneficial properties of QUER are well documented, encompassing its direct antioxidant activity to that of modulating signal transduction pathways [264]. In this context, QUER displays, among others, anti-inflammatory, immunoprotective, neuroprotective, anticarcinogenic and anti-aging effects [259,260,265]. These health-promoting effects are supported

by studies performed in eukaryotic model systems, as well as in animals and humans [266–268].

The budding yeast *Saccharomyces cerevisiae* is a single-celled eukaryote that, exploited as a model system, has proved to help decipher conserved fundamental processes/pathways of multicellular eukaryotes, despite the large evolutionary distance involved. As far as human aging/longevity is concerned, in this yeast, two complementary aging models allow us to simulate the cellular aging of actively proliferating cells, exemplified by fibroblasts, and that of post-mitotic, albeit metabolically active cells, namely myocytes [94,269,270]. The former is the replicative aging model, the latter the chronological aging one. Chronological lifespan (CLS) is the length of time (mean and maximum) that a culture of non-dividing cells remains viable in the stationary phase: viability is estimated by the ability to resume growth and form a colony upon return to a rich, fresh medium [111]. In a standard CLS experiment, yeast cells are grown in synthetic media with 2% glucose [111]. In this condition, growth predominantly relies on a fermentation-based metabolism that allows a fast depletion of available glucose and concomitantly provides an extracellular accumulation of metabolites, particularly the extensive release of ethanol in the medium. Only when glucose becomes limiting does the diauxic shift occur, and cells undergo a highly regulated transition from a fermentative to a respiratory metabolism in which by-products of the

fermentation become substrates and are consumed. The diauxic shift is the turning point between two distinct metabolic states; it is characterized by structural, functional, and physiological rearrangements that involve a huge rewiring of gene expression resulting, among others, in an increase in the metabolic flux through the TCA cycle, in the onset of the glyoxylate shunt and of gluconeogenesis. The last one switches carbon flux toward reserve carbohydrates [135,271]. This contributes, along with antioxidant defence systems, to establish a proper protective state of quiescence that ensures the long-term survival of non-dividing cells during the stationary phase and resumes growth upon refeeding. The ability of cells to perform such rearrangements through a series of interlocking signaling networks is a fundamental aspect that strongly affects CLS [145,272,273]. TORC1-Sch9 and Ras-PKA pathways are two nutrient-sensing pathways that negatively regulate the transition into quiescence, and their inhibition/inactivation at different levels extends CLS [135,274].

On the contrary, impairing the activity of the glyoxylate/gluconeogenic pathway and the accumulation of reserve carbohydrates (in particular trehalose) reduces CLS [113,125,145]. In this context, the NAD^+-dependent deacetylase Sir2, which is the founding member of Sirtuins, deacetylates phosphoenolpyruvate carboxykinase (Pck1) [125], the activity of which is the main flux-controlling step of gluconeogenesis. Pck1 is active in the acetylated form

[125], and *SIR2* deletion correlates with an increase in the acetylated active Pck1, enhancing gluconeogenesis and trehalose content in concert with CLS extension [113,275]. In chronologically aging *sir2*Δ cells, all this is accompanied by a decrease in oxidative stress [115]. The same outcomes are detected after nicotinamide (NAM) supplementation at the diauxic shift [115]. NAM, which is a form of vitamin B3, is an endogenous non-competitive inhibitor of the deacetylation reaction catalyzed by Sirtuins, including Sir2; it shifts the enzymatic reaction toward the reformation of NAD^+ and acetylated target(s) [276,277]. Concerning NAM-supplemented cells, an increase in the acetylated Pck1 is observed due to the lack of Sir2-targeted deacetylation [115]. Conversely, opposite outcomes are detected after resveratrol (RSV) supplementation at the diauxic shift [114]. RSV, a natural non-flavonoid polyphenolic compound, restricts CLS and increases oxidative stress. In RSV-supplemented cells, a reduction of the acetylated Pck1 is observed in concert with a decrease in gluconeogenesis and trehalose stores [114].

Here, we focused on the effects of QUER supplementation at the diauxic shift. The results indicate that QUER determines CLS extension accompanied by a decrease in oxidative stress in line with its inbuilt characteristics of antioxidants. In addition, we show that QUER deeply influences carbon metabolism allowing cells to acquire features useful for better survival during chronological aging. In particular, QUER improves the assimilation of the C2

by-product of yeast fermentation through Sir2-dependent Pck1 activity and glycerol catabolism resulting in trehalose increase. Furthermore, QUER also extends CLS under extreme Calorie Restriction (CR, chronologically aging cells in water) together with enhancement of intracellular glycerol catabolism and trehalose stores, indicating that critical components of the beneficial effects of QUER on CLS are changes in carbon metabolism.

1.2 Materials and methods

1.2.1 Yeast Strains, Growth Conditions and CLS Determination

All yeast strains used in this work were generated by PCR-based methods in a W303-1A background (*MATa ade2-1 his3-11,15 leu2-3,112 trp1-1 ura3-1 can1-100*) and are listed in Table S1. The accuracy of gene replacements and correct deletions/integrations was verified by PCR with flanking and internal primers. Cells were grown in batches at 30°C in a minimal medium (Difco Yeast Nitrogen Base without amino acids, 6.7 g/L) with the indicated carbon source at 2% (3% for glycerol) and supplements added in excess [112]. Cell number was determined during growth using a Coulter Counter-Particle Count and Size Analyzer [278]. Duplication time (Td) was obtained by linear regression of the cell number increase over time on a semi-logarithmic plot. Survival experiments were performed on cells grown in a minimal

medium with 2% *w/v* glucose and supplements added in excess. Samples were collected at different time points to define the growth profile (exponential phase, diauxic shift (Day 0), post-diauxic phase and stationary phase) of the culture [112]. CLS was measured according to [279] by counting colony-forming units (CFU) starting with 72 h (Day 3, first age-point) after Day 0. The number of CFU on Day 3 was considered the initial survival (100%). QUER (dissolved in DMSO, purchased from Sigma-Aldrich) was added at the final concentration of 300 µM. NAM (Sigma-Aldrich, Darmstadt, Germany) at the final concentration of 5 mM. Survival experiments in water (pH adjusted to 3.2) were performed as described [280]. Every 48 h, 300 µM of QUER was added to the culture after washing. Viability was determined by CFU.

1.2.2 Dosage of Metabolites and Enzymatic Assays

At designated time points, aliquots of the yeast cultures were centrifuged, and both pellets (washed twice) and supernatants were collected and frozen at – 80°C until used. Rapid sampling for intracellular metabolite measurements was performed as described [112]. The glucose, G6P, ethanol, acetic acid and glycerol concentrations were determined using enzymatic assays (K-HKGLU, K-ETOH, K-ACET and K-GCROL kits from Megazyme, Bray,

Ireland). Extraction and determination of intracellular trehalose according to [281]. The K-HKGLU kit was used to quantify the released glucose.

Pck1 and Icl1 activities were assayed as previously reported [112]. FAD-dependent glycerol-3-phosphate dehydrogenase (Gut2) activity was determined according to [282]. Total protein concentration was estimated using the BCATM Protein Assay Kit (Thermo Fisher Scientific,Waltham, MA, USA).

1.2.3 Estimation of Superoxide Levels and Lipid Peroxidation

Dihydroethidium (DHE, Sigma-Aldrich) staining was performed to analyze superoxide anion ($O_2^{\cdot -}$) [283]. Cells were counterstained with propidium iodide to discriminate between live and dead cells. A Nikon Eclipse E600 fluorescence microscope equipped with a Nikon Digital Sight DS Qi1 camera was used. Digital images were acquired and processed using Nikon software NIS-Elements (https://www.microscope.healthcare.nikon.com/products/software/nis-elements). Lipid peroxidation was determined by quantifying MDA using the BIOXYTECH® LPO-586™ Colorimetric Assay Kit (OxisResearch, Portland, OR, USA). The assay is based on the reaction of the chromogenic N-methyl-2-phenylindole with MDA forming a stable chromophore with maximum absorbance at 586 nm.

1.2.4 Immunoprecipitation and Western Analysis

Total protein extract preparation, immunoprecipitation and Western analysis were performed as described [113]. Primary antibodies used were anti-HA (12CA5, Roche, Mannheim, Germany) and anti-acetylated-lysine (Ac-K-103, Cell Signaling, Leiden, The Netherlands). Secondary antibodies were purchased from Amersham. Binding was visualized with the ECL Western Blotting Detection Reagent (Amersham Pharmacia Biotech, Milan, Italy). After ECL detection, films were scanned on a Bio-Rad GS-800 calibrated imaging densitometer and quantified with Scion Image software 4.0.3.2.

1.2.5 HM Silencing Assay

Silencing was examined using an α-factor sensitivity halo assay [284] with some modifications [285]. In brief, drops (5 µL of a 10^6 cell/mL dilution) of exponentially growing cells were pin-spotted onto agar plates (2% glucose/minimal medium and appropriate supplements) containing α-factor (2.5 µM final concentration). Then, 5 µL of 5 mM splitomicin (dissolved in DMSO) was loaded on a sterile filter disk placed in the centre of the agar plates to form a concentration gradient of splitomicin. Similarly, a concentration gradient of QUER was formed by loading 5 µL of 300 µM QUER. Plates were

incubated at 30°C for 2/3 days. Cells were also dropped onto plates without pheromones and scored for growth. Both α-factor and splitomicin were purchased from Sigma-Aldrich.

1.2.6 Statistical Analysis of Data

All values are presented as the mean of three independent experiments ± Standard Deviation (SD). Three technical replicates were analyzed in each independent experiment. Statistical significance was assessed by a one-way ANOVA test. The level of statistical significance was set at a *p* value of ≤0.05.

1.3 Results and discussion

1.3.1 Quercetin Supplementation at the Diauxic Shift Extends CLS and Promotes Trehalose Accumulation

Since previous works reported that QUER treatment to yeast cells exponentially growing on glucose increases CLS [286–289], we set out to evaluate whether a similar positive effect could be observed following its supplementation at the onset of chronological aging, namely at the diauxic shift. At the diauxic shift, cells shift from glucose-driven fermentation to ethanol/acetate-driven respiration, and the outcomes of such a metabolic reconfiguration

influence CLS [145,272,273,290,291]. QUER-supplemented cells displayed an increase of both mean and maximum CLS (Figure 1A and Table S2) as well as of the survival integral (Table S2) defined as the area under the CLS curves and calculated according to [292], compared to unsupplemented cells.

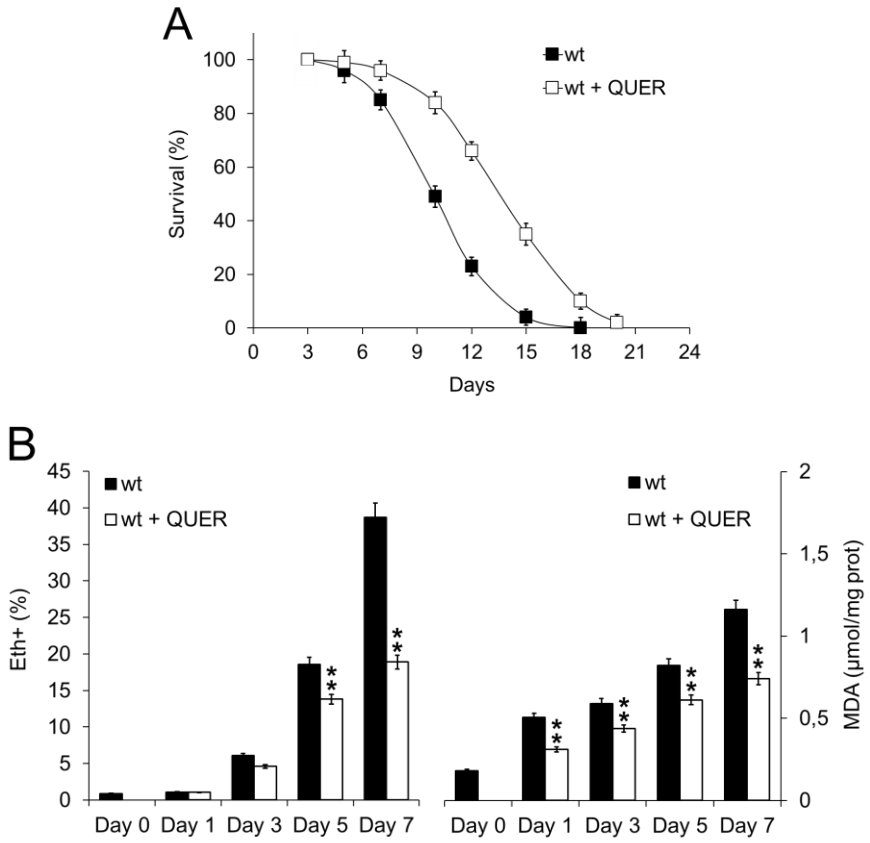

Figure 1. *QUER supplementation at the diauxic shift extends CLS and reduces oxidative stress.* Wildtype (wt) cells were grown in minimal medium/2% glucose and the required supplements in excess (see Materials and Methods). At the diauxic shift (Day 0), quercetin (QUER, 300 µM) was added, and (**A**) survival over time of treated

and untreated cultures was assessed by colony-forming capacity on YEPD plates. 72 h after the diauxic shift (Day 3) was considered the first age point, corresponding to 100% survival. In parallel, for the same cultures (**B**) left: bar charts of the percentage of fluorescent/superoxide positive cells assessed by the superoxide-driven conversion of non-fluorescent dihydroethidium into fluorescent ethidium (Eth) and right: intracellular malondialdehyde (MDA) concentration. All data refer to mean values determined in three independent experiments with three technical replicates each. Standard deviations (SD) are indicated. Statistical significance as assessed by a one-way ANOVA test is indicated (** $p \leq 0.01$).

The CLS extension was accompanied by decreased levels of two oxidative stress biomarkers, such as superoxide anion ($O_2^{\cdot -}$) and malondialdehyde (MDA) (Figure 1B). The former is one of the most potentially harmful ROS, and the latter is a natural end-product of lipid peroxidation: both accumulate as chronological aging progresses, limiting cellular longevity [291,293,294]. The antioxidant activity is a feature shared with other flavonoids and is linked to the chemical structure of this class of molecules, which allows them to scavenge free radicals directly. In addition, the antioxidant property of flavonoids relies on their ability to chelate metal ions, mainly iron ones [295,296]. Iron plays a crucial role in many metabolic processes, and Fe^{2+} participates in the generation of free radicals in the Fenton reaction contributing to oxidative stress. However, in yeast, a decrease in oxidative stress markers (ROS, glutathione oxidation, protein carbonylation and lipid peroxidation) observed after QUER treatment was not associated with iron chelation suggesting that

this beneficial effect of QUER is independent of its intrinsic iron-chelating properties [289].

Starting from the aforementioned results, which align with QUER's antioxidant and anti-aging properties, we decided to analyze the metabolic changes underlying the beneficial effects of QUER supplementation at the diauxic shift. Initially, we measured the enzymatic activity of isocitrate lyase (Icl1), one of the unique enzymes of the glyoxylate shunt, and that of Pck1, the key enzyme of gluconeogenesis.

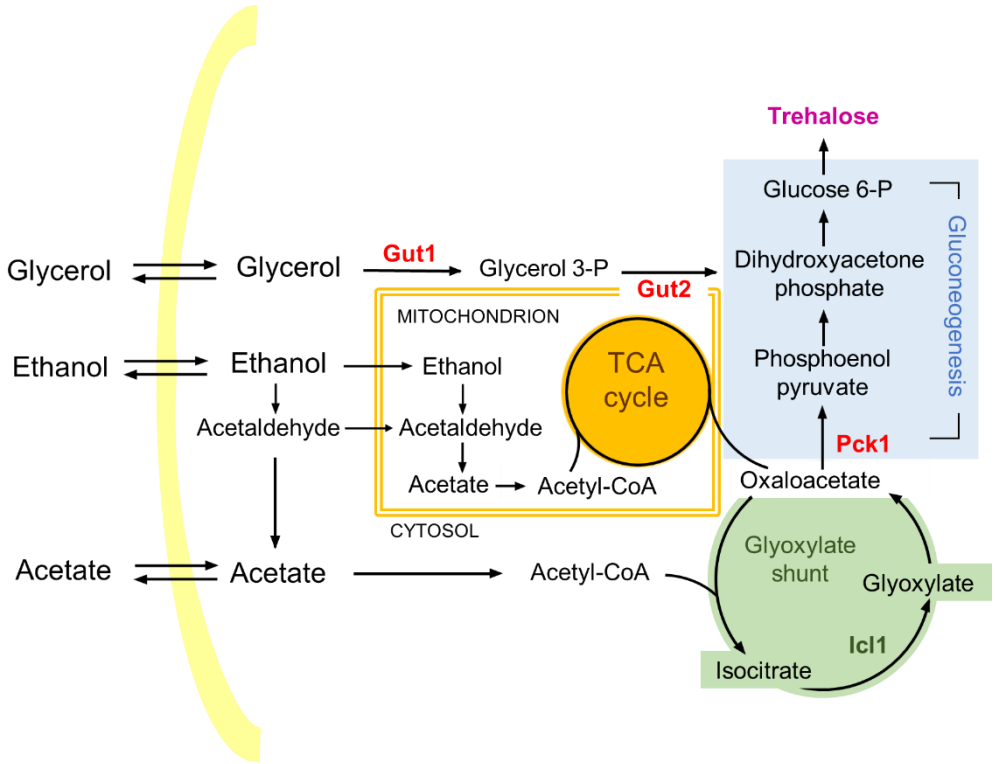

Figure 2. *Scheme of metabolic pathways involved in utilising the main non-fermentable carbon sources during chronological aging.* Three pathways (TCA cycle, glyoxylate shunt and gluconeogenesis) are schematically shown. Gut1, glycerol

kinase; Gut2, mitochondrial glycerol-3-phosphate dehydrogenase; Pck1, phosphoenolpyruvate carboxykinase; Icl1, isocitrate lyase.

The glyoxylate shunt and the gluconeogenesis are anabolic pathways operative during chronological aging and involve using ethanol and acetate (Figure 2). These are C2 compounds, the metabolism of which influences CLS [14,41,42].

In QUER-supplemented cells, the enzymatic activities of Icl1 and Pck1 were higher than those in the unsupplemented ones (Figure 3A), consistent with increased utilization of ethanol and acetate (Figure 3B), indicating an enhancement of glyoxylate/gluconeogenic pathways. Gluconeogenesis allows the production of glucose-6-phosphate (G6P), which is required for trehalose biosynthesis. In QUER-supplemented cells, increased G6P levels and trehalose ones were detected (Figure 3C). Trehalose is a disaccharide stored by chronologically aging cells and is advantageous for their survival [145,146]. In keeping with this finding, gene expression profiles of QUER-treated cells in the exponential phase showed upregulation of genes involved in trehalose biosynthesis associated with an increase in trehalose content and acquisition of oxidative stress resistance [289].

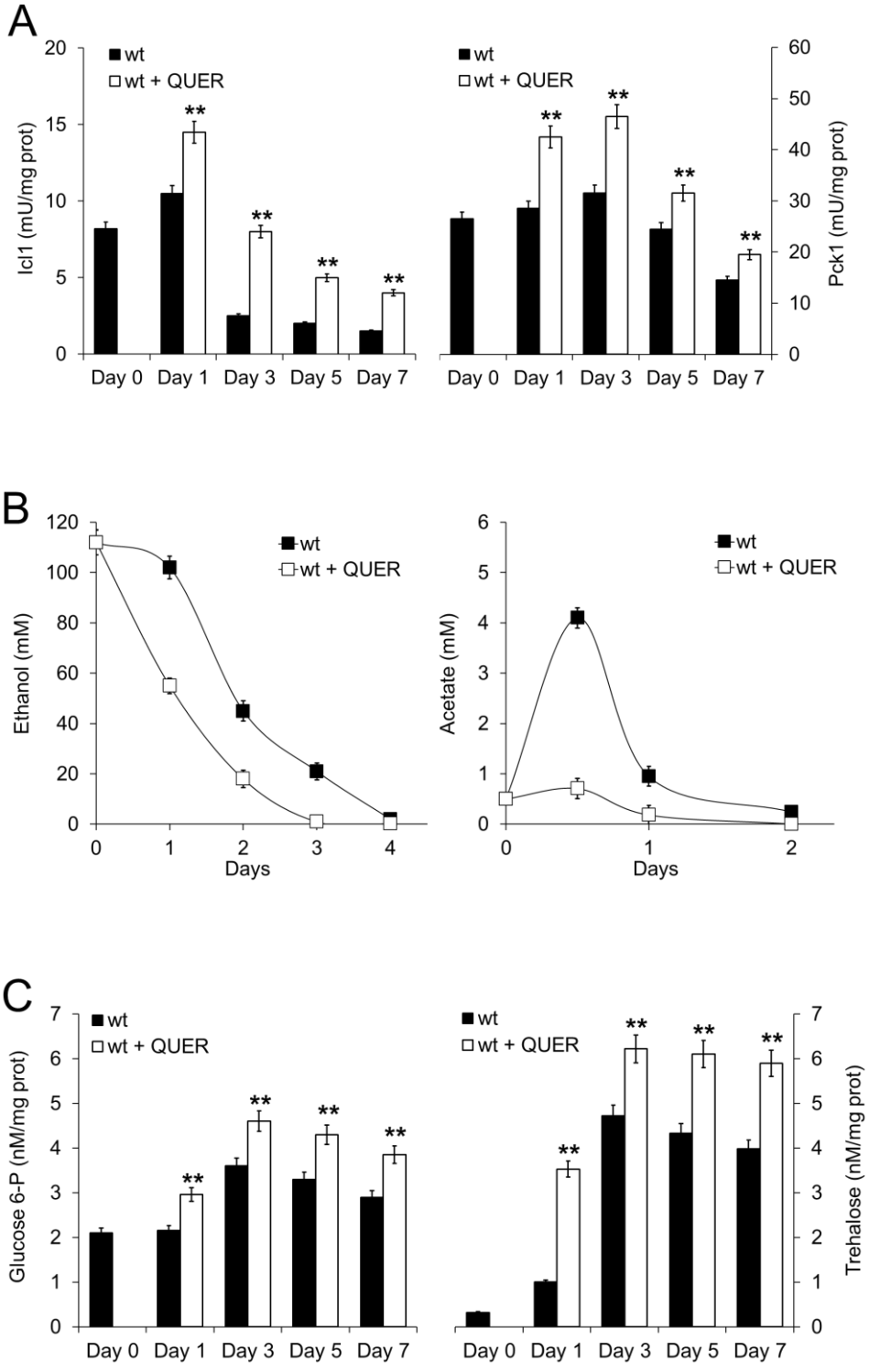
A
wt
wt + QUER
Icl1 (mU/mg prot)
Pck1 (mU/mg prot)
Day 0
Day 1
Day 3
Day 5
Day 7
**
B
Ethanol (mM)
Acetate (mM)
Days
C
Glucose 6-P (nM/mg prot)
Trehalose (nM/mg prot)

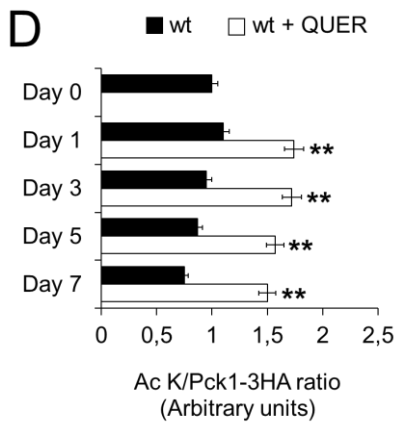

Figure 3. *QUER supplementation at the diauxic shift enhances the glyoxylate/gluconeogenic flux.* At the indicated time points, (**A**) Icl1 and Pck1 enzymatic activities, (**B**) ethanol and acetate levels and (**C**) glucose-6-phosphate (G6P) content along with trehalose one evaluated for both treated and untreated cultures of Figure 1. (**D**) Bar charts of the ratio of Ac-K (acetylated form of Pck1) to Pck1-3HA (total Pck1) values obtained by densitometric quantification of signal intensity of the corresponding bands on Western blots. Wt cells expressing Pck1-3HA were grown and supplied with QUER, as in Figure 1. At different time points, total protein extracts were prepared from treated and untreated cultures and subjected to immunoprecipitation with anti-HA antibodies, followed by Western analysis. Immunodecoration was performed with anti-Ac-K and anti-HA antibodies. All data refer to mean values determined in three independent experiments with three technical replicates each. SD is indicated (** $p \leq 0.01$).

Moreover, as far as Pck1 activity is concerned, its increase in QUER-supplemented cells was associated with an increase in the level of the acetylated active form of the enzyme (Figure 3D). Since Pck1 activity is inhibited by Sir2-mediated deacetylation [114,115,125,275], we wondered whether

QUER could affect Sir2 activity. To this end, an α-factor sensitivity assay was performed.

Sir2 deacetylase activity is essential for gene silencing at *HM loci*, and in a haploid strain, its absence determines a pseudodiploid state [297]. Thus, in the presence of α-factor, *MATa* wild type (wt) cells were arrested in the G1 phase of the cell cycle and did not grow, whilst *sir2*Δ cells grew as they were unresponsive to the pheromone (Figure 4A). Notably, in the presence of QUER, wt cells lost sensitivity to α-factor and grew in the presence of the pheromone. No effect was observed on *sir2*Δ cells (Figure 4A). Similar behaviour was observed for wt cells in the presence of splitomicin, used as a control (Figure 4A). This compound inhibits Sir2 deacetylase activity and creates a conditional phenocopy of a *sir2*Δ mutant [298]. All these data suggest that in the presence of QUER, Sir2 is inhibited, and a pro-longevity anabolic metabolism toward gluconeogenesis and trehalose storage takes place.

To further assess if Sir2 activity is involved in QUER-mediated outcomes, we analyzed the consequences of QUER supplementation at the diauxic shift in the absence of the deacetylase. As previously reported, SIR2 deletion extended CLS (Figure 4B, Table S2) [113-115,298,279] in concert with a reduction of oxidative stress biomarkers (Figure 4C) and increased trehalose levels (Figure 4D) [113-115]. Interestingly, QUER supplementation amplified the CLS extension of the *sir2*Δ mutant (Figure 4B, Table S2), as well as the

decrease of oxidative stress biomarkers (Figure 4C) and the increase of trehalose (Figure 4D). Thus, due to this synergistic effect of QUER supplementation and *SIR2* deletion, it is reasonable to think that Sir2 may only mediate a portion of the effects of QUER and that this compound may also exert its activity on additional targets.

As stated, trehalose production relies upon gluconeogenesis, controlled by Pck1 enzymatic activity. In addition, gluconeogenesis plays a positive role in CLS extension [125,300]. Indeed, the loss of Pck1 strongly decreased both CLS (Figure 4B, Table S2) [113,125] and trehalose content (Figure 4D). Moreover, *SIR2* deletion did not affect either CLS of *pck1*Δ cells (Figure 4B, Table S2) [113,125] or trehalose levels (Figure 4D), indicating that Pck1 is required for the CLS extension and the increase of trehalose stores of chronologically aging *sir2*Δ cells. On the contrary, supplementing QUER to *pck1*Δ cells or *pck1*Δ*sir2*Δ ones resulted in a CLS identical to that of chronologically aging wt cells, although less than that measured for QUER-supplemented wt cells (Figure 4B, Table S2). Notably, the same effect was observed for trehalose content (Figure 4D), indicating that QUER supplementation at the diauxic shift can also promote gluconeogenesis to some extent, regardless of Pck1. Since this enzyme catalyzes the rate-limiting step in gluconeogenesis by converting oxaloacetate to phosphoenolpyruvate (Figure 2), this implies that in the *pck1*Δ mutant, QUER can also fuel gluconeogenesis with other

substrates available during the post-diauxic phase that allow to bypass the requirement of oxaloacetate.

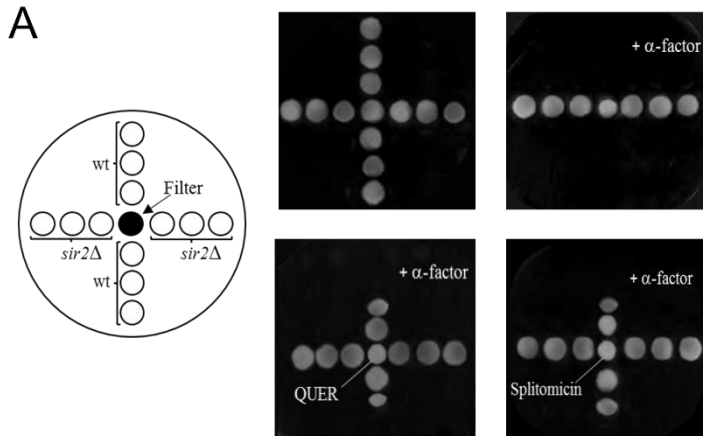

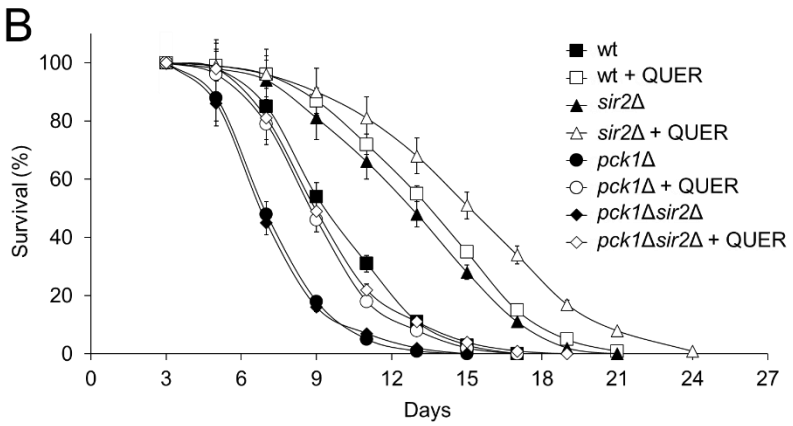

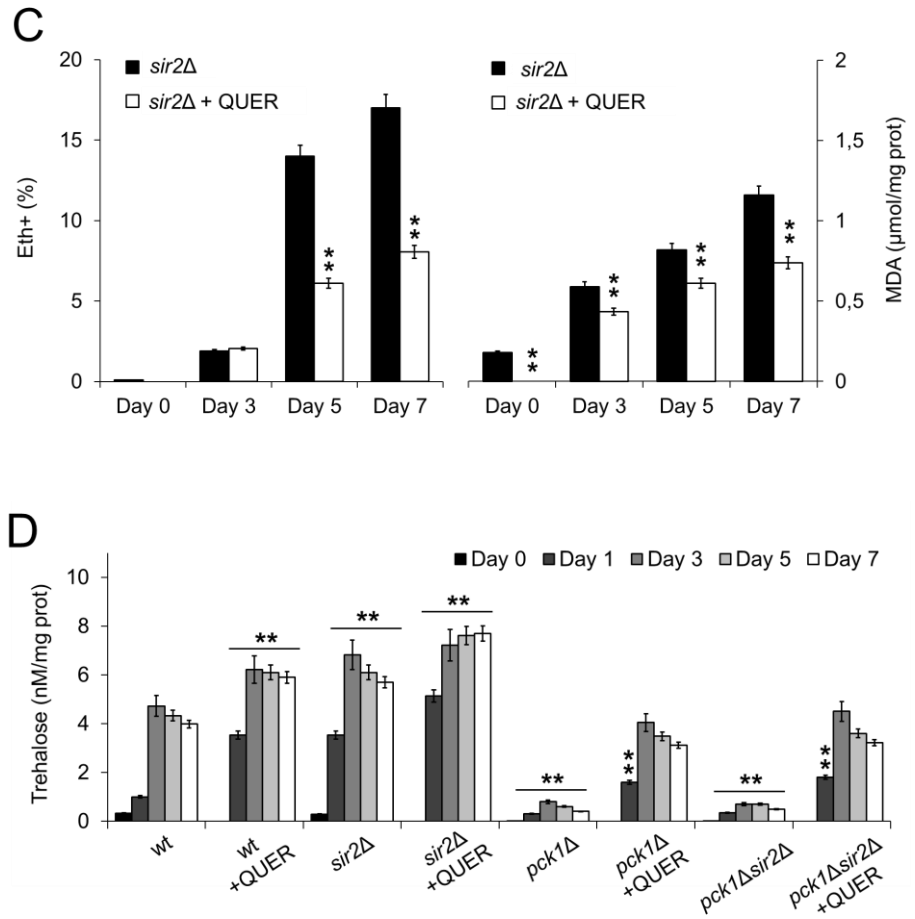

Figure 4. *QUER inhibits Sir2 activity*. (**A**) Wt and *sir2*Δ exponentially growing cells were dropped (5 µL of a 10^6 cells/mL dilution) onto glucose-rich/medium plates (top left), supplemented with 2,5 µM α-factor (top right and bottom left and right). A concentration gradient of QUER was formed by loading 5 µL of 300 µM QUER on a filter disk placed on the agar (bottom left). 5 µL of 5 mM splitomicin was loaded on a filter disk as a control (bottom right). Growth was monitored after three days at 30°C. (**B**) CLS of the indicated strains grown and supplied with QUER as in Figure 1. (**C**) Bar charts of the percentage of intracellular superoxide accumulating cells (Eth) and intracellular malondialdehyde (MDA) concentration. Strains are indicated. (**D**) Intracellular trehalose concentration was evaluated for the indicated cultures. All data refer to mean values determined in three independent experiments with three technical replicates each. SD is shown (** $p \leq 0.01$).

1.3.2 Quercetin Supplementation at the Diauxic Shift Also Enhances Glycerol Catabolism

Glucose-fermenting cells of *S.cerevisiae* produce, in addition to C2 by-products (ethanol and acetate), some glycerol as a by-product for cytosolic redox balancing [301]. Glycerol is transiently accumulated in the culture medium and, after the diauxic shift, is catabolised by the L-glycerol 3-phosphate (L-G3P) pathway [153]. This pathway involves the sequential action of two enzymes: a glycerol kinase encoded by *GUT1* and a L-glycerol-3-phosphate dehydrogenase encoded by *GUT2*. The final product is dihydroxyacetone phosphate that can be channelled into gluconeogenesis, bypassing the step catalyzed by Pck1 (Figure 2). Consequently, in light of the above results, we focused on glycerol catabolism.

In QUER-supplemented chronologically aging wt cells, intracellular (Figure S1) and extracellular glycerol (Figure 5A) were depleted more rapidly than unsupplemented ones. The same behaviour was observed for chronologically aging *pck1*Δ cells. On the contrary, QUER supplementation to the *gut1*Δ culture had no impact on the levels of both intracellular (Figure S1) and extracellular glycerol (Figure 5A). This was also true for the double deletion mutant (*gut1*Δ*pck1*Δ) (Figure 5A). These data are in line with previous reports showing that Pck1 is dispensable when *S.cerevisiae* is growing on a C3 substrate such as glycerol [302,303] and suggest that QUER

supplementation at the diauxic shift enhances glycerol catabolism. Indeed, the glycerol depletion observed for wt cells in the presence of QUER (Figure 5A) was accompanied by a strong increase in the glycerol-3-phosphate dehydrogenase activity (Figure 5B). In *gut1*Δ cells, this enzymatic activity was almost negligible (Figure 5B) due to the lack of the glycerol kinase converting glycerol to glycerol-3-phosphate, which is the substrate of the dehydrogenase (Figure 2).

Concerning ethanol and acetate, since *GUT1* is not required for growth on these C2 compounds [302], in the *gut1*Δ culture, their kinetics of depletion in the medium were like those of the wt culture, and QUER supplementation led to a similar increase (Figure 5C,D). In line with Pck1 role in the utilization of C2 carbon sources, in chronologically aging *pck1*Δ cells and *gut1*Δ*pck1*Δ ones, the depletion of both ethanol and acetate strongly slowed down compared to that of the wt. Furthermore, QUER supplementation had no effect (Figure 5C,D) and this is consistent with the involvement of Pck1 in the increased utilization of ethanol and acetate detected in QUER-supplemented wt cells. In parallel, comparisons of intracellular G6P levels measured in chronologically aging wt cells and in the three mutants clearly showed on the one hand, the different contributions of the L-G3P pathway and the step catalyzed by Pck1 to gluconeogenesis and, on the other, that both routes are required to fuel the gluconeogenic pathway to provide G6P during the post-

diauxic phase (Figures 2 and 5D). In this context, very low G6P levels were detected in the *gut1*Δ*pck1*Δ mutant and were unaffected by QUER supplementation (Figure 5D). On the contrary, supplementing QUER to *pck1*Δ cells, as well as to *gut1*Δ ones, increased the G6P levels, albeit to a lesser degree than those measured for QUER-supplemented wt cells (Figure 5D), correlating well with the notion that QUER impacts on gluconeogenesis at two entry points.

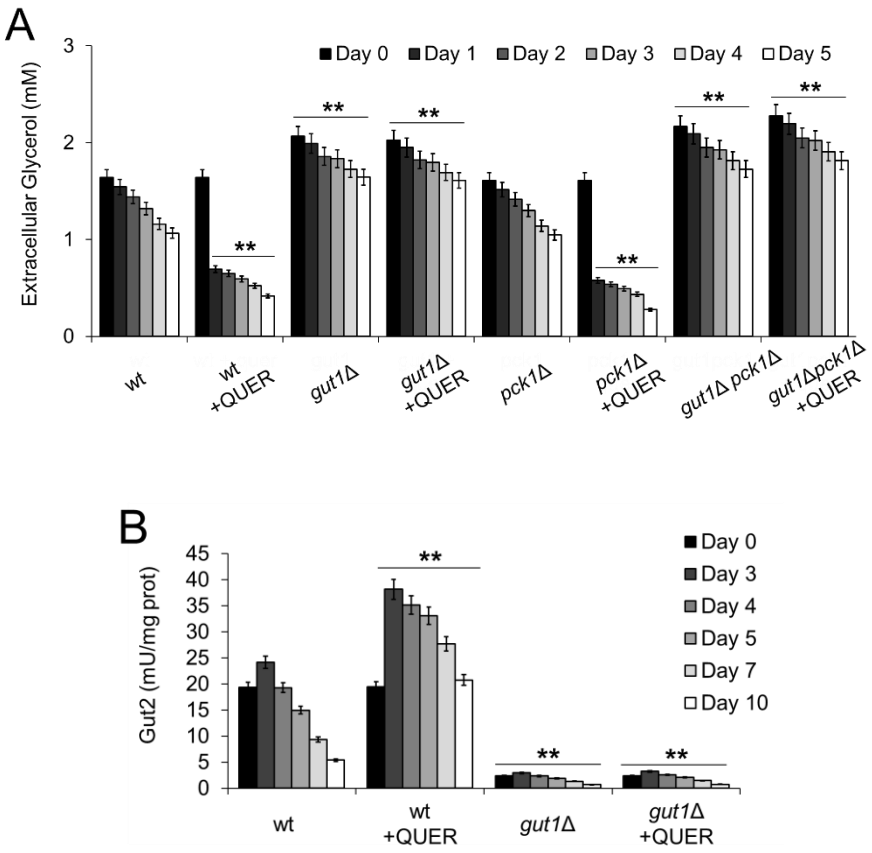

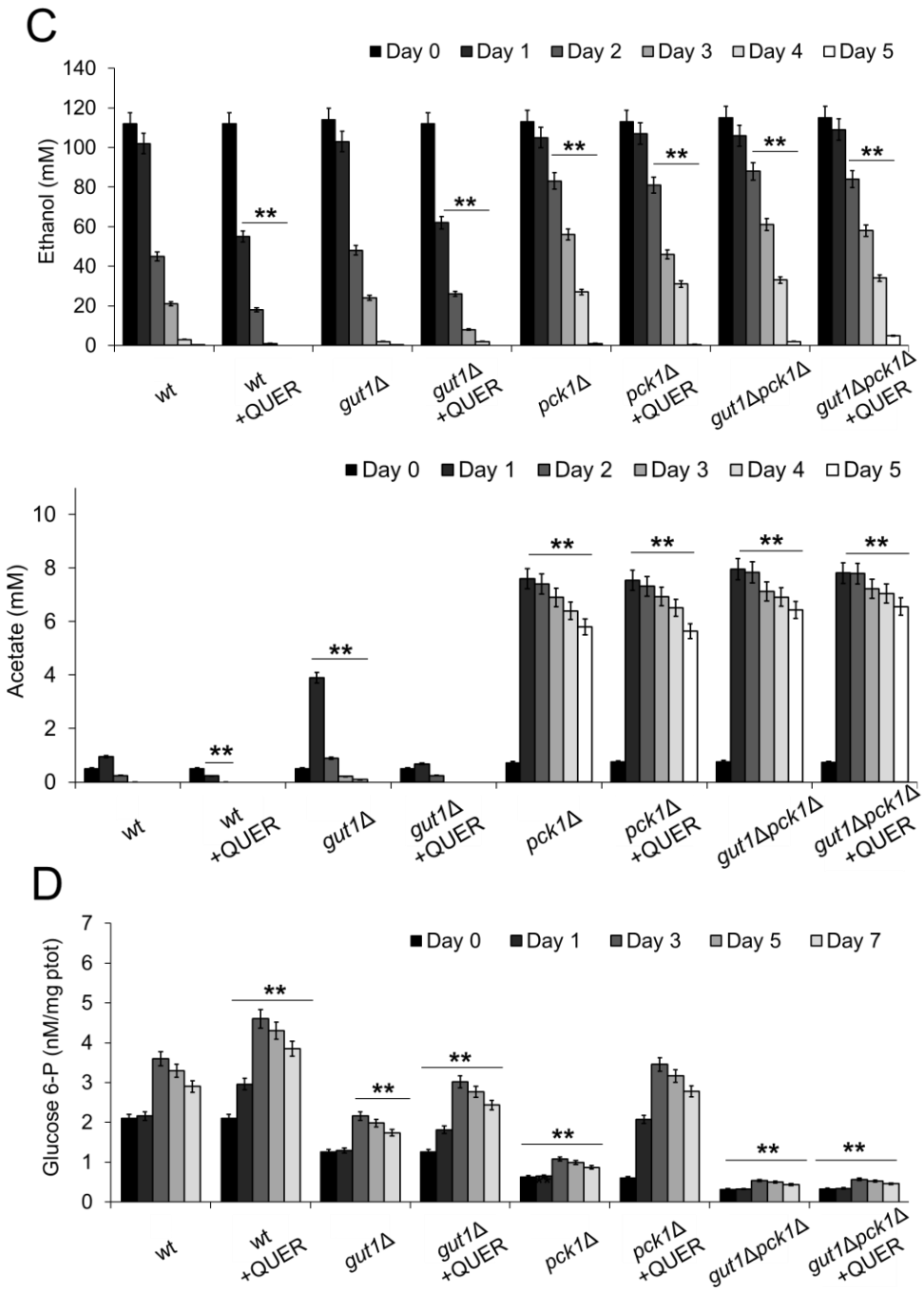

Figure 5. *QUER supplementation at the diauxic shift enhances glycerol catabolism*. Wt, *pck1*Δ, *gut1*Δ and *gut1*Δ*pck1*Δ cells were grown and supplied with QUER as in

Figure 1. At the indicated time points: (**A**) extracellular glycerol levels, (**B**) Gut2 enzymatic activity, (**C**) extracellular ethanol and acetate concentrations and (**D**) glucose-6-phosphate (G6P) content were determined. All data refer to mean values determined in three independent experiments with three technical replicates each. SD is indicated (** $p \leq 0.01$).

We found that NAM, a well-known non-competitive inhibitor of Sir2 activity [276], supplemented at the diauxic shift phenocopies chronologically aging *sir*2Δ cells by inhibiting Sir2-mediated deacetylation of Pck1 [115]. This resulted in an increased CLS (Figure 6A and Table S1) and, among others, increased ethanol/acetate catabolism (Figure 6B) [115]. Thus, NAM was supplied to wt cells at the diauxic shift, and when the NAM stationary culture showed 50% of survival (mean CLS), QUER was added (Figure 6A). In the expired medium, ethanol and acetate were exhausted (Figure 6B), whilst glycerol was still present (Figure 6C). Following QUER supplementation a strong decrease in extracellular glycerol was observed compared to NAM-supplemented cells (Figure 6C), further experimentally reinforcing the finding that QUER enhances glycerol catabolism. Concomitantly, trehalose levels increased (Figure 6D), and CLS was extended (Figure 6A), further supporting the positive correlation between these two parameters.

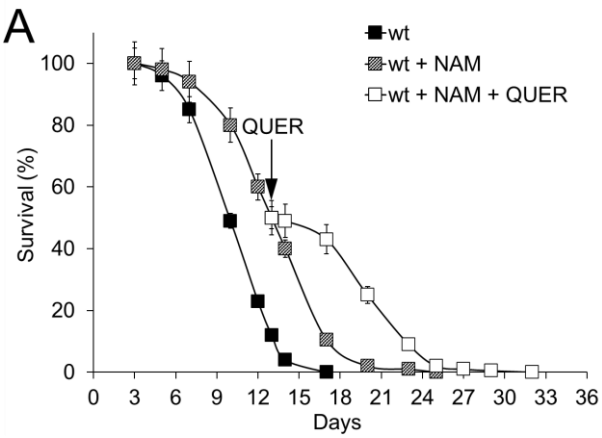
A
wt
wt + NAM
wt + NAM + QUER
QUER
Survival (%)
Days

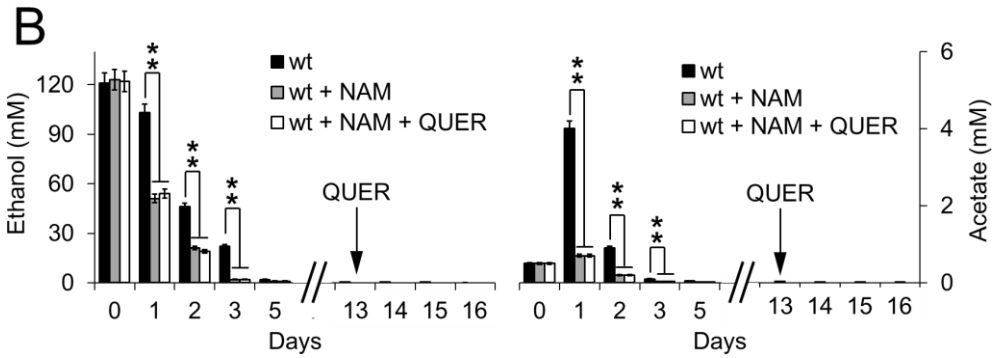
B
wt
wt + NAM
wt + NAM + QUER
QUER
Ethanol (mM)
Acetate (mM)
Days

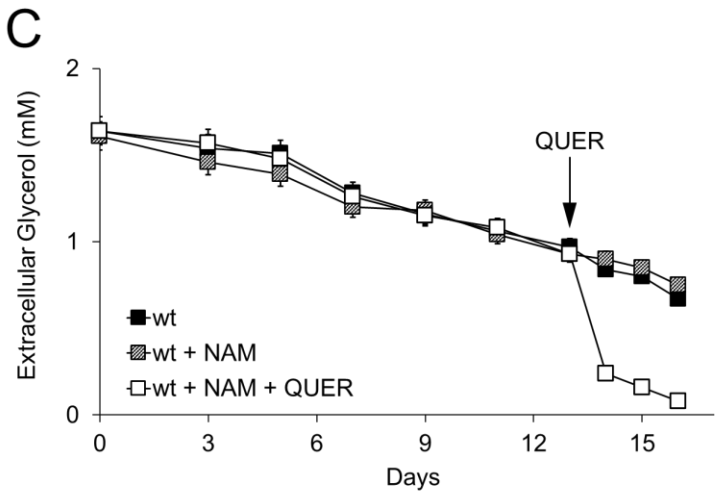
C
QUER
wt
wt + NAM
wt + NAM + QUER
Extracellular Glycerol (mM)
Days

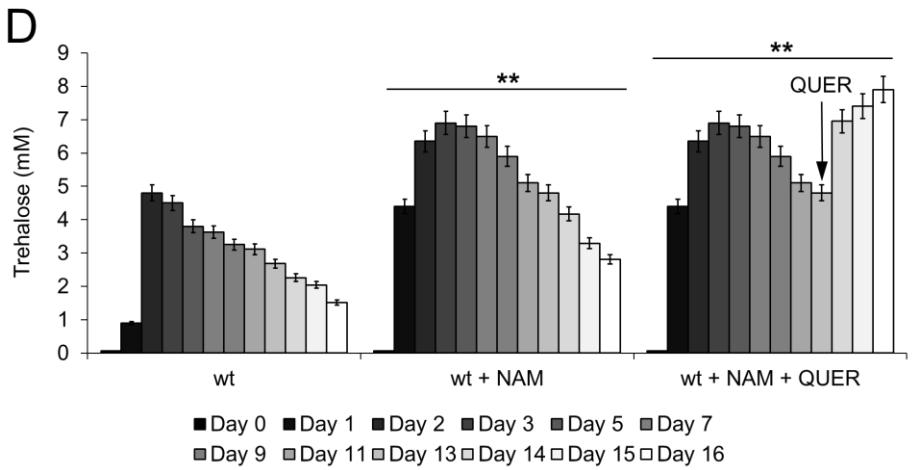

Figure 6. *QUER supplementation during chronological aging further extends the CLS of NAM treated cells*. Wt cells were grown as in Figure 1 and supplied with NAM (5 mM) at the diauxic shift (Day 0). At the time-point where NAM stationary cultures showed 50% of survival (mean CLS), QUER (300 µM) was added. (**A**) The CLS of the indicated cultures is determined in Figure 1. In parallel, (**B**) extracellular ethanol and acetate content, (**C**) extracellular glycerol levels and (**D**) intracellular trehalose concentration were measured. All data refer to mean values determined in three independent experiments with three technical replicates each. SD is indicated (** $p \leq 0.01$).

These data indicate that QUER supplementation at the diauxic shift stimulates the gluconeogenic flux through the L-G3P pathway and Pck1 activity. This leads to improved assimilation of C2 by-products of yeast fermentation and glycerol during the post-diauxic phase and increased reserve carbohydrate trehalose, ensuring long-term survival during chronological aging.

1.3.3. Quercetin Enhances Intracellular Glycerol Catabolism, and Further Extends CLS under Extreme CR

Switching post-diauxic yeast cells from expired medium to water models an extreme condition of CR known to extend CLS remarkably [94,279,304] (Figure 7A and Table S1). In this context, we evaluated the effects of QUER supplementation on wt cells that, after the diauxic shift, were transferred to water, namely in the absence of any extracellular nutrient/carbon/energy source. Supplementing QUER to water amplified the long-lived phenotype of chronological aging cells in water alone (Figure 7A and Table S1). In parallel, measurements of intracellular glycerol and trehalose showed that in the presence of QUER, the utilization of the former increased considerably over time in concert with the increased content of the latter (Figure 7B,C). Hence, QUER brings about trehalose accumulation at the expense of the main compatible solute/osmolyte glycerol, albeit CR-restricted chronological aging cells face an extreme survival-based metabolism. Both trehalose and glycerol are compatible solutes, the accumulation and interplay of which have been shown to occur in yeast during various stress conditions to maximize the probability of cell survival and/or proliferation [305-307]. However, trehalose has more specific roles in protecting proteins and preserving membrane structures, along with being the carbohydrate of choice for surviving

starvation and upon cell cycle reentry from starvation [145,146]. In line with this, its increase is sufficient to improve an “extreme” CLS further.

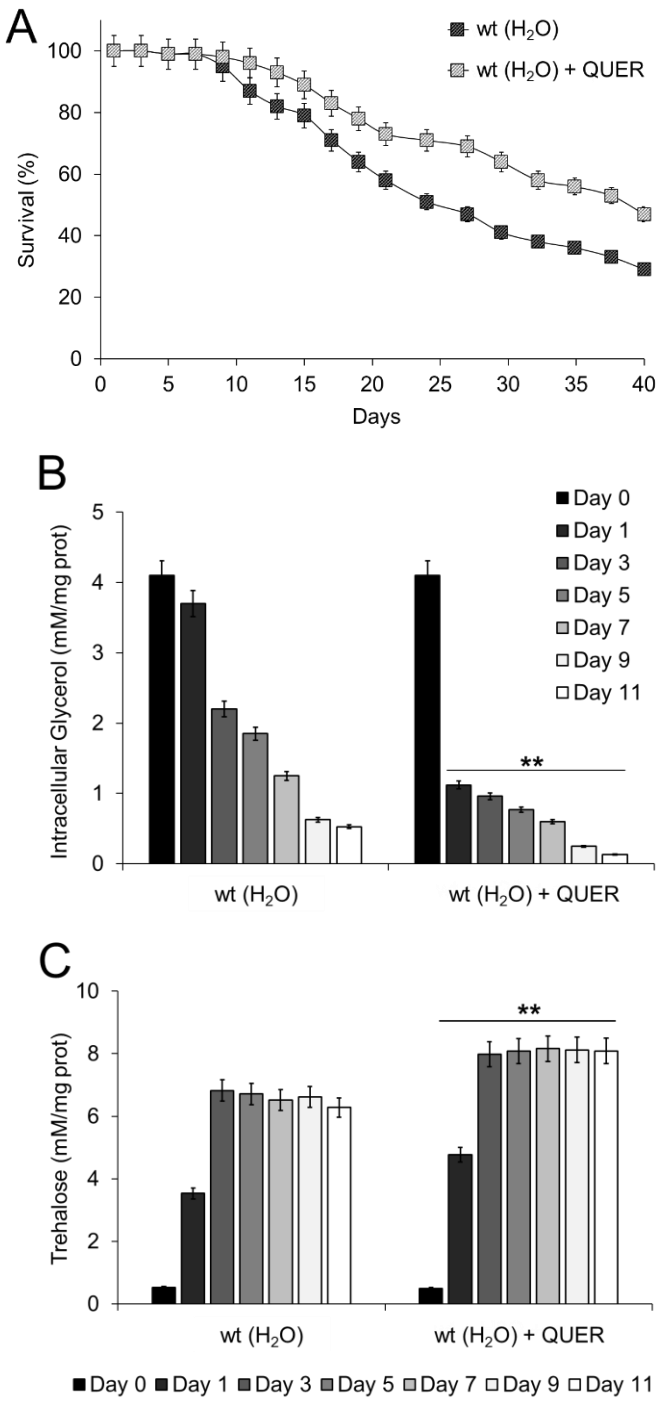

Figure 7. *QUER supplementation further enhances CLS extension under extreme CR*. At the diauxic shift (Day 0) wt cells (grown as in Figure 1) were switched to water (pH adjusted to 3.2) and challenged with QUER (300 μM). Every 48 h cultures were resuspended in fresh water, and each time QUER was added, they were reported. At the indicated time points (**A**) CLS, (**B**) intracellular glycerol and (**C**) trehalose content of cell cultures were determined in parallel after Day 0. All data refer to mean values determined in three independent experiments with three technical replicates each. SD is indicated (** $p \leq 0.01$).

Finally, since glycerol can be utilized by *S.cerevisiae* as a sole carbon/energy source under aerobic conditions, we also analyzed QUER effects on the growth behaviour of wt cells during exponential growth on this C3 compound. A significant decrease in the Td was detected for cells growing on glycerol in the presence of QUER compared to that measured in its absence (Table 1). Similarly, growth on a non-fermentable substrate such as ethanol occurred faster in the presence of QUER, whilst no effect was observed for cells grown on a fermentable substrate such as glucose (Table 1). Taken as a whole, this further indicates that QUER positively affects the catabolism of glycerol and ethanol. This effect is independent of the physiological state of the cells since it takes place in both actively growing cells and chronological aging ones. In these last cells, an enhancement of the anabolic metabolism toward gluconeogenesis and trehalose storage extends the CLS.

Table 1. *QUER promotes respiratory metabolism.*

Medium	Td (h)*
Glycerol	5.44 ± 0.15
Glycerol + QUER	3.35 ± 0.13
Ethanol	4.30 ± 0.15
Ethanol + QUER	3.00 ± 0.16
Glucose	1.40 ± 0.11
Glucose + QUER	1.40 ± 0.13

Duplication time (Td) of wt culture growing on different carbon sources. * Td was calculated as ln2/k, where k is the constant rate of exponential growth. Data represent the average of three independent experiments. Standard deviations are indicated.

1.4 Conclusions

The flavonol QUER is endowed with high antioxidant properties, as proven by many *in vivo* and *in vitro* studies, that provide numerous health-promoting benefits, including anti-aging ones. We found that QUER supplementation at the onset of chronological aging, namely at the diauxic shift, extends yeast CLS. This beneficial effect relies on the influence on carbon metabolism induced by QUER, which leads to improved assimilation of C2 by-products of yeast fermentation and glycerol during the post-diauxic phase. It follows an enhancement of a pro-longevity anabolic metabolism toward gluconeogenesis fuelled at two entry points: the L-G3P pathway and Sir2-dependent Pck1

activity. The outcome is increased reserve carbohydrate trehalose, which ensures long-term survival during chronological aging, thus benefiting cellular longevity.

1.5 Supplementary materials

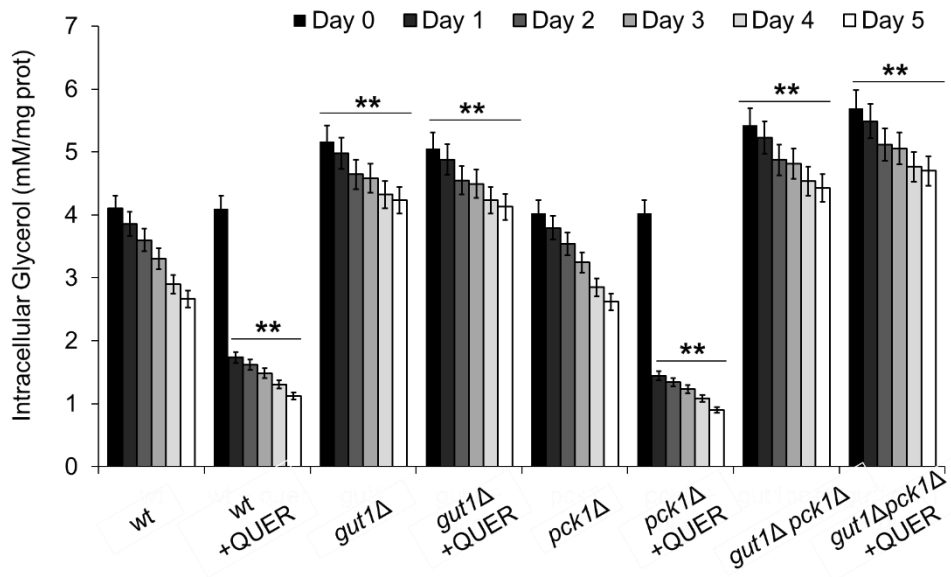

Figure S1. *QUER supplementation at the diauxic shift enhances glycerol catabolism*. Wt, *pck1*Δ, *gut1*Δ and *gut1*Δ*pck1*Δ cells were grown and supplied with quercetin (QUER, 300 µM) at the diauxic shift. At the indicated time-points intracellular glycerol levels were determined. All data refer to mean values determined in three independent experiments with three technical replicates each. SD is indicated (** $p \leq 0.01$).

Table S1. *Yeast strains used in this study.*

Strain	Relevant Genotype	Source
W303-1A	*MAT*a *ade2-1 his3-11,15 leu2-3,112 trp1-1 ura3-1 can1-100*	P.P. Slominski
YVU21	W303-1A *sir2Δ::URA3*	[284]
YVU83	W303-1A *pck1Δ::KlLEU2*	[113]
YVU84	W303-1A *sir2Δ::URA3 pck1Δ::KlLEU2*	[113]
YVU90	W303-1A *PCK1-3HA::KlURA3*	[113]
YVU91	W303-1A *sir2Δ::HIS3 PCK1-3HA::KlURA3*	[113]
YVU97	W303-1A *gut1Δ::HIS3*	This study
YVU98	W303-1A *gut1Δ::HIS3 sir2Δ::URA3*	This study
YVU99	W303-1A *gut1Δ::HIS3 pck1Δ::KlLEU2*	This study

Table S2. *Quantification of chronological survival.*

Strain	Mean CLS	Max CLS	SI CLS curve
wt (W303-1A)	10.30 ± 0.67	14.70 ± 0.29	685.70 ± 67
wt + QUER	13.55 ± 0.51**	18.60 ± 0.45**	996.07 ± 54**
*sir2*Δ	13.12 ± 0.46**	17.80 ± 0.38**	989.43 ± 75**
*sir2*Δ + QUER	15.19 ± 0.32**	20.79 ± 0.57**	1313.00 ± 43**
*pck1*Δ	6.45 ± 0.53**	9.85 ± 0.49**	436.32 ± 29**
*pck1*Δ + QUER	10.19 ± 0.24	14.20 ± 0.17	676.12 ± 63
*pck1*Δ*sir2*Δ	6.71 ± 0.42**	10.00 ± 0.32**	440.31 ± 39**
*pck1*Δ*sir2*Δ + QUER	9.59 ± 0.35	13.50 ± 0.40	675.32 ± 56
wt + NAM	13.06 ± 0.58**	17.24 ± 0.49**	979.53 ± 34**
wt (H_2O)	23.18 ± 0.61**	41.74 ± 0.61**	1416.76 ± 44**
wt (H_2O) + QUER	27.94 ± 0.84**	58.74 ± 0.83**	2068.41 ± 67**

Data referring to the time points where chronological aging cultures showed 50% (Mean CLS) and 10% (Max CLS) of survival as well as survival integral (SI) measured as reported by [292].

CHAPTER 2

Glucosinolates from Seed-Press Cake of Camelina sativa (L.) Crantz Extend Yeast Chronological Lifespan by Modulating Carbon Metabolism and Respiration

by Francesco Abbiati, Ivan Orlandi, Stefania Pagliari,

Luca Campone and Marina Vai

https://doi.org/10.3390/antiox14010080

2.1 Introduction

Glucosinolates (GSLs) are a complex group of nitrogen/sulfur-containing glycosides, produced as secondary metabolites by a large number of plants belonging to the order of Brassicales, which includes the Brassicaceae family. In this family, there are many edible plants, such as Brussels sprouts, cauliflower, garden cress, cabbage, broccoli, and radish, in which the GSL content is particularly abundant [35,37,308]. To date, more than 130 different GSL structures have been well-documented [39]. Structurally, all GSLs have a common core structure characterized by a β-thioglucose linked by a sulfur atom to a (Z)-N-hydroximinosulfate ester and an amino acid-derived, variable side chain (R group) [37,39]. GSLs may be classified in subgroups according to several criteria. The most frequently used is based on the biosynthetic precursor amino acid that categorizes GSLs into aliphatic, aromatic, and indolic GSLs [37,39]. GSLs can be hydrolyzed by endogenous plant myrosinases. These are thioglucosideglucohydrolases (EC 3.2.1.147) and remove glucose of the core structure. The resulting aglicone is unstable and rearranges producing isothiocyanates or other breakdown products, the nature of which depend upon different factors, including the nature of the R group [39,45]. GSLs and/or their breakdown products play important roles in plant protection against biotic and abiotic stresses [309-311], as well as, in agriculture for their biofumigant activity [44]. In addition, these compounds can

provide beneficial effects on human health attributed, among others, to anti-oxidant and anti-inflammatory properties [51,52,312].

Camelina (*Camelina sativa* (L.) Crantz), also known as gold-of-pleasure, false flax, or linseed dodder, is an ancient oilseed plant within the Brassicaceae family [58]. Its crops display interesting agronomic features, such as a good growth under different environmental conditions, rapidly maturing short-season forms (spring and winter cultivars), and low requirements for water, fertilizers, and pesticides [58,61,62,64,313]. Camelina seeds contain three aliphatic GSLs: glucoarabin (9-methyl-sulfinyl-nonyl-glucosinolate, GSL9), glucocamelinin (10-methyl-sulfinyl-decyl-glucosinolate, GSL10), and homoglucocamelinin (11-methylsulfinyl-undecyl-glucosinolate, GSL11) [60]. Furthermore, Camelina seeds have a distinctive content in fatty acids (in particular unsaturated ω-3 and ω-6), which makes Camelina oil well-suited for many industrial and nutritional products ranging from biodiesel and lotions to dietary supplements [314,315]. Following oil extraction, Camelina press cake (PC) is obtained as a by-product and can be employed as cheap protein-rich feed for cattle and poultry [315,317]. This application makes the entire Camelina supply chain a promising example of an environmentally and economically sustainable bio-based process. In this context, Camelina GSL9, GSL10, and GSL11, contained in the PC, have a great potential due to their antioxidant properties that are worth studying, in order to increase the edible PC

valorization. Thus, the objective of the present study was to analyze the effects of these GSLs, purified from Camelina PC, in the budding yeast *Saccharomyces cerevisiae*. This single-celled eukaryote has been highly instrumental as a model system for many purposes from basic to biomedical research. For example, *S.cerevisiae*-based studies have led to the identification/characterization of the nutrient-sensing TOR pathway, that regulates stress, growth, metabolism, and aging from yeast to humans [318,319]. In addition, yeast has been employed to identify natural compounds with anti-aging properties that proved to be functional (exemplified by spermidine) when tested in mammalian systems [320,321].

Here, we report that GSL9, GSL10, and GSL11 display anti-aging properties promoting chronological lifespan (CLS) extension. Such an extension relies on a more efficient phosphorylating respiration state that leads, on the one hand, to a lower superoxide anion ($O_2^{\cdot -}$) content and, on the other, to ATP increase. In addition, a pro-longevity metabolism toward trehalose storage takes place.

2.2 Materials and methods

2.2.1. Preparation and Purification of GSL Extract

Camelina PC was provided by FlaNat Research srl (Milan, Italy) and GSLs were extracted following a published method [322] with slight modifications. PC was homogenized into a fine powder using a grinder (TUBE-MILL 100, IKA, Staufenim Breisgau, Germany). Powdered sample was resuspended in 96% ethanol (ratio: 1 gr/5 mL) and subjected to sonication (2 cycles of 5 min each). Supernatants were filtered through a 0.45 µm PTFE filter. After extraction, GSLs were purified by Solid Phase Extraction (SPE). The SPE Mega Bond Elut NH2 cartridges were activated with methanol and equilibrated with 1% acetic acid in water. The extract was loaded into the NH_3^+ SPE and GSL fraction was eluted with a solution of methanol with 2% NH_4OH. The purified extract was then evaporated, dissolved in water, and freeze-dried. The lyophilized fraction was dissolved in water at 10 mg/mL and filtered with 0.22 µm PES syringe filter before UPLC-DAD-HRMS analysis.

2.2.2 Yeast Strain, Growth Conditions, and CLS Determination

The yeast strain W303-1A (*MATa ade2-1 his3-11,15 leu2-3,112 trp1-1 ura3-1 can1-100*) was grown in batches at 30° C in minimal medium (Difco Yeast Nitrogen Base without amino acids, 6.7 g/L) with 2% *w/v* glucose and the required supplements added in excess: adenine, histidine, and uracil at 200 mg/L and leucine at 500 mg/L [112]. CLS was determined by clonogenic assays [277]. Colony-forming units (CFUs) were counted starting with 72 h (Day 3, first age-point) after the diauxic shift (Day 0). The number of CFUs on Day 3 was considered the initial survival (100%). Cell number, extracellular glucose, and ethanol were measured at different time points during growth in order to characterize the growth profile (exponential phase, diauxic shift, post-diauxic phase, and stationary phase) of the culture [112]. Cell numberwas determined using a Coulter Counter-Particle Count and Size Analyser [278]. Duplication time was calculated as in [278]. Survival integral, namely the area under the CLS curves, was determined according to [292]. Treatments were performed at Day 0. GSL9, GSL10, and GSL11 (purchased from Extrasynthese, Genay, France) were added at the final concentrations of 270, 640, and 90 μM, respectively. Nicotinamide (NAM, Sigma-Aldrich, Darmstadt, Germany) was added at 5 mM final concentration [115].

2.2.3 Dosage of Metabolites and Enzymatic Activities

At designated time points, aliquots of the yeast cultures were centrifuged, and both pellets (washed twice) and supernatants were collected and frozen at - 80 °C until used. Rapid sampling for intracellular metabolite measurements was performed as described [112]. The concentrations of glucose, ethanol, acetate, citrate, succinate, malate, fumarate, and glycerol were determined using enzymatic assays (K-HKGLU, K-ETOH, K-ACET, K-SUCC, K-CITR, K-LMALR, and K-GCROL kits from Megazyme, Bray, Ireland, and MAK060 from Sigma-Aldrich, Darmstadt, Germany). Extraction and determination of intracellular trehalose according to [281]. The K-HKGLU kit was used to quantify the released glucose.

Isocitrate lyase (Icl1) activity was assayed as previously reported [112]. Estimation of succinate dehydrogenase (SDH) activity was performed according to [323] by measuring at 540 nm the formation of formazan due to tetrazolium salt reduction. Glycerol-3-phosphate dehydrogenase (Gut2) activity was determined according to [282]: spheroplasts were prepared with Zymolyase 20T (MP Biomedicals, Solon, OH, USA).

ATP was extracted as described [324] and quantified using the ATP determination kit (Molecular Probes, Thermo Fisher Scientific, Waltham, MA, USA). Cell dry weight was measured as in [325]. Total protein concentration was

assayed using the Pierce™ BCA Protein Assay Kit (Thermo Fisher Scientific, Waltham, MA, USA).

2.2.4 Subcellular Fractionation

Mitochondria were prepared as in [326] with minor modifications. Briefly, at designated time points, about 10^9 cells were harvested by centrifugation and spheroplasts were prepared in the presence of Zymolyase 20T (MP Biomedicals, Solon, OH, USA). Spheroplasts were resuspended in ice-cold homogenization buffer (0.6 M sorbitol, 10 mM Tris-HCl, pH 7.4, 1 mM EDTA, 0.2% *w/v* bovine serum albumin (Sigma-Aldrich, Darmstadt, Germany), containing 1 mM phenylmethylsulfonyl fluoride (Sigma-Aldrich, Darmstadt, Germany) and Complete EDTA-free cocktail of protease inhibitors (Roche Diagnostic, GmbH, Manheim, Germany). Spheroplasts were homogenized with 20 strokes using a Dounce homogenizer (Sigma-Aldrich, Darmstadt, Germany). Then, the homogenate was centrifuged at 1500 rcf for 5 min to remove cell debris and nuclei. The supernatant was clarified by centrifugation at 4000 rcf for 5 min and, finally, pellets of crude mitochondria were collected at 12,000 for 10 min. Pellets of crude mitochondria and the corresponding supernatants were used to measure the concentrations of mitochondrial and cytosolic fumarate, respectively. Subcellular fractions were checked by Western

analysis using anti-3-phosphoglycerate kinase mAb (22C5 from Molecular Probes, Invitrogen, Thermo Fisher Scientific, Waltham, MA, USA) as a cytosolic marker and anti-Tom40 Ab (H-300 from Santa Cruz Biotechnology, Dallas, TX, USA) as a mitochondrial one. Secondary antibodies were purchased from Amersham (Cytiva, Amersham, UK). Detection of Western blots as described [327].

2.2.5 Respiration Assays and Fluorescence Microscopy

The basal oxygen consumption of intact cells was measured at 30 °C using a "Clark-type" oxygen electrode (Oxygraph System, Hansatech Instruments, Nortfolk, UK) as previously reported [304]. The addition of 37.5 mM triethyltin bromide (TET, Sigma-Aldrich, Darmstadt, Germany) and 10 µM of the uncoupler carbonyl cyanide 3-chlorophenylhydrazone (CCCP, Sigma-Aldrich, Darmstadt, Germany) to the oxygraphy chamber accounted for the non-phosphorylating respiration and the maximal/uncoupled respiratory capacity, respectively [115]. The addition of 2 M antimycin A (Sigma-Aldrich, Darmstadt, Germany) accounted for non-mitochondrial oxygen consumption. Respiratory rates for the basal oxygen consumption (J_R), the maximal/uncoupled oxygen consumption (J_{MAX}), and the non-phosphorylating oxygen consumption (J_{TET}) were determined from the slope of a plot of O_2 concentration

against time, divided by the cell number. The net respiration (net_R) was obtained by subtracting J_{TET} from J_R. Index of respiratory competence (IRC) was determined as previously described [328,329]. At different time points, identical samples of the yeast cultures were plated on Yeast Extract Peptone/2% *w/v* glucose (YEPD) agar plates and on YEP/3% *v/v* glycerol (YEPG) plates. IRC was calculated as colonies on YEPG divided by colonies on YEPD times 100%.

Dihydroethidium (DHE, Sigma-Aldrich, Darmstadt, Germany) staining was performed to analyze superoxide anion ($O_2^{\cdot -}$) [283]. The mitochondrial membrane potential was assessed by staining with 3,3′ -dihexyloxacarbocyanine iodide ($DiOC_6$, Molecular Probes, Invitrogen, Thermo Fisher Scientific, Waltham, MA, USA) [330]. Cells were counterstained with propidium iodide to discriminate between live and dead cells. A Nikon Eclipse E600 fluorescence microscope equipped with a Nikon Digital Sight DS Qi1 camera was used. Digital images were acquired and processed using Nikon NIS-Elements BR 4.30.00 64-bit software, https://www.microscope.healthcare.nikon.com/products/software/niselements (accessed on 8 January 2025).

2.2.6 Statistical Analysis

All values are presented as the mean of three independent experiments ± standard deviation (SD). Three technical replicates were analyzed in each independent experiment. Statistical significance was assessed by one-way ANOVA test. The level of statistical significance was set at a p value of ≤ 0.05. All data were processed with Microsoft Excel 2019 (Microsoft Corporation, Redmond, WA, USA) to calculate the average values and standard deviations. Statistical analyses were performed using GraphPad Prism software version 9.5.1 (GraphPad Inc., La Jolla, CA, USA).

2.3 Results and discussion

2.3.1 Characterization of GSL Extract

As a first step, we analyzed, by UPLC-DAD-HRMS, the content of the extract purified from Camelina PC (see Section 2), which was then used in the experiments with *S.cerevisiae* cells. A representative chromatogram is presented in Figure 1, showing that in the purified extract only three aliphatic GSLs were present, namely GSL9, GSL10, and GSL11.

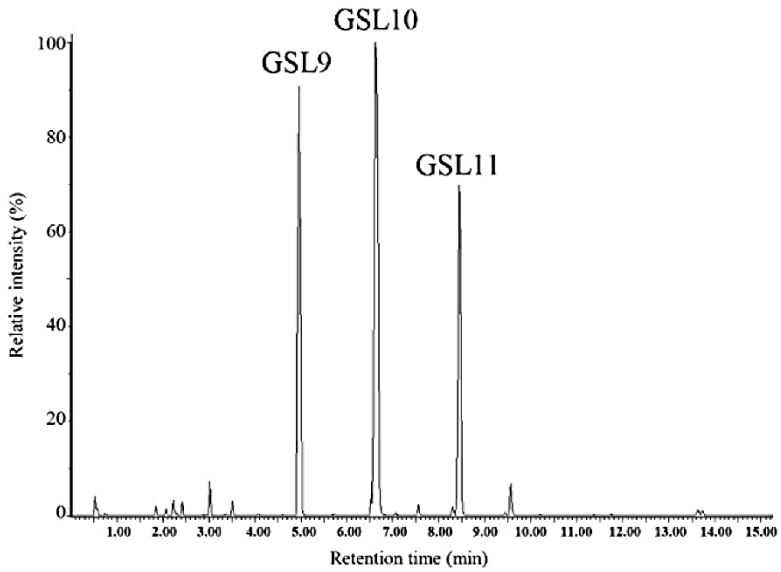

Figure 1. *Representative UPLC-DAD- HRMS chromatogram of GSLs purified from Camelina press cake.*

2.3.2 GSL Extract Increases CLS

Taking advantage of the chronological aging model, which allows us to simulate in *S.cerevisiae* cellular aging of post-mitotic quiescent mammalian cells, we investigated whether the purified GSL extract may have any effect on yeast longevity as well as on cellular metabolism. To this end, in the context of a standard CLS experiment [111], GSL extract was supplemented to cells in a range of different concentrations (from 10 μM to 1.5 mM). Supplementation was done at the diauxic shift (Day 0) because it is at this point that a massive metabolic reconfiguration takes place enabling cells to acquire a set of features required for survival during the quiescent state [272,331]. GSL

extract extended CLS (Figure 2A) showing a dose–response relationship between the increase of both mean and maximum CLS (Table 1) as well as of the survival integral (Table 1 and Figure 2B) and the concentrations of GSL extract. As shown in Table 1 and in the dose–response curve of Figure 2B, the maximal benefit for CLS extension was achieved for 1 mM GSL extract, whilst higher concentration such as 1.5mM could not further enhance cell longevity. Consequently, in this study, 1 mM GSL extract was chosen to investigate the pro-longevity effect of GSL extract on chronological aging. Furthermore, since the GSL extract obtained from Camelina PC only consisted of three GSLs, namely GSL9, GSL10, and GSL11 (Figure 1), we also evaluated the effects on CLS of the three GSLs separately using the amount of each that was present in 1 mM GSL extract. All three GSLs supplied separately increased CLS (Figure 2C), confirming the pro-longevity effect exerted by the GSL extract.

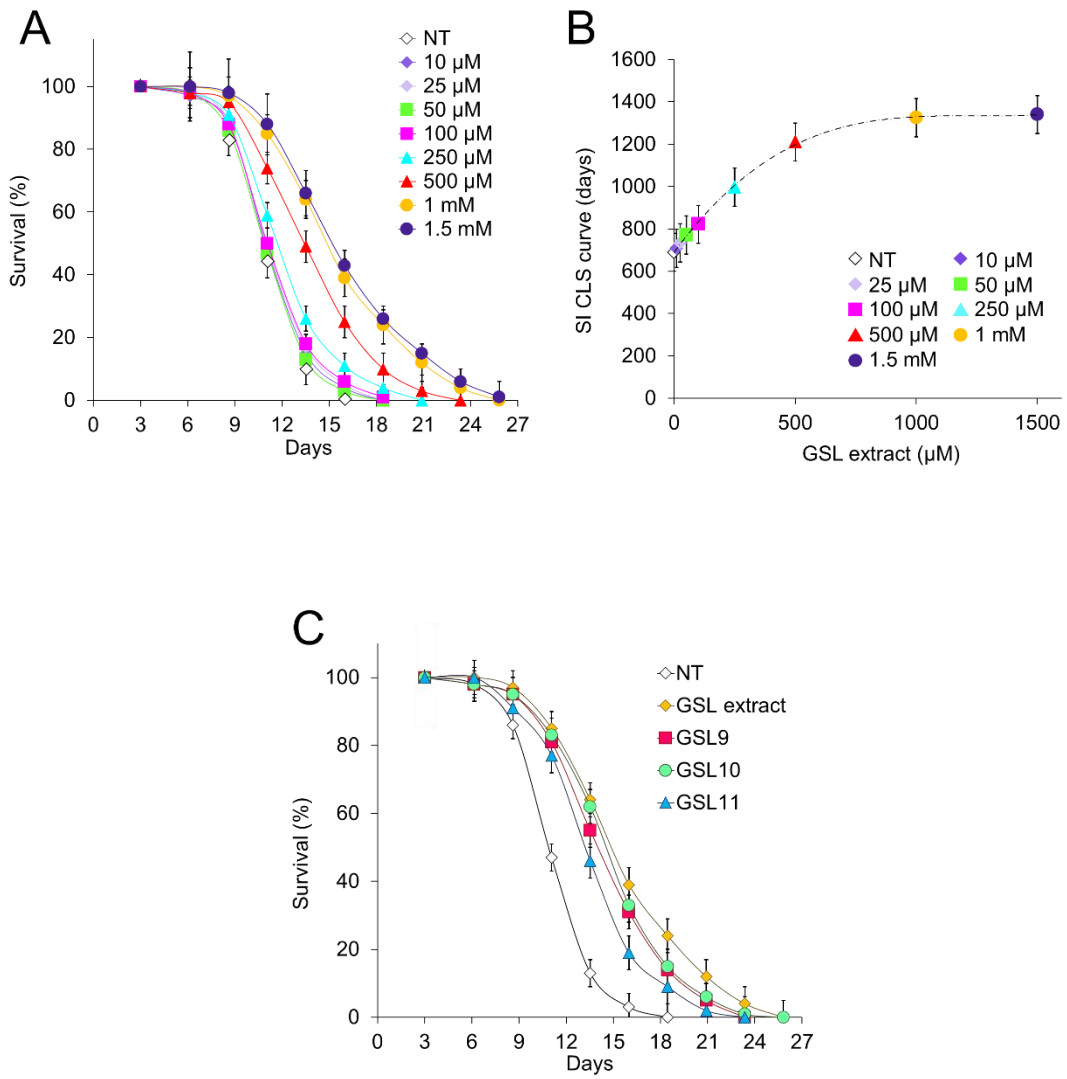

Figure 2. *GSL extract supplementation at the diauxic shift promotes CLS longevity.* Yeast cells were grown in minimal medium/2% glucose and the required supplements in excess (see Section 2). At the diauxic shift (Day 0), different concentrations (from 10 µM to 1.5 mM) of GSL extract were added and (**A**) survival over time of treated and untreated (NT) cultures was determined by colony-forming capacity on YEPD plates. 72 h after the diauxic shift (Day 3) was considered the first age point, corresponding to 100% survival. (**B**) Dose–response relationship of the survival

integral values (SI) versus the concentrations of GSL extract. (**C**) CLS of cells supplied with GSL extract (1 mM) or GSL9, GSL10, and GSL11 separately, at the concentration which was present in 1 mM GSL extract. All data refer to mean values determined in three independent experiments with three technical replicates each. Standard deviations (SD) are indicated.

Table 1. *GSL extract extends CLS showing a dose-response relationship.*

	Mean CLS	**Max CLS**	**SI**
NT	10.90 ± 0.52	13.99 ± 0.56	689.36 ± 60
10 µM GSL extract	10.96 ± 0.21	14.24 ± 0.33	707.98 ± 55
25 µM GSL extract	11.01 ± 0.47	14.60 ± 0.50	734.23 ± 74
50 µM GSL extract	10.89 ± 0.26	13.89 ± 0.42	771.42 ± 67
100 µM GSL extract	11.07 ± 0.39	14.76 ± 0.37	821.40 ± 31
250 µM GSL extract	11.65 ± 0.27*	16.20 ± 0.22*	996.97 ± 58**
500 µM GSL extract	13.38 ± 0.50**	18.50 ± 0.31**	1210.46 ± 40**
1.0 mM GSL extract	14.92 ± 0.21**	21.40 ± 0.29**	1325.25 ± 55**
1.5 mM GSL extract	15.25 ± 0.33**	22.15 ± 0.49**	1340.11 ± 44**

Data referring to the time points where chronological aging cultures of Figure 2A showed 50% (Mean CLS) and 10% (Max CLS) of survival as well as survival integral (SI) measured as in [292]. NT, untreated culture. Standard deviations are indicated (* $p \leq 0.05$ and ** $p \leq 0.01$).

2.3.3 GSL Extract Preserves Mitochondrial Functionality

Longevity is tightly linked to mitochondrial functionality. Indeed, increase of mitochondrial dysfunction is one feature that has been observed in aging

across species and decline of mitochondrial functionality is considered a hallmark of aging [6,291,332]. In *S.cerevisiae*, mitochondrial functionality can be assessed by measuring the IRC, which defines the percentage of viable cells competent to respire [328]. At the diauxic shift, both the unsupplemented culture and that supplemented with the GSL extract were respiration-competent, showing an IRC of about 100% (Figure 3A). Afterwards, as expected [115,333], a time-dependent loss of mitochondrial functionality was observed with increasing chronological age. However, at Day 18 the IRC of the supplemented culture was still about 75% against about 30% of the unsupplemented one (Figure 3A). A similar behavior was observed when GSL9, GSL10, and GSL11 were supplied separately (Figure 3A), indicating that GSLs preserve mitochondrial functionality. In addition, as cells age, mitochondria undergo a gradual loss of the membrane potential along with morphological changes: the mitochondrial tubular network becomes punctiform (also referred to as mitochondrial fragmentation) [334,335]. Fluorescent staining with $DiOC_6$ dye, which accumulates specifically at mitochondrial membranes depending on their membrane potential [330], revealed that already at Day 5 the mitochondrial network of chronologically aging cells underwent fragmentation and punctuated structures appeared (Figure 3B). On the contrary, following GSL extract supplementation, tubular shapes with

bright fluorescence were still present at Day 7 (Figure 3B), suggesting that the mitochondrial functionality is preserved in line with IRC results.

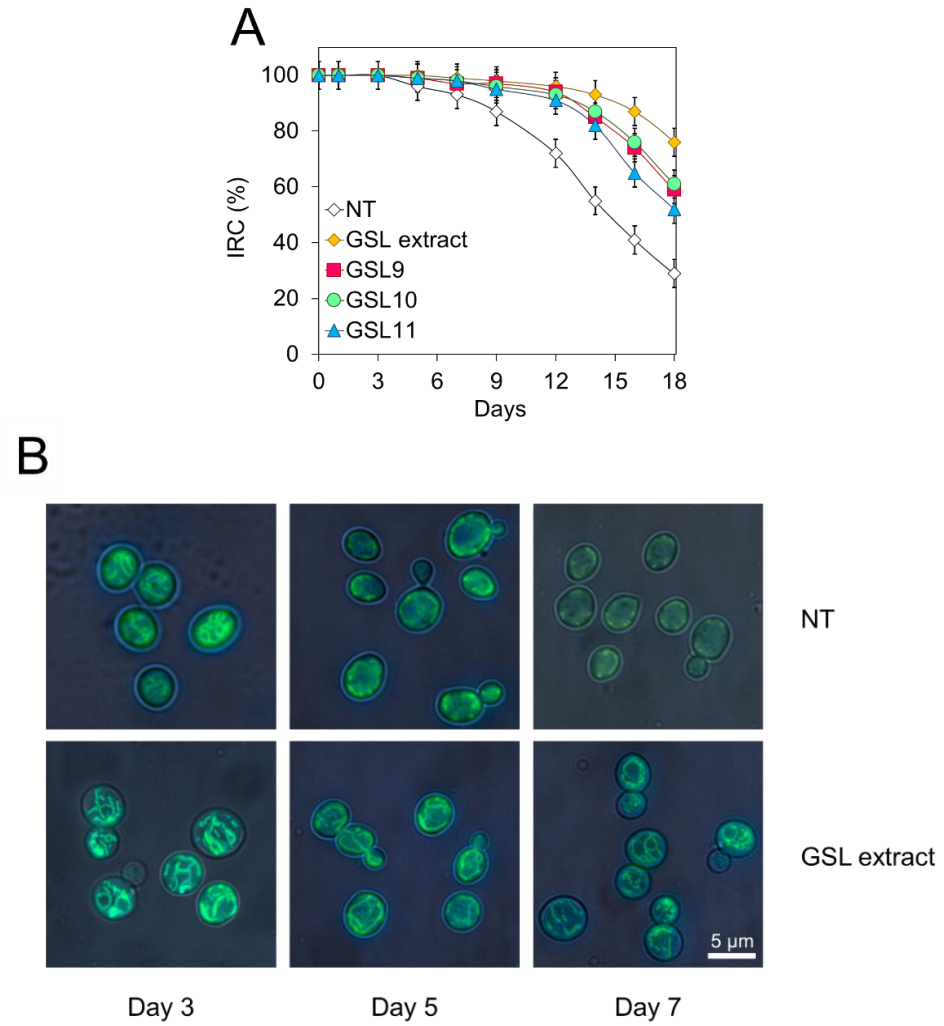

Figure 3. *GSL extract supplementation at the diauxic shift preserves mitochondrial functionality.* Cells were grown and supplied with GSL extract (1 mM) as in Figure 2 and (**A**) starting from Day 0, aliquots of the indicated cultures were serially diluted and plated onto YEPD and YEPG plates in order to determine the index of respiratory competence (IRC). All data refer to mean values determined in three

independent experiments with three technical replicates each. Standard deviations (SD) are indicated. (**B**) Representative images of NT and GSL extract-supplemented cultures stained with $DiOC_6$ to visualize mitochondrial membranes at the indicated time points.

2.3.4 GSL Extract Supplementation at the Diauxic Shift Correlates with a More Efficient Respiration

Considering that following the diauxic shift a respiration-based metabolism takes place and given the influence played by respiration on CLS [336-338], we quantified some respiratory parameters in both supplemented and unsupplemented cultures. When cells were supplied with the GSL extract at the diauxic shift, a slight increase in basal oxygen consumption (J_R) was observed, whilst maximal respiratory capacity (J_{MAX}) was unaffected (Figure 4A,B). Since J_{MAX} was assayed in the presence of the protonophore CCCP, which dissipates the proton gradient across the mitochondrial membrane, it follows that the membrane potential is not influenced by GSL supplementation. Carbon starvation elicits a transition from phosphorylating to non-phosphorylating respiration and an increase in oxidative damage [339]. Interestingly, in supplemented cells, the non-phosphorylating respiration (J_{TET}) was extremely lower than that of the unsupplemented ones (Figure 4C). In such a determination, TET was used to inhibit ATP synthase, allowing oxygen measurement in a condition where the dissipation of the proton gradient due

to ATP synthase-driven proton translocation is inhibited and only proton leak takes place. Consequently, the net respiration ($net_R = J_R - J_{TET}$), which assesses the coupled respiration, in supplemented cells was higher than that of the unsupplemented ones, especially 5 days after the diauxic shift where net_R for the unsupplemented culture was reduced to values close to zero (Figure 4D), indicating that GSL supplementation seems to promote a more efficient coupling of electron transport to ATP generation. In addition, in supplemented cells the value of the ratio between net_R and J_{MAX}, which estimates the fraction of the electron transfer system utilized to drive ATP synthesis [338], was also significantly higher. This was particularly evident as a function of time in culture (Figure 4E), showing that GSL supplementation allows chronologically aging cells to retain a mitochondrial respiration toward a more coupled state for a longer period.

It is well known that electrons may accumulate at intermediate levels of the electron transport chain (ETC) favouring electron leakage. This, in turn, impacts on ROS formation as oxygen can readily accept single electrons generating O_2 reduction intermediates, among which superoxide anions ($O_2^{\cdot -}$). In excess, this radical, directly or converted to other ROS, causes frequently irreversible damage to cellular macromolecules, such as lipids, proteins, and DNA, contributing to the aging process [291,293,341]. GSL supplementation drastically reduced the expected increase of $O_2^{\cdot -}$ that occurs as cells

chronologically age (Figure 4F), in line with the low J_{TET} values measured in the supplemented cells since non-phosphorylating respiration is prone to generate $O_2^{\cdot -}$ [339]. In addition, a lower level of $O_2^{\cdot -}$ produced in the ETC decreases the risk of impairing mitochondrial functionality. This is what takes place in the supplemented cells, the mitochondria of which are functional and with a tubular morphology (Figure 3B). All this correlates with an enhanced CLS.

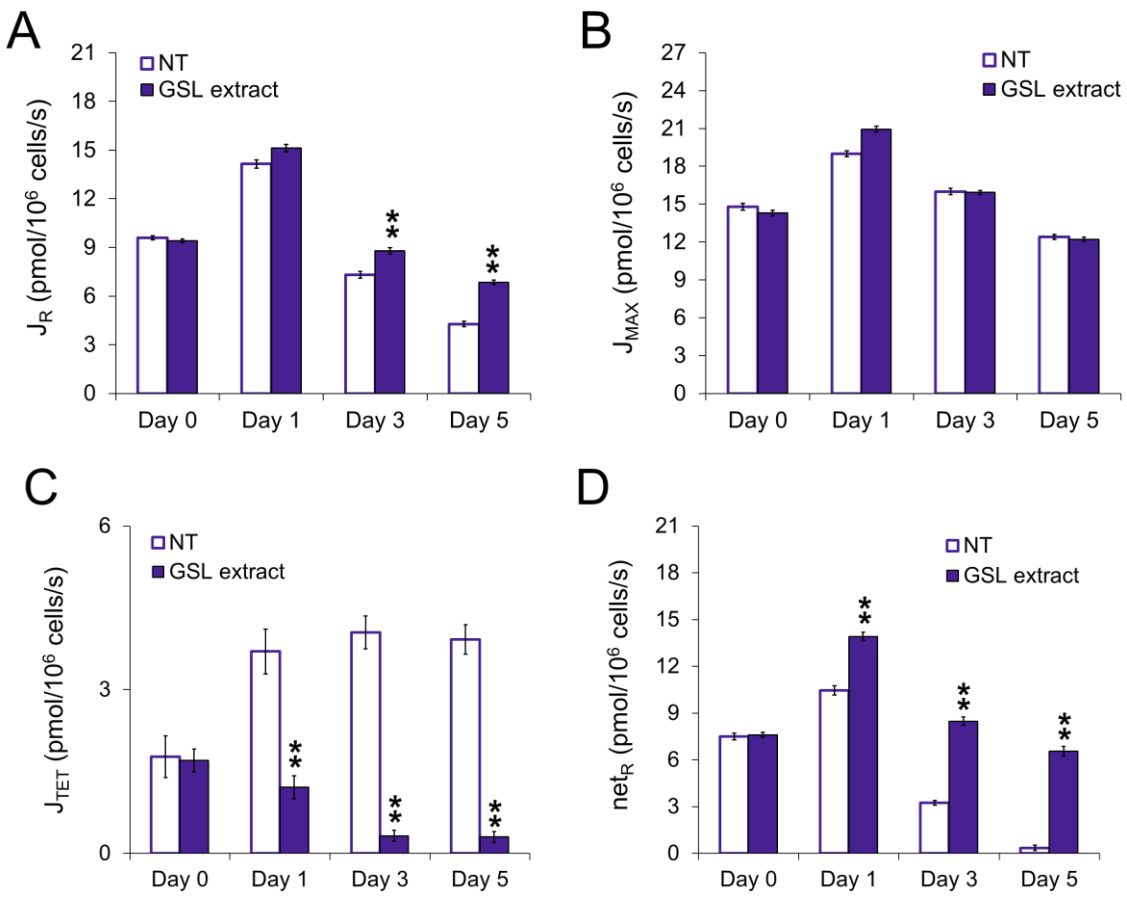

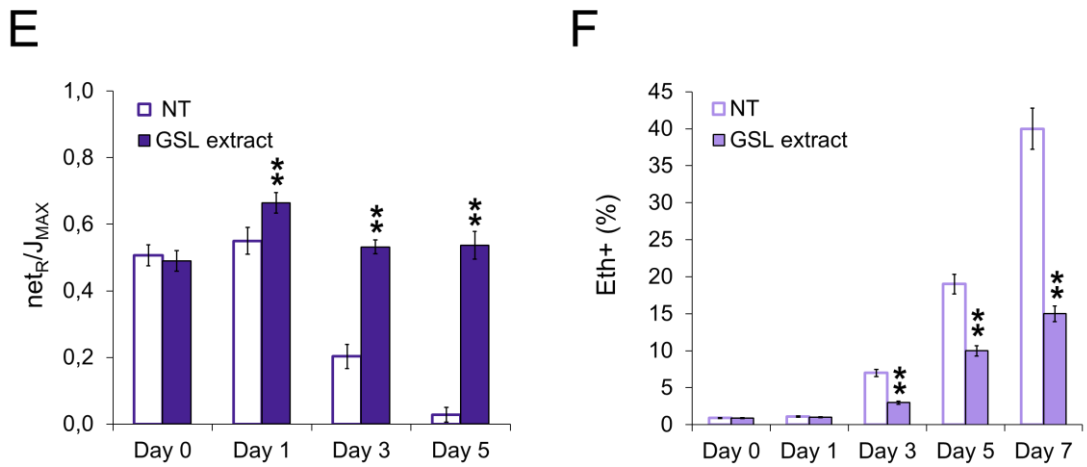

Figure 4. *GSL extract supplementation at the diauxic shift promotes phosphorylating respiration.* Cells were grown and supplied with GSL extract (1 mM), as in Figure 2, and oxygen uptake rates (J) are expressed as pmol/10^6 cells/s. (**A**) Basal respiration rate (J_R), (**B**) uncoupled respiration rate (J_{MAX}), (**C**) non-phosphorylating respiration rate (J_{TET}), (**D**) net respiration ($net_R = J_R - J_{TET}$), and (**E**) fraction of the electron transfer system utilized for ATP synthesis (net_R/J_{MAX}) were measured at the indicated time points. Substrates and inhibitors used in the measurements of the respiratory parameters are detailed in the text. (**F**) Bar charts of the percentage of fluorescent/superoxide positive cells assessed by the superoxide-driven conversion of non-fluorescent dihydroethidium into fluorescent ethidium (Eth). Day 0, diauxic shift. All data refer to mean values determined in three independent experiments with three technical replicates each. SD is indicated. Statistical significance as assessed by one-way ANOVA test is indicated (** $p \leq 0.01$).

2.3.5 GSL Extract Supplementation at the Diauxic Shift Preserves TCA Enzymatic Activities

Mitochondria host the TCA cycle that fulfils a broad range of metabolic activities, from the oxidative generation of reducing equivalents that drive aerobic respiration, to providing building blocks for macromolecule synthesis. TCA enzymatic activities change at the diauxic shift when cellular metabolism shifts from fermentation to respiration, as well as during chronological aging [271,291,342]. Thus, initially, we measured the levels of some intermediates of the TCA cycle, namely citrate, succinate, malate, and fumarate that also have a metabolic connection with the glyoxylate shunt (Figure 5). The latter is activated after glucose depletion and is responsible for the generation of C4 units from C2 ones (ethanol and acetate) by excluding the two decarboxylation steps of the TCA cycle and also operates as an anaplerotic device of the TCA cycle [152,271]. After the diauxic shift, in the unsupplemented culture, the levels of citrate, succinate, malate, and fumarate decreased (Figure 6A–D) as expected [112,329]. On the contrary, in the GSL-supplemented culture, the levels of these intermediates remained higher as cells aged (Figure 6A–D). With regard to succinate, it is released from the glyoxylate shunt into the cytoplasm as a net product and is imported into the mitochondria to feed the TCA cycle [151].

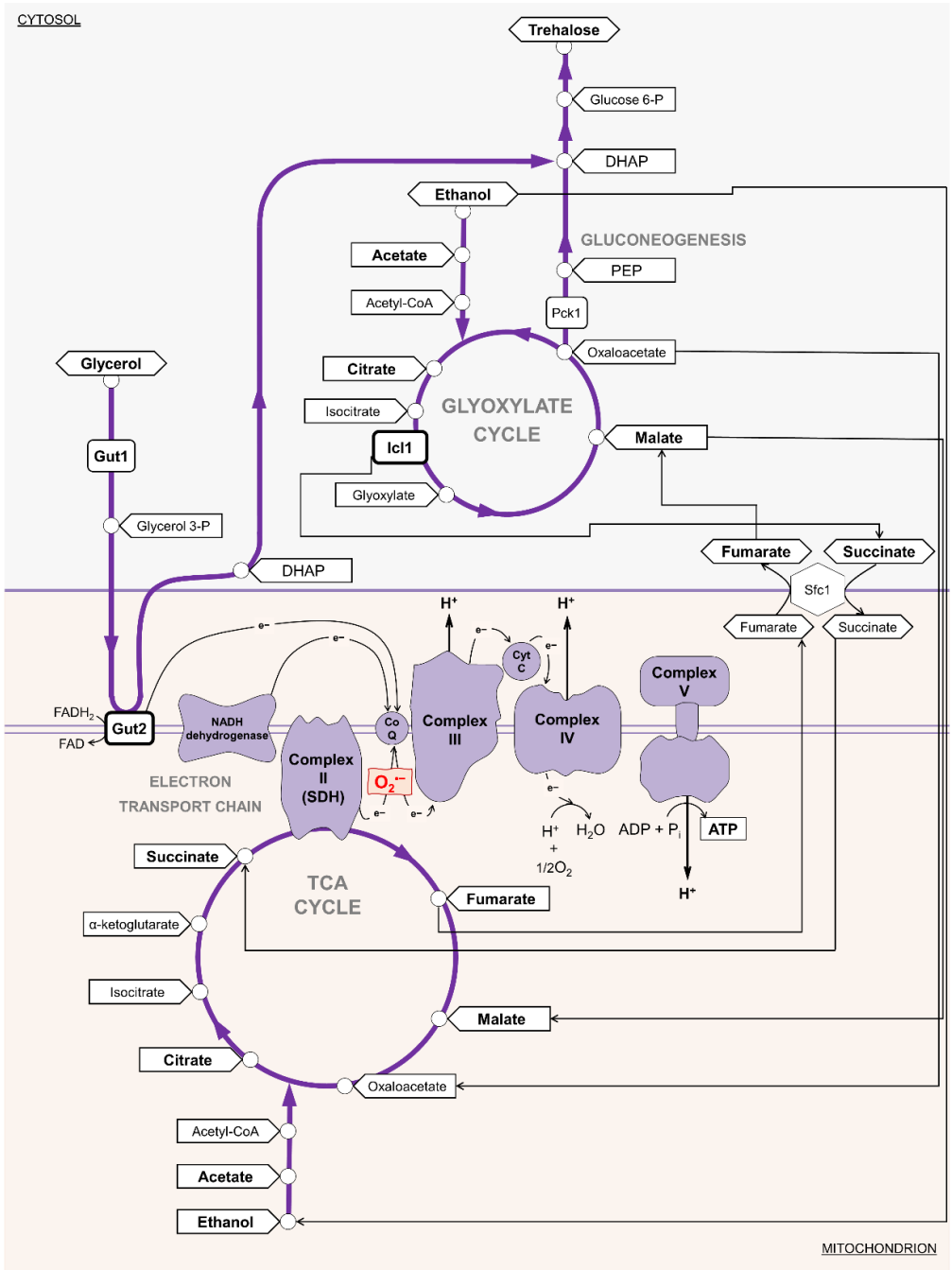

Figure 5. *Scheme of metabolic pathways involved in utilizing the main non-ferment-able carbon sources during chronological aging*. The electron transport chain and

three pathways (the glyoxylate shunt, TCA cycle, and gluconeogenesis) are schematically shown. Icl1, isocitrate lyase; Pck1, phosphoenolpyruvate carboxykinase; Gut1, glycerol kinase; Gut2, mitochondrial glycerol-3-phosphate dehydrogenase; Sfc1, mitochondrial succinate-fumarate transporter; SDH, succinate dehydrogenase complex; PEP, phosphoenolpyruvate; DHAP, dihydroxyacetone phosphate.

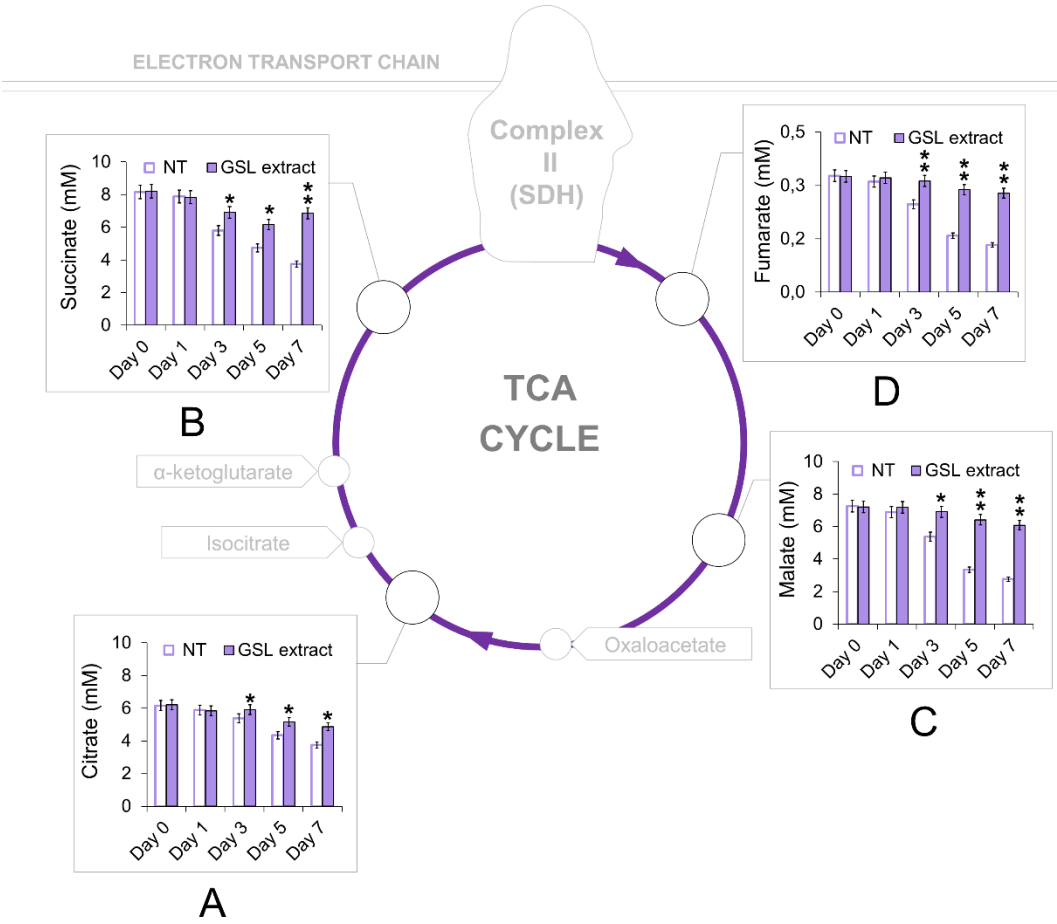

Figure 6. *GSL supplementation at the diauxic shift preserves TCA intermediate contents.* Cells were grown and supplied with GSL extract (1 mM), as in Figure 2, and intracellular concentrations of (**A**) citrate, (**B**) succinate, (**C**) malate, and (**D**)

fumarate were measured at the indicated time points. Day 0, diauxic shift. SDH, succinate dehydrogenase complex. All data refer to mean values determined in three independent experiments with three technical replicates each. SD is indicated (* $p \leq 0.05$ and ** $p \leq 0.01$).

In the latter succinate is oxidized to fumarate by succinate dehydrogenase complex (SDH), also known as Complex II (Figures 5 and 6). This reaction is coupled to the reduction of ubiquinone to ubiquinol, which is the substrate for Complex III in the ETC; in such a way, SDH functionally links the activity of the TCA cycle to the ETC. Starting from the diauxic shift, SDH activity significantly decreased in unsupplemented cells (Figure 7A), in concert with a decrease in the levels of mitochondrial fumarate (Figure 7B) indicative of an aging-associated decline of the TCA cycle flux. In the GSL-supplemented culture SDH enzymatic activity and mitochondrial fumarate content were stably maintained at higher levels (Figure 7A,B). This indicates that GSL extract preserves TCA functioning, which is a feature that is involved in conferring longevity in yeast and other organisms [343-346]. In addition, in the context of chronological aging, mutants deleted in genes encoding subunits of SDH, namely *SDH1*, *SDH2*, and *SDH4*, show the shortest-lived phenotype among 33 single ETC component-deleted strains and higher $O_2^{\cdot -}$ content associated with an impaired mitochondrial efficiency [347].

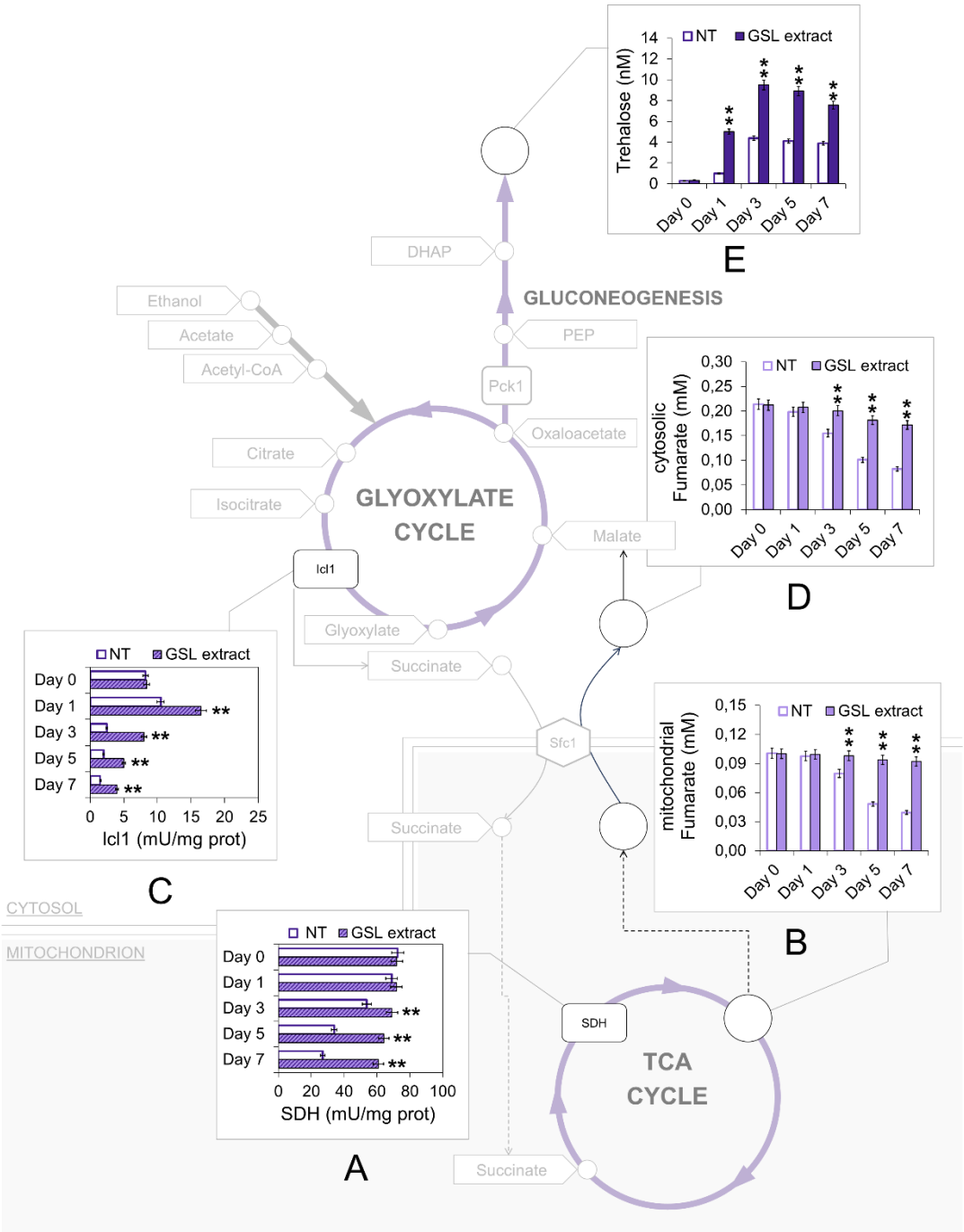

Figure 7. *GSL extract supplementation at the diauxic shift promotes trehalose storage.* At the indicated time points, (**A**) SDH enzymatic activity, (**B**) mitochondrial fumarate, (**C**) Icl1 enzymatic activity, (**D**) cytosolic fumarate, and (**E**) trehalose

content evaluated for both treated and untreated cultures of Figure 2. Day 0, diauxic shift. Icl1, isocitrate lyase; Pck1, phosphoenolpyruvate carboxykinase; Sfc1, mitochondrial succinate-fumarate transporter; SDH, succinate dehydrogenase complex; PEP, phosphoenolpyruvate; DHAP, dihydroxyacetone phosphate. All data refer to mean values determined in three independent experiments with three technical replicates each. SD is indicated (** $p \leq 0.01$).

Interestingly, SDH has a medical significance, considering that its activity has been reported to decline with age in many tissues (brain, liver, heart, and skin) and to be reduced in some age-related diseases, including neurodegenerative disorders. This decline/reduction is associated with an increase of ROS contributing to cellular damage [348-350].

2.3.6 GSL Extract Supplementation at the Diauxic Shift Enhances Glyoxylate/Gluconeogenic Flux and Increased Trehalose Stores Without Affecting Ethanol/Acetate Catabolism

The glyoxylate shunt is composed of five enzymatic reactions, three of which are also present in the TCA cycle, whilst two are unique to the shunt. One of these is that catalyzed by isocitrate lyase (Icl1). This enzyme is solely localized in the cytosol and generates succinate and the name-giving metabolite glyoxylate from isocitrate (Figures 5 and 7). Measurements of Icl1 enzymatic activity revealed a clear increase in the culture supplemented with GSLs

compared with the unsupplemented counterpart (Figure 7C) indicative of an enhancement of the shunt. As stated above, cytosolic succinate is imported into the mitochondria. However, its transfer by the Sfc1 transporter provides cytosolic fumarate. In fact, fumarate is generated exclusively in the TCA cycle. Once in the cytosol fumarate is converted to malate and utilized to refill the glyoxylate shunt and fuel gluconeogenesis (Figures 5 and 7) [351]. The latter, in turn, fuels the synthesis of storage carbohydrates, the accumulation of which contributes to the longevity of chronologically aging cells [145,336]. Following GSL supplementation, cytosolic fumarate levels increased, as well as trehalose content (Figure 7D,E). It is well recognized that the ability of chronologically aging cells to accumulate sufficient trehalose stores ensures, on the one hand, long-term survival during the stationary phase and, on the other, the resumption of growth upon nutrient supply. Hence, an enhancement of intracellular trehalose stores correlates with CLS extension [115,145,146,327]: this is also the case of the culture supplemented with the GSL extract (Figures 2A and 7E).

During the diauxic shift, the glyoxylate shunt is fed by two C2 by-products of the fermentation, namely ethanol and acetate (Figure 5). No difference was observed in the utilization of extracellular ethanol and acetate following GSL supplementation (Figure 8A), suggesting that GSLs did not affect the catabolism of these compounds. Since, our published data indicated that

supplementation at the diauxic shift of nicotinamide (NAM), a form of vitamin B3, extends CLS in concert with an enhancement of the glyoxylate shunt and increased ethanol/acetate catabolism (Figure 8B,C) [115], we analyzed the effects of a combined supplementation of GSL extract and NAM. An additive extension on CLS was produced when GSLs and NAM were provided together at the diauxic shift compared to single supplementations (Figure 8B and Table 2). On the other hand, the fast kinetics of ethanol/acetate depletion in the medium of NAM-supplemented cells was unaffected by GSL supplementation (Figure 8C). A feature of NAM-supplemented cells was also an increase in trehalose content compared with the unsupplemented ones [115], albeit to a lesser degree than that measured for GSL supplementation (Figure 8D). Supplementing NAM and GSLs together resulted in higher trehalose levels than those with GSL extract alone as cells age (Day 9 to Day 13) (Figure 8D). NAM is a non-competitive inhibitor of Sir2 activity [276] and, in the context of chronological aging, its supplementation inhibits Sir2-mediated deacetylation of phosphoenolpyruvate carboxykinase (Pck1) [115]. Pck1 catalyzes the main flux-controlling step of the gluconeogenesis, is active in the acetylated form [125] and is required for the utilization of ethanol/acetate. *SIR2* deletion or inhibition of its enzymatic activity lead to an improved assimilation of these C2 units by the glyoxylate-requiring gluconeogenesis resulting in increased accumulation of trehalose and longevity extension

[113,115,275]. Given the results described above with single/combined supplementations of NAM and GSLs, we may reasonably rule out that Sir2 is the target of GSLs and that other targets/pathways can account for their effects.

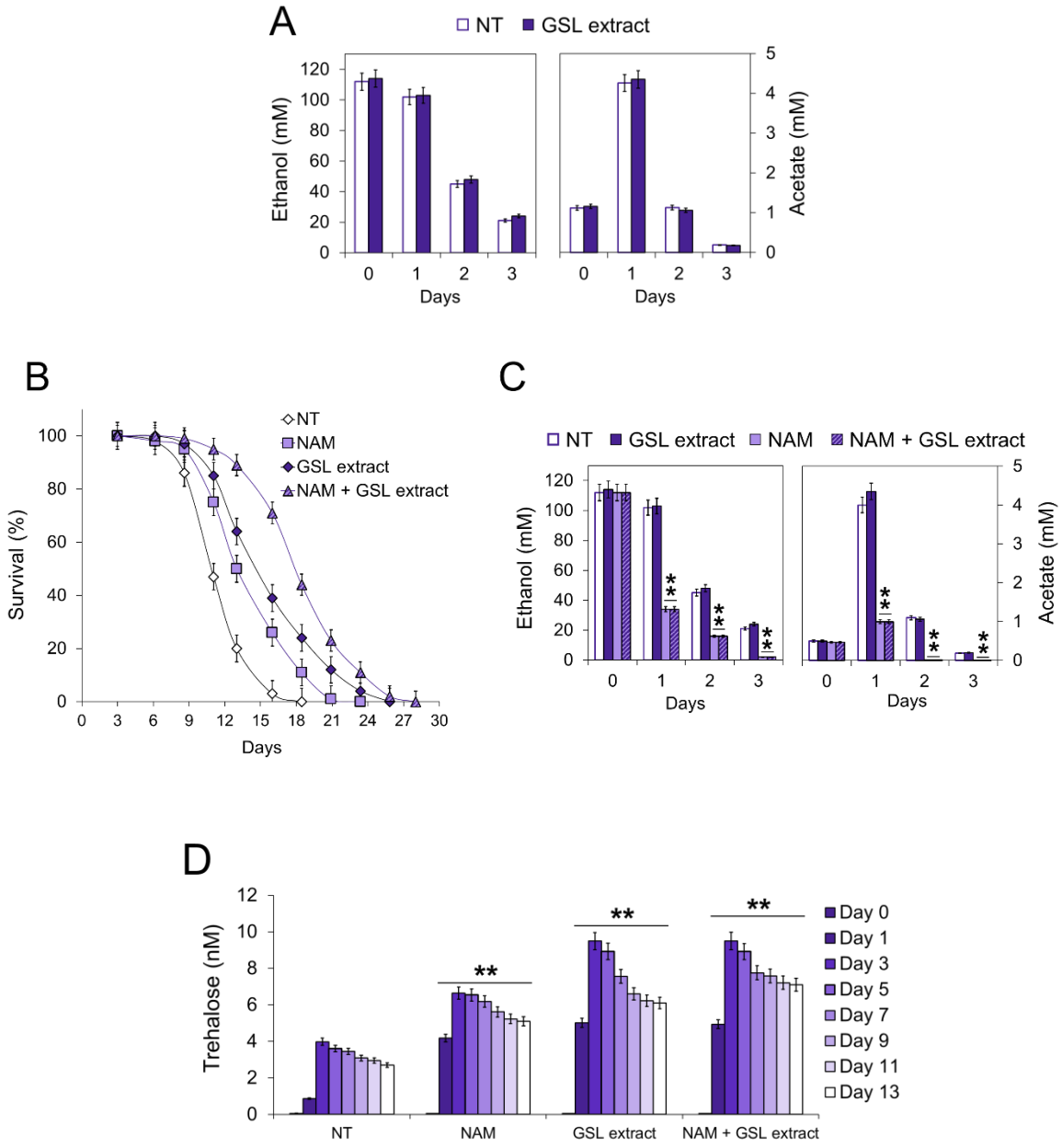

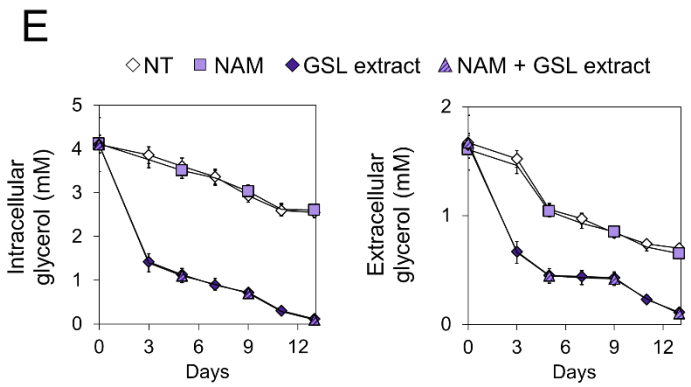

Figure 8. *GSL extract supplementation at the diauxic shift promotes glycerol catabolism resulting in increased accumulation of trehalose and CLS extension.* At the indicated time points, (**A**) bar charts of ethanol and acetate levels evaluated for both GSL extract-treated and untreated cultures of Figure 2. (**B**) CLS of cultures supplemented at Day 0 with NAM (5 mM), GSL extract (1 mM), or NAM + GSL extract. In parallel, (**C**) extracellular ethanol and acetate content, (**D**) intracellular trehalose concentration, and (**E**) intracellular and extracellular glycerol levels were measured. Day 0, diauxic shift. All data refer to mean values determined in three independent experiments with three technical replicates each. SD is indicated (** $p \leq 0.01$).

Table 2. *Effect on CLS of GSL extract and NAM provided together at the diauxic shift.*

	Mean CLS	**Max CLS**	**SI**
NT	10.90 ± 0.52	13.99 ± 0.56	689.36 ± 60
NAM	13.06 ± 0.58**	17.24 ± 0.49**	979.53 ± 34**
GSL extract	14.92 ± 0.21**	21.40 ± 0.29**	1325.25 ± 55**
NAM + GSL extract	17.97 ± 0.39**	23.28 ± 0.23**	1510.06 ± 45**

Data referring to the time points where chronological aging cultures reported in Figure 8B showed 50% (Mean CLS) and 10% (Max CLS) of survival as well as survival

integral (SI) measured as in [292]. NT, untreated culture. Standard deviations are indicated (** $p \leq 0.01$).

2.3.7 Glycerol Catabolism Is Enhanced in GSL-Supplemented Chronologically Aging Cells in Concert with ATP Increase

The L-glycerol 3-phosphate (L-G3P) pathway becomes operative at the diauxic shift, allowing glycerol utilization [153]. Glycerol is a C3 by-product of yeast fermentation and, by the L-G3P pathway, is catabolized to dihydroxyacetone phosphate that can be used to fuel gluconeogenesis downstream of the step catalyzed by Pck1 (Figure 5). In GSL-supplemented chronologically aging cells, intracellular and extracellular glycerol decreased more rapidly than in unsupplemented cells, as well as in NAM-supplemented ones (Figure 8E). The kinetics of glycerol utilization following the combined supplementation of NAM and GSLs was similar to that of GSLs alone (Figure 8E). To further examine the effects on glycerol catabolism of GSLs, the latter were added to NAM-supplemented chronologically aging cells when the culture reached 50% of survival (mean CLS) (Figure 9A). At this time point, extracellular ethanol and acetate were completely depleted (Figure 9B), whilst glycerol was still present (Figure 9C). GSL supplementation determined a strong decrease in intracellular and extracellular glycerol (Figure 9C). This decrease corresponded temporally to the increase in trehalose, the content of which

started to rise again reaching levels higher than those of the single NAM supplementation (Figure 9D). All these changes in the carbon metabolism were accompanied by the extension of CLS (Figure 9A). Taken together all these data indicate that the GSL extract, on the one hand, specifically enhances glycerol catabolism and, on the other, that glycerol utilization is directed toward trehalose biosynthesis.

The enhancement of glycerol catabolism following GSL supplementation was further assessed by measuring the enzymatic activity of the FAD-dependent glycerol-3-phosphate dehydrogenase Gut2. In effect, glycerol catabolism specifically requires Gut1, a cytosolic glycerol kinase that phosphorylates glycerol to glycerol-3-phosphate (G3P). The latter is oxidized to DHAP with a concurrent reduction of FAD to $FADH_2$ by Gut2, which is located in the mitochondrial membrane (Figure 5) [80]. In GSL-supplemented chronologically aging cells, Gut2 activity was higher than that in unsupplemented cells (Figure 10A), matching the increase of glycerol depletion (Figure 8E). It is known that the electron pair of $FADH_2$ is transferred to the mobile electron carrier coenzyme Q, and via the latter to Complex III of the ETC. Electron flux, the final step of which is catalyzed by Complex IV, is coupled to proton pumping across the inner membrane of the mitochondria. The resulting proton motive force fuels ATP synthesis (Figure 5). Measurements of ATP levels showed that, in GSL-supplemented chronologically aging cells, these levels

remained higher than those in unsupplemented ones (Figure 10B). These results mirror respiratory results (Figure 4C,D) which pointed to a more efficient coupling of electron transport to ATP generation following GSL supplementation.

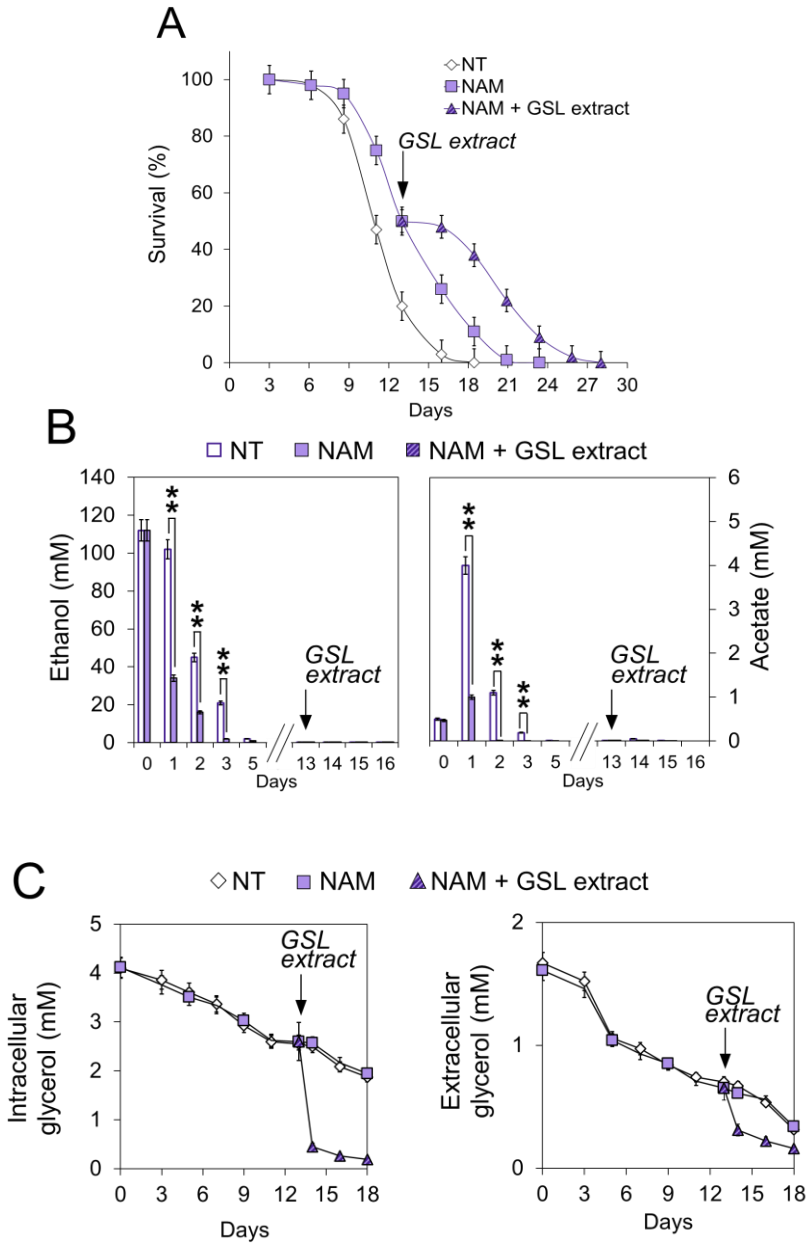

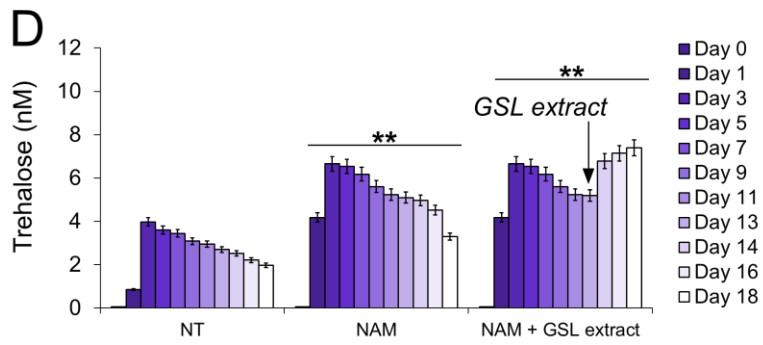

Figure 9. *GSL extract supplementation during chronological aging further extends the CLS of NAM treated cells.* Wt cells were grown as in Figure 2 and supplied with NAM (5 mM) at Day 0. At the time point where NAM stationary cultures showed 50% of survival (mean CLS), GSL extract (1 mM) was added. (**A**) CLS of the indicated cultures. In parallel, (**B**) extracellular ethanol and acetate content, (**C**) intracellular and extracellular glycerol levels, and (**D**) intracellular trehalose concentration were measured. All data refer to mean values determined in three independent experiments with three technical replicates each. SD is indicated (** $p \leq 0.01$).

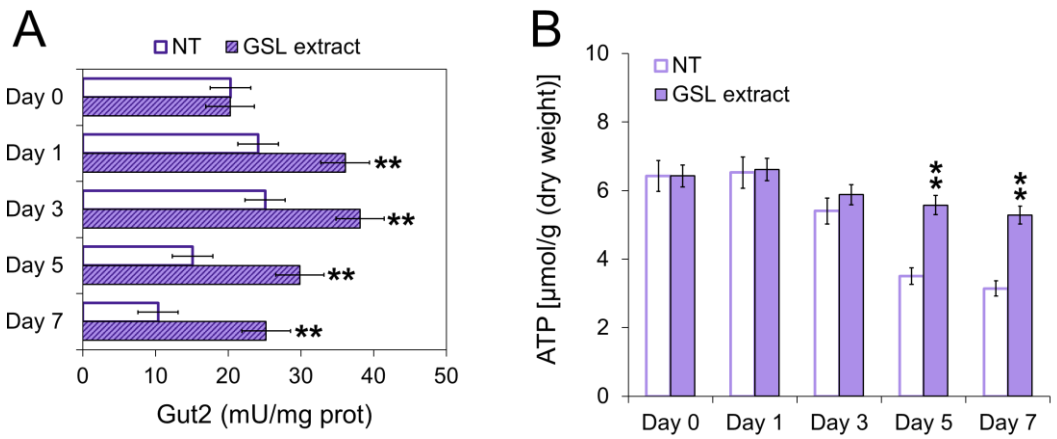

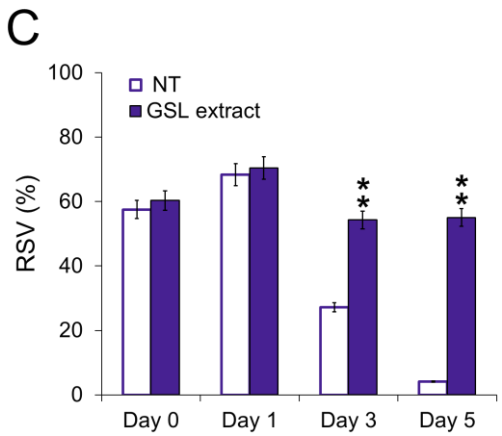

Figure 10. *GSL extract supplementation at the diauxic shift positively affects ATP levels*. At the indicated time points, (**A**) Gut2 enzymatic activity and (**B**) ATP content were evaluated for both treated and untreated cultures of Figure 2. For the same cultures: (**C**) bar charts of the respiration state value (RSV = [net_R / (J_{MAX} − J_{TET})] × 100). Day 0, diauxic shift. All data refer to mean values determined in three independent experiments with three technical replicates each. SD is indicated (** $p \leq 0.01$).

In keeping with this, the respiration state value (RSV), which represents the percentage of stimulation of oxidative phosphorylation compared to basal respiration capacity [339], was higher in GSL-supplemented cells than that in unsupplemented ones (Figure 10C) which is indicative of an increase in the oxidative phosphorylation efficiency. In this context, we can hypothesize, although yet fully speculative, that the increase in Gut2 activity together with that of SDH (Figure 7A), both by delivering electrons to the ETC via ubiquinone, might increase the electron flux through the ETC. This might reduce

electron stalling in the ETC decreasing the probability of unpaired electron leakage to produce ROS. In particular, Complex III generates $O_2^{\cdot -}$ during the Q-cycle linked to the formation of an unstable semiquinone intermediate, which can donate its unpaired electron to oxygen. In general, under some circumstances, increasing the electron flux through the ETC decreases ROS formation [352]. Furthermore, a more efficient electron transfer to ubiquinone by channeling the electrons via the tightly bound $FADH_2$ directly to the respiratory chain might explain the increase in its efficiency. In this regard, it has been observed that the yeast respiratory chain efficiency increased upon raising the growth temperature (from 30 °C up to 37 °C) and this temperature-dependent increase required Gut2 [353].

2.4 Conclusions

The GSL extract, which has been purified by us from a seed-press cake of *C. sativa*, displays a pro-longevity effect for yeast cells experiencing CLS. The increase of both mean and maximum CLS is also observed when the three aliphatic GSLs (GSL9, GSL10, and GSL11), which make up the extract, were supplied separately. CLS extension occurs since GSLs are effective in preserving mitochondrial functionality and drastically reduce the expected increase of $O_2^{\cdot -}$ that takes place as cells chronologically age. In addition, GSLs

have a significant impact on glycerol catabolism, the enhancement of which has positive effects on the phosphorylating respiration state and on the reserve carbohydrate trehalose: both prerequisites for a longer chronological lifespan [115,145,146,327,347]. Additional experiments are required to elucidate the precise molecular mechanism/target underpinning GSL-mediated effects during chronological aging.

CHAPTER 3

Targeting protein aggregation using a cocoa-bean shell extract to reduce α-synuclein toxicity in models of Parkinson's disease

by Farida Tripodi, Alessia Lambiase, Hind Moukham, Giorgia Spandri, Maura Brioschi, Ermelinda Falletta, Annalisa D'Urzo, Marina Vai, Francesco Abbiati, Stefania Pagliari, Andrea Salvo, Mattia Spano, Luca Campone, Massimo Labra and Paola Coccetti

https://doi.org/10.1016/j.crfs.2024.100888

Introduction

The food industry produces a high amount of waste during food processing and production. Under a circular economy perspective, the valorization of these by-products and waste is convenient not only from an economic and environmental point of view, but also because they are rich in active compounds with potentially useful bioactivities [74,354].

Cocoa beans (*Theobroma cacao* L.) are widely used in food production, but also for pharmaceutical and cosmetic purposes [73]. One of the main by-product of cocoa processing is the cocoa bean shell, which is produced in large quantities during the roasting process [74,75]. It has been estimated that global cocoa bean production in the 2015/2016 harvest reached approximately 3972 thousand tons, with the shell making up to 20% of the bean [78,89]. This represents roughly 600 thousand tons, most of which are discarded as waste and remain under-utilised, with limited applications as boiler fuel, animal feed, or fertilizer [78]. However, in recent years, cocoa shells have gained attention as a rich source of phenolic compounds, including caffeine and theobromine [78-82]. These two compounds, belonging to the methylxanthine class, are well-known for their antioxidant and anti-inflammatory properties [355-357], which contribute to mitigating oxidative stress, a key factor in neurodegenerative diseases. While the spotlight is often on

cocoa bean, recent studies suggest that cocoa shells, given their abundant availability and cost-effectiveness, can offer a significant potential as a sustainable resource for developing therapeutic agents [90-92]. Besides, new insights into the toxicological safety of two cocoa shell matrices has been also provided, opening opportunities for their use as functional food and nutraceutical products [82]. Recently, a new environmentally friendly and automated pressurised liquid extraction method has been developed and optimised to selectively recover theobromine and caffeine from cocoa shell by-products [80].

Parkinson's disease (PD), characterised by aberrant aggregates of the presynaptic protein α-synuclein (α-syn), is the second most common neurodegenerative disease [358-360]. Many *in vitro* and *in vivo* models mimicking α-syn pathology have been used over the years [361]; among them, *Saccharomyces cerevisiae* has been extensively employed as a model of synucleinopathies [362-365]. This unicellular eukaryote is a valuable tool in research due to its small size, short generation time, non-pathogenic nature, and ease of genetic manipulation [94]. The deep conservation of cellular mechanisms, such as DNA replication, cell division, and protein folding, from yeast to pluricellular eukaryotes, underscores its relevance for human disease studies. The most commonly used yeast model for Parkinson's disease research involves the heterologous expression of human α-syn, which induces toxicity

associated with aggregate formation, leading to vesicular trafficking impairment, increased oxidative stress and mitochondrial dysfunction, reduced lifespan, disturbed calcium signaling and altered autophagy [363,364,366-368]. As in more complex systems, the autophagic pathway is the major responsible for the clearance of oligomers and toxic aggregates, which cannot be degraded by the proteasome [369].

Although *S.cerevisiae* provides an excellent platform for preliminary studies, pluricellular eukaryotic models such as *Caenorhabditis elegans* [370,371], *Drosophila melanogaster* [372,373] and mice [374] are also extensively employed. Interestingly, a SH-SY5Y cell line overexpressing α-syn through a doxycycline-inducible promoter, is a valuable model for studying the molecular mechanisms underlying neuronal degeneration [375]. This eukaryotic system provides a robust platform for the *in vitro* screening of neuroprotective compounds to evaluate potential pharmaceutical compounds.

Here we show that an extract from cocoa bean shells increases lifespan and reduces reactive oxygen species (ROS) levels in a yeast model of synucleinopathy. Its anti-aging properties are associated with a stimulation of autophagy during the first two days of the stationary phase and a strong anti-aggregation feature both *in vivo* and *in vitro*. Consistently, our data also highlight a significant reduction of toxic α-syn oligomers in neuroblastoma cells

expressing α-syn, supporting the potential use of cocoa bean shell extract as a preventive agent against aggregation and its pathogenic effects.

3.1 Materials and methods

3.2.1 Chemical reagents

All chemicals were purchased from Merck unless otherwise stated. MS-grade solvents used for UPLC analysis, acetonitrile, water, and formic acid were provided by Romil. Reagents for SPR experiments were purchased from Cytiva. Cell culture media and supplements were provided by Euro-clone, Biolog plates and reagents were provided by Rigel Process and Lab.

3.2.2 Cocoa bean shell extract (CBSE) preparation

Cocoa bean shell (Trinitario variety) was kindly provided by a cocoa proces-sor after being roasted at 225 °C for approximately 20 min. The cocoa bean shell extract (CBSE) was obtained by Pressurised Liquid Extraction (PLE) using Dionex ASE350 (Dionex Sunnyvale, CA) as previously reported [80]. Briefly, 1 g of dry matrix, previously blended and sieved (300–600 μm) to obtain homogeneous samples, was extracted in 5 mL stainless steel cells

using 15% EtOH solution, 90 °C temperature, 5 cycles and a static time of 6 min at a pressure of 100 bar. After the extraction the ethanol was removed using a rotary evaporator (G3, heiVAP core, Heidolph Germany) with the bath temperature set at 40 °C and the extract was freeze-dried (ALPHA 1–2 LSC BASIC, Christ Germany) with a yield of 20.68 ±1.25 % of dry matrix.

3.2.3 Chemical characterization and quantitative analysis of caffeine and theobromine

The CBSE was analysed by Synapt G2-Si QToF instrument (equipped with a ZsprayTM ESI-probe) (Waters) coupled with an Acquity UPLC I- Class chromatography system (Waters). The UPLC analyses were carried out by a ACQUITY UPLC HSS T3 column (100 × 2.1 mm, 1.8 µm, Waters) fitted with a VanGuard cartridge (Waters) maintained at a fixed temperature of 35 °C. The products were separated using a linear gradient elution program, which consisted of water (A) and acetonitrile (B) (both with 0.1% formic acid) varying from 5 to 95% B (0–20 min). A flow rate of 0. 4 mL/min and an injection volume of 4 µL were adopted. The PDA acquisition wavelength range was 190–400 nm. For mass spectrometry analyses, both negative and positive ionization modes were applied. The ESI-modes were acquired in the range of 50–1200 m/z with a fixed source temperature of 120 °C and a desolvation temperature of 150 °C. A desolvation gas flow of 600 L/h was employed. The

capillary voltage was 3 kV (positive ionization mode) and - 2 kV (negative ionization mode). The instrument was controlled by a MassLynxTM v4.2 software (Waters). All MS acquisitions were performed the same day, with blank control between injections.

For quantitative analysis, the UPLC system was coupled with a UV detector acquiring data 283 nm. An external standard calibration method was used to quantify theobromine and caffeine in the extract. Standard solutions of theobromine and caffeine, each at a concentration of 1 mg/mL, were properly diluted with H_2O to create six-level calibration curves ranging from 1 to 200 µg/mL. The linearity of each calibration curve was verified using analysis of variance (ANOVA), and the linear model was found appropriate for the concentrations used and each level was acquired in triplicate. The instrument was controlled by a MassLynxTM v4.2 software (Waters). All MS acquisitions were performed the same day, with blank control between injections.

In addition, to detect analytes not visible with mass spectrometry, an NMR analysis was also conducted. Extract aliquots (4.3–4.7 mg) were resuspended in 1 mL deuterated water, containing 50 mM phosphate buffer pH7.4 and 0.4 mM TSP (internal standard). 700 µL of this solution were transferred to NMR tubes and analysed. NMR analyses were performed with a JEOL JNM-ECZ 600R spectrometer (resonance 1H 600.17 MHz) equipped with a 5 mm FG/RO DIGITAL AUTOTUNE probe. Monodimensional experiments

were carried out in the following conditions: 128 scans, 4 dummy scans, pre-saturation of the residual water signal, impulse at 90 °C of 8.3 μs, 64K data points, time of acquisition 7.7 s. For metabolite identification, literature data referred to NMR studies on cocoa samples [376,377] were used. To quantify the identified metabolites in the aqueous solution, the integrals of the selected 1H resonances were measured with respect to TSP as previously described [378]. Three replicates were made, and the results were expressed as μg/mg of extract ±SD.

3.2.4 Proteomic characterization

Proteins present in the CBSE were concentrated and separated from small molecules using molecular cut-off filtration (Amicon 10000 Da MWCO, Merck) with two washes with water. After protein precipitation with 80% Acetonitrile, pellets were resuspended in 25 mmol/L NH_4HCO_3 containing 0.1% RapiGest (Waters Corporation) and sonicated by immersion for 10 s before digestion, as previously described [379]. After 15 min of incubation at 80 °C, proteins were reduced with 5 mmol/L DTT at 60 °C for 15 min, and carbamidomethylated with 10 mmol/L iodoacetamide for 30 min at room temperature in darkness. Digestion was performed with sequencing-grade trypsin

(Promega) (1 µg every 25 µg of proteins) overnight at 37 °C. After digestion, 2% TFA was added to hydrolyze RapiGest and inactivate trypsin.

Tryptic peptides were used for label-free mass spectrometry analysis, LC-MSE, which was performed on a hybrid quadrupole time-of-flight mass spectrometer (Xevo G2-XS, Waters Corporation), coupled with a UPLC H-class system and equipped with an ESI source (Waters Corporation). Samples were injected into an analytical column ACQUITY Premier HSS T3 C18, 100 Å, 1.8 µm, 2.1 mm ×150 mm equipped with a vanguard FIT cartridge (Waters Corporation), for elution at a flow rate of 200 µl/min for 3 min at 2% mobile phase B before increasing the organic solvent B concentration from 2 to 50% over 90 min, using 0.1% v/v formic acid in water as reversed phase solvent A, and 0.1% v/v formic acid in acetonitrile as reversed phase solvent B. All of the lyses were performed in duplicate and analysed by LC-MSE as previously detailed [380]. In particular, in the low-energy MS mode, the data were collected with Masslynx software at a constant collision energy of 6 eV, while in the high-energy mode, fragmentation was achieved by applying a ramp from 15 to 35 eV. Scan time of 0.1 s, capillary voltage of 1 kV, cone voltage of 40 V, source temperature 120 °C, desolvation temperature of 600 °C with desolvation gas at 800 L/h were applied to acquire spectra in the range 50–1990 m/z. The time-of-flight analyzer was externally calibrated using Sodium formate from m/z 50 to 1990, and data were post-acquisition lock mass

corrected using the monoisotopic mass of the doubly charged precursor of [Glu1]-fibrinopeptide B (m/z 785.8426) delivered to the mass spectrometer at 100 fmol/µL. The reference sprayer was sampled every 30 s. The radio frequency (RF) applied to the quadrupole mass analyzer was adjusted in such a way that ions from m/z 300 to 2000 were efficiently transmitted, thus ensuring that any ion with a mass of less than m/z 300 only arose from dissociations in the collision cell. Peak detection and protein identification were performed with PLGS software (v 3.0.3) using a Uniprot *Theobroma cocoa* sequence database (v2024_04, 40947 unreviewed entries, 16 reviewed entries) and NCBI database (167551 entries). The following search criteria were used for protein identification: the default search parameters included the “automatic” setting for mass accuracy (approximately 10 ppm for precursor ions and 25 ppm for product ions); a minimum of one peptide match per protein, a minimum of two consecutive product ion matches per peptide, and a minimum of five total product ion matches per protein; up to one missed cleavage site allowed; carbamidomethyl-cysteine as fixed modification; and methionine oxidation as variable modification.

3.2.5 Yeast strains, growth analysis and chronological lifespan (CLS) determination

The *S. cerevisiae* strains used in this paper are reported in Table 1. Yeast cells were grown at 30 °C in minimal medium (Difco Yeast Nitrogen Base without amino acids 6.7 g/L), with 2% w/v glucose and supplements added in excess [112]. Cell growth was monitored by determining cell number using a Coulter Counter-Particle Count and Size Analyser, as described [278]. In parallel, the extracellular concentration of glucose and ethanol were measured in medium samples collected at different time-points using enzymatic assays (K-HKGLU and K-ETOH Megazyme) [112]. Duplication time (Td) was obtained by linear regression of the cell number increase over time on a semi-logarithmic plot. CLS of Figure 1 was measured according to [279] by counting colony-forming units (CFU) starting with 72 h (day 3, first-age point) after diauxic shift (day 0). The number of CFU on day 3 was considered the initial survival (100%). CBSE, dissolved in 20% ethanol by using an ultrasonic bath at 28 khz frequency and 90 W power for 3 min, was added to yeast cultures at the final concentration of 0.2% w/v. A 25X stock solution was prepared to properly dissolve the raw extract and at the same time to limit perturbations in cell culture medium composition after the supplementation. CLS experiments of Figure 2 and 3 were performed adding CBSE in the exponential phase, as in [381]. Briefly, cells were pre-grown until mid-late exponential

phase and then inoculated at 0.150 OD/mL into flasks containing fresh medium in the presence of CBSE at the final concentration of 0.05%, 0.1% or 0.2% w/v. Then, the medium was filtered through 0.22 µm filters and 0.1 mM ampicillin was added to preserve sterility throughout the duration of the experiments. Survival was assessed by propidium iodide staining (PI) at different time points with the Cytoflex cytofluorimeter (Beckman Coulter) and analysed with the Cytoflex software.

Table 1. *Yeast strains used in this study.*

Strain	Relevant Genotype	Source
wt [empty]	*BY4742 MATα his3Δ1 leu2Δ0 lys2Δ0 ura3Δ0 [pYX242]*	[382]
wt [αSyn]	*BY4742 MATα his3Δ1 leu2Δ0 lys2Δ0 ura3Δ0 [pYX242-SNCA]*	[382]
wt [αSyn] [ATG8-GFP]	*BY4742 MATα his3Δ1 leu2Δ0 lys2Δ0 ura3Δ0 [pYX242-SNCA] [pCu-ATG8-GFP]*	[382]
atg8Δ [αSyn]	*BY4742 MATα his3Δ1 leu2Δ0 lys2Δ0 ura3Δ0 atg8Δ::KanMX [pYX242-SNCA]*	This study

3.2.6 Analysis of reactive oxygen species (ROS) levels

ROS levels were analysed as previously reported [381]. Briefly, yeast cells were collected after 24 h treatment with the extract and 0.2 OD of cells were resuspended in PBS and stained with 5 µg/mL dihydroethidium (DHE) for 10 min. FACS analyses were performed with a Cytoflex cytofluorimeter (Beckman Coulter) and analysed with the Cytoflex software.

3.2.7 Protein extraction and immunoblotting from yeast proteins

Equal amounts of cells were collected and quenched using TCA 6% and lysed in lysis buffer (6 M UREA, 1% SDS, 50 mM Tris-HCl pH7.5, 5 mM EDTA), as reported in [381]. Western blot analysis was performed using anti-GFP antibody (Roche), anti-α-synuclein antibody (Sigma Aldrich) or anti-Cdc34 antibody [383].

3.2.8 Analysis of aggresomes in yeast

The intracellular protein aggresomes were analysed using the PROTEOSTAT® Aggresome detection kit (ENZO Life Sciences). Cells were collected following a 24 h treatment with 0.2% CBSE and 0.2 OD were suspended in PBS buffer and stained with the PROTEOSTAT® Aggresome detection reagent at a dilution of 1:1500 [381]. FACS analyses were conducted using a Cytoflex cytofluorimeter (Beckman Coulter) and analysed with Cytoflex software.

3.2.9 In vitro aggregation of α-syn and ThT assay

α-syn was purchased from Merck and dissolved at 70 μM in PBS. Protein samples (20 μL) were incubated at 37 °C in PBS up to 72 h under constant

shaking at 900 rpm with a thermo-mixer in the absence (cnt) or in the presence of the extract at 0.1 and 0.025 mg/mL or in the presence of caffeine and theobromine solution at 0.01 mg/mL. The ThT binding assay was performed according to [396], using a 20 μM ThT solution in PBS buffer. 180 μL of ThT solution were added to 20 μL of the aggregated α-syn samples, transferred into a black 96-well clear bottom multiwell plate and ThT fluorescence was read at the maximum intensity of fluorescence of 485 nm using a Victor X3 plate reader (PerkinElmer); fluorescence of blank samples was subtracted from the fluorescence values of all samples. In control experiments, no interference of the extract on ThT fluorescence was observed.

3.2.10 Surface plasmon resonance (SPR) analysis

The BIACORE X100 system (Cytiva-Pall) was utilised to analyse molecular interactions between α-syn and the CBSE *via* Surface Plasmon Resonance (SPR). α-syn was immobilised onto a carboxymethylated dextran surface of a CM5 sensor chip using amine-coupling chemistry, as recommended by the manufacturer (Biacore Sensor Surface handbook BR100571), with the instrument temperature set at 25 °C. The amine coupling procedure was performed using HBS-EP running buffer (0.01 M HEPES, 0.15 M NaCl, 0.003 M EDTA, and 0.005% v/v Surfactant P20, pH 7.4) at a flow rate of 5 μL/min.

The CM5 sensor chip was activated by injecting EDC/NHS (1:1) into both flow cells 1 and 2 for 10 min. α-syn was then injected into flow cell 2 at a concentration of 200 µg/mL in 10 mM sodium acetate, pH 3.1, and covalently immobilised at level of 1200 Response Units (RU). The remaining activated sites on the chip were subsequently blocked using 1 M ethanolamine (pH 8.5) in both cells. The association capacity of α-syn was determined by injecting two control antibodies, anti-α-syn (Sigma) recognizing the whole α-syn (positive control) and anti-α-syn33 (Sigma) recognizing α-syn oligomers (negative control), at a dilution of 1:2500 in HBS-EP running buffer at a flow rate of 10 µL/min. The lyophilized CBSE was resuspended in HBS-EP running buffer and injected at multiple concentrations for 5 min at 25 °C and a flow rate of 10 µL/min, with the running buffer injected as a blank under the same conditions. After injection, the analyte solutions were replaced by the running buffer at a continuous flow rate of 10 µL/ min for 5 min. Surface regeneration was achieved by injecting 50 mM NaOH for a contact time of 1 min. Each sensorgram was corrected for the response observed in the control flow cell 1 (no immobilised protein) and normalized to a baseline of 0 RU. The sensorgram curves were acquired using the BiacoreX100 Control software, version 2.0.2 (Cytiva- Pall), in manual run mode.

3.2.11 Biolog OmniLog system

The effect of CBSE was evaluated for its impact on metabolic abilities using various chemical agents. This was done using the Biolog OmniLog Phenotype MicroArray chemical sensitivity panels PM21-PM25, which include 120 chemical compounds at four different concentrations. The Biolog OmniLog System was employed to compare the chemical sensitivity for each drug of *wt[αsyn]* yeast cells with and without 0.2% CBSE. All plates were prepared following the manufacturer's instructions as outlined in the OmniLog ID System User Guide (Biolog). Yeast cell cultures were grown on agar plates at 30 °C and inoculated into 8 mL of minimal medium containing 2% glucose and YNB in sterile glass tubes. The cell suspension was measured using the BIOLOG Turbidimeter (Biolog) until a transmittance of 62% T was achieved. The suspension was prepared according to the BIOLOG PM protocol for yeast cells, using Dye E. 100 µL of cell suspension was added to each well and microplates were incubated in the OmniLog™ system at 30 °C for 72 h. The resistance and sensitivity profiles were compared using the appropriate OmniLog Biolog database (Biolog), with the y-maximum value of each kinetic growth curve being used for the analysis. Ratio between CBSE-treated and control cells were calculated, and compounds which showed a fold change >5 or <0.2 in at least three concentrations for each compound were considered as compounds towards which CBSE increases or decreases sensitivity.

3.2.12 Cell cultures

SH-SY5Y pTet-SNCA-FLAG were purchased from Merck. Cells were cultured on geltrex-coated plates at 37 °C in DMEM/F12 medium, containing 10% fetal bovine serum, 2 mM glutamine, 100 units/mL penicillin and 100 µg/mL streptomycin, in a humidified 5% CO_2 incubator. Doxycycline-inducible α-syn-expressing cells were selected against the antibiotic puromycin with a dose of 2 µg/mL. Induction of α-syn expression was achieved by adding 6 µg/mL doxycycline (doxy, from a 6 mg/mL stock in DMSO) for 48 h or 72 h. The CBSE was resuspended in water, sterile filtered and added to the medium at a final concentration of 150 µg/mL. For immunofluorescence assays, 160.000 cells were seeded on geltrex-coated glass cover slips in wells of a 24 multiwell plate and treated the day after for 48 h.

3.2.13 Protein extraction and immunoblotting for mammalian proteins

Total cell extracts were prepared using RIPA buffer (50 mM Tris-HCl, pH 7.5, 150 mM NaCl, 0.5% sodium deoxycholate, 1% NP-40, 0.1% SDS) plus protease inhibitor cocktail (Roche), and phosphatase inhibitor cocktail (Merck). Protein concentration was determined using the Bradford protein assay (Bio-Rad). Western blot analysis was performed using anti-α-syn antibody

(Merck), anti-phospho-T172-AMPK antibody (Cell Signaling), anti-AMPKα antibody (Cell signalling), anti-p62/SQSTM1 antibody (Merck), anti-phospho-Ser555-ULK1 antibody (Merck), anti-ULK1 antibody (Calbiochem) and anti-vinculin antibody (Sigma).

3.2.14 Immunofluorescence assay

After treating cells with doxycycline (Doxy) alone or in combination with CBSE (Doxy + Cocoa) for 48h, cells were washed with PBS, fixed with 4% formaldehyde for 15 min, and permeabilized with PBS-0.2% Triton X-100 for 10 min. Then, cells were washed three times in blocking solution (PBS-1% BSA), blocked at room temperature for 60 min, and then incubated overnight at 4 °C with the primary antibodies dissolved in blocking solution as follows: anti-oligomer A11 Polyclonal Antibody (1:40, Invitrogen), anti α-syn antibody (1:200, Merck). Then, cells were incubated with anti-rabbit secondary antibody (1:200) conjugated with AlexaFluor488, dissolved in a blocking solution, for 1 h at room temperature shield from light. Glasses were mounted with a DAPI containing mounting solution. The PROTEOSTAT R Protein aggregation assay (ENZO Life Sciences) was used to measure α-syn aggregates in cells as described by the manufacturer's instructions. Briefly, after treating cells as mentioned above, cells were washed carefully twice with 1X PBS,

then fixed with 4% formaldehyde for 30 min at room temperature and permeabilized with Permeabilizing solution for 30 min on ice. Following PBS washes, the slides were dispensed in Proteostat dye and incubated for 30 min at room temperature. All treated slides were washed and mounted with a mounting medium with DAPI for nuclear staining and imaged under a Thunder fluorescence microscope (Leica). Image analysis was performed using the ImageJ software (NIH).

3.2.15 Statistical Analysis

Experiments were conducted in triplicate. Results are presented as mean values ± standard deviations (SD). Statistical data analyses were made using the two-tailed Student's t-test with significance set at $p < 0.05$, or by one-way ANOVA test ($*p \leq 0.05$ and $**p \leq 0.01$).

3.3 Results

3.3.1 Characterization of the cocoa bean shell extract

The cocoa bean shell extract (CBSE), which was optimised and partially characterised previously [80], was subjected to further analyses to better

define its composition. For this purpose, both UPLC-PDA-MS and NMR analyses were performed, and the compounds identified or tentatively identified are described in Tables 2 and 3. The identity of some compounds was achieved on the basis of the accurate mass and the associated errors, isotopic distribution, m/z values comparison with those reported in the literature and using literature databases.

NMR analysis identified and quantified mainly amino acids, such as Ala, Leu, Ile, Val, Phe, Asp, Tyr, and intermediates of TCA cycle such as fumarate, succinate, malate and citrate. The last one, together with lactate and glycerol, were the most abundant ones (Table 2, Figure S1A). MS analysis revealed the presence of the two methylxanthines, caffeine and theobromine (theobromine: 52.74 ± 8.12 µg/mg extract, caffeine: 12.98 ± 3.96 µg/mg extract), and of other less abundant metabolites, like hydroxy-jasmonic acid sulfate, procyanin B, cyanidin-3-O (2″ galloyl)-galactoside, as well as of some unknown compounds that could not be clearly identified (Table 3, Figure S1B).

According to a Bradford quantification, the extract also contained 6 µg/mg of proteins. Although the amount of protein was very low, a proteomic analysis was performed to achieve a characterization. Mass spectrometry analysis of the proteins present in the extract revealed the presence of 5 proteins from *Theobroma cacao* (Table 4), with Vicilins and a 21 kDa seed protein being the most abundant ones according to peptide intensity, as expected from

literature [384]. However, we cannot exclude the presence of other proteins not identified due to low level of annotation in the database of *T. cacao,* although both UniProt and NCBI databases were used.

Table 2. *Metabolities identified by NMR analysis in the ^{1}H spectrum.*

Metabolite	**^{1}H chemical shift (ppm)**	**Multiplicity (J [Hz])**	**Concentration µg/mg ± SD**
Leucine	0.96	d [6.2]	3.37 ± 0.09
Isoleucine	1.01	d [7.1]	1.82 ± 0.02
Valine	1.05	d [7.1]	3.22 ± 0.01
2,3-Butanediole	1.15	d [6.4]	1.51 ± 0.10
Lactate	1.33	d [6.9]	31.56 ± 1.12
Alanine	1.48	d [7.2]	4.64 ± 0.09
Acetate	1.92	s	7.43 ± 0.22
GABA	2.30	t [6.1]	2.42 ± 0.06
Succinate	2.41	s	3.74 ± 0.06
Citrate	2.55	d [15.3]	13.02 ± 0.12
Aspartate	2.82	dd [17.4, 3.8]	1.69 ± 0.01
Glycerol	3.66	dd [11.7, 4.3]	15.90 ± 0.56
Mannitol	3.87	dd [11.9, 2.9]	4.76 ± 0.04
Pyroglutamate	4.18	dd [9.1, 5.9]	7.16 ± 0.03
Malate	4.30	dd [10.2, 2.9]	3.53 ± 0.15
Fumarate	6.53	s	0.08 ± 0.01
Tyrosine	6.90	d [8.4]	1.26 ± 0.02
Phenylalanine	7.43	m	4.03 ± 0.05
Formate	8.46	s	0.46 ± 0.01

Table 3. *Chemical compounds identified or tentatively identified by UPLC-PDA-MS.*

m/z expected	m/z calculated	Ionization mode	Error (ppm)	Molecular formula	Proposed compound	Reference
181.0720	181.0733	M + H	5.5	$C_7H_8N_4O_2$	Theobromine	[80,395]
195.0877	195.0888	M + H	5.9	$C_8H_{10}N_4O_2$	Caffeine	[80]
	263.0636	M + H			Unknown	
	279.0407	M + H			Unknown	
	297.0509	M + H			Unknown	
305.0695	305.0699	M-H	-0.57	$C_{12}H_{18}O_7S$	Hydroxy-jasmonic acid sulfate	[395]
327.0510	327.0517	M-H	-2.06	$C_{17}H_{12}O_7$	Unknown	
399.0838	399.0835	M + H	0.78	$C_{28}H_{14}OS$	Unknown	
	563.1732	M + H			Unknown	
579.1497	579.1486	M + H	1.90	$C_{30}H_{26}O_{12}$	Procyanidin B	[80,394]
601.1188	601.1183	M + H	0.83	$C_{28}H_{24}O_{15}$	Cyanidin-3-O(2''galloyl)-galactoside	[394]
	617.0954	M + H			Unknown	
467.1195	467.1214	M-H	-4.07	$C_{21}H_{24}O_{12}$	Unknown	

3.3.2 Supplementation of CBSE extends CLS of yeast cells expressing human α-syn

Since yeast *S.cerevisiae* has been extensively employed as model system to study the cytotoxic effects of α-syn in PD and other synucleinopathies [365], we wished to test in the context of a standard CLS experiment [385] whether cocoa-shell treatment might have any ameliorating effect on the age-dependent α-syn-mediated cell death [368]. To this end a humanised yeast

model of PD overexpressing human α-syn was used. As shown in Figure 1A, no significant differences were observed in the duplication time (Td) between cells expressing α-syn and wt ones grown on minimal medium in 2% glucose (Figure 1A). Consistently, during the exponential phase, when growth is sustained by a prevalent fermentation-based metabolism, the glucose decrease was accompanied by ethanol accumulation that in both yeast cultures followed the same kinetics (Figure 1B). Once defined the growth profile, CBSE was added to both cultures at the onset of chronological aging, namely at the diauxic shift, and CLS was determined by CFU scoring. In line with previous reports [368], α-syn expression reduced CLS (Figure 1C). Interestingly, CBSE supplementation increased both mean and maximum CLS (Figure 1C and D), as well as the survival integral (SI, Figure 1D), defined as the area under the CLS curves [292]. Indeed, the SI increased by about 38% for wt and 89% for α-syn expressing cells, indicative of a pro-longevity effect of the CBSE. Starting from these results and being specifically interested in α-syn aggregation and its cytotoxic outcome, subsequent analyses were performed only with cells expressing α-syn.

A

Strain	Td (h)
wt [empty]	2.44 ± 0.38
wt [α-syn]	2.49 ± 0.36

B

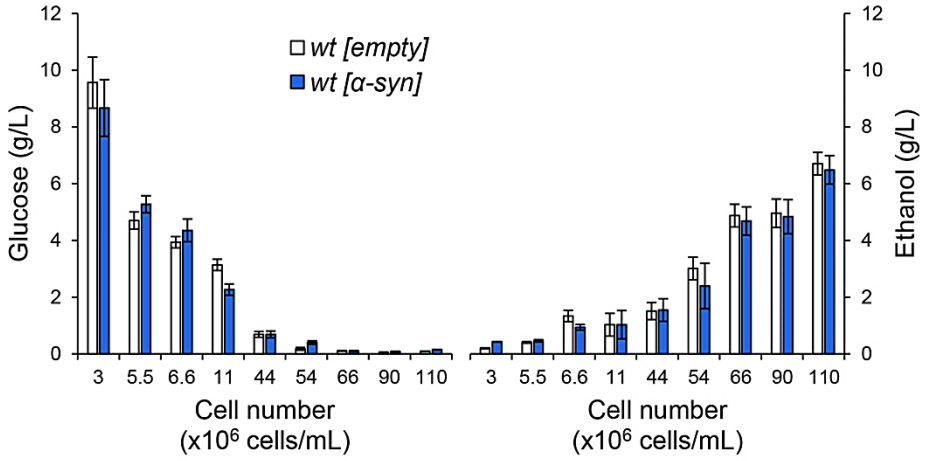

C

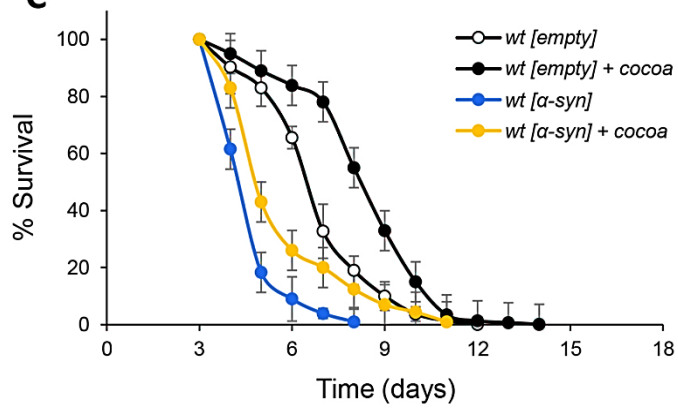

D

Strain	Mean CLS	Max CLS	SI CLS curve
wt [empty]	6.45 ± 0.40	8.93 ± 0.45	315.50 ± 22.01
wt [empty] + cocoa	8.26 ± 0.41**	10.38 ± 0.51**	435.20 ± 21.76**
wt [α-syn]	4.22 ± 0.21**	5.60 ± 0.28**	138.75 ± 6.92**
wt [α-syn] + cocoa	4.79 ± 0.24**	8.22 ± 0.41*	262.50 ± 13.11**

Figure 1. *CBSE supplementation at the diauxic shift extends CLS*. Wild-type (*wt[empty]*) and α-syn overexpressing (*wt[α-syn]*) cells were grown in minimal

medium containing 2% glucose and required supplements in excess. (**A**) Cell growth was monitored by counting cell number over time and duplication time (Td) of wt and α-syn expressing cells was calculated as ln2/k, where k is the constant rate of exponential growth. In parallel, (**B**) extracellular concentration of (left) glucose and (right) ethanol were measured in medium samples collected at different time-points. At the diauxic shift (day 0), CBSE (cocoa) was added and (**C**) survival over time of the indicated strains was assessed by colony-forming capacity on YEPD plates. 72 h after the diauxic shift (day 3) was considered the first age-point, corresponding to 100% survival. (**D**) Quantification of chronological survival: data referring to the time-points (days) where chronological aging cultures showed 50% (Mean CLS) and 10% (Max CLS) of survival, as well as, survival integral (SI) measured as reported [292]. All data refer to mean values determined in three independent experiments with three technical replicates each. Standard deviations (SD) are indicated. *$p \leq 0.05$ and **$p \leq 0.01$.

When CBSE was added to exponentially growing cells, up to 0.2%, no effect on the growth rate was observed (data not shown), while a significant dose-dependent reduction of intracellular ROS was detected 1 day after its addition, supporting an antioxidant effect (Figure 2A). Nevertheless, both the mean and the maximal CLS, as well as the SI increased (more than 70%) only at the highest concentration (0.2%) (Figure 2B), in accordance with the results reported above.

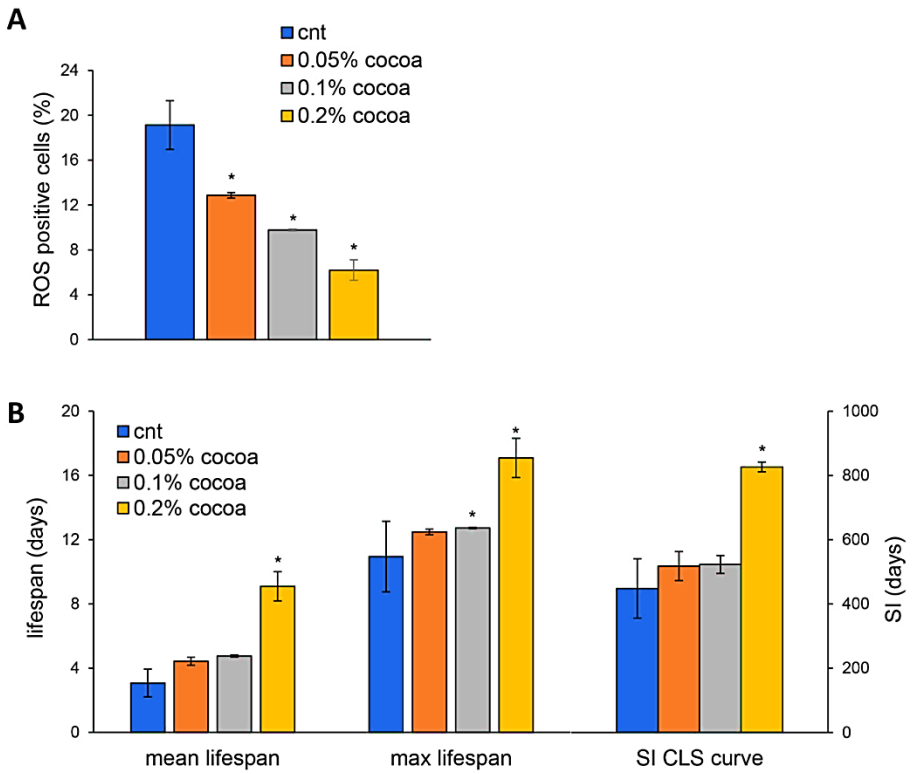

Figure 2. *The CBSE extends yeast lifespan and reduces ROS levels.* (**A**) ROS content of yeast *wt[α-syn]* cells grown in medium containing 2% glucose in the absence or presence of 0.05%, 0.1% or 0.2% CBSE, added in the exponential phase of growth. (**B**) Mean and maximal lifespan and SI of cells in (A). Histograms represent mean ±standard deviation of at least two independent experiments. *p <0.05.

3.3.3 The anti-aging effect is independent from caffeine and theobromine

Since the CBSE contains both metabolites and proteins (Tables 2–4), we performed a size-exclusion fractionation to separate the protein fraction

(molecular weight >10 kDa) from the metabolite fraction and tested them separately on the yeast model. As shown in Figure 4A and B, the metabolite fraction increased mean lifespan and reduced ROS levels (albeit to a lesser extent than the total extract), while the protein fraction showed no significant activity, suggesting that metabolites are the main responsible for the antioxidant and anti-aging effect of the CBSE. This is consistent with the very low amount of protein present in the extract.

Among the metabolites identified in the CBSE, caffeine and theobromine represent about 10% of the total extract (see paragraph 4.3.1). To analyse whether the observed anti-aging effect could be attributed to the presence of these two methylxanthines, α-syn overexpressing cells were treated with caffeine, theobromine or a combination of both, mimicking their abundance in the CBSE. Neither single treatments, nor their combination, showed any anti-aging effect (Figure 4C) or antioxidant properties (Figure 4D), suggesting that the pro-longevity function might depend on other metabolites or result from a synergistic/combined action with other molecules of the CBSE.

Table 4. *List of proteins by LC-MS^E in cocoa extract with the corresponding peptides*

Entry (Database)	Accession	protein Description	protein score	MW	protein matched Products	protein matched Peptides	Cov (%)	Peptide Intensity Sum	Sequence	MH + Error (ppm)	Score
ASP_THECC (Unipot)	P32765	21 KDa seed protein	615	24438	30	7	30.77	203620	(R)HSDDDGQIR(L)	0.9339	6.6629
									(R)SDLD-NGTPVIFSNADSKDDVVR(	0.4055	5.9953
									(R)VSTDVNIEFVPIR(D)	2.7383	5.3816
									(R)RSDLD-NGTPVIFSNADSK(D)	-2.3825	5.2396
									(R)LDNYDNSAGK(W)	-3.3845	5.1266
									(R)ATGQSCPEIVVQR(R)	1.7676	4.8949
A0A061EM85_THECC (Uniprot)	A0A061EM85	Vicilin-A_putative	200	66198	37	9	17.67	75441	(R)QDRR(E)	-1.8736	6.2310

Entry (Database)	Accession	protein Description	protein score	MW	protein matched Products	protein matched Peptides	Cov (%)	Peptide Intensity Sum	Sequence	MH + Error (ppm)	Score
A0A061EM85_THECC (Uniprot)	A0A061EM85	Vicilin-A_putative	200	66198	37	9	17.67	75441	(K)EQER(G)	-0.3204	5.6220
									(K)ELSFGVPSK(L)	1.3752	5.6153
									(R)SEEEEGQQR(N)	-1.5498	5.3042
									(R)GTVVSVPAGSTVYVVSQDNQEK(L)	3.0933	5.2171
									(R)EQEEESEEETGEFQQVK(A)	1.6377	5.1098
									(R)QQEEELQR(Q)	-3.0807	4.8992
									(R)EKLEEILEEQR(G)	-1.8284	4.7921
									(K)LTIAVLALPVNSPQK(V)	-0.6553	4.6108

Entry (Database)	Accession	protein Description	protein score	MW	protein matched Products	protein matched Peptides	Cov (%)	Peptide Intensity Sum	Sequence	MH + Error (ppm)	Score
VCL_THECC (Uniprot)	Q43358	Vicilin	167	61483	32	8	17.33	55233	(R)QDRR(E)	-1.8736	6.2310
									(K)EQER(G)	-0.3204	5.622
									(R)SEEEEGQQR(N)	-1.5498	5.3042
									(R)GTVVSVPAGSTVYVVSQDNQEK(L)	3.0933	5.2171
									(R)EQEEESEEETGEFQQVK(A)	1.6377	5.1098
									(R)QQEEELQR(Q)	-3.0807	4.8992
									(R)EKLEEILEEQR(G)	-1.8284	4.7921
									(K)LTIAVLALPVNSPQK(V)	-0.6553	4.6108

Entry (Database)	Accession	protein Description	protein score	MW	protein matched Products	protein matched Peptides	Cov (%)	Peptide Intensity Sum	Sequence	MH + Error (ppm)	Score
A0A061GTA7_THECC (uniport)	A0A061GTA7	Uncharacterized pro-	117	10317	4	1	7.53	5242	(K)IEEHQSY(-)	-0.1395	5.2605
A0A061GZ27_THECC (Uniprot)	A0A061GZ27	Putative plant transposon protein domanin-con-	100	12772	6	1	13.76	6904	(M)NQCHFSEVSCSICQK(V)	0.6846	4.8622
CAA44494.1 (NCBI)	CAA44494.1	vicilin_partial	1582	54423	81	13	23.7	503177	(R)EQEEESEEETFGEF(-)	0.2798	7.8005
									(R)QDRR(E)	-1.8736	7.1311
									(R)REQEEESEEETFGEF(-)	-0.7810	6.6848
									(R)NNPYYFPK(R)	0.4712	6.3261
									(R)DEEGNFK(I)	-1.2679	6.2127
									(R)SEEEEGQQR(N)	-1.5498	6.2030
									(K)ESYNVQR(G)	2.3721	6.1794

Entry (Database)	Accession	protein Description	protein score	MW	protein matched Products	protein matched Peptides	Cov (%)	Peptide Intensity Sum	Sequence	MH + Error (ppm)	Score
CAA44494.1 (NCBI)	CAA44494.1	vicilin_partial	1582	54423	81	13	23.7	503177	(R)GTVVSVPAG-STVYVVSQDNQEK(L)	3.0933	6.1217
									(K)EQER(G)	-1.8439	5.9501
									(R)QQEEELQR(Q)	-3.0807	5.7974
									(R)EKLEEILEEQR(G)	-1.8284	5.6899
									(K)LTI-AVLALPVNSPG K(Y)	-0.6553	5.5105
									(K)LEEILEEQR(G)	3.2998	5.3213
									(R)EQEEESEEE (T)	1.8693	0
									(R)EQEEESEEET (F)	1.9878	0

Entry (Database)	Accession	protein Description	protein score	MW	protein matched Products	protein matched Peptides	Cov (%)	Peptide Intensity Sum	Sequence	MH + Error (ppm)	Score
CAA44494.1 (NCBI)	CAA44494.1	vicilin_partial	1582	54423	81	13	23.7	503177	(R)EQEEESEEETFGE(F)	-1.9716	0
									(R)EQEEESEEETGEF(-)	0.1171	0
									(R)EQEEESEE(E)	-2.1412	0

3.3.4 The CBSE binds α-syn and reduces its aggregation

In the last years, several data reported that natural extracts could exhibit direct fibrillation-inhibiting effects [386]. Thus, we wondered if the anti-aging effect of the CBSE could be due to a reduction in α-syn aggregation. A very strong decrease of intracellular aggresomes was observed in yeast cells treated with the CBSE for 24 h, with a 5-fold decrease compared to control cells (Figure 4A), showing its potential in reducing the aggregation of misfolded proteins. Thus, to evaluate a direct effect of the extract on the aggregation process, α-syn fibrillation experiments were performed *in vitro* and the ThT emission fluorescence signal was used to quantify fibrils formation over time. In the absence of the CBSE, the ThT fluorescence showed the typical sigmoidal shape, indicating the aggregation of the protein; this behaviour completely disappeared in the presence of the extract (at both concentrations, Figure 4B). Interestingly, caffeine and theobromine together, although had no effect on yeast longevity and ROS content (Figure 3C and D), showed a partial inhibitory effect on the aggregation of α-syn, Figure S2A).

A direct effect of the extract on aggregation would imply a direct interaction among the components of the CBSE and α-syn. To explore this hypothesis, α-syn protein was immobilised on a CM5 sensor chip for surface plasmon resonance (SPR) analysis. To validate the suitability and selectivity of the

chip, anti α-syn (which binds free and aggregated α-syn) and anti-α-syn33 (which binds only α-syn aggregates) antibodies were utilised as positive and negative controls, respectively, and were injected into the SPR system. While the anti-α-syn antibody bound the protein on the chip, the one specific for the aggregated α-syn showed no binding at all (Figure S2B). These results showed that the immobilised α-syn protein on the sensor chip surface was in its non-aggregated form and thus was employed to assess its direct binding with the CBSE. Results obtained from the SPR assay indicate that the CBSE could bind to α-syn protein in a concentration-dependent manner (Figure 4C). Indeed, five increasing concentrations of the extract were tested (0.64 mg/mL, 1.27 mg/mL, 2.54 mg/mL, 5.08 mg/mL and 8 mg/mL) and the response signal increased as a function of the rising concentration of the sample (Figure 4D). This indicates that there are compounds in the CBSE that directly bind to α-syn, and can explain the inhibitory effect on the amyloid aggregation of α-syn (Figure 4B). Finally, we tested caffeine and theobromine, which did not appear to bind to the protein (data not shown). However, considering that the molecular weights of caffeine (194.19 g/mol) and theobromine (180.164 g/mol) are near the detection limit of the instrument (100 Da), we cannot exclude that the binding was not detected due to technical limitations.

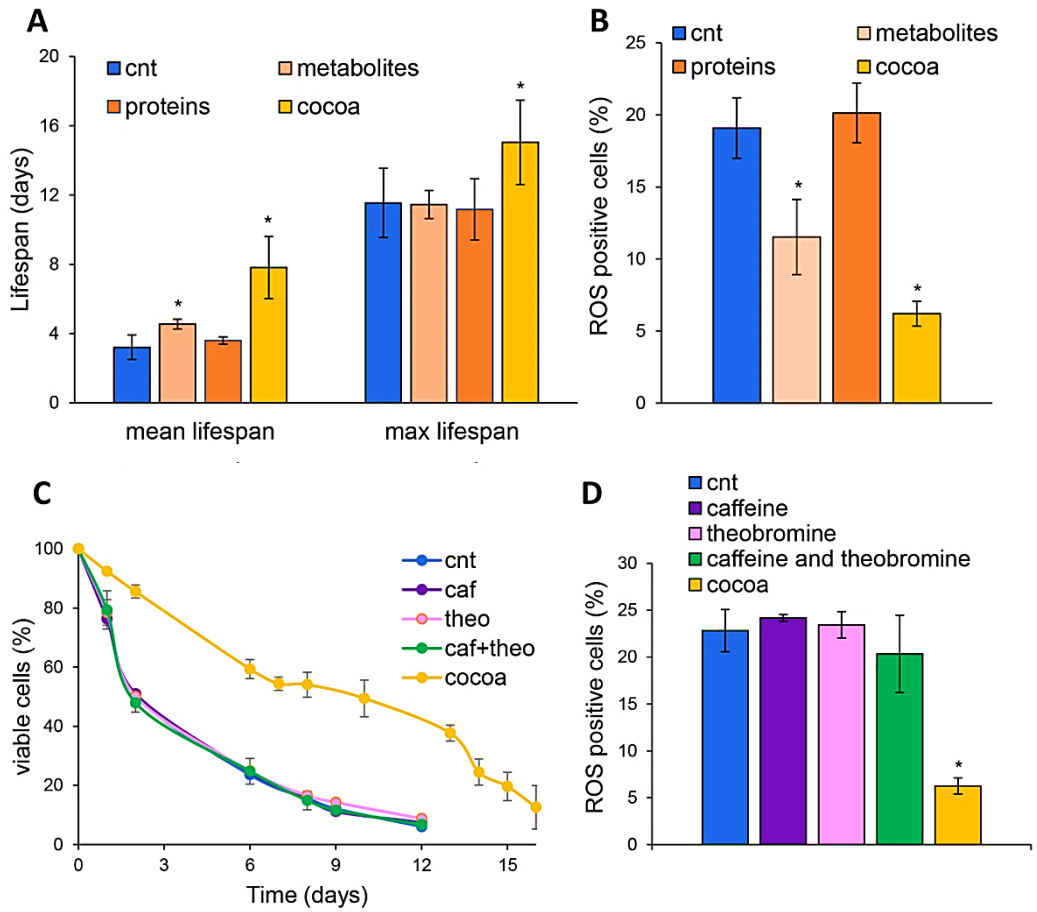

Figure 3. *The effect of the CBSE is independent from caffeine and theobromine.* (**A**) CLS of yeast *wt [α-syn]* cells in medium containing 2% glucose in the absence (cnt) or presence of 0.2% CBSE, and its contained metabolites and proteins. (**B**) ROS content of cells treated for 24 h as in (A). (**C**) CLS of yeast *wt [α-syn]* cells in medium containing 2% glucose in the absence or presence of 0.2% CBSE, caffeine, theobromine or a combination of the two (25.96 µg/mL caffeine and 105.4 µg/mL theobromine). (**D**) ROS content of cells treated for 24 h as in (C). Results are reported as the mean ±standard deviation of three independent experiments. *p <0.05.

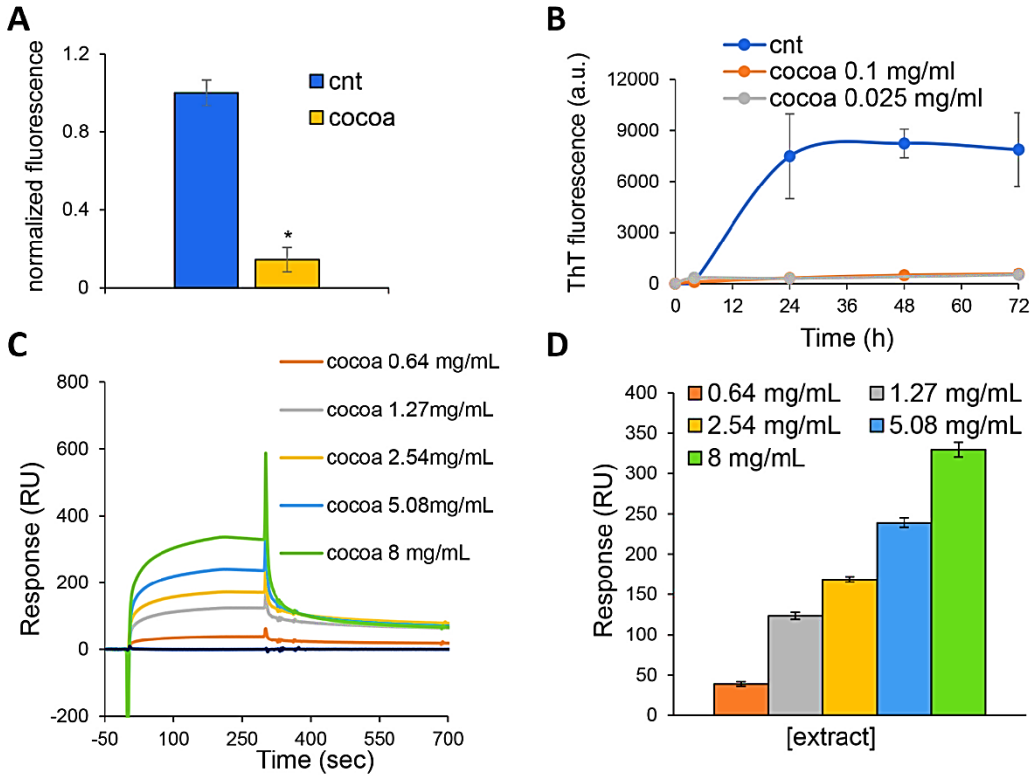

Figure 4. *The CBSE inhibits α-syn aggregation.* (**A**) Fluorescence intensity obtained from flow cytometry analysis of aggresomes of yeast *wt [α-syn]* cells in medium containing 2% glucose in the absence (cnt) or presence of 0.2% CBSE. (**B**) α-syn aggregation process, followed by ThT fluorescence, in the absence (cnt) or presence of the CBSE (0.1 and 0.025 mg/ml). (**C**) SPR sensorgrams of CBSE at different concentrations (8 mg/mL, 5.08 mg/mL, 2.54 mg/mL, 1.27 mg/mL, 0.64 mg/mL) display binding toward α-syn on CM5 sensor chip surface. (**D**) The CBSE shows dose-dependent binding activity to α-syn protein. Results are reported as the mean ±standard deviation of at three independent experiments.

3.3.5 The CBSE stimulates autophagy in yeast cells

In an attempt to identify cellular changes occurring upon treatment with the CBSE, a high throughput screening for sensitivity against antibiotics, chemicals and osmolytes was performed. The chemical resistance and sensitivity profile due to the CBSE of the yeast strain overexpressing α-syn was measured using the Biolog Phenotype MicroArrays PM21-PM25 chemical sensitivity panel, which contains 120 assays of chemical sensitivity. Each plate contains 24 different chemical agents in 4 different concentrations, that were divided into 6 groups based on their structure and function: ions, cyclic compounds, organic compounds, chelators, antibiotics, and nitrogen compounds (Table S1). In the presence of 0.2% extract, yeast cells showed increased resistance to several compounds; interestingly most of them have been described for their effect on autophagy in different models (Figure 5, Table S2).

The autophagic pathway is normally activated in stationary phase cells and is the major process involved in the clearance of α-syn aggregates [364]. Therefore, to evaluate the activation of the autophagic process in cells treated with the CBSE, we monitored the accumulation of free GFP in cells expressing Atg8-GPF fusion protein, whose cleavage is indicative of autophagy activation. Interestingly, a significant increase in the cleavage of Atg8-GFP was observed 1 day, and even more, 2 days after the extract addition,

reflecting the activation of the autophagic process in such condition (Figure 6A and B).

However, in *atg8Δ* cells, CBSE was still able to significantly reduce both intracellular ROS level and aggresomes (Figure 6C and D), suggesting that the stimulation of the autophagic process is not the only pathway involved in the pro-longevity function of the CBSE.

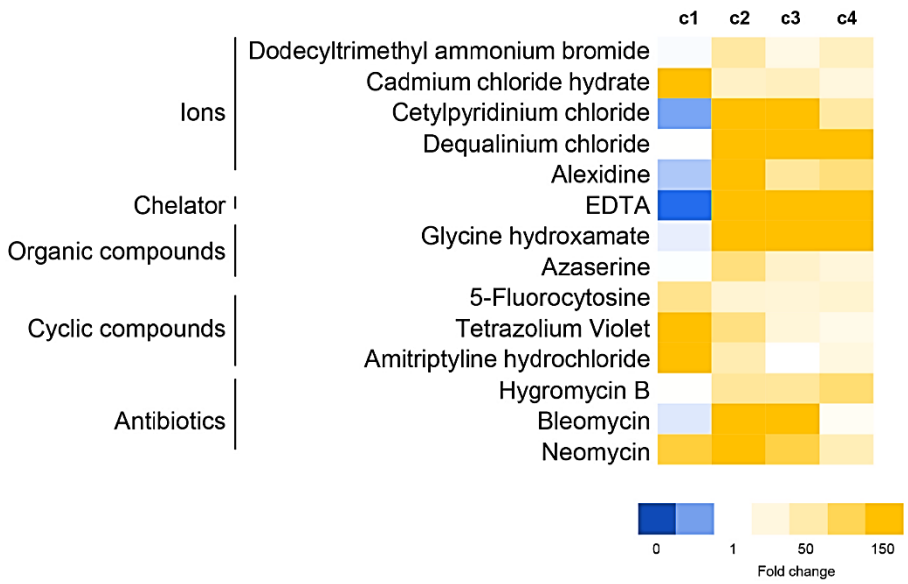

Figure 5. *Drug sensitivity upon CBSE treatment.* Heatmap of sensitivity of *wt[α-syn]* cells to selected drugs in the presence of CBSE compared to the control con-dition, measured by Biolog OmniLog Phenotype MicroArray. Fold changes (treated/cnt) in y-maximum value were calculated and compounds were selected when fold change was >5 or <0.2 in at least three concentrations. Colour scale indicates increased resistance (yellow) or decreased resistance (blue) after 72 h growth.

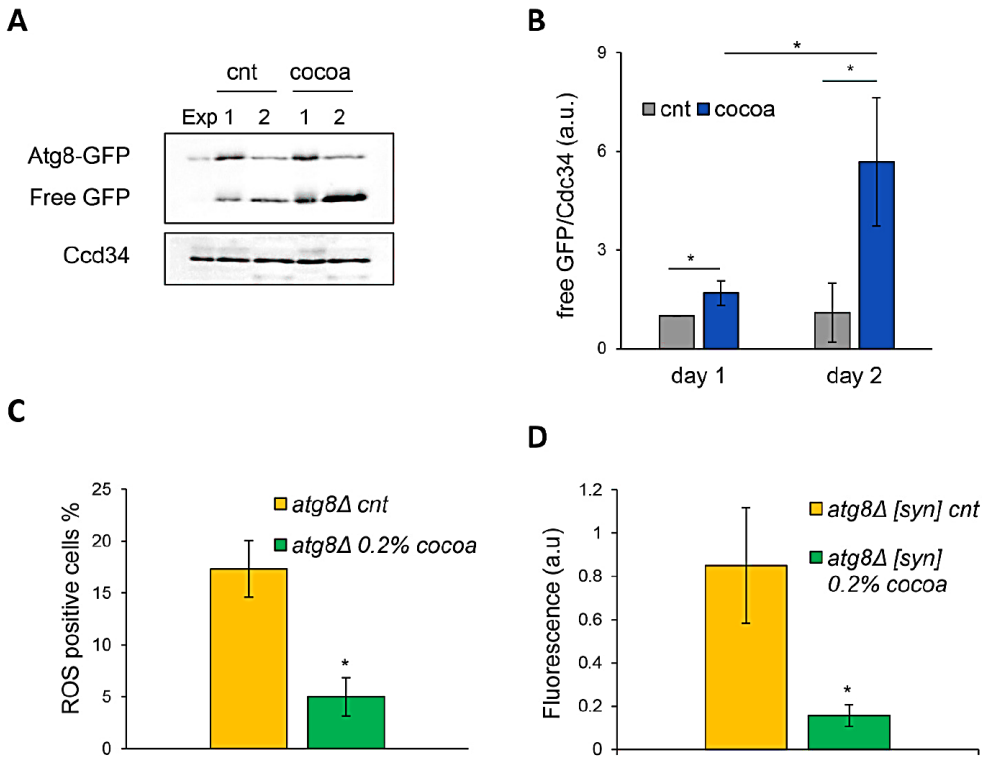

Figure 6. *The CBSE activates autophagy in yeast.* (**A**) Western analysis using anti-GFP antibody on total extracts from *wt[α-syn][Atg8-GFP]* cells treated with 0.2% CBSE for 1 and 2 days. Anti-Cdc34 antibody was used as loading control. (**B**) Quantification of free GFP of three independent experiments performed as in (A). (**C**) ROS content of *atg8Δ[α-syn]* cells in medium containing 2% glucose in the absence (cnt) or presence of 0.2% CBSE for 24 h. (**D**) Fluorescence intensity obtained from flow cytometry analysis of aggresomes of yeast *atg8Δ[α-syn]* cells in medium containing 2% glucose in the absence (cnt) or presence of 0.2% CBSE for 24 h. Results are reported as the mean ±standard deviation. **p* <0.05.

3.3.6 The CBSE reduces α-syn aggregates in neuroblastoma cells

In order to further investigate the effects of the CBSE, we turned to SH-SY5Y neuroblastoma cells expressing α-syn under a doxycycline- inducible promoter [375]. As expected, doxycycline induced an increase of monomeric α-syn level, which was not affected by treatment with the CBSE both at 48 h and 72 h (Figure 7A–C). Although the extract induced the phosphorylation of the energy sensor AMPK, no change of either pULK1 or p62 level was observed, suggesting that the CBSE does not activate the autophagic pathway in neuroblastoma cells (Figure 7A and B).

One of the key processes for the pathogenesis of Parkinson's disease is the assembly of toxic oligomeric species of α-syn. Then, since we have shown that the CBSE is able to bind and inhibit α-syn aggregation (Figure 4), the level of α-syn oligomers was investigated in neuroblastoma cells treated with the CBSE. Strikingly, a significant reduction of α-syn oligomers, as well as of intracellular aggresomes were observed upon CBSE treatment (Figure 7D and E). These data suggest that the CBSE prevents the formation of toxic oligomeric species and not their clearance through the autophagic degradation.

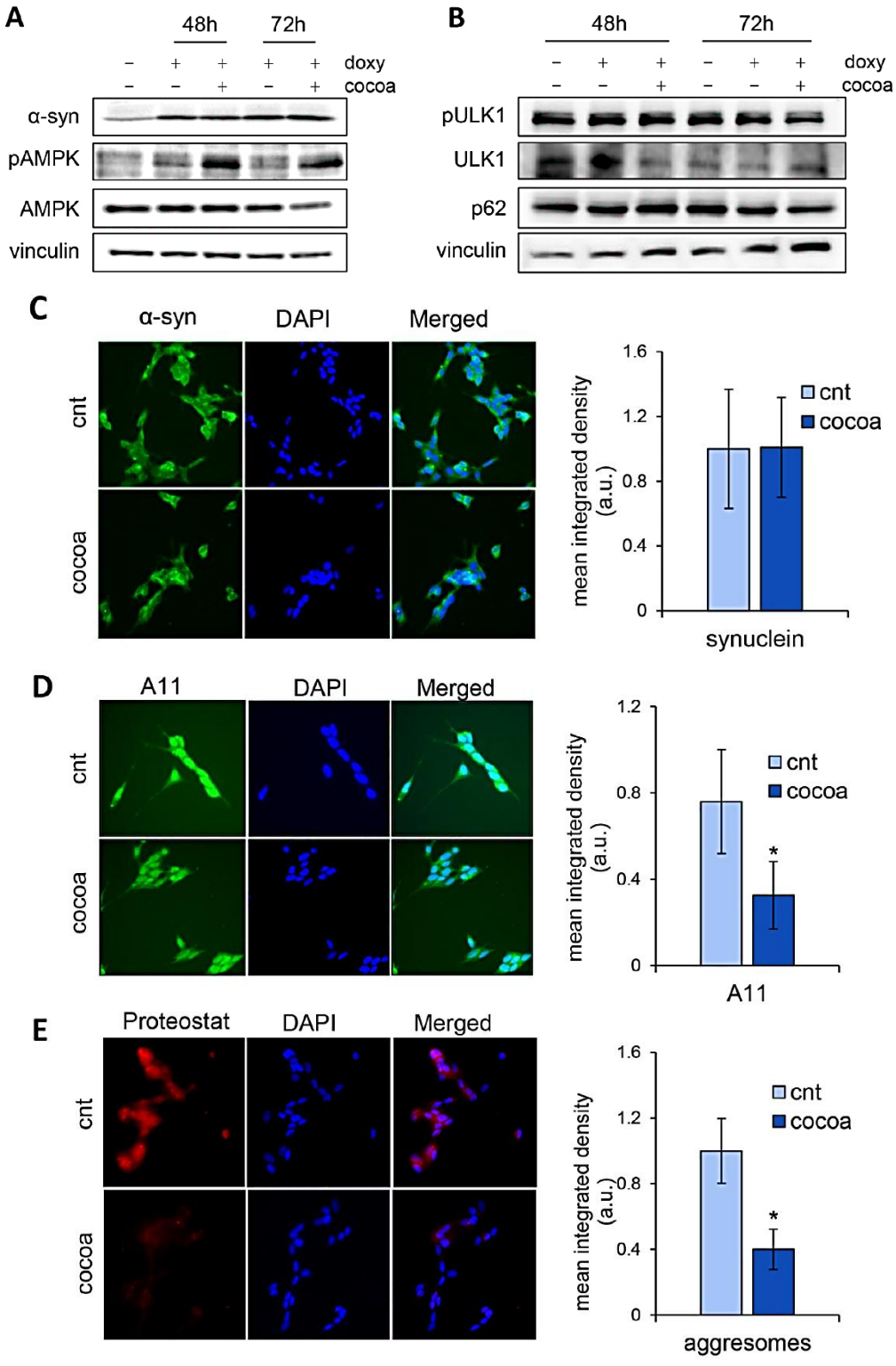
A
48h
72h
doxy
cocoa
α-syn
pAMPK
AMPK
vinculin
B
48h
72h
doxy
cocoa
pULK1
ULK1
p62
vinculin
C
α-syn
DAPI
Merged
cnt
cocoa
mean integrated density (a.u.)
1.6
1.2
0.8
0.4
0
cnt
cocoa
synuclein
D
A11
DAPI
Merged
cnt
cocoa
mean integrated density (a.u.)
1.2
0.8
0.4
0
cnt
cocoa
*
A11
E
Proteostat
DAPI
Merged
cnt
cocoa
mean integrated density (a.u.)
1.6
1.2
0.8
0.4
0
cnt
cocoa
*
aggresomes

Figure 7. *The CBSE reduces α-syn toxicity in neuroblastoma cells.* (**A–B**) Western blot analysis using anti-α-syn, anti-phospho-T172-AMPK, anti-AMPKα, anti- vinculin antibodies (A) and anti-p62/SQSTM1 anti-phospho-Ser555-ULK1, anti-ULK1 and anti-vinculin antibodies (B) on protein extracts from SH-SY5Y pTet- SNCA-FLAG cells untreated, treated with doxycycline or treated with doxycycline and 150 μg/mL CBSE for 48 and 72 h. (**C**) Representative immunofluorescence (60x) images of SH-SY5Y cells treated with doxycycline (Doxy) alone and in combination with 150 μg/ml CBSE (Doxy +Cocoa) for 48 h, immunolabeled with anti α-syn antibody (**C**), A11 anti-oligomer antibody (**D**), and Proteostat R dye (**E**). Nuclei were stained by DAPI (Blue). Histograms represent mean ±standard deviation of cell fluorescence quantified with the ImageJ software.

3.4 Discussion

Accumulation of pathological protein aggregates is associated with a wide range of human diseases. Among these, aggregates of β-amyloid, p- tau or α-syn in the brain are found in patients with Alzheimer's and Parkinson's diseases and correlate with the progression of neurodegeneration [387]. Considering the consequent induction of neurotoxicity and neuronal loss, there is an increasing interest in the study of secondary metabolites, such as terpenes, flavonoids and phenols, able to inhibit protein aggregation and/or stimulate the clearance of these toxic aggregates. In recent years, the protective effects of a number of bioactive compounds have been highlighted on a wide variety of diseases, among which neurodegenerative ones [386,388].

In the context of the research of still unexplored bioactive molecules, nature is an unlimited reservoir for the discovery of novel therapeutics not only against broad-spectrum diseases, but also for applications in the cosmetic and food industries. In line with this, the valorization of by-products generated by the conventional linear food industry is an emerging strategy to identify new potential useful bioactivities and to reduce food waste.

In the present study we have employed this approach for the utilisation of cocoa bean shells, a by-product typically discarded during the roasting process of cocoa beans [80].

Here we show that CBSE, obtained by a green extraction and rich in amino acids, organic acids and methylxanthines (Tables 2 and 3), strongly improves yeast longevity and reduces the toxicity of human α-syn, by decreasing intracellular protein aggregates (Figures 1, 2, 4 and 7). Different eukaryotic models, yeast cells and a neuroblastoma cell line, were used to verify the bioactivity of the CBSE. Although the effects identified are not completely superimposable in the two systems, this approach highlights the importance of using multiple models to better identify all the biological pathways that contribute to the neuroprotective activity of natural compounds. Indeed, while CBSE stimulates autophagy in the yeast model of PD (Figure 6), this is not the case in neuroblastoma cells, even if the stress responsive kinase AMP-activated protein kinase (AMPK) is activated (Figure 7). We consider this result

particularly relevant because energy metabolism defects are commonly described in neurodegeneration and several studies reported the implication of AMPK in various signalling pathways that are involved in the progression of neurodegeneration [389]. Thus, the stimulation of both autophagy and AMPK signalling appears to represent as two complementary responses induced by CBSE which together contribute to protect the cell from the toxicity of misfolded proteins.

Results obtained by surface plasmon resonance (SPR) assays indicate also that CBSE binds α-syn protein in a concentration-dependent manner, supporting a direct association of the cacao-bean shell extract with monomers of α-syn by preventing its aggregation into toxic oligomers and amyloid fibrils (Figure 4B–D). What remains to be elucidated are the specific compounds exerting this role. Although caffeine and theobromine, as well as the very small fraction of proteins contained in the extract, do not have any effect on yeast longevity and ROS content (Figure 3), the methylxanthines together show a partial inhibitory effect on the aggregation of α-syn *in vitro* (Figure S2A). The protective functions of methylxanthines are well documented, since they reduce inflammation and preserve cognitive functions [92,390-392]. Then, the inactivity of both caffeine and theobromine in our yeast model could suggest a possible synergistic or combined role of different molecules within the extract.

The promising results obtained in this study represents the first step for the development of the CBSE as a neuroprotective agent. In order to address if the reported bioactivity may be relevant also under physiological conditions, CBSE bioavailability, absorption rate and metabolism need to be further investigated both in animal models and in clinical studies. In addition, to reach the brain, the active compounds of CBSE have to pass through the gastrointestinal tract and to cross the blood brain barrier, without losing any efficacy. Remarkably, toxicology studies performed in mice, both in acute and subchronic assays, indicate that the oral administration of both cacao shell flour or extracts is safe, without significant histopathological alterations [82]. In line with this, an interesting approach of encapsulation has been reported to enrich chocolate bars with phenolic antioxidant compounds extracted from cocoa bean shells [393].

3.5 Supplementary materials

A

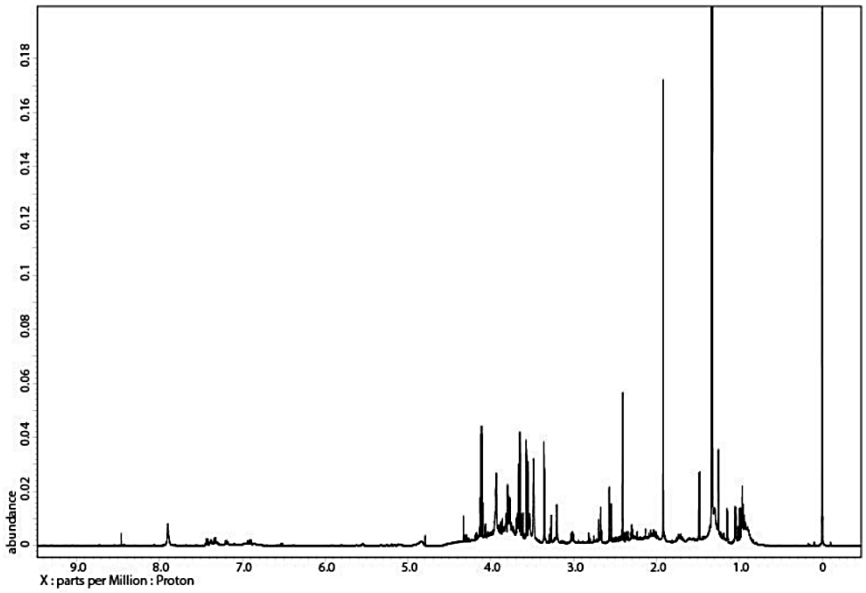

B

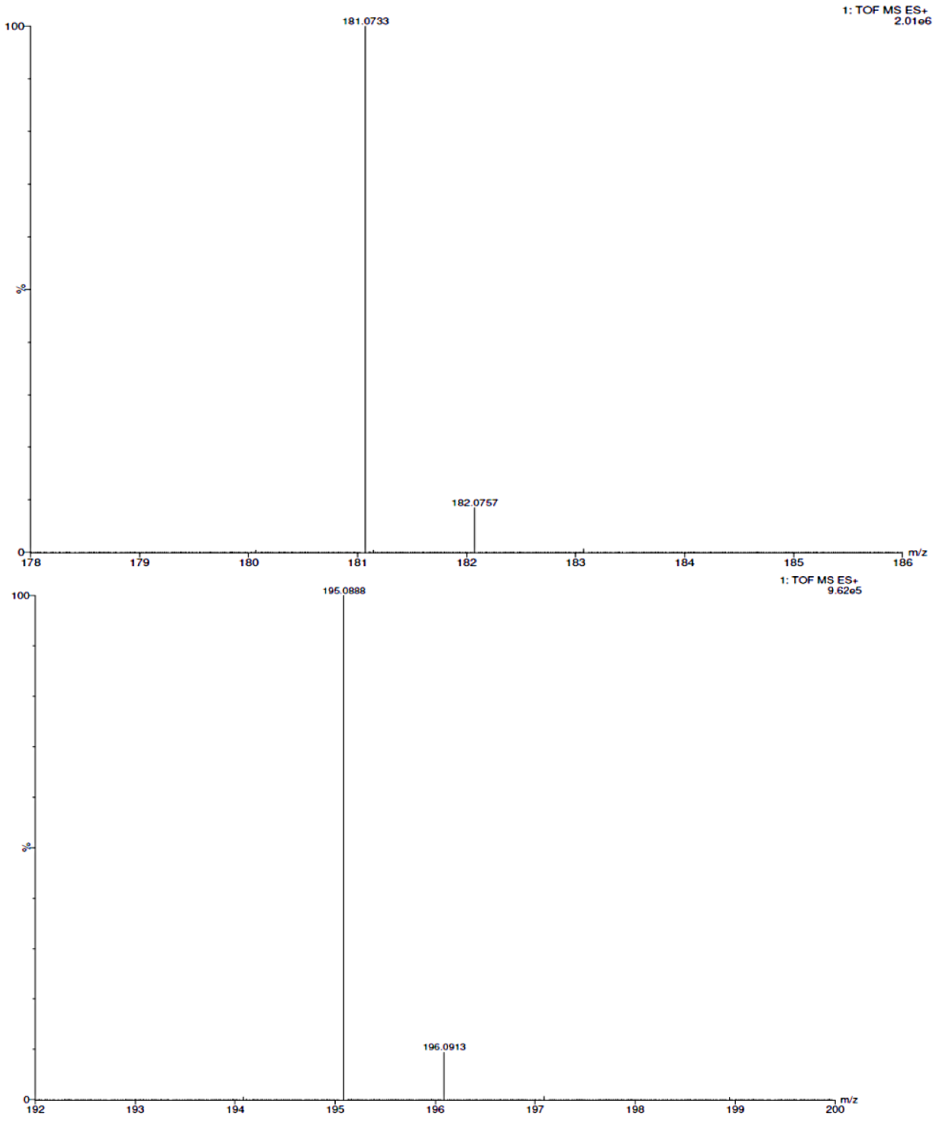
1: TOF MS ES+
2.01e6
181.0733
182.0757
100
%
0
178
179
180
181
182
183
184
185
186
m/z
1: TOF MS ES+
9.62e5
195.0888
196.0913
100
%
0
192
193
194
195
196
197
198
199
200
m/z

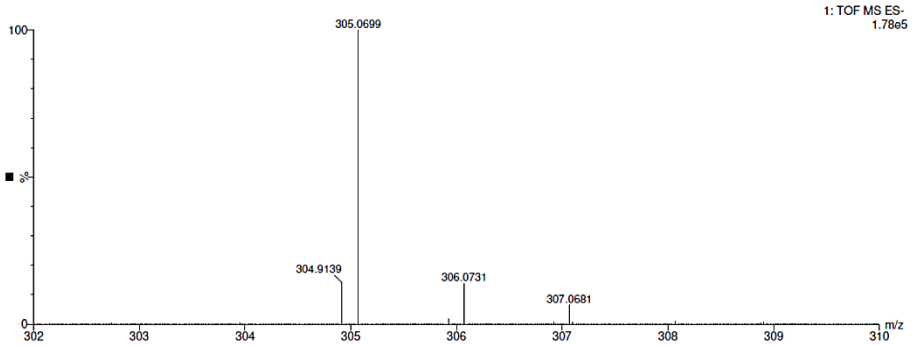
1: TOF MS ES-
1.78e5
305.0699
304.9139
306.0731
307.0681
m/z

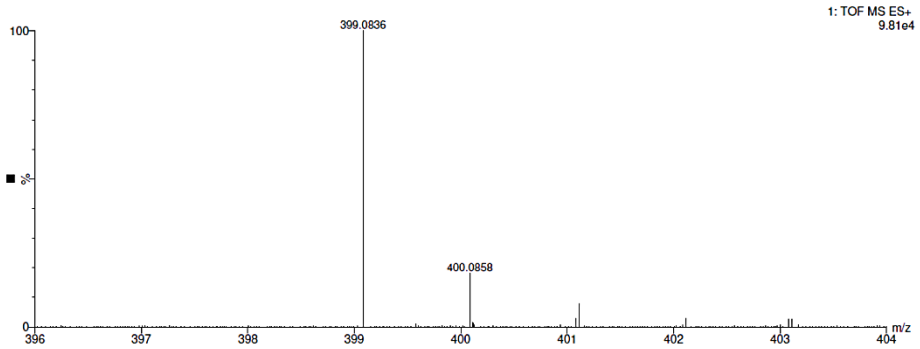
1: TOF MS ES+
9.81e4
399.0836
400.0858
m/z

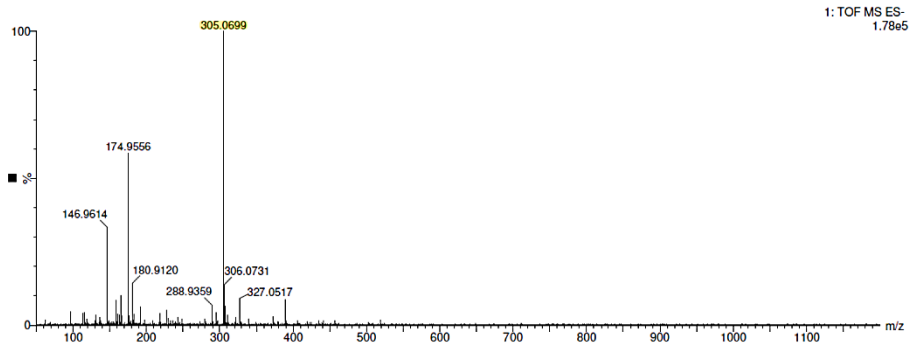
1: TOF MS ES-
1.78e5
305.0699
174.9556
146.9614
180.9120
306.0731
288.9359
327.0517
m/z

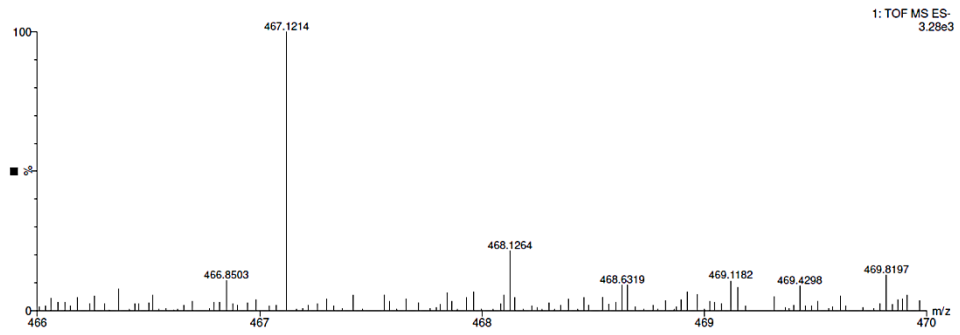
1: TOF MS ES-
3.28e3
467.1214
468.1264
466.8503
468.6319
469.1182
469.4298
469.8197
m/z

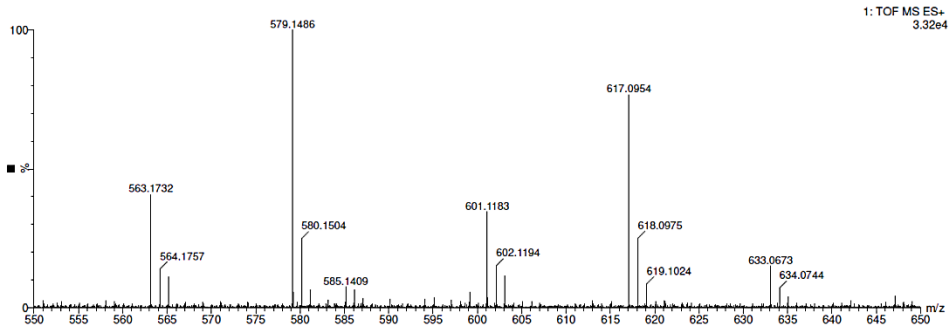

Figure S1. (**A**) 600.17 MHz 1H NMR spectrum of cocoa bean shell extract solubilized in D_2O containing 50 mM phosphate buffer pH7.4 and 0.4 mM TSP as internal standard. (**B**) MS spectra of the metabolites reported in Table 3.

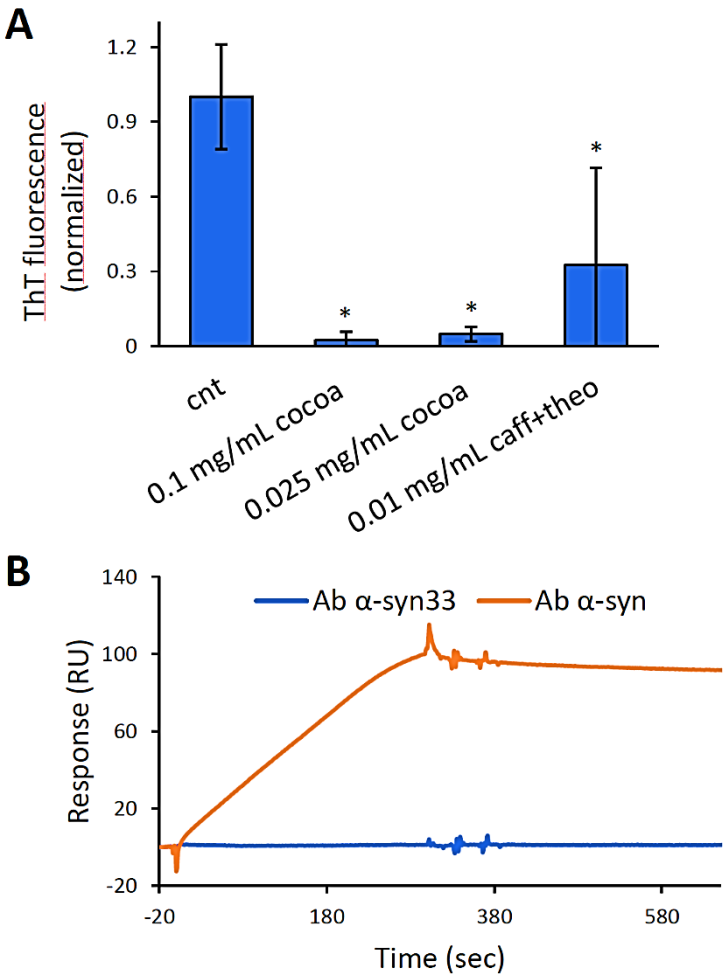

Figure S2. (**A**) α-syn aggregation process, followed by ThT fluorescence, in the absence (cnt) or presence of the 0.01 mg/mL of caffeine and theobromine. (**B**) The bioactivity of the CM5 sensor chip was determined by injecting positive (Ab anti-α-syn) and negative (Ab anti-α-syn33) controls onto immobilised α-syn protein.

Table S1. PM21-PM25 chemical compounds divided into functional groups. Drugs from plates PMs 21–25 divided into 6 groups, based on their structure and function: ions, cyclic compounds, organic compounds, chelators, antibiotics and nitrogen compounds. These 24 different chemical agents are presented in 4 different concentrations. The data presented for each drug concentration represent the ratio between the y-maximum value of cells grown with the cocoa-shell treatment and the untreated control.

Groups	Drugs	Conc. 1	Conc. 2	Conc. 3	Conc. 4
	Sodium dichromate	0.568	0.624	7.381	2.483
	Sodium arsenate	0.841	0.441	0.263	0.553
	Sodium arsenite	0.623	0.603	3.281	0.355
	Sodium cyanate	0.211	0.416	0.846	0.712
	Sodium orthovanadate	0.628	8.260	3.682	0.995
	Sodium selenate	0.538	0.738	0.637	0.562
	Sodium selenite	0.655	0.655	0.698	0.990
	Sodium cyanide	0.440	4.112	1.891	14.762
	Sodium thiosulfate	1.605	0.276	0.281	1.838
	Sodium metasilicate	0.883	0.891	0.395	1.333
Ions	Sodium metaborate tetrahydrate	0.695	0.842	4.864	24.808
	Sodium (meta)periodate	0.834	0.979	0.645	0.417
	Sodium metavanadate	0.827	10.249	2.406	0.795
	Sodium fluoride	0.504	0.580	0.350	0.384
	Potassium chromate	0.328	0.982	28.241	84.368
	Copper (II) sulfate	0.747	20.745	5.493	4.990
	Thallium(I) acetate	0.941	2.938	0.198	0.037
	Cadmium chloride hydrate	61.403	12.128	13.669	7.381
	Cobalt(II) chloride hexahydrate	0.842	0.775	1.138	24.255
	Cupric chloride dihydrate	0.885	0.709	3.532	0.475
	Manganese(II) chloride	0.833	0.780	1.465	2.444

	Magnesium chloride	1.027	0.854	0.836	0.804
	Nickel chloride	0.591	0.645	0.698	0.979
	Zinc chloride	15.230	0.056	0.231	0.019
	Benzethonium chloride	0.007	1.035	105.006	16.826
	Protamine sulfate	0.562	0.580	0.617	1.352
	Poly-L-lysine hydrochloride	0.611	3.562	3.156	0.527
	Cetylpyridinium chloride	0.425	86.487	135.200	18.796
	Domiphen bromide	0.820	0.906	112.782	93.627
	Ammonium sulfate	0.540	5.319	1.545	0.032
	Lithium chloride	0.943	0.747	30.688	12.906
	Aluminum sulfate	0.780	0.386	3.144	1.803
	Dequalinium chloride	1.332	100.927	85.825	131.658
	Methyl viologen dichloride hydrate	4.242	0.089	3.603	0.076
	Dodecyltrimethyl ammonium bromide	0.975	18.914	6.043	13.221
	Alexidine	0.652	71.948	20.141	26.238
Cyclic Compounds	Promethazine	0.577	6.096	1.007	0.028
	Chlorpromazine hydrochloride	712.891	63.116	51.796	1.000
	Cycloheximide	0.762	0.732	0.488	0.528
	Trifluoperazine	6.548	3.298	1.187	1.732
	Thioridazine hydrochloride	0.721	81.016	14.520	1.000
	Fluconazole	0.726	0.482	1.386	0.240
	Tamoxifen	0.680	3.988	1.103	2.973
	Miconazole nitrate	2.408	3.024	0.661	0.622
	Tetrazolium Violet	67.922	25.351	8.318	5.290
	Amitriptyline hydrochloride	94.348	16.094	1.000	7.009
	Zaragozic acid A	0.859	0.621	0.441	0.027
	Berberine chloride	0.535	0.534	0.768	2.818
Organic Compounds	L-Aspartic acid β-hydroxamate	0.527	0.272	1.930	0.192
	L-Glutamic acid g-hydroxamate	0.920	0.325	1.284	14.924

L-Arginine hydroxamate	0.273	0.766	1.242	97.123
Glycine hydroxamate	0.900	125.862	130.341	57.425
D,L-Serine hydroxamate	0.710	4.095	0.980	0.779
D-Serine	0.921	0.789	1.847	0.423
Thialysine	0.641	0.379	0.094	0.616
5-Fluorocytosine	22.995	9.564	8.840	10.070
5-Fluorouracil	0.434	0.590	0.082	0.017
Propiconazole	1.019	0.945	1.717	7.836
Sodium benzoate	0.658	0.595	0.415	0.295
Hydroxyurea	0.927	0.974	1.464	34.670
Azaserine	0.994	26.104	11.241	8.007
Urea hydrogen peroxide	0.882	0.707	0.835	0.647
Succinic acid	0.589	0.749	4.131	6.484
Malic acid	0.812	0.747	116.117	11.930
Tartaric acid	0.716	0.863	1.350	0.473
Fumaric acid	0.556	0.729	0.392	0.029
Cinnamic acid	0.728	0.603	0.821	0.256
Fluorodeoxyuridine	0.739	0.884	0.645	0.026
Sodium caprylate	0.669	0.000	0.785	0.380
Sodium salicylate	0.871	1.452	1.116	1.159
Glycine hydrochloride	0.305	0.768	6.428	1.666
Caffeine	0.581	0.585	-0.028	0.407
Chloroalanine hydrochloride	0.639	1.207	1.000	24.164
2-Deoxy-D-glucose	0.934	0.049	0.694	0.026
Clomiphene citrate	0.744	10.841	1.258	0.524
Ibuprofen	0.575	0.527	0.009	0.009
Chloroquine	0.904	1.952	95.179	1.149
Guanidine hydrochloride	0.561	0.472	16.468	15.944
Myclobutanil	0.881	0.671	0.911	0.120

	Niaproof	0.204	0.327	0.013	1.221
	Polymyxin B	0.681	0.808	131.563	31.240
	Miltefosine	0.764	0.537	70.027	80.424
	FCCP	0.771	0.722	0.610	0.017
	CCCP	0.536	0.699	1.534	2.951
	Triclosan	0.536	19.741	1.574	14.318
Chelators	1-Hydroxypyridine-2-thione	0.659	0.714	0.873	0.327
	EDTA	0.060	139.272	131.186	59.347
	BAPTA	0.694	0.755	108.205	2.685
	EGTA	3.324	5.524	1.920	7.977
	Sodium pyrophosphate decahydrate	0.898	0.005	0.038	0.501
	Benzamidine	0.430	14.517	13.875	1.269
	2,2`-Dipyridyl	0.936	0.806	0.614	17.780
Antibiotics	Nystatin	0.601	0.428	17.862	12.708
	D-Cycloserine	8.931	3.427	1.049	1.153
	Apramycin sulfate	0.322	0.680	0.980	1.703
	Blasticidin hydrochloride	0.185	0.982	0.617	0.186
	Chlortetracycline hydrochloride	0.570	0.962	3.965	0.878
	Kanamycin monosulfate	0.804	0.394	0.177	1.119
	Paromomycin	9.092	3.369	2.545	1.473
	Isoniazid	0.664	2.075	10.869	1.815
	Bleomycin	0.859	128.058	60.042	3.171
	Doxycycline hyclate	0.748	0.129	0.921	2.946
	Tobramycin	0.652	34.116	24.032	3.491
	Hygromycin B	1.575	20.553	20.219	28.204
	Neomycin	38.855	117.128	36.588	14.900
	Pentamidine isethionate	0.770	1.049	0.030	2.279
	6-Azauracil	0.786	0.629	0.935	1.873

	Diamide	0.419	0.623	0.000	2.044
	Thiourea	0.088	0.604	12.648	0.425
	4-Aminopyridine	0.131	0.353	29.848	37.486
	Sodium azide	0.477	0.853	0.278	25.055
Nitrogen compounds	Sodium nitrite	0.748	0.898	1.132	1.314
	Cisplatin	8.866	9.519	4.374	11.550
	Aminacrine	1.193	7.287	1.707	2.750
	3-Amino-1,2,4-triazole	0.588	0.632	143.026	39.586
	4-Nitroquinoline-N-oxide	0.860	0.737	0.725	0.984
	Hydroxylamine hydrochloride	0.861	0.698	1.060	0.001
	Compound 48/80	0.386	2.525	136.429	61.358

Table S2. *Compounds towards which cocoa-shell extract alters sensitivity, reported in Figure 5*. Compounds were selected when the fold change (ratio between y-maximum value of CBSE treated vs control cells) was >5 or <0.2 in at least three concentrations. Drugs are categorised according to their structure and function, and their specific effects are described alongside the pertinent reference.

Groups	Drugs	Effects	References
Ions	Dodecyltrimethyl ammonium bromide	ability to promote disaggregation of the fibrillar assembly (*in vitro*)	[397]
	Cadmium chloride hydrate	autophagy inducer (in hepatocytes)	[398]
	Cetylpyridinium chloride	antimicrobial effect (drug dose-dependently inhibit mitochondrial complex 1 and potent and dose-dependent AMPK inducer)	[399]

	Dequalinium chloride	act as an inducer and/or stabilizer of the protofibrils of α-synuclein (*in vitro*)	[400]
	Alexidine	antimicrobial effect	[401]
Chelators	EDTA	autophagy inducer (in *A. fumigatus*)	[402]
Organic Compounds	Glycine hydroxamate	autophagy inhibitor (in neuron through the AMPK pathway both *in vitro* and *in vivo*)	[403]
	Azaserine	antioxidant effect	[404]
Cyclic Compounds	5-Fluorocytosine	autophagy inducer (in BGC-823 cells)	[405]
	Tetrazolium Violet	apoptotic inducer (antitumor effect in Human Lung Cancer A549 cells)	[406]
	Amitriptyline hydrochloride	autophagy inhibitor (not block the beginning of autophagy, block its turnover, via inhibiting autophagosome maturation in neuronal cells)	[407]
Antibiotics	Hygromycin B	inhibit growth (in *S.cerevisiae*)	[408]
	Bleomycin	autophagy inducer (in idiopathic pulmonary fibrosis)	[409]
	Neomycin	autophagy inducer (in both cochlear HCs and HEIOC-1 cells after neomycin injury)	[410]

OUTLOOK

In the context of an increasing average age in industrialized countries, which is not accompanied by a corresponding improvement in quality of life and is marked by a rise in age-related diseases, this thesis provides compelling evidence for the potential pro-longevity effects of three dietary supplements as safe strategies to support healthy aging.

Specifically, the flavonol QUER, recognised by the Food and Drug Administration (FDA) as General Recognised as Safe, exhibits strong antioxidant properties, as demonstrated by numerous *in vivo* and *in vitro* studies, and offers a range of health-promoting benefits, including anti-aging effects. Our findings show that QUER supplementation at the onset of chronological aging, namely at the diauxic shift, extends the CLS of yeast. This beneficial effect is linked to QUER-induced modulation of carbon metabolism, which enhances the assimilation of C2 fermentation by-products and of glycerol during the post-diauxic phase. This metabolic shift promotes a pro-longevity anabolic state *via* gluconeogenesis, supported by both the L-G3P pathway and Sir2-dependent Pck1 activity. This results in increased accumulation of trehalose, which is the carbohydrate sustaining long-term survival during aging and contributes to cellular longevity.

The GSL extract, purified from the seed-press cake of *Camelina sativa*, which is a by-product of Camelina oil production, also exerts a pro-longevity effect in yeast undergoing chronological aging. Both mean and maximum CLS are significantly extended in a dose dependent manner, even when the three constituent aliphatic GSLs (GSL9, GSL10 and GSL11) are administered individually. This effect is attributed to the preservation of mitochondrial function and a marked reduction in superoxide accumulation. Furthermore, GSLs enhance glycerol catabolism, which positively influences the phosphorylating respiratory state and trehalose levels, both essential for extended CLS.

Finally, using yeast and neuroblastoma cell models overexpressing human α-syn, we demonstrate that CBSE, an extract derived from cocoa bean shell, the by-product of the cocoa processing, significantly reduces protein aggregation and oxidative stress, while promoting cellular longevity. Chemical characterization reveals the presence of amino acids, organic acids, glycerol, lactate and methylxanthines (caffeine and theobromine), although the anti-aging effects are independent of the latter. CBSE activates autophagy in yeast, whereas in neuroblastoma cells it stimulates AMPK signaling. Surface plasmon resonance assays confirm that CBSE binds α-syn in a concentration-dependent manner, inhibiting its aggregation into toxic oligomers. These findings support the potential of CBSE as a nutraceutical candidate for preventing neurodegenerative diseases associated with protein misfolding.

Although this thesis presents promising insights into the anti-aging potential of QUER, GSL extract and CBSE, further investigations are necessary to elucidate the precise molecular mechanisms and cellular targets involved in their effects during chronological aging. Moreover, while *S.cerevisiae* serves as a valuable model system, it has inherent limitations. As a unicellular eukaryote, yeast cannot replicate complex multicellular processes such as inflammation, synaptic transmission or tissue-specific physiology. Additionally, differences in metabolic profiles and gene regulation between yeast and multicellular eukaryotes may limit the translational relevance of some findings.

Given these constraints, the results presented in this thesis require validation in more complex biological systems, including mammalian cells and animal models, to assess their applicability to human health.

Despite these limitations, yeast remains a fundamental molecular model in biomedical research. Similarly, this doctoral journey has been a formative experience, offering not only scientific growth but also personal and professional development. It has been a path of challenges and compromises, yet rich in opportunities: the chance to be continually inspired by the vastness of scientific knowledge and its many areas still unexplored; the opportunity to design and refine a research project, confronting the gap between theoretical ideas and biological reality; the privilege of engaging with fellow researchers, sharing knowledge and mentoring new students. Much like the yeast model,

I view this PhD not as a conclusion, but as a starting point, a foundation upon which to build the complex system of my future, step by step.

REFERENCES LIST

1- Troen B. R. (2003). The biology of aging. *The Mount Sinai journal of medicine, New York*, *70*(1), 3–22.

2- Kanasi, E., Ayilavarapu, S., & Jones, J. (2016). The aging population: demographics and the biology of aging. *Periodontology 2000*, *72*(1), 13–18. https://doi.org/10.1111/prd.12126

3- Guo, J., Huang, X., Dou, L., Yan, M., Shen, T., Tang, W., & Li, J. (2022). Aging and aging-related diseases: from molecular mechanisms to interventions and treatments. *Signal transduction and targeted therapy*, *7*(1), 391. https://doi.org/10.1038/s41392-022-01251-0

4- Tenchov, R., Sasso, J. M., Wang, X., & Zhou, Q. A. (2024). Aging Hallmarks and Progression and Age-Related Diseases: A Landscape View of Research Advancement. *ACS chemical neuroscience*, *15*(1), 1–30. https://doi.org/10.1021/acschemneuro.3c00531

5- da Costa, J. P., Vitorino, R., Silva, G. M., Vogel, C., Duarte, A. C., & Rocha-Santos, T. (2016). A synopsis on aging-Theories, mechanisms and future prospects. *Ageing research reviews*, *29*, 90–112. https://doi.org/10.1016/j.arr.2016.06.005

6- López-Otín, C., Blasco, M. A., Partridge, L., Serrano, M., & Kroemer, G. (2023). Hallmarks of aging: An expanding universe. *Cell*, *186*(2), 243–278. https://doi.org/10.1016/j.cell.2022.11.001

7- López-Otín, C., Blasco, M. A., Partridge, L., Serrano, M., & Kroemer, G. (2013). The hallmarks of aging. *Cell*, *153*(6), 1194–1217. https://doi.org/10.1016/j.cell.2013.05.039

8- Nutraceuticals Market Insights; Report ID: SQMIG35I2228; Region: Global; Published Date: June, 2025; Pages: 196; Tables: 66; Figures: 75

9- Puri, V., Nagpal, M., Singh, I., Singh, M., Dhingra, G. A., Huanbutta, K., Dheer, D., Sharma, A., & Sangnim, T. (2022). A Comprehensive

Review on Nutraceuticals: Therapy Support and Formulation Challenges. *Nutrients*, *14*(21), 4637. https://doi.org/10.3390/nu14214637

10- Jain, S., Purohit, A., Nema, P., Vishwakarma, H., & Jain, P. K. (2022). A Brief Review on Nutraceuticals and its Application. *Asian Journal of Dental and Health Sciences*, *2*(1), 7–13. https://doi.org/10.22270/ajdhs.v2i1.10

11- Jain, N., Radhakrishnan, A., & Kuppusamy, G. (2022). Review on nutraceuticals: phase transition from preventive to protective care. *Journal of complementary & integrative medicine*, *19*(3), 553–570. https://doi.org/10.1515/jcim-2022-0026

12- Chopra, A. S., Lordan, R., Horbańczuk, O. K., Atanasov, A. G., Chopra, I., Horbańczuk, J. O., Jóźwik, A., Huang, L., Pirgozliev, V., Banach, M., Battino, M., & Arkells, N. (2022). The current use and evolving landscape of nutraceuticals. *Pharmacological research*, *175*, 106001 https://doi.org/10.1016/j.phrs.2021.106001

13- AlAli, M., Alqubaisy, M., Aljaafari, M. N., AlAli, A. O., Baqais, L., Molouki, A., Abushelaibi, A., Lai, K. S., & Lim, S. E. (2021). Nutraceuticals: Transformation of Conventional Foods into Health Promoters/Disease Preventers and Safety Considerations. *Molecules (Basel, Switzerland)*, *26*(9), 2540. https://doi.org/10.3390/molecules26092540

14- Trendelenburg, A. U., Scheuren, A. C., Potter, P., Müller, R., & Bellantuono, I. (2019). Geroprotectors: A role in the treatment of frailty. *Mechanisms of ageing and development*, *180*, 11–20. https://doi.org/10.1016/j.mad.2019.03.002

15- Metchnikoff, E. The Prolongation of Life: Optimistic Studies. (1908) *William Heinemann Ltd*. London, UK.

16- Rivero-Segura, N. A., Zepeda-Arzate, E. A., Castillo-Vazquez, S. K., Fleischmann-delaParra, P., Hernández-Pineda, J., Flores-Soto, E., García-delaTorre, P., Estrella-Parra, E. A., & Gomez-Verjan, J. C. (2024). Exploring the Geroprotective Potential of Nutraceuticals. *Nutrients*, *16*(17), 2835. https://doi.org/10.3390/nu16172835

17-Deepika, & Maurya, P. K. (2022). Health Benefits of Quercetin in Age-Related Diseases. *Molecules (Basel, Switzerland)*, *27*(8), 2498. https://doi.org/10.3390/molecules27082498
18-de Oliveira, M. R., Nabavi, S. M., Braidy, N., Setzer, W. N., Ahmed, T., & Nabavi, S. F. (2016). Quercetin and the mitochondria: A mechanistic view. *Biotechnology advances*, *34*(5), 532–549. https://doi.org/10.1016/j.biotechadv.2015.12.014
19-Carrillo-Martinez, E. J., Flores-Hernández, F. Y., Salazar-Montes, A. M., Nario-Chaidez, H. F., & Hernández-Ortega, L. D. (2024). Quercetin, a Flavonoid with Great Pharmacological Capacity. *Molecules (Basel, Switzerland)*, *29*(5), 1000. https://doi.org/10.3390/molecules29051000
20-Andres, S., Pevny, S., Ziegenhagen, R., Bakhiya, N., Schäfer, B., Hirsch-Ernst, K. I., & Lampen, A. (2018). Safety Aspects of the Use of Quercetin as a Dietary Supplement. *Molecular nutrition & food research*, *62*(1), 10.1002/mnfr.201700447. https://doi.org/10.1002/mnfr.201700447
21-Mutha, R. E., Tatiya, A. U., & Surana, S. J. (2021). Flavonoids as natural phenolic compounds and their role in therapeutics: an overview. *Future journal of pharmaceutical sciences*, *7*(1), 25. https://doi.org/10.1186/s43094-020-00161-8
22-Roy, A., Khan, A., Ahmad, I., Alghamdi, S., Rajab, B. S., Babalghith, A. O., Alshahrani, M. Y., Islam, S., & Islam, M. R. (2022). Flavonoids a Bioactive Compound from Medicinal Plants and Its Therapeutic Applications. *BioMed research international*, *2022*, 5445291. https://doi.org/10.1155/2022/5445291
23-Kaşıkcı, M. B., Bağdatlıoğlu, N. (2016) Bioavailability of Quercetin. *Current Research in Nutrition Food Science*, *4*. http://dx.doi.org/10.12944/CRNFSJ.4.Special-Issue-October.20
24-Mariani, C., Braca, A., Vitalini, S., De Tommasi, N., Visioli, F., & Fico, G. (2008). Flavonoid characterization and in vitro antioxidant activity of Aconitum anthora L. (Ranunculaceae). *Phytochemistry*, *69*(5), 1220–1226. https://doi.org/10.1016/j.phytochem.2007.12.009
25-Colunga Biancatelli, R. M. L., Berrill, M., Catravas, J. D., & Marik, P. E. (2020). Quercetin and Vitamin C: An Experimental, Synergistic

Therapy for the Prevention and Treatment of SARS-CoV-2 Related Disease (COVID-19). *Frontiers in immunology*, *11*, 1451. https://doi.org/10.3389/fimmu.2020.01451

26- Vogt, T., Zimmermann, E., Grimm, R., Meyer, M., & Strack, D. (1997). Are the characteristics of betanidin glucosyltransferases from cell-suspension cultures of Dorotheanthus bellidiformis indicative of their phylogenetic relationship with flavonoid glucosyltransferases? *Planta*, *203*(3), 349–361. https://doi.org/10.1007/s004250050201

27- Winkel-Shirley B. (2001). Flavonoid biosynthesis. A colorful model for genetics, biochemistry, cell biology, and biotechnology. *Plant physiology*, *126*(2), 485–493. https://doi.org/10.1104/pp.126.2.485

28- Tronina, T., Łużny, M., Dymarska, M., Urbaniak, M., Kozłowska, E., Piegza, M., Stępień, Ł., & Janeczko, T. (2023). Glycosylation of Quercetin by Selected Entomopathogenic Filamentous Fungi and Prediction of Its Products' Bioactivity. *International journal of molecular sciences*, *24*(14), 11857. https://doi.org/10.3390/ijms241411857

29- Golmohammadi, M., Elmaghraby, D. A., Ramírez-Coronel, A. A., Rakhimov, N., Mohammed, S. S., Romero-Parra, R. M., Jawad, M. A., Zamanian, M. Y., Soltani, A., Taheri, N., Kianifar, F., & Vousooghi, N. (2023). A comprehensive view on the quercetin impact on bladder cancer: Focusing on oxidative stress, cellular, and molecular mechanisms. *Fundamental & clinical pharmacology*, *37*(5), 900–909. https://doi.org/10.1111/fcp.12896

30- Ulusoy, H. G., & Sanlier, N. (2020). A minireview of quercetin: from its metabolism to possible mechanisms of its biological activities. *Critical reviews in food science and nutrition*, *60*(19), 3290–3303. https://doi.org/10.1080/10408398.2019.1683810

31- Li, Y., Zhou, S., Li, J., Sun, Y., Hasimu, H., Liu, R., & Zhang, T. (2015). Quercetin protects human brain microvascular endothelial cells from fibrillar β-amyloid1-40-induced toxicity. *Acta pharmaceutica Sinica. B*, *5*(1), 47–54. https://doi.org/10.1016/j.apsb.2014.12.003

32-Aghababaei, F., & Hadidi, M. (2023). Recent Advances in Potential Health Benefits of Quercetin. *Pharmaceuticals (Basel, Switzerland)*, *16*(7), 1020. https://doi.org/10.3390/ph16071020
33-Qi, Y., Guo, L., Jiang, Y., Shi, Y., Sui, H., & Zhao, L. (2020). Brain delivery of quercetin-loaded exosomes improved cognitive function in AD mice by inhibiting phosphorylated tau-mediated neurofibrillary tangles. *Drug delivery*, *27*(1), 745–755. https://doi.org/10.1080/10717544.2020.1762262
34-Bravi, E., Falcinelli, B., Mallia, G., Marconi, O., Royo-Esnal, A., & Benincasa, P. (2023). Effect of Sprouting on the Phenolic Compounds, Glucosinolates, and Antioxidant Activity of Five *Camelina sativa* (L.) Crantz Cultivars. *Antioxidants (Basel, Switzerland)*, *12*(8), 1495. https://doi.org/10.3390/antiox12081495
35-Fahey, J. W., Zalcmann, A. T., & Talalay, P. (2001). The chemical diversity and distribution of glucosinolates and isothiocyanates among plants. *Phytochemistry*, *56*(1), 5–51. https://doi.org/10.1016/s0031-9422(00)00316-2
36-Clarke, D. B. Glucosinolates, structures and analysis in food. (2010) *Anal. Methods*, *2*, 310-325. https://doi.org/10.1039/B9AY00280D
37-Halkier, B. A., & Gershenzon, J. (2006). Biology and biochemistry of glucosinolates. *Annual review of plant biology*, *57*, 303–333. https://doi.org/10.1146/annurev.arplant.57.032905.105228
38-Sturm, C., & Wagner, A. E. (2017). Brassica-Derived Plant Bioactives as Modulators of Chemopreventive and Inflammatory Signaling Pathways. *International journal of molecular sciences*, *18*(9), 1890. https://doi.org/10.3390/ijms18091890
39-Blažević, I., Montaut, S., Burčul, F., Olsen, C. E., Burow, M., Rollin, P., & Agerbirk, N. (2020). Glucosinolate structural diversity, identification, chemical synthesis and metabolism in plants. *Phytochemistry*, *169*, 112100. https://doi.org/10.1016/j.phytochem.2019.112100
40-Jeon, B. W., Oh, M., Kim, H. S., Kim, E. O., & Chae, W. B. (2022). Glucosinolate variation among organs, growth stages and seasons suggests its dominant accumulation in sexual over asexual-reproductive organs in white radish. *Scientia Horticulturae*, *291*,110617.

https://doi.org/10.1016/j.scienta.2021.110617
41-Falk, K. L., Kästner, J., Bodenhausen, N., Schramm, K., Paetz, C., Vassão, D. G., Reichelt, M., von Knorre, D., Bergelson, J., Erb, M., Gershenzon, J., & Meldau, S. (2014). The role of glucosinolates and the jasmonic acid pathway in resistance of Arabidopsis thaliana against molluscan herbivores. *Molecular ecology*, *23*(5), 1188–1203. https://doi.org/10.1111/mec.12610
42-Li, N., Wu, X., Zhuang, W., Wu, C., Rao, Z., Du, L., & Zhou, Y. (2022). Cruciferous vegetable and isothiocyanate intake and multiple health outcomes. *Food chemistry*, *375*, 131816. https://doi.org/10.1016/j.foodchem.2021.131816
43-Holst, B., & Williamson, G. (2004). A critical review of the bioavailability of glucosinolates and related compounds. *Natural product reports*, *21*(3), 425–447. https://doi.org/10.1039/b204039p
44-Ziedan, E. H. (2022). A review of the efficacy of biofumigation agents in the control of soil-borne plant diseases. *Journal of Plant Protection Research*, *62*(1), 1-11. https://doi.org/10.24425/jppr.2022.140292
45-Agerbirk, N., & Olsen, C. E. (2012). Glucosinolate structures in evolution. *Phytochemistry*, *77*, 16–45. https://doi.org/10.1016/j.phytochem.2012.02.005
46-Alexandre, E. M. C., Moreira, S. A., Pinto, C. A., Pintado, M. & Saraiva, J. A. (2020) Chapter 7 - Analysis of glucosinolates content in food products. Editor(s): Charis M. Galanakis, Glucosinolates: Properties, Recovery, and Applications, *Academic Press*, 213-250. https://doi.org/10.1016/B978-0-12-816493-8.00007-X
47-Baenas, N., Cartea, M. E., Moreno, D. A., Tortosa, M. & Francisco, M. (2020) Chapter 6 - Processing and cooking effects on glucosinolates and their derivatives. Editor(s): Charis M. Galanakis, Glucosinolates: Properties, Recovery, and Applications, *Academic Press*, 181–212. https://doi.org/10.1016/B978-0-12-816493-8.00006-8
48-Galanakis, C. M. (2020) Chapter 8 - Recovery techniques, stability, and applications of glucosinolates.cations of Glucosinolates. Editor(s): Charis M. Galanakis, Glucosinolates: Properties, Recovery, and Applications, *Academic Press*, 251-280. https://doi.org/10.1016/B978-0-12-816493-8.00008-1

49-Brown, P. D. & Morra, M. J. (1995) Glucosinolate-containing plant tissues as bioherbicides. *Journal of Agricultural and Food Chemistry*, *43*(12), 3070-3074. https://doi.org/10.1021/jf00060a015

50-Borges, A., Abreu, A. C., Ferreira, C., Saavedra, M. J., Simões, L. C., & Simões, M. (2015). Antibacterial activity and mode of action of selected glucosinolate hydrolysis products against bacterial pathogens. *Journal of food science and technology*, *52*(8), 4737–4748. https://doi.org/10.1007/s13197-014-1533-1

51-Zhao, A., Jeffery, E. H., & Miller, M. J. (2022). Is Bitterness Only a Taste? The Expanding Area of Health Benefits of Brassica Vegetables and Potential for Bitter Taste Receptors to Support Health Benefits. *Nutrients*, *14*(7), 1434. https://doi.org/10.3390/nu14071434

52-Connolly, E. L., Sim, M., Travica, N., Marx, W., Beasy, G., Lynch, G. S., Bondonno, C. P., Lewis, J. R., Hodgson, J. M., & Blekkenhorst, L. C. (2021). Glucosinolates From Cruciferous Vegetables and Their Potential Role in Chronic Disease: Investigating the Preclinical and Clinical Evidence. *Frontiers in pharmacology*, *12*, 767975. https://doi.org/10.3389/fphar.2021.767975

53-Barba, F. J., Nikmaram, N., Roohinejad, S., Khelfa, A., Zhu, Z., & Koubaa, M. (2016). Bioavailability of Glucosinolates and Their Breakdown Products: Impact of Processing. *Frontiers in nutrition*, *3*, 24. https://doi.org/10.3389/fnut.2016.00024

54-Bheemreddy, R. M., & Jeffery, E. H. (2007). The metabolic fate of purified glucoraphanin in F344 rats. *Journal of agricultural and food chemistry*, *55*(8), 2861–2866. https://doi.org/10.1021/jf0633544

55-Michaelsen, S., Otte, J., Simonsen, L.-O., & Sørensen, H. (1994) Absorption and degradation of individual intact glucosinolates in the digestive tract of rodents. *Acta Agriculturae Scandinavica, Section A – Animal Science*, *44*, 25–37.

56-Zubr, J. (1997) Oil-Seed Crop: Camelina sativa. *Industrial Crops and Products*, *6*, 113-119. https://doi.org/10.1016/S0926-6690(96)00203-8

57-Vollmann, J., Moritz, T., Kargl, C., Baumgartner, S., & Wagentristl, H. (2007) Agronomic Evaluation of Camelina Genotypes Selected for

Seed Quality Characteristics. *Industrial Crops and Products*, *26*, 270-277. https://doi.org/10.1016/j.indcrop.2007.03.017

58-Berti, M., Gesch, R., Eynck, C., Anderson, J., & Cermak, S. (2016) Camelina Uses, Genetics, Genomics, Production, and Management. *Industrial Crops and Products*, *94*, 690–710. https://doi.org/10.1016/j.indcrop.2016.09.034

59-Zanetti, F., Alberghini, B., Marjanović Jeromela, A. Grahovac, N., Rajković, D., Kiprovski, & B. Monti, A. (2021) Camelina, an ancient oilseed crop actively contributing to the rural renaissance in Europe. A review. *Agronomy for Sustainable Development*, *41*, 2. https://doi.org/10.1007/s13593-020-00663-y

60-Vaughn, S. F., & Berhow, M. A. (2005) Glucosinolate hydrolysis products from various plant sources: pH effects, isolation, and purification. *Industrial Crops and Products*, *21*(2), 193−202. https://doi.org/10.1016/j.indcrop.2004.03.004

61-Sydor, M., Kurasiak-Popowska, D., Stuper-Szablewska, K., & Rogozin´ski, T. (2022) Camelina sativa. Status quo and future perspectives. *Industrial Crops and Products*, *187*, 115531. https://doi.org/10.1016/j.indcrop.2022.115531

62-Walia, M. K., Zanetti, F., Gesch, R. W., Krzy˙zaniak, M., Eynck, C., Puttick, D., & Monti, A. (2021) Winter camelina seed quality in different growing environments across Northern America and Europe. *Industrial Crops and Products*, *169*, 113639. https://doi.org/10.1016/j.indcrop.2021.113639

63-Royo-Esnal, A., Edo-Tena, E., Torra, J., Recasens, J. & Gesch, R. W. (2017) Using fitness parameters to evaluate three oilseed *Brassicaceae* species as potential oil crops in two contrasting environments. *Industrial Crops and Products*, *95*, 148–155. https://doi.org/10.1016/j.indcrop.2016.10.020

64-Royo-Esnal, A., & Valencia-Gredilla, F. (2018). Camelina as a Rotation Crop for Weed Control in Organic Farming in a Semiarid Mediterranean Climate. *Agriculture*, *8*(10), 156. https://doi.org/10.3390/agriculture8100156

65-Angelini, L. G., Abou Chehade, L., Foschi, L., & Tavarini, S. (2020). Performance and Potentiality of Camelina (*Camelina sativa* L. Crantz)

Genotypes in Response to Sowing Date under Mediterranean Environment. *Agronomy*, *10*(12), 1929. https://doi.org/10.3390/agronomy10121929

66- Orczewska-Dudek, S., & Pietras, M. (2019). The Effect of Dietary *Camelina sativa* Oil or Cake in the Diets of Broiler Chickens on Growth Performance, Fatty Acid Profile, and Sensory Quality of Meat. *Animals : an open access journal from MDPI*, *9*(10), 734. https://doi.org/10.3390/ani9100734

67- Szumacher-Strabel, M., Cieślak, A., Zmora, P., Pers-Kamczyc, E., Bielińska, S., Stanisz, M., & Wójtowski, J. (2011). Camelina sativa cake improved unsaturated fatty acids in ewe's milk. *Journal of the science of food and agriculture*, *91*(11), 2031–2037. https://doi.org/10.1002/jsfa.4415

68- Rusconi, M., & Conti, A. (2010). Theobroma cacao L., the Food of the Gods: a scientific approach beyond myths and claims. *Pharmacological research*, *61*(1), 5–13. https://doi.org/10.1016/j.phrs.2009.08.008

69- Lachenaud, P., Sounigo, O., & Sallée, B. (2005). Les cacaoyers spontanés de Guyane française: état des recherches. *Acta Botanica Gallica*, *152*(3), 325–346. https://doi.org/10.1080/12538078.2005.10515493

70- Bekele, F., & Phillips-Mora, W. (2019). Cacao (*Theobroma cacao* L.) Breeding. In: Al-Khayri, J., Jain, S., & Johnson, D. (eds) Advances in Plant Breeding Strategies: Industrial and Food Crops. Springer, Cham. https://doi.org/10.1007/978-3-030-23265-8_12

71- Jean-Marie, E., Bereau, D., & Robinson, J. C. (2021). Benefits of Polyphenols and Methylxanthines from Cocoa Beans on Dietary Metabolic Disorders. *Foods (Basel, Switzerland)*, *10*(9), 2049. https://doi.org/10.3390/foods10092049

72- Beg, M. S., Ahmad, S., Jan, K., & Bashir, K. (2017). Status, Supply Chain and Processing of Cocoa—A Review. *Trends in Food Science & Technology*, *66*, 108–116. https://doi.org/10.1016/j.tifs.2017.06.007

73- Mazzutti, S., Gonçalves Rodrigues, L. G., Mezzomo, N., Venturi, V., & Salvador Ferreira, S. R. (2018). Integrated green-based processes using supercritical CO_2 and pressurized ethanol applied to recover

antioxidant compouds from cocoa (*Theobroma cacao*) bean hulls. *The Journal of Supercritical Fluids*, *135*, 52–59. https://doi.org/10.1016/j.supflu.2017.12.039

74- Panak Balentić, J., Ačkar, Đ., Jokić, S., Jozinović, A., Babić, J., Miličević, B., Šubarić, D., & Pavlović, N. (2018). Cocoa Shell: A By-Product with Great Potential for Wide Application. *Molecules (Basel, Switzerland)*, *23*(6), 1404. https://doi.org/10.3390/molecules23061404

75- Okiyama, D. C. G., Navarro, S. L. B., & Rodrigues, C. E. C. (2017). Cocoa shell and its compounds: applications in the food industry. *Trends in Food Science & Technology*, *63*, 103–112. https://doi.org/10.1016/j.tifs.2017.03.007.

76- Kim, J., Kim, J., Shim, J., Lee, C. Y., Lee, K. W., & Lee, H. J. (2014). Cocoa phytochemicals: recent advances in molecular mechanisms on health. *Critical reviews in food science and nutrition*, *54*(11), 1458–1472. https://doi.org/10.1080/10408398.2011.641041

77- Martin, M. Á., & Ramos, S. (2021). Impact of cocoa flavanols on human health. *Food and chemical toxicology : an international journal published for the British Industrial Biological Research Association*, *151*, 112121. https://doi.org/10.1016/j.fct.2021.112121

78- Okiyama, D. C. G., Soares, I. D., & Cuevas, M. S., Crevelin, E. J., Moraes L. A. B, Melo M. P., Oliveira A. L., & Rodrigues C. E. C. (2018). Pressurized liquid extraction of flavanols and alkaloids from cocoa bean shell using ethanol as solvent. *Food Research International*, 114, 20–29. https://doi.org/10.1016/j.foodres.2018.07.055

79- Arlorio, M., Coïsson, J.D., Travaglia, F., Varsaldi, F., Miglio, G., Lombardi, G., & Martelli, A. (2005). Antioxidant and biological activity of phenolic pigments from *Theobroma cacao* hulls extracted with supercritical CO_2. *Food Research International*, *38*, 1009–1014. https://doi.org/10.1016/j.foodres.2005.03.012

80- Pagliari, S., Celano, R., Rastrelli, L., Sacco, E., Arlati, F., Labra, M., & Campone, L. (2022). Extraction of methylxanthines by pressurized hot water extraction from cocoa shell by-product as natural source of functional ingredient. *LWT*, *170*, 114115.

https://doi.org/10.1016/j.lwt.2022.114115
81- Visioli, F., Bernardini, E., Poli, A., & Paoletti, R. (2012). Chocolate and Health: A Brief Review of the Evidence. In: Conti, A., Paoletti, R., Poli, A., & Visioli, F. (eds) Chocolate and Health. Springer, Milano. https://doi.org/10.1007/978-88-470-2038-2_5
82- Gil-Ramírez, A., Cañas, S., Cobeta, I.M., Rebollo-Hernanz, M., Rodríguez-Rodríguez, P., Benítez, V., Arribas, S. M., Martín-Cabrejas M. A., Aguilera, Y. (2024). Uncovering cocoa shell as a safe bioactive food ingredient: nutritional and toxicological breakthroughs. *Future Foods*, *10*, 100461. https://doi.org/10.1016/j.fufo.2024.100461
83- Wollgast, J., & Anklam, E. (2000). Review on polyphenols in *Theobroma cacao*: changes in composition during the manufacture of chocolate and methodology for identification and quantification. *Food Research International*, *33*, 423–447. https://doi.org/10.1016/S0963-9969(00)00068-5
84- Ortega, N., Romero, M. P., Macià, A., Reguant, J., Anglès, N., Morelló, J. R., & Motilva, M. J. (2008). Obtention and characterization of phenolic extracts from different cocoa sources. *Journal of agricultural and food chemistry*, *56*(20), 9621–9627. https://doi.org/10.1021/jf8014415
85- Sánchez-Rabaneda, F., Jáuregui, O., Casals, I., Andrés-Lacueva, C., Izquierdo-Pulido, M., & Lamuela-Raventós, R. M. (2003). Liquid chromatographic/electrospray ionization tandem mass spectrometric study of the phenolic composition of cocoa (Theobroma cacao). *Journal of mass spectrometry : JMS*, *38*(1), 35–42. https://doi.org/10.1002/jms.395
86- Borchers, A. T., Keen, C. L., Hannum, S.M., & Gershwin, M.E. (2000) Cocoa and chocolate: composition, bioavailability, and health implications. *Journal of Medicinal Food*, *3*, 77–105. https://doi.org/10.1089/109662000416285
87- Rios, L. Y., Bennett, R. N., Lazarus, S. A., Rémésy, C., Scalbert, A., & Williamson, G. (2002). Cocoa procyanidins are stable during gastric transit in humans. *The American journal of clinical nutrition*, *76*(5), 1106–1110. https://doi.org/10.1093/ajcn/76.5.1106

88-Tušek, K., Valinger, D., Jurina, T., Sokač Cvetnić, T., Gajdoš Kljusurić, J., & Benković, M. (2024). Bioactives in Cocoa: Novel Findings, Health Benefits, and Extraction Techniques. *Separations*, *11*(4), 128. https://doi.org/10.3390/separations11040128

89-Soares, T. F., & Oliveira, M. B. P. P. (2022). Cocoa By-Products: Characterization of Bioactive Compounds and Beneficial Health Effects. *Molecules (Basel, Switzerland)*, *27*(5), 1625. https://doi.org/10.3390/molecules27051625

90-Rojo-Poveda, O., Barbosa-Pereira, L., Zeppa, G., & Stévigny, C. (2020). Cocoa Bean Shell-A By-Product with Nutritional Properties and Biofunctional Potential. *Nutrients*, *12*(4), 1123. https://doi.org/10.3390/nu12041123

91-Cinar, Z. Ö., Atanassova, M., Tumer, T. B., Caruso, G., Antika, G., Sharma, S., Sharifi-Rad, J., & Pezzani, R. (2021). Cocoa and cocoa bean shells role in human health: an updated review. *Journal of Food Composition and Analysis*, *103*, 104115. https://doi.org/10.1016/j.jfca.2021.104115

92-Sánchez, M., Laca, A., Laca, A., & Díaz, M. (2023). Cocoa Bean Shell: A By-Product with High Potential for Nutritional and Biotechnological Applications. *Antioxidants (Basel, Switzerland)*, *12*(5), 1028. https://doi.org/10.3390/antiox12051028

93-Kaeberlein, M. (2010). Lessons on longevity from budding yeast. *Nature*, *464*(7288), 513–519. https://doi.org/10.1038/nature08981.

94-Longo, V. D., Shadel, G. S., Kaeberlein, M., & Kennedy, B. (2012). Replicative and chronological aging in Saccharomyces cerevisiae. *Cell metabolism*, *16*(1), 18–31. https://doi.org/10.1016/j.cmet.2012.06.002.

95-Sampaio-Marques, B., Burhans, W. C., & Ludovico, P. (2014). Longevity pathways and maintenance of the proteome: the role of autophagy and mitophagy during yeast ageing. *Microbial cell (Graz, Austria)*, *1*(4), 118–127. https://doi.org/10.15698/mic2014.04.136.

96-Mortimer R. K. (2000). Evolution and variation of the yeast (Saccharomyces) genome. *Genome research*, *10*(4), 403–409. https://doi.org/10.1101/gr.10.4.403.

97- Goffeau, A., Barrell, B. G., Bussey, H., Davis, R. W., Dujon, B., Feldmann, H., Galibert, F., Hoheisel, J. D., Jacq, C., Johnston, M., Louis, E. J., Mewes, H. W., Murakami, Y., Philippsen, P., Tettelin, H., & Oliver, S. G. (1996). Life with 6000 genes. *Science (New York, N.Y.)*, *274*(5287), 546–567. https://doi.org/10.1126/science.274.5287.546.

98- Bassett, D. E., Jr, Boguski, M. S., & Hieter, P. (1996). Yeast genes and human disease. *Nature*, *379*(6566), 589–590. https://doi.org/10.1038/379589a0.

99- Miller-Fleming, L., Giorgini, F., & Outeiro, T. F. (2008). Yeast as a model for studying human neurodegenerative disorders. *Biotechnology journal*, *3*(3), 325–338. https://doi.org/10.1002/biot.200700217

100- Sampaio-Marques, B., & Ludovico, P. (2015). Sirtuins and proteolytic systems: implications for pathogenesis of synucleinopathies. *Biomolecules*, *5*(2), 735–757. https://doi.org/10.3390/biom5020735

101- Sampaio-Marques, B., & Ludovico, P. (2018). Linking cellular proteostasis to yeast longevity. *FEMS yeast research*, *18*(5), 10.1093/femsyr/foy043. https://doi.org/10.1093/femsyr/foy043

102- Smith, M. G., & Snyder, M. (2006). Yeast as a model for human disease. *Current protocols in human genetics*, *Chapter 15*, https://doi.org/10.1002/0471142905.hg1506s48

103- Meunier, B., Fisher, N., Ransac, S., Mazat, J. P., & Brasseur, G. (2013). Respiratory complex III dysfunction in humans and the use of yeast as a model organism to study mitochondrial myopathy and associated diseases. *Biochimica et biophysica acta*, *1827*(11-12), 1346–1361. https://doi.org/10.1016/j.bbabio.2012.11.015

104- Camacho-Pereira, J., Tarragó, M. G., Chini, C. C. S., Nin, V., Escande, C., Warner, G. M., Puranik, A. S., Schoon, R. A., Reid, J. M., Galina, A., & Chini, E. N. (2016). CD38 Dictates Age-Related NAD Decline and Mitochondrial Dysfunction through an SIRT3-Dependent Mechanism. *Cell metabolism*, *23*(6), 1127–1139. https://doi.org/10.1016/j.cmet.2016.05.006

105- Kurat, C. F., Natter, K., Petschnigg, J., Wolinski, H., Scheuringer, K., Scholz, H., Zimmermann, R., Leber, R., Zechner, R., & Kohlwein, S. D. (2006). Obese yeast: triglyceride lipolysis is functionally conserved from mammals to yeast. *The Journal of biological chemistry*, *281*(1), 491–500. https://doi.org/10.1074/jbc.M508414200

106- Howitz, K. T., Bitterman, K. J., Cohen, H. Y., Lamming, D. W., Lavu, S., Wood, J. G., Zipkin, R. E., Chung, P., Kisielewski, A., Zhang, L. L., Scherer, B., & Sinclair, D. A. (2003). Small molecule activators of sirtuins extend Saccharomyces cerevisiae lifespan. *Nature*, *425*(6954), 191–196. https://doi.org/10.1038/nature01960

107- Mohammadi, S., Saberidokht, B., Subramaniam, S., & Grama, A. (2015). Scope and limitations of yeast as a model organism for studying human tissue-specific pathways. *BMC systems biology*, *9*, 96. https://doi.org/10.1186/s12918-015-0253-0

108- Mortimer, R. K., & Johnston, J. R. (1959). Life span of individual yeast cells. *Nature*, *183*(4677), 1751–1752. https://doi.org/10.1038/1831751a0

109- Ölmez, T. T., Moreno, D. F., Liu, P., Johnson, Z. M., McGinnis, M. M., Tu, B. P., Hochstrasser, M., & Acar, M. (2023). Sis2 regulates yeast replicative lifespan in a dose-dependent manner. *Nature communications*, *14*(1), 7719. https://doi.org/10.1038/s41467-023-43233-y

110- Müller, I., Zimmermann, M., Becker, D., & Flömer, M. (1980). Calendar life span versus budding life span of Saccharomyces cerevisiae. *Mechanisms of ageing and development*, *12*(1), 47–52. https://doi.org/10.1016/0047-6374(80)90028-7

111- Fabrizio, P., & Longo, V. D. (2003). The chronological life span of Saccharomyces cerevisiae. *Aging cell*, *2*(2), 73–81. https://doi.org/10.1046/j.1474-9728.2003.00033.x

112- Orlandi, I., Coppola, D. P., & Vai, M. (2014). Rewiring yeast acetate metabolism through *MPC1* loss of function leads to mitochondrial damage and decreases chronological lifespan. *Microbial cell (Graz, Austria)*, *1*(12), 393–405. https://doi.org/10.15698/mic2014.12.178

113- Casatta, N., Porro, A., Orlandi, I., Brambilla, L., & Vai, M. (2013). Lack of Sir2 increases acetate consumption and decreases extracellular pro-aging factors. *Biochimica et biophysica acta*, *1833*(3), 593–601. https://doi.org/10.1016/j.bbamcr.2012.11.008

114- Orlandi, I., Stamerra, G., Strippoli, M., & Vai, M. (2017). During yeast chronological aging resveratrol supplementation results in a short-lived phenotype Sir2-dependent. *Redox biology*, *12*, 745–754. https://doi.org/10.1016/j.redox.2017.04.015

115- Orlandi, I., Pellegrino Coppola, D., Strippoli, M., Ronzulli, R., & Vai, M. (2017). Nicotinamide supplementation phenocopies SIR2 inactivation by modulating carbon metabolism and respiration during yeast chronological aging. *Mechanisms of ageing and development*, *161*(Pt B), 277–287. https://doi.org/10.1016/j.mad.2016.06.006

116- Alugoju, P., Palanisamy, C. P., Anthikapalli, N. V. A., Jayaraman, S., Prasanskulab, A., Chuchawankul, S., Dyavaiah, M., & Tencomnao, T. (2024). Exploring the anti-aging potential of natural products and plant extracts in budding yeast *Saccharomyces cerevisiae*: A review. *F1000Research*, *12*, 1265. https://doi.org/10.12688/f1000research.141669.2

117- Busti, S., Coccetti, P., Alberghina, L., & Vanoni, M. (2010). Glucose signaling-mediated coordination of cell growth and cell cycle in Saccharomyces cerevisiae. *Sensors (Basel, Switzerland)*, *10*(6), 6195–6240. https://doi.org/10.3390/s100606195

118- Ozcan, S., & Johnston, M. (1995). Three different regulatory mechanisms enable yeast hexose transporter (HXT) genes to be induced by different levels of glucose. *Molecular and cellular biology*, *15*(3), 1564–1572. https://doi.org/10.1128/MCB.15.3.1564

119- Diderich, J. A., Schepper, M., van Hoek, P., Luttik, M. A., van Dijken, J. P., Pronk, J. T., Klaassen, P., Boelens, H. F., de Mattos, M. J., van Dam, K., & Kruckeberg, A. L. (1999). Glucose uptake kinetics and transcription of HXT genes in chemostat cultures of Saccharomyces cerevisiae. *The Journal of biological chemistry*, *274*(22), 15350–15359. https://doi.org/10.1074/jbc.274.22.15350

120- Flikweert, M. T., Kuyper, M., van Maris, A. J., Kötter, P., van Dijken, J. P., & Pronk, J. T. (1999). Steady-state and transient-state analysis of growth and metabolite production in a Saccharomyces cerevisiae strain with reduced pyruvate-decarboxylase activity. *Biotechnology and bioengineering*, *66*(1), 42–50. https://doi.org/10.1002/(sici)1097-0290(1999)66:1<42::aid-bit4>3.0.co;2-l

121- Jitrapakdee, S., Adina-Zada, A., Besant, P. G., Surinya, K. H., Cleland, W. W., Wallace, J. C., & Attwood, P. V. (2007). Differential regulation of the yeast isozymes of pyruvate carboxylase and the locus of action of acetyl CoA. *The international journal of biochemistry & cell biology*, *39*(6), 1211–1223. https://doi.org/10.1016/j.biocel.2007.03.016

122- Herzig, S., Raemy, E., Montessuit, S., Veuthey, J. L., Zamboni, N., Westermann, B., Kunji, E. R., & Martinou, J. C. (2012). Identification and functional expression of the mitochondrial pyruvate carrier. *Science (New York, N.Y.)*, *337*(6090), 93–96. https://doi.org/10.1126/science.1218530

123- Bender, T., Pena, G., & Martinou, J. C. (2015). Regulation of mitochondrial pyruvate uptake by alternative pyruvate carrier complexes. *The EMBO journal*, *34*(7), 911–924. https://doi.org/10.15252/embj.201490197

124- Bowman, S. B., Zaman, Z., Collinson, L. P., Brown, A. J., & Dawes, I. W. (1992). Positive regulation of the LPD1 gene of Saccharomyces cerevisiae by the HAP2/HAP3/HAP4 activation system. *Molecular & general genetics : MGG*, *231*(2), 296–303. https://doi.org/10.1007/BF00279803

125- Lin, Y. Y., Lu, J. Y., Zhang, J., Walter, W., Dang, W., Wan, J., Tao, S. C., Qian, J., Zhao, Y., Boeke, J. D., Berger, S. L., & Zhu, H. (2009). Protein acetylation microarray reveals that NuA4 controls key metabolic target regulating gluconeogenesis. *Cell*, *136*(6), 1073–1084. https://doi.org/10.1016/j.cell.2009.01.033

126- Guarente, L., & Picard, F. (2005). Calorie restriction--the SIR2 connection. *Cell*, *120*(4), 473–482. https://doi.org/10.1016/j.cell.2005.01.029

127- Lillie, S. H., & Pringle, J. R. (1980). Reserve carbohydrate metabolism in Saccharomyces cerevisiae: responses to nutrient limitation. *Journal of bacteriology*, *143*(3), 1384–1394. https://doi.org/10.1128/jb.143.3.1384-1394.1980

128- Wang, Z., Wilson, W. A., Fujino, M. A., & Roach, P. J. (2001). Antagonistic controls of autophagy and glycogen accumulation by Snf1p, the yeast homolog of AMP-activated protein kinase, and the cyclin-dependent kinase Pho85p. *Molecular and cellular biology*, *21*(17), 5742–5752. https://doi.org/10.1128/MCB.21.17.5742-5752.2001

129- Wilson, W. A., Wang, Z., & Roach, P. J. (2002). Systematic identification of the genes affecting glycogen storage in the yeast Saccharomyces cerevisiae: implication of the vacuole as a determinant of glycogen level. *Molecular & cellular proteomics : MCP*, *1*(3), 232–242. https://doi.org/10.1074/mcp.m100024-mcp200

130- François, J., & Parrou, J. L. (2001). Reserve carbohydrates metabolism in the yeast Saccharomyces cerevisiae. *FEMS microbiology reviews*, *25*(1), 125–145. https://doi.org/10.1111/j.1574-6976.2001.tb00574.x

131- De Virgilio, C., Simmen, U., Hottiger, T., Boller, T., & Wiemken, A. (1990). Heat shock induces enzymes of trehalose metabolism, trehalose accumulation, and thermotolerance in Schizosaccharomyces pombe, even in the presence of cycloheximide. *FEBS letters*, *273*(1-2), 107–110. https://doi.org/10.1016/0014-5793(90)81062-s

132- De Virgilio, C., Hottiger, T., Dominguez, J., Boller, T., & Wiemken, A. (1994). The role of trehalose synthesis for the acquisition of thermotolerance in yeast. I. Genetic evidence that trehalose is a thermoprotectant. *European journal of biochemistry*, *219*(1-2), 179–186. https://doi.org/10.1111/j.1432-1033.1994.tb19928.x

133- Crowe, J. H., Hoekstra, F. A., & Crowe, L. M. (1992). Anhydrobiosis. *Annual review of physiology*, *54*, 579–599. https://doi.org/10.1146/annurev.ph.54.030192.003051

134- Hottiger, T., De Virgilio, C., Hall, M. N., Boller, T., & Wiemken, A. (1994). The role of trehalose synthesis for the acquisition of thermotolerance in yeast. II. Physiological concentrations of trehalose

increase the thermal stability of proteins in vitro. *European journal of biochemistry*, *219*(1-2), 187–193. https://doi.org/10.1111/j.1432-1033.1994.tb19929.x

135- De Virgilio C. (2012). The essence of yeast quiescence. *FEMS microbiology reviews*, *36*(2), 306–339. https://doi.org/10.1111/j.1574-6976.2011.00287.x

136- Wiemken A. (1990). Trehalose in yeast, stress protectant rather than reserve carbohydrate. *Antonie van Leeuwenhoek*, *58*(3), 209–217. https://doi.org/10.1007/BF00548935

137- Bell, W., Klaassen, P., Ohnacker, M., Boller, T., Herweijer, M., Schoppink, P., Van der Zee, P., & Wiemken, A. (1992). Characterization of the 56-kDa subunit of yeast trehalose-6-phosphate synthase and cloning of its gene reveal its identity with the product of CIF1, a regulator of carbon catabolite inactivation. *European journal of biochemistry*, *209*(3), 951–959. https://doi.org/10.1111/j.1432-1033.1992.tb17368.x

138- Bell, W., Sun, W., Hohmann, S., Wera, S., Reinders, A., De Virgilio, C., Wiemken, A., & Thevelein, J. M. (1998). Composition and functional analysis of the Saccharomyces cerevisiae trehalose synthase complex. *The Journal of biological chemistry*, *273*(50), 33311–33319. https://doi.org/10.1074/jbc.273.50.33311

139- De Virgilio, C., Bürckert, N., Bell, W., Jenö, P., Boller, T., & Wiemken, A. (1993). Disruption of TPS2, the gene encoding the 100-kDa subunit of the trehalose-6-phosphate synthase/phosphatase complex in Saccharomyces cerevisiae, causes accumulation of trehalose-6-phosphate and loss of trehalose-6-phosphate phosphatase activity. *European journal of biochemistry*, *212*(2), 315–323. https://doi.org/10.1111/j.1432-1033.1993.tb17664.x

140- Vuorio, O. E., Kalkkinen, N., & Londesborough, J. (1993). Cloning of two related genes encoding the 56-kDa and 123-kDa subunits of trehalose synthase from the yeast Saccharomyces cerevisiae. *European journal of biochemistry*, *216*(3), 849–861. https://doi.org/10.1111/j.1432-1033.1993.tb18207.x

141- Reinders, A., Bürckert, N., Hohmann, S., Thevelein, J. M., Boller, T., Wiemken, A., & De Virgilio, C. (1997). Structural analysis of

the subunits of the trehalose-6-phosphate synthase/phosphatase complex in Saccharomyces cerevisiae and their function during heat shock. *Molecular microbiology*, *24*(4), 687–695. https://doi.org/10.1046/j.1365-2958.1997.3861749.x

142- DeRisi, J. L., Iyer, V. R., & Brown, P. O. (1997). Exploring the metabolic and genetic control of gene expression on a genomic scale. *Science (New York, N.Y.)*, *278*(5338), 680–686. https://doi.org/10.1126/science.278.5338.680

143- Vandercammen, A., François, J., & Hers, H. G. (1989). Characterization of trehalose-6-phosphate synthase and trehalose-6-phosphate phosphatase of Saccharomyces cerevisiae. *European journal of biochemistry*, *182*(3), 613–620. https://doi.org/10.1111/j.1432-1033.1989.tb14870.x

144- Londesborough, J., & Vuorio, O. E. (1993). Purification of trehalose synthase from baker's yeast. Its temperature-dependent activation by fructose 6-phosphate and inhibition by phosphate. *European journal of biochemistry*, *216*(3), 841–848. https://doi.org/10.1111/j.1432-1033.1993.tb18206.x

145- Cao, L., Tang, Y., Quan, Z., Zhang, Z., Oliver, S. G., & Zhang, N. (2016). Chronological Lifespan in Yeast Is Dependent on the Accumulation of Storage Carbohydrates Mediated by Yak1, Mck1 and Rim15 Kinases. *PLoS genetics*, *12*(12), e1006458. https://doi.org/10.1371/journal.pgen.1006458

146- Shi, L., Sutter, B. M., Ye, X., & Tu, B. P. (2010). Trehalose is a key determinant of the quiescent metabolic state that fuels cell cycle progression upon return to growth. *Molecular biology of the cell*, *21*(12), 1982–1990. https://doi.org/10.1091/mbc.e10-01-0056

147- Thevelein J. M. (1984). Regulation of trehalose mobilization in fungi. *Microbiological reviews*, *48*(1), 42–59. https://doi.org/10.1128/mr.48.1.42-59.1984

148- Jules, M., Guillou, V., François, J., & Parrou, J. L. (2004). Two distinct pathways for trehalose assimilation in the yeast Saccharomyces cerevisiae. *Applied and environmental microbiology*, *70*(5), 2771–2778. https://doi.org/10.1128/AEM.70.5.2771-2778.2004

149- Jules, M., Beltran, G., François, J., & Parrou, J. L. (2008). New insights into trehalose metabolism by Saccharomyces cerevisiae: NTH2 encodes a functional cytosolic trehalase, and deletion of TPS1 reveals Ath1p-dependent trehalose mobilization. *Applied and environmental microbiology*, *74*(3), 605–614. https://doi.org/10.1128/AEM.00557-07

150- Parrou, J. L., Jules, M., Beltran, G., & François, J. (2005). Acid trehalase in yeasts and filamentous fungi: localization, regulation and physiological function. *FEMS yeast research*, *5*(6-7), 503–511. https://doi.org/10.1016/j.femsyr.2005.01.002

151- Lee, Y. J., Jang, J. W., Kim, K. J., & Maeng, P. J. (2011). TCA cycle-independent acetate metabolism via the glyoxylate cycle in Saccharomyces cerevisiae. *Yeast (Chichester, England)*, *28*(2), 153–166. https://doi.org/10.1002/yea.1828

152- Strijbis, K., & Distel, B. (2010). Intracellular acetyl unit transport in fungal carbon metabolism. *Eukaryotic cell*, *9*(12), 1809–1815. https://doi.org/10.1128/EC.00172-10

153- Klein, M., Swinnen, S., Thevelein, J. M., & Nevoigt, E. (2017). Glycerol metabolism and transport in yeast and fungi: established knowledge and ambiguities. *Environmental microbiology*, *19*(3), 878–893. https://doi.org/10.1111/1462-2920.13617

154- Johannes P. van Dijken, W. Alexander Scheffers, Redox balances in the metabolism of sugars by yeasts, *FEMS Microbiology Reviews*, Volume 1, Issue 3-4, April 1986, Pages 199–224. https://doi.org/10.1111/j.1574-6968.1986.tb01194.x

155- Ansell, R., Granath, K., Hohmann, S., Thevelein, J. M., & Adler, L. (1997). The two isoenzymes for yeast NAD+-dependent glycerol 3-phosphate dehydrogenase encoded by GPD1 and GPD2 have distinct roles in osmoadaptation and redox regulation. *The EMBO journal*, *16*(9), 2179–2187. https://doi.org/10.1093/emboj/16.9.2179

156- Wei, M., Fabrizio, P., Madia, F., Hu, J., Ge, H., Li, L. M., & Longo, V. D. (2009). Tor1/Sch9-regulated carbon source substitution is as effective as calorie restriction in life span extension. *PLoS genetics*, *5*(5), e1000467. https://doi.org/10.1371/journal.pgen.1000467

157- Nevoigt, E., & Stahl, U. (1997) Osmoregulation and glycerol metabolism in the yeast *Saccharomyces cerevisiae*. *FEMS Microbiology Reviews*, *21*(3), 231–241. https://doi.org/10.1111/j.1574-6976.1997.tb00352.x

158- Larsson, K., Ansell, R., Eriksson, P., & Adler, L. (1993). A gene encoding sn-glycerol 3-phosphate dehydrogenase (NAD+) complements an osmosensitive mutant of Saccharomyces cerevisiae. *Molecular microbiology*, *10*(5), 1101–1111. https://doi.org/10.1111/j.1365-2958.1993.tb00980.x

159- Albertyn, J., Hohmann, S., Thevelein, J. M., & Prior, B. A. (1994). GPD1, which encodes glycerol-3-phosphate dehydrogenase, is essential for growth under osmotic stress in Saccharomyces cerevisiae, and its expression is regulated by the high-osmolarity glycerol response pathway. *Molecular and cellular biology*, *14*(6), 4135–4144. https://doi.org/10.1128/mcb.14.6.4135-4144.1994

160- Wang, H. T., Rahaim, P., Robbins, P., & Yocum, R. R. (1994). Cloning, sequence, and disruption of the Saccharomyces diastaticus DAR1 gene encoding a glycerol-3-phosphate dehydrogenase. *Journal of bacteriology*, *176*(22), 7091–7095. https://doi.org/10.1128/jb.176.22.7091-7095.1994

161- Haurie, V., Perrot, M., Mini, T., Jenö, P., Sagliocco, F., & Boucherie, H. (2001). The transcriptional activator Cat8p provides a major contribution to the reprogramming of carbon metabolism during the diauxic shift in Saccharomyces cerevisiae. *The Journal of biological chemistry*, *276*(1), 76–85. https://doi.org/10.1074/jbc.M008752200

162- Hedges, D., Proft, M., & Entian, K. D. (1995). CAT8, a new zinc cluster-encoding gene necessary for derepression of gluconeogenic enzymes in the yeast Saccharomyces cerevisiae. *Molecular and cellular biology*, *15*(4), 1915–1922. https://doi.org/10.1128/MCB.15.4.1915

163- Young, E. T., Dombek, K. M., Tachibana, C., & Ideker, T. (2003). Multiple pathways are co-regulated by the protein kinase Snf1 and the transcription factors Adr1 and Cat8. *The Journal of biological chemistry*, *278*(28), 26146–26158. https://doi.org/10.1074/jbc.M301981200

164- Roth, S., Kumme, J., & Schüller, H. J. (2004). Transcriptional activators Cat8 and Sip4 discriminate between sequence variants of the carbon source-responsive promoter element in the yeast Saccharomyces cerevisiae. *Current genetics*, *45*(3), 121–128. https://doi.org/10.1007/s00294-003-0476-2

165- Grandier-Vazeille, X., Bathany, K., Chaignepain, S., Camougrand, N., Manon, S., & Schmitter, J. M. (2001). Yeast mitochondrial dehydrogenases are associated in a supramolecular complex. *Biochemistry*, *40*(33), 9758–9769. https://doi.org/10.1021/bi010277r

166- Grauslund, M., & Rønnow, B. (2000). Carbon source-dependent transcriptional regulation of the mitochondrial glycerol-3-phosphate dehydrogenase gene, GUT2, from Saccharomyces cerevisiae. *Canadian journal of microbiology*, *46*(12), 1096–1100. https://doi.org/10.1139/w00-105

167- Lu, L., Roberts, G., Simon, K., Yu, J., & Hudson, A. P. (2003). Rsf1p, a protein required for respiratory growth of Saccharomyces cerevisiae. *Current genetics*, *43*(4), 263–272. https://doi.org/10.1007/s00294-003-0398-z

168- Roberts, G. G., & Hudson, A. P. (2006). Transcriptome profiling of Saccharomyces cerevisiae during a transition from fermentative to glycerol-based respiratory growth reveals extensive metabolic and structural remodeling. *Molecular genetics and genomics : MGG*, *276*(2), 170–186. https://doi.org/10.1007/s00438-006-0133-9

169- Lu, L., Roberts, G. G., Oszust, C., & Hudson, A. P. (2005). The YJR127C/ZMS1 gene product is involved in glycerol-based respiratory growth of the yeast Saccharomyces cerevisiae. *Current genetics*, *48*(4), 235–246. https://doi.org/10.1007/s00294-005-0023-4

170- Roberts, G. G., 3rd, & Hudson, A. P. (2009). Rsf1p is required for an efficient metabolic shift from fermentative to glycerol-based respiratory growth in S. cerevisiae. *Yeast (Chichester, England)*, *26*(2), 95–110. https://doi.org/10.1002/yea.1655

171- Zaman, S., Lippman, S. I., Schneper, L., Slonim, N., & Broach, J. R. (2009). Glucose regulates transcription in yeast through a network of signaling pathways. *Molecular systems biology*, *5*, 245.

https://doi.org/10.1038/msb.2009.2
172- Creamer, D. R., Hubbard, S. J., Ashe, M. P., & Grant, C. M. (2022). Yeast Protein Kinase A Isoforms: A Means of Encoding Specificity in the Response to Diverse Stress Conditions?. *Biomolecules*, *12*(7), 958. https://doi.org/10.3390/biom12070958
173- Robertson, L. S., & Fink, G. R. (1998). The three yeast A kinases have specific signaling functions in pseudohyphal growth. *Proceedings of the National Academy of Sciences of the United States of America*, *95*(23), 13783–13787. https://doi.org/10.1073/pnas.95.23.13783
174- Ptacek, J., Devgan, G., Michaud, G., Zhu, H., Zhu, X., Fasolo, J., Guo, H., Jona, G., Breitkreutz, A., Sopko, R., McCartney, R. R., Schmidt, M. C., Rachidi, N., Lee, S. J., Mah, A. S., Meng, L., Stark, M. J., Stern, D. F., De Virgilio, C., Tyers, M., … Snyder, M. (2005). Global analysis of protein phosphorylation in yeast. *Nature*, *438*(7068), 679–684. https://doi.org/10.1038/nature04187
175- Thevelein, J. M., & de Winde, J. H. (1999). Novel sensing mechanisms and targets for the cAMP-protein kinase A pathway in the yeast Saccharomyces cerevisiae. *Molecular microbiology*, *33*(5), 904–918. https://doi.org/10.1046/j.1365-2958.1999.01538.x
176- Schneper, L., Düvel, K., & Broach, J. R. (2004). Sense and sensibility: nutritional response and signal integration in yeast. *Current opinion in microbiology*, *7*(6), 624–630. https://doi.org/10.1016/j.mib.2004.10.002
177- Santangelo G. M. (2006). Glucose signaling in Saccharomyces cerevisiae. *Microbiology and molecular biology reviews : MMBR*, *70*(1), 253–282. https://doi.org/10.1128/MMBR.70.1.253-282.2006
178- Zeller, C. E., Parnell, S. C., & Dohlman, H. G. (2007). The RACK1 ortholog Asc1 functions as a G-protein beta subunit coupled to glucose responsiveness in yeast. *The Journal of biological chemistry*, *282*(34), 25168–25176. https://doi.org/10.1074/jbc.M702569200
179- Griffioen, G., Anghileri, P., Imre, E., Baroni, M. D., & Ruis, H. (2000). Nutritional control of nucleocytoplasmic localization of cAMP-dependent protein kinase catalytic and regulatory subunits in Saccharomyces cerevisiae. *The Journal of biological chemistry*, *275*(2), 1449–1456. https://doi.org/10.1074/jbc.275.2.1449

180- Moir, R. D., Lee, J., Haeusler, R. A., Desai, N., Engelke, D. R., & Willis, I. M. (2006). Protein kinase A regulates RNA polymerase III transcription through the nuclear localization of Maf1. *Proceedings of the National Academy of Sciences of the United States of America*, *103*(41), 15044–15049. https://doi.org/10.1073/pnas.0607129103

181- Cai, Y., & Wei, Y. H. (2015). Distinct regulation of Maf1 for lifespan extension by Protein kinase A and Sch9. *Aging*, *7*(2), 133–143. https://doi.org/10.18632/aging.100727.

182- Werner-Washburne, M., Brown, D., & Braun, E. (1991). Bcy1, the regulatory subunit of cAMP-dependent protein kinase in yeast, is differentially modified in response to the physiological status of the cell. *The Journal of biological chemistry*, *266*(29), 19704–19709. https://doi.org/10.1016/S0021-9258(18)55049-3.

183- Griffioen, G., Branduardi, P., Ballarini, A., Anghileri, P., Norbeck, J., Baroni, M. D., & Ruis, H. (2001). Nucleocytoplasmic distribution of budding yeast protein kinase A regulatory subunit Bcy1 requires Zds1 and is regulated by Yak1-dependent phosphorylation of its targeting domain. *Molecular and cellular biology*, *21*(2), 511–523. https://doi.org/10.1128/MCB.21.2.511-523.2001

184- Lee, P., Cho, B. R., Joo, H. S., & Hahn, J. S. (2008). Yeast Yak1 kinase, a bridge between PKA and stress-responsive transcription factors, Hsf1 and Msn2/Msn4. Molecular microbiology, 70(4), 882–895. https://doi.org/10.1111/j.1365-2958.2008.06450.x

185- Görner, W., Durchschlag, E., Martinez-Pastor, M. T., Estruch, F., Ammerer, G., Hamilton, B., Ruis, H., & Schüller, C. (1998). Nuclear localization of the C2H2 zinc finger protein Msn2p is regulated by stress and protein kinase A activity. *Genes & development*, *12*(4), 586–597. https://doi.org/10.1101/gad.12.4.586

186- Görner, W., Durchschlag, E., Wolf, J., Brown, E. L., Ammerer, G., Ruis, H., & Schüller, C. (2002). Acute glucose starvation activates the nuclear localization signal of a stress-specific yeast transcription factor. *The EMBO journal*, *21*(1-2), 135–144. https://doi.org/10.1093/emboj/21.1.135

187- Garreau, H., Hasan, R. N., Renault, G., Estruch, F., Boy-Marcotte, E., & Jacquet, M. (2000). Hyperphosphorylation of Msn2p and Msn4p in response to heat shock and the diauxic shift is inhibited by cAMP in Saccharomyces cerevisiae. *Microbiology (Reading, England)*, *146 (Pt 9)*, 2113–2120.

https://doi.org/10.1099/00221287-146-9-2113
188- Reinders, A., Bürckert, N., Boller, T., Wiemken, A., & De Virgilio, C. (1998). Saccharomyces cerevisiae cAMP-dependent protein kinase controls entry into stationary phase through the Rim15p protein kinase. *Genes & development*, *12*(18), 2943–2955. https://doi.org/10.1101/gad.12.18.2943
189- Talarek, N., Cameroni, E., Jaquenoud, M., Luo, X., Bontron, S., Lippman, S., Devgan, G., Snyder, M., Broach, J. R., & De Virgilio, C. (2010). Initiation of the TORC1-regulated G0 program requires Igo1/2, which license specific mRNAs to evade degradation via the 5'-3' mRNA decay pathway. *Molecular cell*, *38*(3), 345–355. https://doi.org/10.1016/j.molcel.2010.02.039
190- Luo, X., Talarek, N., & De Virgilio, C. (2011). Initiation of the yeast G0 program requires Igo1 and Igo2, which antagonize activation of decapping of specific nutrient-regulated mRNAs. *RNA biology*, *8*(1), 14–17. https://doi.org/10.4161/rna.8.1.13483
191- Budovskaya, Y. V., Stephan, J. S., Reggiori, F., Klionsky, D. J., & Herman, P. K. (2004). The Ras/cAMP-dependent protein kinase signaling pathway regulates an early step of the autophagy process in Saccharomyces cerevisiae. *The Journal of biological chemistry*, *279*(20), 20663–20671. https://doi.org/10.1074/jbc.M400272200
192- Budovskaya, Y. V., Stephan, J. S., Deminoff, S. J., & Herman, P. K. (2005). An evolutionary proteomics approach identifies substrates of the cAMP-dependent protein kinase. *Proceedings of the National Academy of Sciences of the United States of America*, *102*(39), 13933–13938. https://doi.org/10.1073/pnas.0501046102
193- Stephan, J. S., Yeh, Y. Y., Ramachandran, V., Deminoff, S. J., & Herman, P. K. (2009). The Tor and PKA signaling pathways independently target the Atg1/Atg13 protein kinase complex to control autophagy. *Proceedings of the National Academy of Sciences of the United States of America*, *106*(40), 17049–17054. https://doi.org/10.1073/pnas.0903316106
194- González, A., & Hall, M. N. (2017). Nutrient sensing and TOR signaling in yeast and mammals. *The EMBO journal*, *36*(4), 397–408. https://doi.org/10.15252/embj.201696010
195- Seto B. (2012). Rapamycin and mTOR: a serendipitous discovery and implications for breast cancer. *Clinical and translational medicine*, *1*(1), 29. https://doi.org/10.1186/2001-1326-1-29

196- Loewith, R., Jacinto, E., Wullschleger, S., Lorberg, A., Crespo, J. L., Bonenfant, D., Oppliger, W., Jenoe, P., & Hall, M. N. (2002). Two TOR complexes, only one of which is rapamycin sensitive, have distinct roles in cell growth control. *Molecular cell*, *10*(3), 457–468. https://doi.org/10.1016/s1097-2765(02)00636-6
197- Wullschleger, S., Loewith, R., & Hall, M. N. (2006). TOR signaling in growth and metabolism. *Cell*, *124*(3), 471–484. https://doi.org/10.1016/j.cell.2006.01.016
198- De Virgilio, C., & Loewith, R. (2006). Cell growth control: little eukaryotes make big contributions. *Oncogene*, *25*(48), 6392–6415. https://doi.org/10.1038/sj.onc.1209884
199- Nicastro, R., Péli-Gulli, M. P., Caligaris, M., Jaquenoud, M., Dokládal, L., Alba, J., Tripodi, F., Pillet, B., Brunner, M., Stumpe, M., Muneshige, K., Hatakeyama, R., Dengjel, J., & De Virgilio, C. (2025). TORC1 autonomously controls its spatial partitioning via the Rag GTPase tether Tco89. *Cell reports*, *44*(5), 115683. https://doi.org/10.1016/j.celrep.2025.115683
200- Urban, J., Soulard, A., Huber, A., Lippman, S., Mukhopadhyay, D., Deloche, O., Wanke, V., Anrather, D., Ammerer, G., Riezman, H., Broach, J. R., De Virgilio, C., Hall, M. N., & Loewith, R. (2007). Sch9 is a major target of TORC1 in Saccharomyces cerevisiae. *Molecular cell*, *26*(5), 663–674. https://doi.org/10.1016/j.molcel.2007.04.020
201- Wanke, V., Cameroni, E., Uotila, A., Piccolis, M., Urban, J., Loewith, R., & De Virgilio, C. (2008). Caffeine extends yeast lifespan by targeting TORC1. *Molecular microbiology*, *69*(1), 277–285. https://doi.org/10.1111/j.1365-2958.2008.06292.x
202- Teng, X., & Hardwick, J. M. (2019). Whi2: a new player in amino acid sensing. *Current genetics*, *65*(3), 701–709. https://doi.org/10.1007/s00294-018-00929-9
203- Nakashima, S., Morinaka, K., Koyama, S., Ikeda, M., Kishida, M., Okawa, K., Iwamatsu, A., Kishida, S., & Kikuchi, A. (1999). Small G protein Ral and its downstream molecules regulate endocytosis of EGF and insulin receptors. *The EMBO journal*, *18*(13), 3629–3642. https://doi.org/10.1093/emboj/18.13.3629
204- Nicastro, R., Sardu, A., Panchaud, N., & De Virgilio, C. (2017). The Architecture of the Rag GTPase Signaling Network. *Biomolecules*, *7*(3), 48. https://doi.org/10.3390/biom7030048
205- Binda, M., Péli-Gulli, M. P., Bonfils, G., Panchaud, N., Urban, J., Sturgill, T. W., Loewith, R., & De Virgilio, C. (2009). The Vam6 GEF

controls TORC1 by activating the EGO complex. *Molecular cell*, *35*(5), 563–573.
https://doi.org/10.1016/j.molcel.2009.06.033

206- Gao, M., & Kaiser, C. A. (2006). A conserved GTPase-containing complex is required for intracellular sorting of the general amino-acid permease in yeast. *Nature cell biology*, *8*(7), 657–667.
https://doi.org/10.1038/ncb1419

207- Powis, K., Zhang, T., Panchaud, N., Wang, R., De Virgilio, C., & Ding, J. (2015). Crystal structure of the Ego1-Ego2-Ego3 complex and its role in promoting Rag GTPase-dependent TORC1 signaling. *Cell research*, *25*(9), 1043–1059.
https://doi.org/10.1038/cr.2015.86

208- Zhang, T., Péli-Gulli, M. P., Zhang, Z., Tang, X., Ye, J., De Virgilio, C., & Ding, J. (2019). Structural insights into the EGO-TC-mediated membrane tethering of the TORC1-regulatory Rag GTPases. *Science advances*, *5*(9), eaax8164.
https://doi.org/10.1126/sciadv.aax8164

209- Panchaud, N., Péli-Gulli, M. P., & De Virgilio, C. (2013). Amino acid deprivation inhibits TORC1 through a GTPase-activating protein complex for the Rag family GTPase Gtr1. *Science signaling*, *6*(277), ra42.
https://doi.org/10.1126/scisignal.2004112

210- Panchaud, N., Péli-Gulli, M. P., & De Virgilio, C. (2013). SEACing the GAP that nEGOCiates TORC1 activation: evolutionary conservation of Rag GTPase regulation. *Cell cycle (Georgetown, Tex.)*, *12*(18), 2948–2952.
https://doi.org/10.4161/cc.26000

211- Péli-Gulli, M. P., Sardu, A., Panchaud, N., Raucci, S., & De Virgilio, C. (2015). Amino Acids Stimulate TORC1 through Lst4-Lst7, a GTPase-Activating Protein Complex for the Rag Family GTPase Gtr2. *Cell reports*, *13*(1), 1–7.
https://doi.org/10.1016/j.celrep.2015.08.059

212- Ukai, H., Araki, Y., Kira, S., Oikawa, Y., May, A. I., & Noda, T. (2018). Gtr/Ego-independent TORC1 activation is achieved through a glutamine-sensitive interaction with Pib2 on the vacuolar membrane. *PLoS genetics*, *14*(4), e1007334.
https://doi.org/10.1371/journal.pgen.1007334

213- De Virgilio, C., & Loewith, R. (2006). The TOR signalling network from yeast to man. *The international journal of biochemistry & cell biology*, *38*(9), 1476–1481.
https://doi.org/10.1016/j.biocel.2006.02.013

214- Caligaris, M., Sampaio-Marques, B., Hatakeyama, R., Pillet, B., Ludovico, P., De Virgilio, C., Winderickx, J., & Nicastro, R. (2023). The Yeast Protein Kinase Sch9 Functions as a Central Nutrient-Responsive Hub That Calibrates Metabolic and Stress-Related Responses. *Journal of fungi (Basel, Switzerland)*, *9*(8), 787. https://doi.org/10.3390/jof9080787

215- Caligaris, M., Nicastro, R., Hu, Z., Tripodi, F., Hummel, J. E., Pillet, B., Deprez, M. A., Winderickx, J., Rospert, S., Coccetti, P., Dengjel, J., & De Virgilio, C. (2023). Snf1/AMPK fine-tunes TORC1 signaling in response to glucose starvation. eLife, 12, e84319. https://doi.org/10.7554/eLife.84319

216- Deprez, M. A., Eskes, E., Wilms, T., Ludovico, P., & Winderickx, J. (2018). pH homeostasis links the nutrient sensing PKA/TORC1/Sch9 ménage-à-trois to stress tolerance and longevity. *Microbial cell (Graz, Austria)*, *5*(3), 119–136. https://doi.org/10.15698/mic2018.03.618

217- Tate, J. J., Rai, R., & Cooper, T. G. (2015). Nitrogen starvation and TorC1 inhibition differentially affect nuclear localization of the Gln3 and Gat1 transcription factors through the rare glutamine tRNACUG in Saccharomyces cerevisiae. *Genetics*, *199*(2), 455–474. https://doi.org/10.1534/genetics.114.173831

218- Hatakeyama, R., Péli-Gulli, M. P., Hu, Z., Jaquenoud, M., Garcia Osuna, G. M., Sardu, A., Dengjel, J., & De Virgilio, C. (2019). Spatially Distinct Pools of TORC1 Balance Protein Homeostasis. *Molecular cell*, *73*(2), 325–338.e8. https://doi.org/10.1016/j.molcel.2018.10.040

219- Hu, Z., Raucci, S., Jaquenoud, M., Hatakeyama, R., Stumpe, M., Rohr, R., Reggiori, F., De Virgilio, C., & Dengjel, J. (2019). Multilayered Control of Protein Turnover by TORC1 and Atg1. *Cell reports*, *28*(13), 3486–3496.e6. https://doi.org/10.1016/j.celrep.2019.08.069

220- Noda T. (2017). Autophagy in the context of the cellular membrane-trafficking system: the enigma of Atg9 vesicles. *Biochemical Society transactions*, *45*(6), 1323–1331. https://doi.org/10.1042/BST20170128

221- Hatakeyama, R., & De Virgilio, C. (2019). A spatially and functionally distinct pool of TORC1 defines signaling endosomes in yeast. *Autophagy*, *15*(5), 915–916. https://doi.org/10.1080/15548627.2019.1580107

222- Henne, W. M., Buchkovich, N. J., & Emr, S. D. (2011). The ESCRT pathway. *Developmental cell*, *21*(1), 77–91. https://doi.org/10.1016/j.devcel.2011.05.015

223- Morshed, N., Ralvenius, W. T., Nott, A., Watson, L. A., Rodriguez, F. H., Akay, L. A., Joughin, B. A., Pao, P. C., Penney, J., LaRocque, L., Mastroeni, D., Tsai, L. H., & White, F. M. (2020). Phosphoproteomics identifies microglial Siglec-F inflammatory response during neurodegeneration. *Molecular systems biology*, *16*(12), e9819. https://doi.org/10.15252/msb.20209819

224- Yao, W., Chen, Y., Chen, Y., Zhao, P., Liu, J., Zhang, Y., Jiang, Q., Wu, C., Xie, Y., Fan, S., Ye, M., Wang, Y., Feng, Y., Bai, X., Fan, M., Feng, S., Wang, J., Cui, Y., Xia, H., Ma, C., … Yi, C. (2023). TOR-mediated Ypt1 phosphorylation regulates autophagy initiation complex assembly. *The EMBO journal*, *42*(19), e112814. https://doi.org/10.15252/embj.2022112814

225- González, A., Shimobayashi, M., Eisenberg, T., Merle, D. A., Pendl, T., Hall, M. N., & Moustafa, T. (2015). TORC1 promotes phosphorylation of ribosomal protein S6 via the AGC kinase Ypk3 in Saccharomyces cerevisiae. *PloS one*, *10*(3), e0120250. https://doi.org/10.1371/journal.pone.0120250

226- Yerlikaya, S., Meusburger, M., Kumari, R., Huber, A., Anrather, D., Costanzo, M., Boone, C., Ammerer, G., Baranov, P. V., & Loewith, R. (2016). TORC1 and TORC2 work together to regulate ribosomal protein S6 phosphorylation in Saccharomyces cerevisiae. *Molecular biology of the cell*, *27*(2), 397–409. https://doi.org/10.1091/mbc.E15-08-0594

227- Dokládal, L., Stumpe, M., Pillet, B., Hu, Z., Garcia Osuna, G. M., Kressler, D., Dengjel, J., & De Virgilio, C. (2021). Global phosphoproteomics pinpoints uncharted Gcn2-mediated mechanisms of translational control. *Molecular cell*, *81*(9), 1879–1889.e6. https://doi.org/10.1016/j.molcel.2021.02.037

228- Jorgensen, P., Rupes, I., Sharom, J. R., Schneper, L., Broach, J. R., & Tyers, M. (2004). A dynamic transcriptional network communicates growth potential to ribosome synthesis and critical cell size. *Genes & development*, *18*(20), 2491–2505. https://doi.org/10.1101/gad.1228804

229- Lempiäinen, H., Uotila, A., Urban, J., Dohnal, I., Ammerer, G., Loewith, R., & Shore, D. (2009). Sfp1 interaction with TORC1 and Mrs6 reveals feedback regulation on TOR signaling. *Molecular cell*, *33*(6), 704–716. https://doi.org/10.1016/j.molcel.2009.01.034

230- Loewith, R., & Hall, M. N. (2011). Target of rapamycin (TOR) in nutrient signaling and growth control. *Genetics*, *189*(4), 1177–1201. https://doi.org/10.1534/genetics.111.133363

231- Cecil, J. H., Padilla, C. M., Lipinski, A. A., Langlais, P. R., Luo, X., & Capaldi, A. P. (2025). The Molecular Logic of Gtr1/2 and Pib2 Dependent TORC1 Regulation in Budding Yeast. *bioRxiv : the preprint server for biology*, 2023.12.06.570342. https://doi.org/10.1101/2023.12.06.570342
232- Zeng, Q., Araki, Y., & Noda, T. (2024). Pib2 is a cysteine sensor involved in TORC1 activation in Saccharomyces cerevisiae. *Cell reports*, *43*(1), 113599. https://doi.org/10.1016/j.celrep.2023.113599
233- Coccetti, P., Nicastro, R., & Tripodi, F. (2018). Conventional and emerging roles of the energy sensor Snf1/AMPK in *Saccharomyces cerevisiae*. *Microbial cell (Graz, Austria)*, *5*(11), 482–494. https://doi.org/10.15698/mic2018.11.655
234- Hong, S. P., & Carlson, M. (2007). Regulation of snf1 protein kinase in response to environmental stress. *The Journal of biological chemistry*, *282*(23), 16838–16845. https://doi.org/10.1074/jbc.M700146200
235- Simpson-Lavy, K., & Kupiec, M. (2023). Glucose Inhibits Yeast AMPK (Snf1) by Three Independent Mechanisms. *Biology*, *12*(7), 1007. https://doi.org/10.3390/biology12071007
236- Nicastro, R., Tripodi, F., Guzzi, C., Reghellin, V., Khoomrung, S., Capusoni, C., Compagno, C., Airoldi, C., Nielsen, J., Alberghina, L., & Coccetti, P. (2015). Enhanced amino acid utilization sustains growth of cells lacking Snf1/AMPK. *Biochimica et biophysica acta*, *1853*(7), 1615–1625. https://doi.org/10.1016/j.bbamcr.2015.03.014
237- Hedbacker, K., & Carlson, M. (2008). SNF1/AMPK pathways in yeast. *Frontiers in bioscience : a journal and virtual library*, *13*, 2408–2420. https://doi.org/10.2741/2854
238- Crute, B. E., Seefeld, K., Gamble, J., Kemp, B. E., & Witters, L. A. (1998). Functional domains of the alpha1 catalytic subunit of the AMP-activated protein kinase. *The Journal of biological chemistry*, *273*(52), 35347–35354. https://doi.org/10.1074/jbc.273.52.35347
239- Sanz, P., Viana, R., & Garcia-Gimeno, M. A. (2016). AMPK in Yeast: The SNF1 (Sucrose Non-fermenting 1) Protein Kinase Complex. *Experientia supplementum (2012)*, *107*, 353–374. https://doi.org/10.1007/978-3-319-43589-3_14
240- Chen, L., Jiao, Z. H., Zheng, L. S., Zhang, Y. Y., Xie, S. T., Wang, Z. X., & Wu, J. W. (2009). Structural insight into the

autoinhibition mechanism of AMP-activated protein kinase. *Nature*, *459*(7250), 1146–1149. https://doi.org/10.1038/nature08075

241- Vincent, O., Townley, R., Kuchin, S., & Carlson, M. (2001). Subcellular localization of the Snf1 kinase is regulated by specific beta subunits and a novel glucose signaling mechanism. Genes & development, 15(9), 1104–1114. https://doi.org/10.1101/gad.879301

242- Leech, A., Nath, N., McCartney, R. R., & Schmidt, M. C. (2003). Isolation of mutations in the catalytic domain of the snf1 kinase that render its activity independent of the snf4 subunit. *Eukaryotic cell*, *2*(2), 265–273. https://doi.org/10.1128/EC.2.2.265-273.2003

243- Wilson, W. A., Hawley, S. A., & Hardie, D. G. (1996). Glucose repression/derepression in budding yeast: SNF1 protein kinase is activated by phosphorylation under derepressing conditions, and this correlates with a high AMP:ATP ratio. *Current biology : CB*, *6*(11), 1426–1434. https://doi.org/10.1016/s0960-9822(96)00747-6

244- Rubenstein, E. M., McCartney, R. R., Zhang, C., Shokat, K. M., Shirra, M. K., Arndt, K. M., & Schmidt, M. C. (2008). Access denied: Snf1 activation loop phosphorylation is controlled by availability of the phosphorylated threonine 210 to the PP1 phosphatase. *The Journal of biological chemistry*, *283*(1), 222–230. https://doi.org/10.1074/jbc.M707957200

245- Maziarz, M., Shevade, A., Barrett, L., & Kuchin, S. (2016). Springing into Action: Reg2 Negatively Regulates Snf1 Protein Kinase and Facilitates Recovery from Prolonged Glucose Starvation in Saccharomyces cerevisiae. *Applied and environmental microbiology*, *82*(13), 3875–3885. https://doi.org/10.1128/AEM.00154-16

246- Ruiz, A., Xu, X., & Carlson, M. (2011). Roles of two protein phosphatases, Reg1-Glc7 and Sit4, and glycogen synthesis in regulation of SNF1 protein kinase. *Proceedings of the National Academy of Sciences of the United States of America*, *108*(16), 6349–6354. https://doi.org/10.1073/pnas.1102758108

247- Mayer, F. V., Heath, R., Underwood, E., Sanders, M. J., Carmena, D., McCartney, R. R., Leiper, F. C., Xiao, B., Jing, C., Walker, P. A., Haire, L. F., Ogrodowicz, R., Martin, S. R., Schmidt, M. C., Gamblin, S. J., & Carling, D. (2011). ADP regulates SNF1, the Saccharomyces cerevisiae homolog of AMP-activated protein kinase. *Cell metabolism*, *14*(5), 707–714.

https://doi.org/10.1016/j.cmet.2011.09.009
248- Papamichos-Chronakis, M., Gligoris, T., & Tzamarias, D. (2004). The Snf1 kinase controls glucose repression in yeast by modulating interactions between the Mig1 repressor and the Cyc8-Tup1 co-repressor. *EMBO reports*, *5*(4), 368–372. https://doi.org/10.1038/sj.embor.7400120
249- Treitel, M. A., Kuchin, S., & Carlson, M. (1998). Snf1 protein kinase regulates phosphorylation of the Mig1 repressor in Saccharomyces cerevisiae. *Molecular and cellular biology*, *18*(11), 6273–6280. https://doi.org/10.1128/MCB.18.11.6273
250- Chandrashekarappa, D. G., McCartney, R. R., O'Donnell, A. F., & Schmidt, M. C. (2016). The β subunit of yeast AMP-activated protein kinase directs substrate specificity in response to alkaline stress. *Cellular signalling*, *28*(12), 1881–1893. https://doi.org/10.1016/j.cellsig.2016.08.016
251- Serra-Cardona, A., Canadell, D., & Ariño, J. (2015). Coordinate responses to alkaline pH stress in budding yeast. *Microbial cell (Graz, Austria)*, *2*(6), 182–196. https://doi.org/10.15698/mic2015.06.205
252- Mizuno, T., Muroi, K., & Irie, K. (2020). Snf1 AMPK positively regulates ER-phagy via expression control of Atg39 autophagy receptor in yeast ER stress response. *PLoS genetics*, *16*(9), e1009053. https://doi.org/10.1371/journal.pgen.1009053
253- Vincent, O., & Carlson, M. (1999). Gal83 mediates the interaction of the Snf1 kinase complex with the transcription activator Sip4. *The EMBO journal*, *18*(23), 6672–6681. https://doi.org/10.1093/emboj/18.23.6672
254- Ratnakumar, S., Kacherovsky, N., Arms, E., & Young, E. T. (2009). Snf1 controls the activity of adr1 through dephosphorylation of Ser230. *Genetics*, *182*(3), 735–745. https://doi.org/10.1534/genetics.109.103432
255- Shi, S., Chen, Y., Siewers, V., & Nielsen, J. (2014). Improving production of malonyl coenzyme A-derived metabolites by abolishing Snf1-dependent regulation of Acc1. *mBio*, *5*(3), e01130-14. https://doi.org/10.1128/mBio.01130-14
256- De Wever, V., Reiter, W., Ballarini, A., Ammerer, G., & Brocard, C. (2005). A dual role for PP1 in shaping the Msn2-dependent transcriptional response to glucose starvation. *The EMBO journal*, *24*(23), 4115–4123. https://doi.org/10.1038/sj.emboj.7600871
257- Yao, W., Li, Y., Wu, L., Wu, C., Zhang, Y., Liu, J., He, Z., Wu, X., Lu, C., Wang, L., Zhong, H., Hong, Z., Xu, S., Liu, W., & Yi, C.

(2020). Atg11 is required for initiation of glucose starvation-induced autophagy. *Autophagy*, *16*(12), 2206–2218. https://doi.org/10.1080/15548627.2020.1719724

258- Singh, P., Arif, Y., Bajguz, A., & Hayat, S. (2021). The role of quercetin in plants. *Plant physiology and biochemistry : PPB*, *166*, 10–19. https://doi.org/10.1016/j.plaphy.2021.05.023

259- Grewal, A. K., Singh, T. G., Sharma, D., Sharma, V., Singh, M., Rahman, M. H., Najda, A., Walasek-Janusz, M., Kamel, M., Albadrani, G. M., Akhtar, M. F., Saleem, A., & Abdel-Daim, M. M. (2021). Mechanistic insights and perspectives involved in neuroprotective action of quercetin. *Biomedicine & pharmacotherapy = Biomedecine & pharmacotherapie*, *140*, 111729. https://doi.org/10.1016/j.biopha.2021.111729

260- Dabeek, W. M., & Marra, M. V. (2019). Dietary Quercetin and Kaempferol: Bioavailability and Potential Cardiovascular-Related Bioactivity in Humans. *Nutrients*, *11*(10), 2288. https://doi.org/10.3390/nu11102288

261- Costa, L. G., Garrick, J. M., Roquè, P. J., & Pellacani, C. (2016). Mechanisms of Neuroprotection by Quercetin: Counteracting Oxidative Stress and More. *Oxidative medicine and cellular longevity*, *2016*, 2986796. https://doi.org/10.1155/2016/2986796

262- Skrovankova, S., Sumczynski, D., Mlcek, J., Jurikova, T., & Sochor, J. (2015). Bioactive Compounds and Antioxidant Activity in Different Types of Berries. *International journal of molecular sciences*, *16*(10), 24673–24706. https://doi.org/10.3390/ijms161024673

263- Slimestad, R., Fossen, T., & Vågen, I. M. (2007). Onions: a source of unique dietary flavonoids. *Journal of agricultural and food chemistry*, *55*(25), 10067–10080. https://doi.org/10.1021/jf0712503

264- Xu, D., Hu, M. J., Wang, Y. Q., & Cui, Y. L. (2019). Antioxidant Activities of Quercetin and Its Complexes for Medicinal Application. *Molecules (Basel, Switzerland)*, *24*(6), 1123. https://doi.org/10.3390/molecules24061123

265- Carrizzo, A., Izzo, C., Forte, M., Sommella, E., Di Pietro, P., Venturini, E., Ciccarelli, M., Galasso, G., Rubattu, S., Campiglia, P., Sciarretta, S., Frati, G., & Vecchione, C. (2020). A Novel Promising Frontier for Human Health: The Beneficial Effects of Nutraceuticals in Cardiovascular Diseases. *International journal of molecular sciences*, *21*(22), 8706.

https://doi.org/10.3390/ijms21228706
266- Zahoor, H., Watchaputi, K., Hata, J., Pabuprapap, W., Suksamrarn, A., Chua, L. S., & Soontorngun, N. (2022). Model yeast as a versatile tool to examine the antioxidant and anti-ageing potential of flavonoids, extracted from medicinal plants. *Frontiers in pharmacology*, *13*, 980066. https://doi.org/10.3389/fphar.2022.980066
267- Carregosa, D., Mota, S., Ferreira, S., Alves-Dias, B., Loncarevic-Vasiljkovic, N., Crespo, C. L., Menezes, R., Teodoro, R., & Santos, C. N. d. (2021). Overview of Beneficial Effects of (Poly)phenol Metabolites in the Context of Neurodegenerative Diseases on Model Organisms. *Nutrients*, *13*(9), 2940. https://doi.org/10.3390/nu13092940
268- Gómez-Linton, D. R., Alavez, S., Alarcón-Aguilar, A., López-Diazguerrero, N. E., Konigsberg, M., & Pérez-Flores, L. J. (2019). Some naturally occurring compounds that increase longevity and stress resistance in model organisms of aging. *Biogerontology*, *20*(5), 583–603. https://doi.org/10.1007/s10522-019-09817-2
269- Longo, V. D., & Kennedy, B. K. (2006). Sirtuins in aging and age-related disease. *Cell*, *126*(2), 257–268. https://doi.org/10.1016/j.cell.2006.07.002
270- MacLean, M., Harris, N., & Piper, P. W. (2001). Chronological lifespan of stationary phase yeast cells; a model for investigating the factors that might influence the ageing of postmitotic tissues in higher organisms. *Yeast (Chichester, England)*, *18*(6), 499–509. https://doi.org/10.1002/yea.701
271- Zampar, G. G., Kümmel, A., Ewald, J., Jol, S., Niebel, B., Picotti, P., Aebersold, R., Sauer, U., Zamboni, N., & Heinemann, M. (2013). Temporal system-level organization of the switch from glycolytic to gluconeogenic operation in yeast. *Molecular systems biology*, *9*, 651. https://doi.org/10.1038/msb.2013.11
272- Zhang, N., & Cao, L. (2017). Starvation signals in yeast are integrated to coordinate metabolic reprogramming and stress response to ensure longevity. *Current genetics*, *63*(5), 839–843. https://doi.org/10.1007/s00294-017-0697-4
273- Pan, Y., Schroeder, E. A., Ocampo, A., Barrientos, A., & Shadel, G. S. (2011). Regulation of yeast chronological life span by TORC1 via adaptive mitochondrial ROS signaling. *Cell metabolism*, *13*(6), 668–678. https://doi.org/10.1016/j.cmet.2011.03.018

274- Powers, R. W., 3rd, Kaeberlein, M., Caldwell, S. D., Kennedy, B. K., & Fields, S. (2006). Extension of chronological life span in yeast by decreased TOR pathway signaling. *Genes & development*, *20*(2), 174–184. https://doi.org/10.1101/gad.1381406
275- Vall-Llaura, N., Mir, N., Garrido, L., Vived, C., & Cabiscol, E. (2019). Redox control of yeast Sir2 activity is involved in acetic acid resistance and longevity. *Redox biology*, *24*, 101229. https://doi.org/10.1016/j.redox.2019.101229
276- Sauve, A. A., Wolberger, C., Schramm, V. L., & Boeke, J. D. (2006). The biochemistry of sirtuins. *Annual review of biochemistry*, *75*, 435–465. https://doi.org/10.1146/annurev.biochem.74.082803.133500
277- Jackson, M. D., Schmidt, M. T., Oppenheimer, N. J., & Denu, J. M. (2003). Mechanism of nicotinamide inhibition and transglycosidation by Sir2 histone/protein deacetylases. *The Journal of biological chemistry*, *278*(51), 50985–50998. https://doi.org/10.1074/jbc.M306552200
278- Vanoni, M., Vai, M., Popolo, L., & Alberghina, L. (1983). Structural heterogeneity in populations of the budding yeast Saccharomyces cerevisiae. *Journal of bacteriology*, *156*(3), 1282–1291. https://doi.org/10.1128/jb.156.3.1282-1291.1983
279- Fabrizio, P., Gattazzo, C., Battistella, L., Wei, M., Cheng, C., McGrew, K., & Longo, V. D. (2005). Sir2 blocks extreme life-span extension. *Cell*, *123*(4), 655–667. https://doi.org/10.1016/j.cell.2005.08.042
280- Hu, J., Wei, M., Mirzaei, H., Madia, F., Mirisola, M., Amparo, C., Chagoury, S., Kennedy, B., & Longo, V. D. (2014). Tor-Sch9 deficiency activates catabolism of the ketone body-like acetic acid to promote trehalose accumulation and longevity. *Aging cell*, *13*(3), 457–467. https://doi.org/10.1111/acel.12202
281- Lee, D. H., & Goldberg, A. L. (1998). Proteasome inhibitors cause induction of heat shock proteins and trehalose, which together confer thermotolerance in Saccharomyces cerevisiae. *Molecular and cellular biology*, *18*(1), 30–38. https://doi.org/10.1128/MCB.18.1.30
282- Guerra, D. G., Decottignies, A., Bakker, B. M., & Michels, P. A. (2006). The mitochondrial FAD-dependent glycerol-3-phosphate dehydrogenase of Trypanosomatidae and the glycosomal redox balance of insect stages of Trypanosoma brucei and Leishmania spp. *Molecular and biochemical parasitology*, *149*(2), 155–169.

https://doi.org/10.1016/j.molbiopara.2006.05.006
283- Madeo, F., Fröhlich, E., Ligr, M., Grey, M., Sigrist, S. J., Wolf, D. H., & Fröhlich, K. U. (1999). Oxygen stress: a regulator of apoptosis in yeast. *The Journal of cell biology*, *145*(4), 757–767. https://doi.org/10.1083/jcb.145.4.757
284- Valtz, N., & Peter, M. (1997). Functional analysis of FAR1 in yeast. *Methods in enzymology*, *283*, 350–365. https://doi.org/10.1016/s0076-6879(97)83029-7
285- Calzari, L., Orlandi, I., Alberghina, L., & Vai, M. (2006). The histone deubiquitinating enzyme Ubp10 is involved in rDNA locus control in Saccharomyces cerevisiae by affecting Sir2p association. *Genetics*, *174*(4), 2249–2254. https://doi.org/10.1534/genetics.106.063099
286- Alugoju, P., Janardhanshetty, S. S., Subaramanian, S., Periyasamy, L., & Dyavaiah, M. (2018). Quercetin Protects Yeast Saccharomyces cerevisiae pep4 Mutant from Oxidative and Apoptotic Stress and Extends Chronological Lifespan. *Current microbiology*, *75*(5), 519–530. https://doi.org/10.1007/s00284-017-1412-x
287- Alugoju, P., Periyasamy, L., & Dyavaiah, M. (2020). Protective effect of quercetin in combination with caloric restriction against oxidative stress-induced cell death of Saccharomyces cerevisiae cells. *Letters in applied microbiology*, *71*(3), 272–279. https://doi.org/10.1111/lam.13313
288- Alugoju, P., Periyasamy, L., & Dyavaiah, M. (2018). Quercetin enhances stress resistance in *Saccharomyces cerevisiae tel1* mutant cells to different stressors. *Journal of food science and technology*, *55*(4), 1455–1466. https://doi.org/10.1007/s13197-018-3062-9
289- Belinha, I., Amorim, M. A., Rodrigues, P., de Freitas, V., Moradas-Ferreira, P., Mateus, N., & Costa, V. (2007). Quercetin increases oxidative stress resistance and longevity in Saccharomyces cerevisiae. *Journal of agricultural and food chemistry*, *55*(6), 2446–2451. https://doi.org/10.1021/jf063302e
290- Orlandi, I., Alberghina, L., & Vai, M. (2020). Nicotinamide, Nicotinamide Riboside and Nicotinic Acid-Emerging Roles in Replicative and Chronological Aging in Yeast. *Biomolecules*, *10*(4), 604. https://doi.org/10.3390/biom10040604
291- Baccolo, G., Stamerra, G., Coppola, D. P., Orlandi, I., & Vai, M. (2018). Mitochondrial Metabolism and Aging in Yeast. *International review of cell and molecular biology*, *340*, 1–33. https://doi.org/10.1016/bs.ircmb.2018.05.001

292- Murakami, C., & Kaeberlein, M. (2009). Quantifying yeast chronological life span by outgrowth of aged cells. *Journal of visualized experiments : JoVE*, (27), 1156. https://doi.org/10.3791/1156

293- Breitenbach, M., Rinnerthaler, M., Hartl, J., Stincone, A., Vowinckel, J., Breitenbach-Koller, H., & Ralser, M. (2014). Mitochondria in ageing: there is metabolism beyond the ROS. *FEMS yeast research*, *14*(1), 198–212. https://doi.org/10.1111/1567-1364.12134

294- Pan Y. (2011). Mitochondria, reactive oxygen species, and chronological aging: a message from yeast. *Experimental gerontology*, *46*(11), 847–852. https://doi.org/10.1016/j.exger.2011.08.007

295- Kejík, Z., Kaplánek, R., Masařík, M., Babula, P., Matkowski, A., Filipenský, P., Veselá, K., Gburek, J., Sýkora, D., Martásek, P., & Jakubek, M. (2021). Iron Complexes of Flavonoids-Antioxidant Capacity and Beyond. *International journal of molecular sciences*, *22*(2), 646. https://doi.org/10.3390/ijms22020646

296- Khokhar, S., Owusu Apenten, R.K. (2003) Iron binding characteristics of phenolic compounds: Some tentative structure-activity relations. *Food Chemistry*, *81*, 133–140. https://doi.org/10.1016/S0308-8146(02)00394-1

297- Gartenberg, M. R., & Smith, J. S. (2016). The Nuts and Bolts of Transcriptionally Silent Chromatin in Saccharomyces cerevisiae. *Genetics*, *203*(4), 1563–1599. https://doi.org/10.1534/genetics.112.145243

298- Bedalov, A., Gatbonton, T., Irvine, W. P., Gottschling, D. E., & Simon, J. A. (2001). Identification of a small molecule inhibitor of Sir2p. *Proceedings of the National Academy of Sciences of the United States of America*, *98*(26), 15113–15118. https://doi.org/10.1073/pnas.261574398

299- Smith, D. L., Jr, McClure, J. M., Matecic, M., & Smith, J. S. (2007). Calorie restriction extends the chronological lifespan of Saccharomyces cerevisiae independently of the Sirtuins. *Aging cell*, *6*(5), 649–662. https://doi.org/10.1111/j.1474-9726.2007.00326.x

300- Onken, B., Kalinava, N., & Driscoll, M. (2020). Gluconeogenesis and PEPCK are critical components of healthy aging and dietary restriction life extension. *PLoS genetics*, *16*(8), e1008982. https://doi.org/10.1371/journal.pgen.1008982

301- Bakker, B. M., Overkamp, K. M., van Maris AJ, Kötter, P., Luttik, M. A., van Dijken JP, & Pronk, J. T. (2001). Stoichiometry and compartmentation of NADH metabolism in Saccharomyces cerevisiae. *FEMS microbiology reviews*, *25*(1), 15–37. https://doi.org/10.1111/j.1574-6976.2001.tb00570.x

302- Xiberras, J., Klein, M., & Nevoigt, E. (2019). Glycerol as a substrate for Saccharomyces cerevisiae based bioprocesses - Knowledge gaps regarding the central carbon catabolism of this 'non-fermentable' carbon source. *Biotechnology advances*, *37*(6), 107378. https://doi.org/10.1016/j.biotechadv.2019.03.017

303- Xiberras, J., Klein, M., Prosch, C., Malubhoy, Z., & Nevoigt, E. (2020). Anaplerotic reactions active during growth of Saccharomyces cerevisiae on glycerol. *FEMS yeast research*, *20*(1), foz086. https://doi.org/10.1093/femsyr/foz086

304- Orlandi, I., Ronzulli, R., Casatta, N., & Vai, M. (2013). Ethanol and acetate acting as carbon/energy sources negatively affect yeast chronological aging. *Oxidative medicine and cellular longevity*, *2013*, 802870. https://doi.org/10.1155/2013/802870

305- Persson, S., Shashkova, S., Österberg, L., & Cvijovic, M. (2022). Modelling of glucose repression signalling in yeast Saccharomyces cerevisiae. *FEMS yeast research*, *22*(1), foac012. https://doi.org/10.1093/femsyr/foac012

306- Li, L., Ye, Y., Pan, L., Zhu, Y., Zheng, S., & Lin, Y. (2009). The induction of trehalose and glycerol in Saccharomyces cerevisiae in response to various stresses. *Biochemical and biophysical research communications*, *387*(4), 778–783. https://doi.org/10.1016/j.bbrc.2009.07.113

307- Estruch F. (2000). Stress-controlled transcription factors, stress-induced genes and stress tolerance in budding yeast. *FEMS microbiology reviews*, *24*(4), 469–486. https://doi.org/10.1111/j.1574-6976.2000.tb00551.x

308- Nguyen, V. P. T., Stewart, J., Lopez, M., Ioannou, I., & Allais, F. (2020). Glucosinolates: Natural Occurrence, Biosynthesis, Accessibility, Isolation, Structures, and Biological Activities. *Molecules (Basel, Switzerland)*, *25*(19), 4537. https://doi.org/10.3390/molecules25194537

309- Abuyusuf, M., Rubel, M. H., Kim, H. T., Jung, H. J., Nou, I. S., & Park, J. I. (2023). Glucosinolates and Biotic Stress Tolerance in Brassicaceae with Emphasis on Cabbage: A Review. *Biochemical genetics*, *61*(2), 451–470. https://doi.org/10.1007/s10528-022-10269-6

310- Chowdhury, P. (2022). Glucosinolates and Its Role in Mitigating Abiotic and Biotic Stress in Brassicaceae. *IntechOpen.* http://dx.doi.org/10.5772/intechopen.102367

311- Del Carmen Martínez-Ballesta, M., Moreno, D. A., & Carvajal, M. (2013). The physiological importance of glucosinolates on plant response to abiotic stress in Brassica. *International journal of molecular sciences*, *14*(6), 11607–11625. https://doi.org/10.3390/ijms140611607

312- Maina, S., Misinzo, G., Bakari, G., & Kim, H. Y. (2020). Human, Animal and Plant Health Benefits of Glucosinolates and Strategies for Enhanced Bioactivity: A Systematic Review. *Molecules (Basel, Switzerland)*, *25*(16), 3682. https://doi.org/10.3390/molecules25163682

313- Royo-Esnal, A., Edo-Tena, E., Torra, J., Recasens, J., & Gesch, R. W. (2017) Using fitness parameters to evaluate three oilseed Brassicaceae species as potential oil crops in two contrasting environments. *Industrial Crops and Products*, *95*, 148‑155. https://doi.org/10.1016/j.indcrop.2016.10.020

314- Arshad, M., Mohanty, A. K., Van Acker, R., Riddle, R., Todd, J., Khalil, H., & Misra, M. (2022). Valorization of camelina oil to biobased materials and biofuels for new industrial uses: a review. *RSC advances*, *12*(42), 27230–27245. https://doi.org/10.1039/d2ra03253h

315- Neupane, D., Lohaus, R. H., Solomon, J. K. Q., & Cushman, J. C. (2022). Realizing the Potential of *Camelina sativa* as a Bioenergy Crop for a Changing Global Climate. *Plants (Basel, Switzerland)*, *11*(6), 772. https://doi.org/10.3390/plants11060772

316- Riaz, R., Ahmed, I., Sizmaz, O., & Ahsan, U. (2022). Use of *Camelina sativa* and By-Products in Diets for Dairy Cows: A Review. *Animals : an open access journal from MDPI*, *12*(9), 1082. https://doi.org/10.3390/ani12091082

317- Juodka, R., Nainienė, R., Juškienė, V., Juška, R., Leikus, R., Kadžienė, G., & Stankevičienė, D. (2022). Camelina (*Camelina sativa* (L.) Crantz) as Feedstuffs in Meat Type Poultry Diet: A Source of Protein and n-3 Fatty Acids. *Animals : an open access journal from MDPI*, *12*(3), 295. https://doi.org/10.3390/ani12030295

318- Liu, G. Y., & Sabatini, D. M. (2020). mTOR at the nexus of nutrition, growth, ageing and disease. *Nature reviews. Molecular cell biology*, *21*(4), 183–203. https://doi.org/10.1038/s41580-019-0199-y

319- González, A., & Hall, M. N. (2017). Nutrient sensing and TOR signaling in yeast and mammals. *The EMBO journal*, *36*(4), 397–408. https://doi.org/10.15252/embj.201696010

320- Hofer, S. J., Daskalaki, I., Bergmann, M., Friščić, J., Zimmermann, A., Mueller, M. I., Abdellatif, M., Nicastro, R., Masser, S., Durand, S., Nartey, A., Waltenstorfer, M., Enzenhofer, S., Faimann, I., Gschiel, V., Bajaj, T., Niemeyer, C., Gkikas, I., Pein, L., Cerrato, G., … Madeo, F. (2024). Spermidine is essential for fasting-mediated autophagy and longevity. *Nature cell biology*, *26*(9), 1571–1584. https://doi.org/10.1038/s41556-024-01468-x

321- Zimmermann, A., Hofer, S., Pendl, T., Kainz, K., Madeo, F., & Carmona-Gutierrez, D. (2018). Yeast as a tool to identify anti-aging compounds. *FEMS yeast research*, *18*(6), foy020. https://doi.org/10.1093/femsyr/foy020

322- Pagliari, S., Giustra, C. M., Magoni, C., Celano, R., Fusi, P., Forcella, M., Sacco, G., Panzeri, D., Campone, L., & Labra, M. (2022). Optimization of ultrasound-assisted extraction of naturally occurring glucosinolates from by-products of *Camelina sativa* L. and their effect on human colorectal cancer cell line. *Frontiers in nutrition*, *9*, 901944. https://doi.org/10.3389/fnut.2022.901944

323- Kregiel, D., Berlowska, J., & Ambroziak,W. (2008) Succinate dehydrogenase activity assay *in situ* with blue tetrazolium salt in crabtree-positive *Saccharomyces cerevisiae* strain. *Food Technology and Biotechnology*, *46*(4), 376‑380. https://api.semanticscholar.org/CorpusID:44229136

324- Gonzalez, B., François, J., & Renaud, M. (1997). A rapid and reliable method for metabolite extraction in yeast using boiling buffered ethanol. *Yeast (Chichester, England)*, *13*(14), 1347–1355. https://doi.org/10.1002/(SICI)1097-0061(199711)13:14<1347::AID-YEA176>3.0.CO;2-O

325- Agrimi, G., Brambilla, L., Frascotti, G., Pisano, I., Porro, D., Vai, M., & Palmieri, L. (2011). Deletion or overexpression of mitochondrial NAD+ carriers in Saccharomyces cerevisiae alters cellular NAD and ATP contents and affects mitochondrial metabolism and the rate of glycolysis. *Applied and environmental microbiology*, *77*(7), 2239–2246. https://doi.org/10.1128/AEM.01703-10

326- Meisinger, C., Pfanner, N., & Truscott, K. N. (2006). Isolation of yeast mitochondria. *Methods in molecular biology (Clifton, N.J.)*, *313*, 33–39. https://doi.org/10.1385/1-59259-958-3:033

327- Abbiati, F., Garagnani, S. A., Orlandi, I., & Vai, M. (2023). Sir2 and Glycerol Underlie the Pro-Longevity Effect of Quercetin during Yeast Chronological Aging. *International journal of molecular sciences*, *24*(15), 12223. https://doi.org/10.3390/ijms241512223
328- Parrella, E., & Longo, V. D. (2008). The chronological life span of Saccharomyces cerevisiae to study mitochondrial dysfunction and disease. *Methods (San Diego, Calif.)*, *46*(4), 256–262. https://doi.org/10.1016/j.ymeth.2008.10.004
329- Orlandi, I., Stamerra, G., & Vai, M. (2018). Altered Expression of Mitochondrial NAD^+ Carriers Influences Yeast Chronological Lifespan by Modulating Cytosolic and Mitochondrial Metabolism. *Frontiers in genetics*, *9*, 676. https://doi.org/10.3389/fgene.2018.00676
330- Koning, A. J., Lum, P. Y., Williams, J. M., & Wright, R. (1993). DiOC6 staining reveals organelle structure and dynamics in living yeast cells. *Cell motility and the cytoskeleton*, *25*(2), 111–128. https://doi.org/10.1002/cm.970250202
331- Sun, S., & Gresham, D. (2021). Cellular quiescence in budding yeast. *Yeast (Chichester, England)*, *38*(1), 12–29. https://doi.org/10.1002/yea.3545
332- Sun, N., Youle, R. J., & Finkel, T. (2016). The Mitochondrial Basis of Aging. *Molecular cell*, *61*(5), 654–666. https://doi.org/10.1016/j.molcel.2016.01.028
333- Orlandi, I., Casatta, N., & Vai, M. (2012). Lack of Ach1 CoA-Transferase Triggers Apoptosis and Decreases Chronological Lifespan in Yeast. *Frontiers in oncology*, *2*, 67. https://doi.org/10.3389/fonc.2012.00067
334- Sharma, A., Smith, H. J., Yao, P., & Mair, W. B. (2019). Causal roles of mitochondrial dynamics in longevity and healthy aging. *EMBO reports*, *20*(12), e48395. https://doi.org/10.15252/embr.201948395
335- Knorre, D. A., Popadin, K. Y., Sokolov, S. S., & Severin, F. F. (2013). Roles of mitochondrial dynamics under stressful and normal conditions in yeast cells. *Oxidative medicine and cellular longevity*, *2013*, 139491. https://doi.org/10.1155/2013/139491
336- Ocampo, A., Liu, J., Schroeder, E. A., Shadel, G. S., & Barrientos, A. (2012). Mitochondrial respiratory thresholds regulate yeast chronological life span and its extension by caloric restriction. *Cell metabolism*, *16*(1), 55–67. https://doi.org/10.1016/j.cmet.2012.05.013

337- Aerts, A. M., Zabrocki, P., Govaert, G., Mathys, J., Carmona-Gutierrez, D., Madeo, F., Winderickx, J., Cammue, B. P., & Thevissen, K. (2009). Mitochondrial dysfunction leads to reduced chronological lifespan and increased apoptosis in yeast. *FEBS letters*, *583*(1), 113–117. https://doi.org/10.1016/j.febslet.2008.11.028

338- Bonawitz, N. D., Rodeheffer, M. S., & Shadel, G. S. (2006). Defective mitochondrial gene expression results in reactive oxygen species-mediated inhibition of respiration and reduction of yeast life span. *Molecular and cellular biology*, *26*(13), 4818–4829. https://doi.org/10.1128/MCB.02360-05

339- Aguilaniu, H., Gustafsson, L., Rigoulet, M., & Nyström, T. (2001). Protein oxidation in G0 cells of Saccharomyces cerevisiae depends on the state rather than rate of respiration and is enhanced in pos9 but not yap1 mutants. *The Journal of biological chemistry*, *276*(38), 35396–35404. https://doi.org/10.1074/jbc.M101796200

340- Gnaiger, E. (2014) Mitochondrial Pathways and Respiratory Control. An Introduction to OXPHOS Analysis, 4th ed.; OROBOROS MiPNet. Publications: Innsbruck, Austria, pp. 1‑81.

341- Barros, M. H., da Cunha, F. M., Oliveira, G. A., Tahara, E. B., & Kowaltowski, A. J. (2010). Yeast as a model to study mitochondrial mechanisms in ageing. *Mechanisms of ageing and development*, *131*(7-8), 494–502. https://doi.org/10.1016/j.mad.2010.04.008

342- Samokhvalov, V., Ignatov, V., & Kondrashova, M. (2004). Inhibition of Krebs cycle and activation of glyoxylate cycle in the course of chronological aging of Saccharomyces cerevisiae. Compensatory role of succinate oxidation. *Biochimie*, *86*(1), 39–46. https://doi.org/10.1016/j.biochi.2003.10.019

343- Borkum J. M. (2023). The Tricarboxylic Acid Cycle as a Central Regulator of the Rate of Aging: Implications for Metabolic Interventions. *Advanced biology*, *7*(7), e2300095. https://doi.org/10.1002/adbi.202300095

344- Janssens, G. E., Grevendonk, L., Schomakers, B. V., Perez, R. Z., van Weeghel, M., Schrauwen, P., Hoeks, J., & Houtkooper, R. H. (2023). A metabolomic signature of decelerated physiological aging in human plasma. *GeroScience*, *45*(6), 3147–3164. https://doi.org/10.1007/s11357-023-00827-0

345- Jing, J. L., Ning, T. C. Y., Natali, F., Eisenhaber, F., & Alfatah, M. (2022). Iron Supplementation Delays Aging and Extends Cellular Lifespan through Potentiation of Mitochondrial Function. *Cells*, *11*(5), 862. https://doi.org/10.3390/cells11050862

346- Mota-Martorell, N., Jové, M., Borrás, C., Berdún, R., Obis, È., Sol, J., Cabré, R., Pradas, I., Galo-Licona, J. D., Puig, J., Viña, J., & Pamplona, R. (2021). Methionine transsulfuration pathway is upregulated in long-lived humans. *Free radical biology & medicine*, *162*, 38–52. https://doi.org/10.1016/j.freeradbiomed.2020.11.026

347- Kwon, Y. Y., Choi, K. M., Cho, C., & Lee, C. K. (2015). Mitochondrial Efficiency-Dependent Viability of Saccharomyces cerevisiae Mutants Carrying Individual Electron Transport Chain Component Deletions. *Molecules and cells*, *38*(12), 1054–1063. https://doi.org/10.14348/molcells.2015.0153

348- Goetzman, E., Gong, Z., Zhang, B., & Muzumdar, R. (2023). Complex II Biology in Aging, Health, and Disease. *Antioxidants (Basel, Switzerland)*, *12*(7), 1477. https://doi.org/10.3390/antiox12071477

349- Wang, Q., Li, M., Zeng, N., Zhou, Y., & Yan, J. (2023). Succinate dehydrogenase complex subunit C: Role in cellular physiology and disease. *Experimental biology and medicine (Maywood, N.J.)*, *248*(3), 263–270. https://doi.org/10.1177/15353702221147567

350- Kang, W., Suzuki, M., Saito, T., & Miyado, K. (2021). Emerging Role of TCA Cycle-Related Enzymes in Human Diseases. *International journal of molecular sciences*, *22*(23), 13057. https://doi.org/10.3390/ijms222313057

351- Palmieri, L., Lasorsa, F. M., De Palma, A., Palmieri, F., Runswick, M. J., & Walker, J. E. (1997). Identification of the yeast ACR1 gene product as a succinate-fumarate transporter essential for growth on ethanol or acetate. *FEBS letters*, *417*(1), 114–118. https://doi.org/10.1016/s0014-5793(97)01269-6

352- Berry, B. J., Trewin, A. J., Amitrano, A. M., Kim, M., & Wojtovich, A. P. (2018). Use the Protonmotive Force: Mitochondrial Uncoupling

and Reactive Oxygen Species. *Journal of molecular biology*, *430*(21), 3873–3891. https://doi.org/10.1016/j.jmb.2018.03.025

353- Postmus, J., Tuzun, I., Bekker, M., Müller, W. H., Teixeira de Mattos, M. J., Brul, S., & Smits, G. J. (2011). Dynamic regulation of mitochondrial respiratory chain efficiency in Saccharomyces cerevisiae. *Microbiology (Reading, England)*, *157*(Pt 12), 3500–3511. https://doi.org/10.1099/mic.0.050039-0

354- Oreopoulou, V., & Ruß, W.D. (2007). Utilization of by-products and treatment of waste in the food industry. *Springer US*. https://api.semanticscholar.org/CorpusID:106440784

355- Rebollo-Hernanz, M., Zhang, Q., Aguilera, Y., Martín-Cabrejas, M. A., & de Mejia, E. G. (2019). Cocoa Shell Aqueous Phenolic Extract Preserves Mitochondrial Function and Insulin Sensitivity by Attenuating Inflammation between Macrophages and Adipocytes In Vitro. *Molecular nutrition & food research*, *63*(10), e1801413. https://doi.org/10.1002/mnfr.201801413

356- Rebollo-Hernanz, M., Aguilera, Y., Martin-Cabrejas, M. A., & Gonzalez de Mejia, E. (2022). Phytochemicals from the Cocoa Shell Modulate Mitochondrial Function, Lipid and Glucose Metabolism in Hepatocytes via Activation of FGF21/ERK, AKT, and mTOR Pathways. *Antioxidants (Basel, Switzerland)*, *11*(1), 136. https://doi.org/10.3390/antiox11010136

357- Cadoná, F. C., Dantas, R. F., de Mello, G. H., & Silva-Jr, F. P. (2022). Natural products targeting into cancer hallmarks: An update on caffeine, theobromine, and (+)-catechin. *Critical reviews in food science and nutrition*, *62*(26), 7222–7241. https://doi.org/10.1080/10408398.2021.1913091

358- Poewe, W., Seppi, K., Tanner, C. M., Halliday, G. M., Brundin, P., Volkmann, J., Schrag, A. E., & Lang, A. E. (2017). Parkinson disease. *Nature reviews. Disease primers*, *3*, 17013. https://doi.org/10.1038/nrdp.2017.13

359- Calabresi, P., Mechelli, A., Natale, G., Volpicelli-Daley, L., Di Lazzaro, G., & Ghiglieri, V. (2023). Alpha-synuclein in Parkinson's disease and other synucleinopathies: from overt neurodegeneration back to early synaptic dysfunction. *Cell death & disease*, *14*(3), 176. https://doi.org/10.1038/s41419-023-05672-9

360- Fields, C. R., Bengoa-Vergniory, N., & Wade-Martins, R. (2019). Targeting Alpha-Synuclein as a Therapy for Parkinson's Disease. *Frontiers in molecular neuroscience*, *12*, 299. https://doi.org/10.3389/fnmol.2019.00299

361- Delenclos, M., Burgess, J. D., Lamprokostopoulou, A., Outeiro, T. F., Vekrellis, K., & McLean, P. J. (2019). Cellular models of alpha-synuclein toxicity and aggregation. *Journal of neurochemistry*, *150*(5), 566–576. https://doi.org/10.1111/jnc.14806

362- Fruhmann, G., Seynnaeve, D., Zheng, J., Ven, K., Molenberghs, S., Wilms, T., Liu, B., Winderickx, J., & Franssens, V. (2017). Yeast buddies helping to unravel the complexity of neurodegenerative disorders. *Mechanisms of ageing and development*, *161*(Pt B), 288–305. https://doi.org/10.1016/j.mad.2016.05.002

363- Sampaio-Marques, B., Pereira, H., Santos, A. R., Teixeira, A., & Ludovico, P. (2018). Caloric restriction rescues yeast cells from alpha-synuclein toxicity through autophagic control of proteostasis. *Aging*, *10*(12), 3821–3833. https://doi.org/10.18632/aging.101675

364- Sampaio-Marques, B., Guedes, A., Vasilevskiy, I., Gonçalves, S., Outeiro, T. F., Winderickx, J., Burhans, W. C., & Ludovico, P. (2019). α-Synuclein toxicity in yeast and human cells is caused by cell cycle re-entry and autophagy degradation of ribonucleotide reductase 1. *Aging cell*, *18*(4), e12922. https://doi.org/10.1111/acel.12922

365- Tenreiro, S., Franssens, V., Winderickx, J., & Outeiro, T. F. (2017). Yeast models of Parkinson's disease-associated molecular pathologies. *Current opinion in genetics & development*, *44*, 74–83. https://doi.org/10.1016/j.gde.2017.01.013

366- Tenreiro, S., Rosado-Ramos, R., Gerhardt, E., Favretto, F., Magalhães, F., Popova, B., Becker, S., Zweckstetter, M., Braus, G. H., & Outeiro, T. F. (2016). Yeast reveals similar molecular mechanisms underlying alpha- and beta-synuclein toxicity. *Human molecular genetics*, *25*(2), 275–290. https://doi.org/10.1093/hmg/ddv470

367- Outeiro, T. F., & Lindquist, S. (2003). Yeast cells provide insight into alpha-synuclein biology and pathobiology. *Science (New York, N.Y.)*, *302*(5651), 1772–1775. https://doi.org/10.1126/science.1090439

368- Büttner, S., Bitto, A., Ring, J., Augsten, M., Zabrocki, P., Eisenberg, T., Jungwirth, H., Hutter, S., Carmona-Gutierrez, D., Kroemer,

G., Winderickx, J., & Madeo, F. (2008). Functional mitochondria are required for alpha-synuclein toxicity in aging yeast. *The Journal of biological chemistry*, *283*(12), 7554–7560. https://doi.org/10.1074/jbc.M708477200

369- Popova, B., Kleinknecht, A., & Braus, G. H. (2015). Posttranslational Modifications and Clearing of α-Synuclein Aggregates in Yeast. *Biomolecules*, *5*(2), 617–634. https://doi.org/10.3390/biom5020617

370- da Silva, L. P. D., da Cruz Guedes, E., Fernandes, I. C. O., Pedroza, L. A. L., da Silva Pereira, G. J., & Gubert, P. (2024). Exploring Caenorhabditis elegans as Parkinson's Disease Model: Neurotoxins and Genetic Implications. *Neurotoxicity research*, *42*(1), 11. https://doi.org/10.1007/s12640-024-00686-3

371- Hughes, S., van Dop, M., Kolsters, N., van de Klashorst, D., Pogosova, A., & Rijs, A. M. (2022). Using a *Caenorhabditis elegans* Parkinson's Disease Model to Assess Disease Progression and Therapy Efficiency. *Pharmaceuticals (Basel, Switzerland)*, *15*(5), 512. https://doi.org/10.3390/ph15050512

372- Sanz, F. J., Solana-Manrique, C., Muñoz-Soriano, V., Calap-Quintana, P., Moltó, M. D., & Paricio, N. (2017). Identification of potential therapeutic compounds for Parkinson's disease using Drosophila and human cell models. *Free radical biology & medicine*, *108*, 683–691. https://doi.org/10.1016/j.freeradbiomed.2017.04.364

373- Avallone, R., Rustichelli, C., Filaferro, M., & Vitale, G. (2024). Chemical Characterization and Beneficial Effects of Walnut Oil on a *Drosophila melanogaster* Model of Parkinson's Disease. *Molecules (Basel, Switzerland)*, *29*(17), 4190. https://doi.org/10.3390/molecules29174190

374- Dovonou, A., Bolduc, C., Soto Linan, V., Gora, C., Peralta Iii, M. R., & Lévesque, M. (2023). Animal models of Parkinson's disease: bridging the gap between disease hallmarks and research questions. *Translational neurodegeneration*, *12*(1), 36. https://doi.org/10.1186/s40035-023-00368-8

375- Vasquez, V., Mitra, J., Perry, G., Rao, K. S., & Hegde, M. L. (2018). An Inducible Alpha-Synuclein Expressing Neuronal Cell Line Model for Parkinson's Disease1. *Journal of Alzheimer's disease : JAD*, *66*(2), 453–460. https://doi.org/10.3233/JAD-180610

376- Caligiani, A., Acquotti, D., Cirlini, M., & Palla, G. (2010). 1H NMR study of fermented cocoa (Theobroma cacao L.) beans. *Journal of agricultural and food chemistry*, *58*(23), 12105–12111.

https://doi.org/10.1021/jf102985w
377- Caligiani, A., Palla, L., Acquotti, D., Marseglia, A., & Palla, G. (2014). Application of 1H NMR for the characterisation of cocoa beans of different geographical origins and fermentation levels. *Food chemistry*, *157*, 94–99. https://doi.org/10.1016/j.foodchem.2014.01.116
378- Spano, M., Goppa, L., Girometta, C. E., Giusti, A. M., Rossi, P., Cartabia, M., Savino, E., & Mannina, L. (2024). Dehydrated mycelia (*Cordyceps militaris, Grifola frondosa, Hericium erinaceus* and *Laricifomes officinalis*) as Novel Foods: a comprehensive NMR study. *LWT*, *199*, 116123. https://doi.org/10.1016/j.lwt.2024.116123
379- Brioschi, M., Lento, S., Tremoli, E., & Banfi, C. (2013). Proteomic analysis of endothelial cell secretome: a means of studying the pleiotropic effects of Hmg-CoA reductase inhibitors. *Journal of proteomics*, *78*, 346–361. https://doi.org/10.1016/j.jprot.2012.10.003
380- Brioschi, M., Eligini, S., Crisci, M., Fiorelli, S., Tremoli, E., Colli, S., & Banfi, C. (2014). A mass spectrometry-based workflow for the proteomic analysis of in vitro cultured cell subsets isolated by means of laser capture microdissection. *Analytical and bioanalytical chemistry*, *406*(12), 2817–2825. https://doi.org/10.1007/s00216-014-7724-9
381- Tripodi, F., Falletta, E., Leri, M., Angeloni, C., Beghelli, D., Giusti, L., Milanesi, R., Sampaio-Marques, B., Ludovico, P., Goppa, L., Rossi, P., Savino, E., Bucciantini, M., & Coccetti, P. (2022). Anti-Aging and Neuroprotective Properties of *Grifola frondosa* and *Hericium erinaceus* Extracts. *Nutrients*, *14*(20), 4368. https://doi.org/10.3390/nu14204368
382- Tripodi, F., Lombardi, L., Guzzetti, L., Panzeri, D., Milanesi, R., Leri, M., Bucciantini, M., Angeloni, C., Beghelli, D., Hrelia, S., Onorato, G., Di Schiavi, E., Falletta, E., Nonnis, S., Tedeschi, G., Labra, M., & Coccetti, P. (2020). Protective effect of *Vigna unguiculata* extract against aging and neurodegeneration. *Aging*, *12*(19), 19785–19808. https://doi.org/10.18632/aging.104069
383- Coccetti, P., Tripodi, F., Tedeschi, G., Nonnis, S., Marin, O., Fantinato, S., Cirulli, C., Vanoni, M., & Alberghina, L. (2008). The CK2 phosphorylation of catalytic domain of Cdc34 modulates its activity at the G1 to S transition in Saccharomyces cerevisiae. *Cell cycle (Georgetown, Tex.)*, *7*(10), 1391–1401. https://doi.org/10.4161/cc.7.10.5825

384- Rawel, H. M., Huschek, G., Sagu, S. T., & Homann, T. (2019). Cocoa Bean Proteins-Characterization, Changes and Modifications due to Ripening and Post-Harvest Processing. *Nutrients*, *11*(2), 428. https://doi.org/10.3390/nu11020428

385- Fabrizio, P., & Longo, V. D. (2007). The chronological life span of Saccharomyces cerevisiae. *Methods in molecular biology (Clifton, N.J.)*, *371*, 89–95. https://doi.org/10.1007/978-1-59745-361-5_8

386- Moukham, H., Lambiase, A., Barone, G. D., Tripodi, F., & Coccetti, P. (2024). Exploiting Natural Niches with Neuroprotective Properties: A Comprehensive Review. *Nutrients*, *16*(9), 1298. https://doi.org/10.3390/nu16091298

387- Wilson, D. M., 3rd, Cookson, M. R., Van Den Bosch, L., Zetterberg, H., Holtzman, D. M., & Dewachter, I. (2023). Hallmarks of neurodegenerative diseases. *Cell*, *186*(4), 693–714. https://doi.org/10.1016/j.cell.2022.12.032

388- Pohl, F., & Kong Thoo Lin, P. (2018). The Potential Use of Plant Natural Products and Plant Extracts with Antioxidant Properties for the Prevention/Treatment of Neurodegenerative Diseases: In Vitro, In Vivo and Clinical Trials. *Molecules (Basel, Switzerland)*, *23*(12), 3283. https://doi.org/10.3390/molecules23123283

389- Domise, M., & Vingtdeux, V. (2016). AMPK in Neurodegenerative Diseases. *Experientia supplementum (2012)*, *107*, 153–177. https://doi.org/10.1007/978-3-319-43589-3_7

390- Dong, X., Li, S., Sun, J., Li, Y., & Zhang, D. (2020). Association of Coffee, Decaffeinated Coffee and Caffeine Intake from Coffee with Cognitive Performance in Older Adults: National Health and Nutrition Examination Survey (NHANES) 2011-2014. *Nutrients*, *12*(3), 840. https://doi.org/10.3390/nu12030840

391- Eskelinen, M. H., & Kivipelto, M. (2010). Caffeine as a protective factor in dementia and Alzheimer's disease. *Journal of Alzheimer's disease : JAD*, *20 Suppl 1*, S167–S174. https://doi.org/10.3233/JAD-2010-1404

392- Valada, P., Alçada-Morais, S., Cunha, R. A., & Lopes, J. P. (2022). Thebromine Targets Adenosine Receptors to Control Hippocampal Neuronal Function and Damage. *International journal of molecular sciences*, *23*(18), 10510. https://doi.org/10.3390/ijms231810510

393- Grassia, M., Messia, M. C., Marconi, E., Demirkol, Ő. Ş., Erdoğdu, F., Sarghini, F., Cinquanta, L., Corona, O., & Planeta, D. (2021). Microencapsulation of Phenolic Extracts from Cocoa Shells to

Enrich Chocolate Bars. *Plant foods for human nutrition (Dordrecht, Netherlands)*, *76*(4), 449–457. https://doi.org/10.1007/s11130-021-00917-4

394- Alves, P, Guedes, J., Serrano, L., Martins, M., Sousa, D., da Silva, G., Riceli, P., & Zampieri, D. (2023). UPLC-QTOF-MSE-Based metabolic profile to screening candidates of biomarkers of dwarf-cashew clones resistant and susceptible to anthracnose (Colleto-trichum gloeosporioides (penz) penz. & sacc.). *Journal of the Brazilian Chemical Society*, *34*, 1652–1668. https://doi.org/10.21577/0103- 5053.20230097.

395- Greño, M., Herrero, M., Cifuentes, A., Marina M. L., & Castro-Puyana, M. (2022). Assessment of cocoa powder changes during the alkalization process using untargeted metabolomics. *LWT, 172*, 114207. https://doi.org/10.1016/j.lwt.2022.114207

396- LeVine H., 3rd (1999). Quantification of beta-sheet amyloid fibril structures with thioflavin T. *Methods in enzymology*, *309*, 274–284. https://doi.org/10.1016/s0076-6879(99)09020-5

397- Pandey, N. K., Ghosh, S., & Dasgupta, S. (2013). Effect of sur-factants on preformed fibrils of human serum albumin. *International journal of biological macromolecules*, *59*, 39–45. https://doi.org/10.1016/j.ijbiomac.2013.04.014

398- Niture, S., Lin, M., Qi, Q., Moore, J. T., Levine, K. E., Fernando, R. A., & Kumar, D. (2021). Role of Autophagy in Cadmium-Induced Hepatotoxicity and Liver Diseases. *Journal of toxicology*, *2021*, 9564297. https://doi.org/10.1155/2021/9564297

399- Allen, S. A., Datta, S., Sandoval, J., Tomilov, A., Sears, T., Woolard, K., Angelastro, J. M., & Cortopassi, G. A. (2020). Cetylpyri-dinium chloride is a potent AMP-activated kinase (AMPK) inducer and has therapeutic potential in cancer. *Mitochondrion*, *50*, 19–24. https://doi.org/10.1016/j.mito.2019.09.009

400- Lee, C. H., Kim, H. J., Lee, J. H., Cho, H. J., Kim, J., Chung, K. C., Jung, S., & Paik, S. R. (2006). Dequalinium-induced protofibril for-mation of alpha-synuclein. *The Journal of biological chemis-try*, *281*(6), 3463–3472. https://doi.org/10.1074/jbc.M505307200

401- Kim, H. S., Woo Chang, S., Baek, S. H., Han, S. H., Lee, Y., Zhu, Q., & Kum, K. Y. (2013). Antimicrobial effect of alexidine and chlorhexidine against Enterococcus faecalis infection. *International journal of oral science*, *5*(1), 26–31. https://doi.org/10.1038/ijos.2013.11

402- Richie, D. L., Fuller, K. K., Fortwendel, J., Miley, M. D., McCarthy, J. W., Feldmesser, M., Rhodes, J. C., & Askew, D. S. (2007). Unexpected link between metal ion deficiency and autophagy in Aspergillus fumigatus. *Eukaryotic cell*, *6*(12), 2437–2447. https://doi.org/10.1128/EC.00224-07

403- Cai, C. C., Zhu, J. H., Ye, L. X., Dai, Y. Y., Fang, M. C., Hu, Y. Y., Pan, S. L., Chen, S., Li, P. J., Fu, X. Q., & Lin, Z. L. (2019). Glycine Protects against Hypoxic-Ischemic Brain Injury by Regulating Mitochondria-Mediated Autophagy via the AMPK Pathway. *Oxidative medicine and cellular longevity*, *2019*, 4248529. https://doi.org/10.1155/2019/4248529

404- Rajapakse, A. G., Ming, X. F., Carvas, J. M., & Yang, Z. (2009). The hexosamine biosynthesis inhibitor azaserine prevents endothelial inflammation and dysfunction under hyperglycemic condition through antioxidant effects. *American journal of physiology. Heart and circulatory physiology*, *296*(3), H815–H822. https://doi.org/10.1152/ajpheart.00756.2008

405- He, X. X., Huang, C. K., & Xie, B. S. (2018). Autophagy inhibition enhanced 5-FU-induced cell death in human gastric carcinoma BGC-823 cells. *Molecular medicine reports*, *17*(5), 6768–6776. https://doi.org/10.3892/mmr.2018.8661

406- Zhang, X. H., Zhang, N., Lu, J. M., Kong, Q. Z., & Zhao, Y. F. (2012). Tetrazolium violet induced apoptosis and cell cycle arrest in human lung cancer a549 cells. *Biomolecules & therapeutics*, *20*(2), 177–182. https://doi.org/10.4062/biomolther.2012.20.2.177

407- Kwon, Y., Bang, Y., Moon, S. H., Kim, A., & Choi, H. J. (2020). Amitriptyline interferes with autophagy-mediated clearance of protein aggregates via inhibiting autophagosome maturation in neuronal cells. *Cell death & disease*, *11*(10), 874. https://doi.org/10.1038/s41419-020-03085-6

408- Kaster, K. R., Burgett, S. G., & Ingolia, T. D. (1984). Hygromycin B resistance as dominant selectable marker in yeast. *Current genetics*, *8*(5), 353–358. https://doi.org/10.1007/BF00419824

409- Yue, Y. L., Zhang, M. Y., Liu, J. Y., Fang, L. J., & Qu, Y. Q. (2022). The role of autophagy in idiopathic pulmonary fibrosis: from mechanisms to therapies. *Therapeutic advances in respiratory disease*, *16*, 17534666221140972. https://doi.org/10.1177/17534666221140972

410- He, Z., Guo, L., Shu, Y., Fang, Q., Zhou, H., Liu, Y., Liu, D., Lu, L., Zhang, X., Ding, X., Liu, D., Tang, M., Kong, W., Sha, S., Li, H.,

Gao, X., & Chai, R. (2017). Autophagy protects auditory hair cells against neomycininduced damage. *Autophagy*, *13*(11), 1884–1904. https://doi.org/10.1080/15548627.2017.1359449

SHORT CV

Education:

- 2020: Bachelor's degree in Biotechnology at Università degli Studi di Milano-Bicocca (Graduation grade: 98/110)
- 2022: Master's degree in Industrial Biotechnology at Università degli Studi di Milano-Bicocca (Graduation grade: 110/110 with honors)
    - Thesis project: 'Cofattori nicotinammidici e longevità: rapporti fra NAD e stress ossidativo durante l'invecchiamento cronologico in lievito'

Professional experience:

- Apr/2017-Present: Volunteer emergency responder at Misericordia di Arese
- Apr/2021-Present: Emergency responder Instructor
- Jul/2019-Jun/2020: Assitant waiter at Fabbrica di Pedavena – Cesate
- Nov/2022-Oct/2025: Doctoral Research in Tecnologie Convergenti per i Sistemi Biomolecolari (TeCSBi) XXXVIII cycle supported by a fellowship from Ministero dell'Università e della Ricerca (percorso 99R – 1 – Percorso Standard, cat. amm. 975 – Posti Ordinari) at Università degli Studi di Milano-Bicocca
    - Thesis project: 'Bioactive compounds and healthy aging: searching for new nutraceuticals through the experimental model of chronological aging in yeast'
    - **Publications**:
        - Abbiati, F.; Garagnani, S.A.; Orlandi, I.; Vai, M. (2023). *Int. J. Mol. Sci. 24, 12223.* https://doi.org/10.3390/ijms241512223
        - Tripodi, F., *et al.* (2024). *Curr. Res. Food Sci. 9,* 100888

https://doi.org/10.1016/j.crfs.2024.100888

- Abbiati, F.; Orlandi, I.; Pagliari, S.; Campone, L.; Vai, M. (2025). *Antioxidants*, *14*, 80 https://doi.org/10.3390/antiox14010080

- **Conferences, congresses and seminars**:
  - Poster in BtBsDay 2022
    13/Dec/2022, Università degli Studi di Milano-Bicocca.
  - Poster in “Visioni di Futuro: ricerca, cittadinanza e sviluppo sostenibile”
    30/Nov/2023, Università degli Studi di Milano-Bicocca. IRIS code: PEN-3657
  - Poster in BtBsDay 2024
    8/Feb/2024, Università degli Studi di Milano-Bicocca.
  - “Genomica: tecnologie avanzate”, 2024, FISV Federazione Italiana Scienze della Vita.
    25-26/Jen/2024, Università degli Studi di Milano.
  - “Advanced Technologies in Single Cell Omics” 2025, FISV Federazione Italiana Scienze della Vita.
    4-5/Feb/2025, Università degli Studi di Milano.
- **Didactic laboratory-workshops** with high-school students for the project “Piano Lauree Scientifiche” and “Laboratori didattici per l’insegnamento delle scienze di base su tematiche di Biologia e Biotecnologie” of Dipartimento di Biotecnologie e Bioscienze-Università degli Studi di Milano-Bicocca:
  - Public tenders code: 22CE314 (2022); 22CE154 (2022); PNRR M4C1-24 (2024); 24CE360 (2024); PNRR M4C1-24 (2025)
- **Lab supervisor** of master students and bachelor interns

- Sep/2024-Dec/2024 Visiting PhD Student in Professor Claudio De Virgilio Laboratory at Université de Fribourg/Universität Freiburg:
    - https://www.unifr.ch/bio/en/groups/de-virgilio/
    - Student Mobility for Traineeships Grant Agreement 2024-2025

Skills

Teamwork, Problem solving, Team building, Cell cultures (yeast), Enzymatic assays, Gene editing, PCR, Gel electrophoresis, Protein expression, Protein purification, Western blotting, *In vitro* kinase assay, Fluorescence microscopy, Image processing, Phenotypic characterization (Biolog's OmniLog®), Scientific writing

Languages

Italian, English (B2)

ACKNOWLEDGMENTS

I would like to express my heartfelt gratitude to Professor Marina Vai and Professor Ivan Orlandi for giving me the incredible opportunity to embark on this PhD journey and for guiding me throughout these years.

I am also deeply thankful to Professor Claudio De Virgilio and his research group for welcoming me into their lab and for accompanying me through truly special months of professional and personal growth. I will always cherish the people and the unforgettable moments I experienced in Fribourg. A special thank you goes to Dr. Marco Caligaris, mentor, friend, teacher and true scientist and to Professor Raffaele Nicastro, guide and friend. Without him, my doctoral experience and, also my life, would not have been the same.

I would like to express my gratitude to my family, including my grandparents, who always trust my choices.

And especially I want to thank Marta, for being by my side through every moment, supporting and enduring me even when things weren't going so well.

I am also grateful to my fellow volunteers at Misericordia di Arese, particularly the members of Squadra 5 and Squadra 3, for being a constant presence during my PhD years. I cannot leave out Mett, Den, Chiara, Costi, Venni and

Licia, whose inclusive spirit and curiosity about the health of my yeast cultures always made me smile.

A heartfelt thank you goes to Marco, Tom, Barbara and Laura, PhD companions and partners in laughter. I also extend my thanks to all the researchers, professors, thesis students, interns and fellow PhD candidates I've met along the way.

Last but certainly not least, I want to thank Anna, Stefano, Luca and Davide, lab mates and friends, who have been the foundation of this journey.